OPTIMIZING SELECTIVITY IN HETEROCYCLE C-H FUNCTIONALIZATION THROUGH COMPUTATIONAL DESIGN

Thesis submitted for the

Degree of Doctor of Philosophy

Department of Chemistry

Trinity 2015

Sami Khawar Jaffar

Linacre College

University of Oxford

Abstract

This thesis describes the application of quantum chemical methods to understand Pd-catalyzed C-H activation of aromatic and heteroaromatic molecules, with a view to establishing the factors that enable predictions of site-selectivity to be made. The first chapter introduces palladium catalyzed C-C bond formation and the synthetic field of direct (C-H/C-X) and oxidative cross-couplings (C-H/C-H), the postulated mechanisms of C-H activation, and the theoretical background to the project. The focus of Chapter 2 is the mechanism and site-selectivity of Pd catalyzed direct arylation of N-methyl indole. The mechanism is shown to proceed via a concerted metalation deprotonation of N-methyl indole followed by transmetalation with $PhB(OH)_2$. Importantly, this second step determines the C2 regioselectivity observed experimentally, and the key transition structure is stabilized through a π-polar bond between AcOH and the C2-C3 π system of indole.

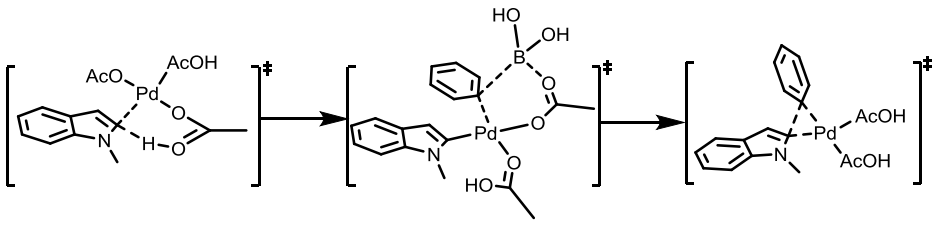

Figure 1. The direct arylation of N-methyl indole discussed in Chapter 2.

In Chapter 3 we apply DFT calculations to examine the mechanism of Pd catalyzed activation of N-methyl indole in an oxidative cross-coupling. Calculations predict the mechanism to proceed via initial C-H activation of the indole followed by C-H activation of benzene. Concerted metalation deprotonation is favoured, and assisted by coordinating solvent molecules. Alternative mechanisms, previously postulated in the literature, are calculated and do not support observed experimental results.

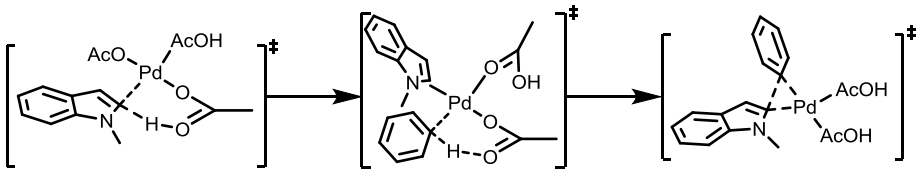

Figure 2. Mechanism of N-methyl indole arylation analyzed in Chapter 3.

We extend our examination into the C-H activation and oxidative arylation of N-acetyl indole by investigating a co-catalyst Pd/Cu system in Chapter 4. Calculations

demonstrate that a Pd-Cu dimer is energetically viable and leads to initial cleavage at C3. The regioselectivity of the mechanism is determined through the subsequent C-H activation of benzene and completed with a facile reductive elimination step.

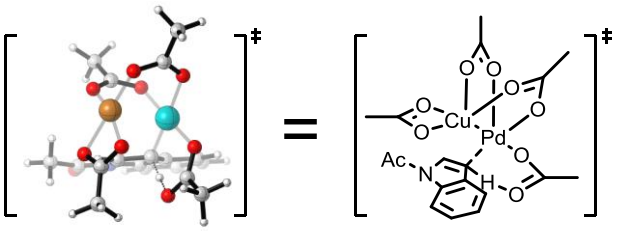

Figure 3. Mechanism of N-acetyl indole C-H activation as studied in Chapter 4.

In Chapter 5 we apply a combination of DFT and kinetic modelling on the trifluoroacetic acid (TFA) tuned homocoupling of benzene and the heterocoupling of benzene and anisole. Concentration terms are applied with the implementation of transition state theory to develop kinetic models. Various catalytic models are investigated to show that $Pd(OTFA)_2$, formed at high concentrations of TFA, favours homocoupling, while at lower TFA concentrations the catalytic species will be $Pd(OAc)_2$-TFA which favours heterocoupling.

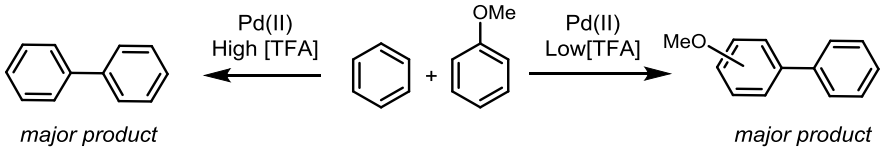

Figure 4. TFA tuned coupling of simple arenes using a Pd(II) catalytic system studied in Chapter 5.

Finally, Chapter 6 presents DFT studies on the Pd-catalyzed homocoupling and chemoselectivity of *p*-xylene. $Pd(OTFA)_2$ is computed to display greater activity than $Pd(OAc)_2$ in oxidative C-H cross coupling. Benzylic (sp^3) C-H activation of *p*-xylene is computed to be relatively difficult compared with sp^2 activation, but can nonetheless occur via an eight membered intermolecular deprotonation transition state.

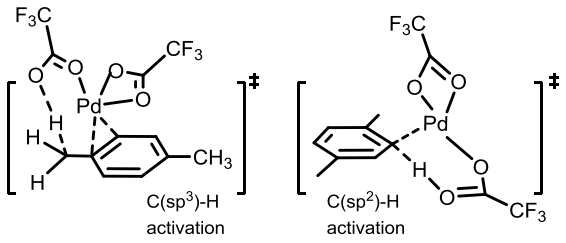

Figure 5. Chapter 6 investigates sp^2-sp^2 and sp^2-sp^3 coupling of *p*-xylene.

Contents

Acknowledgements

First and foremost, I would like to convey my sincerest gratitude to Professor Robert Paton for providing me with the opportunity to pursue this research in his lab, being eternally patient, incredibly supportive and for providing his invaluable advice and guidance throughout my D.Phil.

I am also grateful to my industrial supervisor Dr. Simone Tomasi for his guidance and suggestions throughout the course of my D.Phil especially during my CASE placement at AstraZeneca, Macclesfield and the various funding bodies who supported this research, including EPSRC, AstraZeneca, Linacre EPA Cephalosporin Fund, the Linacre House Trust, Oxford E-Research Centre (OeRC) and the National Service for Computational Chemistry Software (NSCCS).

I'd like to thank all members of the McGrady group with whom I have shared many important discussions, especially Tobias and Daniel. Thank you to all the members of the Paton lab, past and present, especially fellow D.Phil comrades Kelvin, Willian and Ace (Rob) who have made the lab an engaging and exciting place to pursue computational chemistry.

Last but certainly by no means least, I'd like to thank my family. Grandad (*Nana*), Mum (*Ammi*), Dad (*Abbu*), my sister Saima and my wife, Zahraa. Without all of your unconditional love, understanding and support I could not have *never* made it this far, I am forever indebted to you all, thank you.

I dedicate this D.Phil to my late grandmother, *Nanu*.

Glossary of abbreviations and acronyms

Å	angstrom(s), 10^{-10} m
Ac	acetyl, $COCH_3$
AcOH	acetic acid, CH_3COOH
AO	Atomic orbital
Ar	aromatic group
Atm	atmospheres (1 atm = 1.01 x 10^5 Pascal)
au	atomic units
B3LYP	hybrid density functional incorporating Becke exchange with Lee-Yang-Parr correlation
BDE	bond dissociation energy
cat.	catalytic
CCSD(T)	coupled cluster with perturbative estimate for connected triples
CEPA	coupled electron pair approximation
CMD	concerted metalation deprotonation
CP	carbopalladation
CPCM	conductor-like polarizable continuum model
DMA	N,N-dimethylacetamide
DMF	N,N-dimethylformamide
DFT	density functional theory
DZ	double zeta
EAS	electrophilic aromatic substitution
ECP	effective core potential
equiv.	equivalents
ESP	electrostatic potential map

GGA	generalised gradient approximation
GTO	Gaussian-type orbital
HF	Hartree-Fock
IRC	intrinsic reaction coordinate
K	Kelvin
kcal mol^{-1}	kilocalorie per mole
KIE	kinetic isotope effect
LANL	Los Alamos National Laboratory
LDA	local density approximation
MAE	mean absolute error
M06-2X	Minnesota 06 density functional of Truhlar
Me	methyl group, CH_3
MP2	Møller-Plesset second order perturbation theory
NAO	natural atomic orbital
NBO	natural bond orbital
NBI	natural binding index
NPA	natural population analysis
OAc	acetate anion, CH_3COO^-
OMe	methoxy group, $-OCH_3$
OPiv	pivalate anion, $(CH_3)_3COO^-$
OTFA	trifluoroacetate (or triflate) anion, CF_3COO^-
PCM	polarizable continuum model
$Pd(OAc)_2$	palladium (II) diacetate
$Pd(OTFA)_2$	palladium (II) trifluoroacetate
PES	potential energy surface

Ph	phenyl group, C_6H_5
PivOH	pivalic acid, $(CH_3)_3COOH$
RE	reductive elimination
RMSD	root mean squared deviation
RT	room temperature
SCRF	self-consistent reaction field polarizable continuum model
S_E3	intermolecular base assisted deprotonation mechanism
STO	Slater-type orbital
SZ	single zeta
TFA	trifluoroacetic acid, CF_3COOH
TM-4d set	benchmark data of 30 experimental enthalpies of formation involving second row transition metals
Tol	Toluene, C_7H_8
TS	transition state (first order saddle point)
TST	transition state theory
TZ	triple zeta
UFF	Universal Force Field
ωB97XD	dispersion corrected density functional of Head-Gordon
ZPE	Zero-point (vibrational) energy

Author's declaration

The thesis is an account of work carried out by the author in the Department of Chemistry, University of Oxford under the supervision of Professor Robert S. Paton and AstraZeneca, Macclesfield, under the supervision of Dr. Simone Tomasi. No part of this thesis has previously been submitted for a degree in this University or elsewhere. The work of other authors has been freely drawn and is duly acknowledged in the text. A list of references is given at the end of each chapter.

Doctoral work and that described in this thesis has been featured externally as follows:

Jackson, K.; Jaffar, S.K.; Paton, R.S. "Computational Organic Chemistry" *Annu. Rep. Prog. Chem., Sect. B: Org. Chem*, **2013**, *109*, 235.

Jaffar, S.K.; Tomasi, S.; Paton, R.S. "DFT studies into the mechanism and regioselectivity of C2 arylation of N-methyl indole with $PhB(OH)_2$" **2015**, *manuscript in preparation*.

Jaffar, S.K.; Tomasi, S.; Paton, R.S. "Quantum chemical studies on the mechanism and selectivity of indole direct arylations", *Abst. Pap. Am. Chem. Soc.* **2013**, *245*, 287-COMP (presented at 245th American Chemical Society Meeting, 9th April 2013, New Orleans, LA).

Sami Khawar Jaffar

Chapter 1

Theoretical methods & Pd catalyzed C-C bond formation

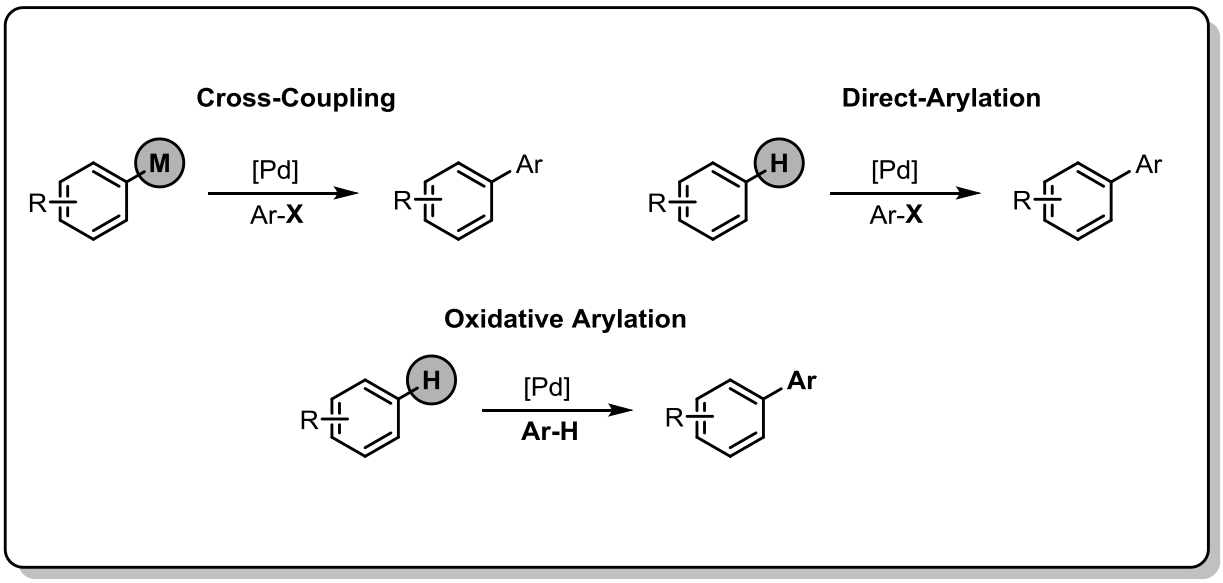

1.1 Theoretical Methods

1.1.1 *ab initio* methods

The fundamental underlying concept behind all *ab initio* methods is the Schrödinger equation, shown here in its non-relativistic, time-independent form (**1)**:

$$H\Psi = E\Psi \quad \textbf{(1)}$$

In this equation *H*, represents the *Hamiltonian*, an operator which provides the total energy value for the system, *E*, when applied to the wavefunction Ψ. The Hamiltonian operator contains terms for kinetic energy of the electrons and nuclei, electrostatic interaction energy and the internuclear repulsion energy and operates on the function Ψ. Any function Ψ that satisfies the Schrödinger equation is known as the eigenfunction (of *H*) which will have its own related energies, i.e. eigenvalue. The variation principle allows different trial wavefunctions to be evaluated on the basis that the one giving the lowest energy, i.e. lowest eigenvalue *E*, is the best possible approximation to the ground state of the system.

For chemical reactions of many-body systems however, the Schrödinger equation cannot be solved exactly. The complexity of the problem can be reduced significantly by separating the motion of the nuclei (translation, vibration and rotation of the molecule) and the electronic motion through the Born-Oppenheimer Approximation[1] which allows for the Schrödinger equation for electronic motion to be solved for a fixed separation of nuclei. This is possible due to the relative disparity between the average speed of electron and nuclei[I], and as such, describing the movement of electrons with respect to fixed nuclear coordinates is a sound assumption. Therefore, the Born-Oppenheimer Approximation can be written as follows (**2**):

$$\Psi = \Psi_n \Psi_e \quad \textbf{(2)}$$

[I] Average speed of an electron in the hydrogen atom is ~1000 times the speed of a proton. This means that, to an approximation, the nuclei are effectively stationary on the timescale of electron movement; or, conversely, that as the nuclei move, the electrons move infinitely faster, that is, they react to nuclear changes instantaneously.

Where the approximation of the total wavefunction is given by the product of an electronic wavefunction Ψ_e (a function of only electronic coordinates) and nuclear wavefunction Ψ_n (a function of only the nuclear coordinates). Thus, implementing this approximation, the Schrödinger equation for electronic motion can be rewritten as **(3)**

$$H_e\Psi_e = E_e\Psi_e \quad \textbf{(3)}$$

The Schrödinger equation includes only electron kinetic energy, electron attraction (to nuclei) and interelectronic interactions. The internuclear repulsion, V_{nuc}, (nuclear-nuclear repulsion energy) is added to the energy obtained from the equation. The Hamiltonian, H_e, is obtained after applying the Born-Oppenheimer Approximation and neglecting relativity is given by (**4**):

$$H_e = -\frac{1}{2}\sum_i^n \nabla_i^2 - \sum_I^N \sum_i^n \frac{Z_I}{r_{Ii}} + \sum_{i<j}^n \frac{1}{r_{Ii}} + V_{nuc} \quad \textbf{(4)}$$

Solving the Born-Oppenheimer Approximation for the electronic Schrödinger equation, for a set of fixed nuclear coordinates, provides an electronic energy (*E*) and wavefunction Ψ. Repeating for other nuclear configurations leads to the creation of an associated potential energy surface (PES). The creation of a complete PES is achievable once the electronic Schrödinger equation has been solved for all nuclear configurations.[II]

The wavefunction Ψ, is dependent upon all coordinates of the molecule, however, the electronic wavefunction can be separated into a product of functions reliant on one electron, as proposed by Hartree (**5**):

$$\Psi_1(R_1), \Psi_2(R_2) \ldots \Psi_n(R_n) = \phi_1(R_1)\phi_2(R_2) \ldots \phi_n(R_n) \quad \textbf{(5)}$$

This wavefunction would solve the Schrödinger equation completely. However, it cannot account for the instantaneous electron-electron repulsive term in the Hamiltonian. This particular problem is addressed through another approximation, whereby an expression which describes the repulsion felt by an electron by the average position of the other electrons, V_i^{eff} (**6**) is applied. It is noted that such an approximation

[II] The creation of a comprehensive PES for a system larger than 3-4 atoms is largely unattainable due to the extensive nature of a 3N-6 dimension space (where N=number of atoms).

is by no means trivial, as it eliminates the ability of an electron to respond instantaneously to the movement of another electron (i.e. it neglects instantaneous electron-electron repulsions, also referred to as dynamic correlations).

$$\left(-\frac{1}{2}\nabla i^2 - \sum_l^N \frac{Z_i}{r_{li}} + V_i^{eff}\right)\phi_i = E_i\Psi_i \quad \textbf{(6)}$$

An iterative scheme is required in order to solve the Hartree equations as V_i^{eff} is dependent upon all of the functions, ϕ_i. Therefore a scheme producing improved functions through an iterative process, thus resulting in improved effective potential operators V_i^{eff}, is utilized. This is continuous and ceases once the functions, ϕ_i are constant, and is termed the self-consistent field (SCF).

The separated wavefunction (**4**), however, was contentious, as it does not satisfy the criteria of the Pauli Exclusion Principle.[2] The form of a multi-electron wavefunction must obey the antisymmetry principle, and therefore, upon changing coordinates of the electron, it is necessary for the wavefunction to change sign. Fock[3,4] suggested the implementation of the Slater determinant **(7)**, which helps in the construction of an antisymmetric wavefunction[5] and satisfies the Pauli Exclusion Principle:

$$\Psi_{(R1,R2..Rn)} = \frac{1}{\sqrt{n!}}\begin{vmatrix} \phi_1(e_1) & \phi_2(e_1) & \phi_n(e_1) \\ \phi_1(e_2) & \phi_2(e_2) & \phi_n(e_2) \\ \cdots & \cdots & \cdots \\ \phi_1(e_n) & \phi_2(e_n) & \phi_n(e_n) \end{vmatrix} = \left|\phi_1,\phi_2 \ldots \phi_n\right| \quad \textbf{(7)}$$

Each one of the one-electron wavefunctions is then expressed as a linear combination of one-electron functions, ϕ(**8**), or also known as the linear combination of atomic orbital (LCAO) approximation:

$$\emptyset_i = \sum_\mu^k c_{i\mu}\chi_\mu \quad \textbf{(8)}$$

where μ spans all of the AOs χ of every atom in the molecule (a total of *k* AOs), and $c_{i\mu}$ is the expansion coefficient of AO χ_μ in MO ϕ_i, also known as *molecular orbital expansion coefficients* and is determined from the iterative solution of the Hartree-Fock SCF equations.[6] These one-electron functions are commonly termed a *basis set*.[7] The solution is provided through an iterative process where the coefficients are produced through an initial guess, which is refined upon each iteration until convergence is reached.

1.1.2. Basis sets

In theory, an infinite basis set is required to solve the HF SCF equations as this would provide an ideal description of electron probability density (i.e. provide the lowest, ground state energy). However, expanding the wavefunction by applying an infinite number of functions is not practical since solution of the SCF equation scales as N^4 (where N= number of basis functions) and thus alternative solutions must be pursued. Therefore, mathematical functions which reproduce a good wavefunction efficiently have been the focus of development. Such development has utilized the variation principle, which states, "*any wavefunction constructed as a linear combination of orthonormal functions will have its energy greater than or equal to the lowest energy (E0) of the system*". As such, truncated expansions can be judged on their quality by assessing the associated energy. An expansion which can provide a lower energy is closer to the genuine solution of the Schrödinger equation, essentially produces a better wavefunction.

A natural starting point would be to utilise functions which resemble the hydrogenic atomic orbitals, known as Slater Type Orbitals (STOs).[8] These orbitals are of the form e^{-r}, and thus mimic the exact solution of the Schrödinger equation for a single electron atom. However, more commonly used are Gaussian Type Orbitals (GTOs) which use Gaussian functions (e^{-r^2}) to mimic Slater-type orbitals. The major advantage of using GTOs is that the product of two Gaussian functions centred on different points is another Gaussian centred between the original centres, so the integrals become much easier to compute. Multiple Gaussian functions are summed together to give a shape better approximating an STO. Thus, GTOs are computationally more efficient; however, their radial component differs from STOs, as they are continuously differentiable as opposed to having a cusp (present in STOs). Therefore, to adequately mimic the proper radial shape of STOs, multiple GTOs are required. Although computationally this may become expensive, it now commonplace in theoretical calculations of many body systems to utilize GTOs. This pioneering work was enabled by Sir John Pople, through development of basis sets (amongst other quantum mechanical theory) and the magnitude of such QM development was recognised with the 1998 *Nobel Prize for Chemistry*.

The basis functions in GTOs required to adequately describe a typical organic system (up to and beyond 100s of atoms) must allow for core electrons to approach the nucleus and valence electrons to delocalize. Therefore single zeta (SZ) basis sets, where one function is used for every occupied orbital are inadequate and are commonly cast aside in preference for double zeta (DZ) basis sets (where the size of the basis set is doubled). Pople provided an alternative,[9,10] through split-valence basis sets, where SZ was used in the core and DZ or TZ (triple zeta) for the valence electrons. With most chemistry routinely focussing on the valence electrons in reactions, this provided a suitable alternative. Additional basis functions can help address the deficiencies in describing electron distribution through polarization functions (denoted commonly as *), and the electron density through diffuse functions (denoted commonly as +).

Polarization functions allow for the valence space to be described in more accuracy as they add a set of functions which improve basis set flexibility. Thus, d functions are added for carbon, and p for hydrogen therefore including AOs with angular momentum one greater than in the valence space. Diffuse functions decay more slowly away from the nucleus and allow for electron density to be expanded into a larger volume which is essential when dealing with anionic or other electron rich atoms and molecules. Here, an additional set of functions of the same AOs as the valence space are added – therefore carbon has an extra set of s and p orbitals.

1.1.3. Møller-Plesset Perturbation theory

In HF theory the main approximation is that an electron's motion can be described by a single-particle function which is not explicitly dependent on instantaneous motions of the other electrons. Therefore, electron correlation (i.e. instantaneous electron-electron interaction) is neglected. Møller and Plesset[11] incorporated perturbation theory to the molecular system, allowing the perturbation component to account for electron correlation. The second-order correction (MP2) method expresses the wavefunction as a linear combination of solutions of the Hamiltonian. This accounts for excitations of electrons into unoccupied orbitals. Spin-component scaled (SCS) MP2[12,13] is a variation of the MP2 method, which empirically scales the correlation energy for same-spin electron (SS, by a factor of 0.33) separately to electrons with opposite spin (OS, by a factor of 1.2). Although accurate, the MP2 method (N^5) scales at a much larger cost than traditional DFT (N^3) and converges more slowly with respect to basis set size.

1.1.4. Coupled Cluster (CC) theory

Coupled Cluster (CC) Theory [14] enables the electron Schrödinger equation to be solved accurately by utilizing the HF wavefunction with the addition of an operator that produces a linear combination of excited determinants. The precept of CC methods allows for the full Configuration Interaction (CI) wavefunction to be described. This wavefunction is the exact wavefunction found in the basis set approximation, and therefore electron correlation can be estimated with far more accuracy than previously described methods.

Although computationally demanding (scaling at N^6, where N is number of basis functions) variations on this method have displayed impressive accuracy when evaluating small organic systems. The incorporation of perturbative triples excitations in the CCSD(T) method is commonly used as the computational chemistry gold standard to yield energy changes within ~1 kcal/mol of experimental values.

1.1.5. Density functional theory (DFT)

The importance of density functional theory (DFT) was recognized in 1998 with a *Nobel Prize in Chemistry* for Walter Kohn for his role in the development of DFT. Hohenberg and Kohn provided the fundamental theorems that are the basis for DFT – which allows the electron density of a molecule to be used to resolve the molecular energy (as opposed to solving the electronic wavefunction).[15] Thus, given the electron density it would be possible to calculate the ground state energy of a system through solving the universal Kohn-Sham functional[16] which described the kinetic energy of non-interacting electrons (**9**). However, the term accounting for interelectronic interaction or *exchange-correlation functional* within the Kohn-Sham equations is unknown.

$$E[\rho(\boldsymbol{r})] = \underbrace{T_e[\rho(\boldsymbol{r})]}_{\text{Kinetic energy of non-interacting}} + \underbrace{V_{nu}[\rho(\boldsymbol{r})]}_{\text{Nuclear-electron attraction term}} + \underbrace{V_{el}[\rho(\boldsymbol{r})]}_{\text{Electron-electron repulsion term}} + \underbrace{E_{XC}[\rho(\boldsymbol{r})]}_{\text{Exchange Correlation functional}} \quad \textbf{(9)}$$

The exchange-correlation function has many variations, as approximations are routinely applied to account for this 'catch-all' term. These approximations are an exchange (E_X) and correlation (E_C) term (**10**), written in terms of the electron density $\rho(\boldsymbol{r})$ (which is a functional of energy density,$(\boldsymbol{\varepsilon})$:

$$E_{XC}[\rho(\boldsymbol{r})] = E_X[\rho(\boldsymbol{r})] + E_C[\rho(\boldsymbol{r})] = \int \rho(\boldsymbol{r})\, \boldsymbol{\varepsilon_X}[\rho(\boldsymbol{r})] d\boldsymbol{r} + \int \rho(\boldsymbol{r})\, \boldsymbol{\varepsilon_c}[\rho(\boldsymbol{r})] d\boldsymbol{r} \quad \textbf{(10)}$$

The variations applied to account for the exchange-correlation term is described within a hierarchal system, termed by Perdew as 'Jacob's Ladder'[17,18] where the bottom of the ladder consists of HF theory and the top aspires to the 'perfect functional'. Amidst these two levels there are a set of five rungs, with the first consisting of the Local Density Approximation (LDA) where the value of the energy density ($\boldsymbol{\varepsilon}$) is dependent and determined from the uniform electron density. Ascending to the second rung, the Generalised Gradient Approximation (GGA) functionals offer an improvement on LDA functionals by extending to incorporate the first derivative of the electron density as well as the electron density itself.

Meta GGA functionals (such as M06-2X,[19] M06-L[20]) also incorporate the kinetic energy density, or the Laplacian of the density, and as with the M06 family can be

highly parametrized to fit experimental data or high accuracy computational data. The fourth rung is occupied by hyper-GGA/ hybrid functionals (such as B3LYP [21,22]) where various % of LDA, GGA and HF exchange are used to account for the exchange-correlation term. These are also parametrized against experimental data to provide for better accuracy. For example, in the popular B3LYP functional (**11**), the exchange correlation term is as follows:

$$E_{XC}^{B3LYP} = (1-a)E_X^{LSDA} - \mathrm{a}E_X^{HF} + b\Delta E_X^B + (1-c)E_C^{LSDA} + cE_C^{LYP} \quad \textbf{(11)}$$

Where *a*= 0.20, *b*=0.72 and *c*=0.81.E_X^{HF}: Hartree-Fock exact exchange functional, E_C^{LSDA}= LDA correlation, E_X^{LSDA}=LDA exchange, E_X^B= Becke 88 exchange functional, E_C^{LYP}= Lee-Yang-Parr correlation functional.

The fifth rung consists of this ladder consists of double-hybrid functionals (such as Grimme's B2PLYP[23]) which uses the unoccupied Kohn-Sham orbitals and employs HF exchange and perturbation correlation to describe the exchange-correlation. These are computationally expensive relative to traditional hybrid functionals, due to an incorporated Møller-Plesset second order calculation within these methods.

Hybrid-GGA functionals as used in this thesis have featured prominently within the computational study of organic and organometallic systems, producing comparable accuracy, and in some cases outperforming higher level *ab initio* methods[24] with a significant reduction in computational cost (DFT scales as N^3, with HF methods N^4 and MP2 N^5, where N=the number of basis functions). Computational studies into the gas phase enthalpies of formation of the TM-4d set against the relativistic pseudopotential correlation consistent Composite Approach (rp-ccCA)[III], showed that hybrid functions such as dispersion-corrected ωB97XD (6.5 kcal/mol) displayed competitive mean absolute deviation (MAD) to double hybrid methods, B2GP-PLYP (4.3 kcal/mol) and mPW2-PLYP (5.2 kcal/mol) at a fraction of the computational cost.[25]

DFT suffers from certain well documented pitfalls, such as the lack of systematic improvement through increasing basis set size, which is possible in HF methods. Treating a particular system, especially when calculating energies of transition metals,

[III] The correlation consistent composite approach (ccCA) is a first-principles-based composite approach for main group and first and second-row transition metal species. ccCA applies B3LYP optimization for geometries and frequencies, HF for molecular orbitals, MP2 and CCSD(T) for electron correlation energies and has been shown to outperform MP2/MP4 for accuracy and reliability in the W4 dataset.

requires prudent selection of functional as different functionals can introduce extreme variation from the true energy. Therefore it is appropriate to ensure suitable benchmarking undertaken and the chosen functional correlates well with the available experimental observables and data from correlated wavefunction theory calculations.

Another notable issue is the deficiency of many DFT functionals to completely disregard or poorly treat London dispersion interactions (i.e. long-range interactions) which play an important part in the accurate treatment of organic systems.[26] This has received much attention, especially in the development of contemporary functionals and dispersion has been incorporated into through various approaches.[27] The most popular approach has been one which applies an atom-pairwise London-dispersion correction scheme (DFT-D)[28] to correct for the $-C_6/R^6$ dependence of the dispersion interaction energy on the interatomic (molecular) distances for DFT functionals lacking adequate long-range dispersion interactions. This has given rise to functionals of the form B3LYP-D, where D indicates the added dispersion term, and further work (notably by Grimme) has created a family of dispersion corrections – through D1 to the most recent D3. A range of functionals incorporating the damped atom-pairwise correction has emerged, most notably with long-range corrected functionals such as ωB97XD[29] which has been shown to remedy the systematic overestimation of internuclear distances in ruthenium-based olefin metathesis catalyst precursors.[30] The relative lack of computational cost between dispersion corrected (i.e. ωB97XD) and non-corrected (ωB97X) provide and the additional benefits of accounting for dispersion create a convincing case to employ dispersion when applying DFT functionals, succinctly summarized by Stefan Grimme, *"Any dispersion-correction is better than none"*.[IV]

[IV] As expressed in his talk on "*Effect of London Dispersion Energy on the Thermochemical Properties of Molecules*" WATOC 2011, Santiago de Compostela, Monday 18th July 2011

1.1.6. Solvation

The treatment of solute molecules in computational chemistry is an area of much debate and development. The extent of the solvent space that needs to be adequately covered, for most organic systems, cannot be done with a quantum mechanical treatment due to the size of these systems. Additionally, many conformations need to be sampled in order to elucidate the free energy of the system. Thus alternative approaches have to be employed.

One such approach is to apply a homogenous dielectric medium across the entire system, essentially averaging out the effects of the solvent. This is often referred to as a continuum, and the most widely used method is the Self-Consistent Reaction field (SCRF) method. Here, a cavity is created in which the solute molecule is held, with the solvent then placed within this cavity. Terms accounting for cavitation, electrostatic and non-electrostatic interactions account for the total solvation energy[V] and the solvation free energy in the SCRF (**12**) can be defined as:

$$\Delta G_{solvation} = \Delta G_{cav} + \Delta G_{disp} + \Delta G_{rep} + \Delta G_{elec} \quad \textbf{(12)}$$

Where, ΔG_{cav} is the energetic cost of creating the cavity, ΔG_{disp} accounts for the dispersive interactions between solvent and solute, ΔG_{rep} accounts for repulsive interactions between solvent and solute and ΔG_{elec} accounts for the electrostatic interactions between solvent and solute. The solvent field effectively polarizes the solute electron density and *vice versa*. There are many variations of the solvent approaches which can be employed, including SMD (*Density based solvation model*)[31] and the more conventional PCM (*polarizable continuum method*) described by Equation **12**.[32] Our work utilizes an extension of the PCM method, known as C-PCM (*conductor-like polarizable continuum model*), in which the solvent is treated as a conductor thus impacting the polarization charge of accessible surface area between both solute and solvent. The benefits inherent to this method[VI] have led this to become a popular choice of method for the treatment of solvation energies of neutral and ionic

[V] This is also known as the implicit solvent model

[VI] (1)Faster computational time (2) high quality results for solvents with high permittivity, and good results for solvents with low permittivity (compared with PCM).

organic species where the mean absolute deviation from 70 experimental values is 2.6 kcal/mol.[33]

Alternatively, a hybrid method whereby explicit solvent molecules are explicitly modelled in addition to the aforementioned dielectric treatment (i.e. added CPCM correction) allows for a more detailed treatment. Long range and local solvation effects are both accounted for, with the explicit molecules receiving quantum mechanical treatment (local effects) and the dielectric field accounting for long-range effects. Explicit coordination of solvent molecules has been shown to be important in assisting Pd catalyzed C-H functionalizations of arenes, modelled (with DFT) using the hybrid method.[34] We utilise the hybrid method in this thesis, where quantum mechanical treatment is applied to explicit solvent molecules that ligate to vacant sites of Pd(0)/Pd(II) to better describe coordination effects of the solvent medium used in experiment.

1.1.7. Potential Energy Surface (PES)

The potential energy surface (PES) is a function of *3N-6* (*x,y,z* coordinates, *N*= number of atoms) dimensions. In transition state modelling creating or mapping out the PES for a reaction consists of characterising ground state and transition state structures. Therefore, a reaction proceeding from reactants to TS to products (where these points of interest or *critical points* are located through quantum mechanical calculations) allow for the construction of the associated PES to the reaction.

Locating ground state structures consists of minimizing the energy with respect to all internuclear coordinates, reaching a *local energy minimum*. This point is assessed through a geometry optimization, where a set of coordinates and a starting geometry is optimized till certain optimization criteria are fulfilled. The gradient of the energy is analyzed and the Hessian matrix (a matrix of second derivatives with respect to the coordinates) is evaluated. If all associated eigenvalues (force constants) are positive, the structure corresponds to a ground state structure or *local energy minimum*. However, if there is one negative eigenvalue, then the structure is a first order *saddle point*, and corresponds to a transition state. Thus, location of a transition state geometry is far more challenging, and more sensitive to initial structure than ground state

geometries.[35] In this thesis all saddle points were located using the Gaussian 09 package through the implementation of the Berny algorithm[36] which requires the initial guess (and hence some knowledge of the curvature around the saddle point of the PES). To generate a good starting point a PES scan is often required. Identification and verification of stationary points as either minima or TSs is performed through analysis of the harmonic vibrational frequencies. Minima have all real vibrational frequencies whereas TS (i.e. saddle points) display a single imaginary frequency due to a negative force constant.

1.1.8. Transition State Theory (TST)

The reaction rate constant (k) is a useful method of understanding the kinetics inherent to a reaction. The simplest equation to understand kinetics in a chemical reaction can be attributed as an empirical relationship, as expressed by the Arrhenius equation (**13**):

$$k = Ae^{\frac{-E_a}{RT}} \quad \textbf{(13)}$$

where A is the *pre-exponential factor*, E_a is the *activation energy*, R is the *universal gas constant* and T is the *absolute temperature*.

Mathematical manipulation of the Arrhenius equation can provide a term to describe the activation energy, E_a, and thus the activation barrier in chemical reactions (**14**):

$$E_a = RT^2 \frac{d(\ln k)}{dT} \quad \textbf{(14)}$$

Alternatively, Transition State Theory (TST) can be used to calculate the reaction rate constant through applying the Eyring equation (**15**). Here, there is an assumption regarding the transmission coefficient (which is an additional prefactor in TST), that no recrossing is involved from reactants to product (i.e. the transition state, TS, always proceeds to the product, never reverting to reactants). Thus following this convention, the Eyring equation can be written as:

$$k = \frac{K_b T}{h} e^{\frac{-\Delta G^{\ddagger}}{RT}} \quad \textbf{(15)}$$

where K_B is the Boltzmann constant, $\Delta G^{\ddagger}$ is the *Gibbs energy of activation*, h is Planck's constant, R is the *universal gas constant* and T is the *absolute temperature*.

The calculation of $\Delta G^{\ddagger}$ within Chapter 6 (where TST is applied) can be summarised in **Figure 1**, where the value of $\Delta G^{\ddagger}$ is calculated as $AB_{pre} \rightarrow AB^{\ddagger}$. This value is extracted in two scenarios, where the reaction proceeds with a low energy precomplex relative to reactants (i.e. AB_{pre} is kinetically favourable) or when the precomplex is higher in energy relative to the reactants (i.e. AB_{pre} requires energy). The barrier height between the TS and precomplex provides resultant $\Delta G^{\ddagger}$.

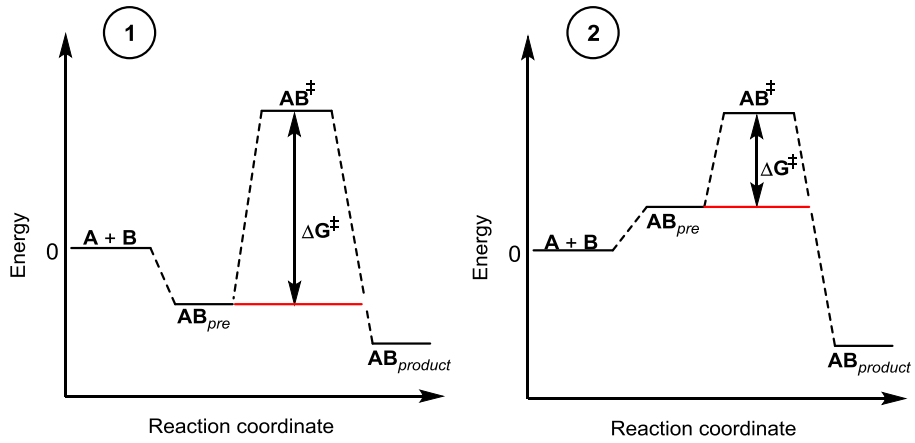

Figure 1. The energy calculated for $\Delta G^{\ddagger}$ for (**1**) the reaction proceeding with an energetically favourable precomplex (AB_{pre}) to TS ($AB^{\ddagger}$) and (**2**) where energy is required to form the precomplex (AB_{pre}) before proceeding to the TS ($AB^{\ddagger}$).

1.2. Pd catalyzed C-C bond formation

1.2.1. Cross coupling

The construction of new C-C bonds underpins the synthesis of many new organic compounds of significant complexity and creation of such molecules has been made tractable through the application of transition metal catalyzed reactions.[37] Traditional cross coupling methods (**Figure 2**) have focused on an organometallic reagent (R^1-X) and organometallic nucleophile (R^2-m) coming together to form a new C-C bond in the presence of a metal (M).

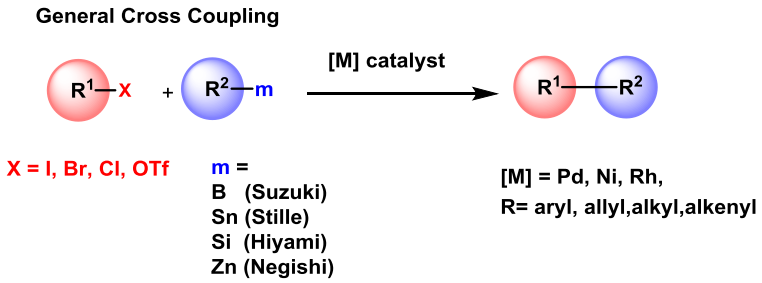

Figure 2. General scheme for a transition-metal catalyzed cross coupling for the creation of new C-C bonds

Transition metal catalyzed C-C methods have an immense scope to couple organic functional groups and are extensively applied.[38] Their importance was acknowledged by the award of the 2010 Nobel Prize for Chemistry to Heck, Suzuki and Negishi recognizing their work in the field of Pd catalyzed cross couplings. Palladium catalyzed cross couplings have grown in prominence since the inception of the Heck (or Heck-Mizori) reaction[39,40,41] which is most commonly conducted with an electron deficient olefin (e.g. styrene) coupling with an aryl/alkenyl halide.

Kumada[42] illustrated the potential of Palladium catalysis in the construction of biaryl linkers through his cross-coupling methodology which utilized a Grignard reagent coupled with an organohalide through a Pd(0)/Pd(II) catalytic cycle. The Negishi cross coupling provided an alternative transition metal catalyzed cross coupling *via* an organozinc and organohalide substrate with Pd or Ni as the catalytic transition metal[43] (although Pd based catalysis has been utilized prominently as yields are significantly higher compared with Ni), and in subsequent years Stille[44] and Suzuki[45] published synthetic approaches to constructing biaryls, again employing Pd(0) as the catalytic species.

However, these seminal cross couplings required a sacrificial metalating agent, with the Stille coupling employing toxic organostannane as one of the coupling partners and the Suzuki coupling utilizing relatively stable and less hazardous organoborane. Having to employ metalated arenes in these seminal cross-couplings resulted in inevitable amounts of stoichiometric toxic waste byproduct, an unwanted consequence of this method. Furthermore, prefunctionalization of the coupling partners inserted additional undesirable steps in the synthetic procedure, combining in an unwanted increase in step economy and atom economy. An efficient and environmentally benign alternative was sought, and achieved through the form of *direct arylation* reactions.

1.2.2. Direct arylation

C-X functionalization, where an X-type ligand (X= halide/psuedohalide) can be incorporated to prefunctionalize a (hetero)arene subsequent to biaryl formation with an unfunctionalized (C-H) (hetero)arene falls into the category of direct arylations. Such functionalizations can provide a powerful synthetic approach towards the formation of biaryl linkers and an attractive alternative to the traditional transition-metal catalyzed cross-couplings of Suzuki, Heck, Stille and Negishi (**Figure 3**).

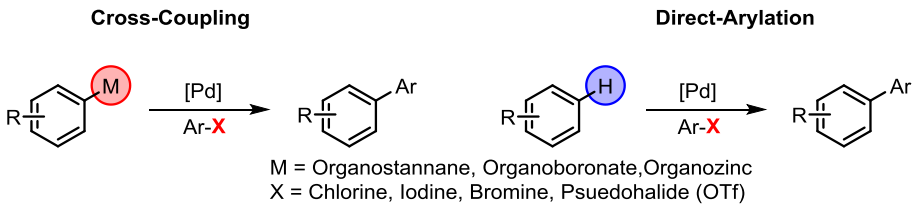

Figure 3. Cross coupling with traditional cross coupling methods (left) and direct arylation methods (right)

A common aspect amongst traditional transition metal cross couplings (i.e. C-X + C-X) reactions was the multistep approach in creating a new C-C bond. The ubiquity of the C-H bond in organic molecules means that methods of C-H activation must contend with the inherent challenge of selecting a desired position for reaction among many possibilities, due to the inherent strength of the C-H bond (bond dissociation enthalpy, BDE ~100-120 kcal/mol). Activating an arene (e.g. benzene, naphthalene, anisole, mesitylene) is further complicated due to low acidity of the C-H bond and the lack of directing groups that may influence, through coordination, C-H bond cleavage.

However, despite these challenges protocols aimed at pre-activating with a halide or pseudohalide, thus creating a C-X bond initially, can allow for directed functionalization through introducing electronic/functional group bias. Direct arylations seek to only prefunctionalize one substrate (conventionally the electron deficient of the two coupling partners) subsequently reducing unwanted waste byproduct associated with traditional metal-catalyzed cross coupling.

Ames[46] displayed an early example of such direct arylation reactions in 1982 (**Figure 4**) where direct intramolecular arylation reaction with a Palladium (II) diacetate catalyst afforded the cyclization product following Heck's synthetic protocol. Subsequently, Ames and coworkers optimized the protocol to allow for the intramolecular direct arylation synthesis of a variety of heterocycles, as illustrated in the synthesis of dibenzofuran.

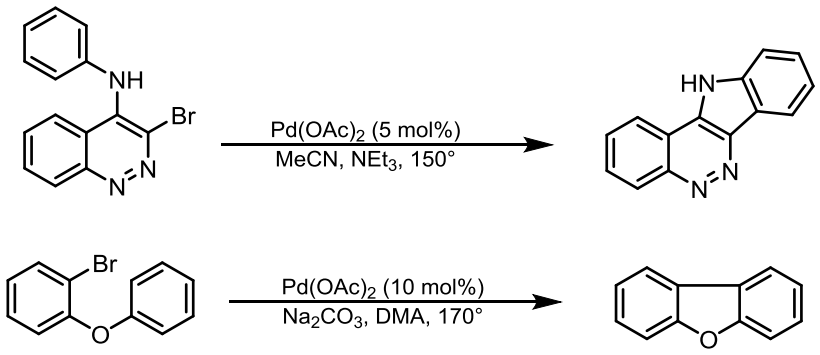

Figure 4. Ames direct intramolecular arylation reactions following the Heck synthetic protocol.

Ohta's seminal work detailing the direct arylation of N-substituted indoles at both the C2[47] and C3[48] position allowed for the evolution of the direct arylation methodology to initiate coupling of chloropyrazine to N-substituted indoles. The regioselectivity of the reaction was seemingly influenced by substitution at the N-1 position, where incorporation of alkyl groups yielded the C2 arylated product. Contrastingly N-Tosyl indole yielded the C3 arylated product with the only noticeable difference in reaction conditions being the initial catalytic loading of $Pd(PPh_3)_4$ (**Figure 5**).

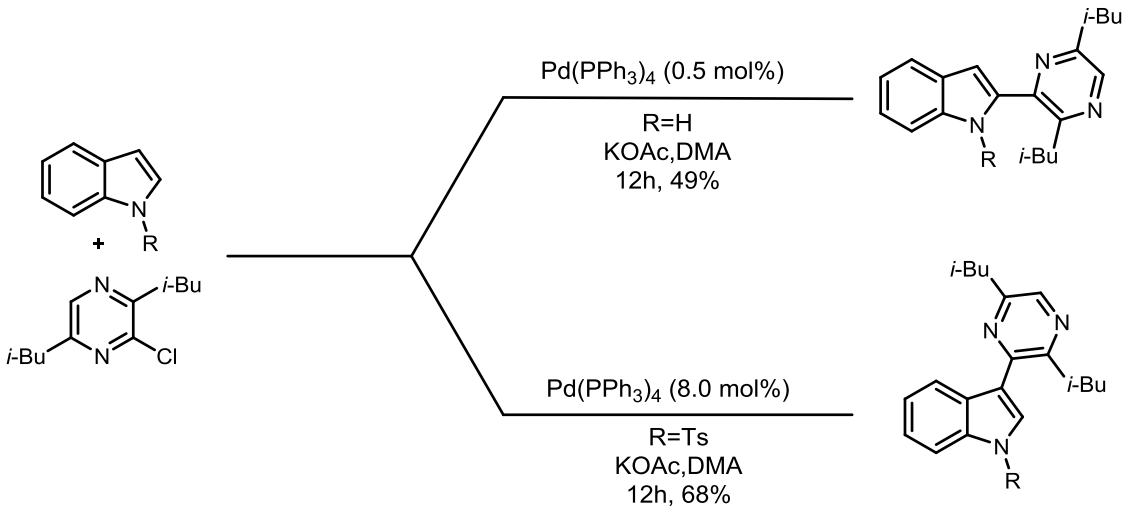

Figure 5. Ohta's seminal work applying direct arylation methodology for N-indoles.

As direct arylation methodologies emerged, Dyler[49] demonstrated the regioselective direct arylation of polar hydrocarbons, such as Azulene with iodobenzene. The Pd(II) catalyzed protocol allowed for selective coupling at the electron rich C1 position, and more importantly it highlighted the opportunity to employ less reactive aromatic arenes in order to undertake direct functionalizations. This influenced a body of work which saw the direct arylation of benzene and toluene from Fagnou[50], Lu[51] and Charlette[52] illustrating the ability to form a variety of biaryls using $Pd(OAc)_2$ as the catalytic species.

1.2.3. Direct arylation of indoles

Indoles are a privileged motif in natural products and pharmaceutical agents. As such, their functionalization is an important synthetic procedure leading to biologically active compounds.[53] The ability to functionalize indoles and affix functional groups (e.g. aromatics) is therefore highly desirable within the synthetic and pharmaceutical communities. It is evident that progress in achieving this aim has benefitted substantially from the advent of direct arylation reactions, where usually the electron-poor aryl has been prefunctionalized.[54]

After Ohta's seminal work utilizing the direct arylation reaction with N-substituted indoles in 1985, the methodology was revisited two decades later when Sames and coworkers[55] used the direct arylation methodology to couple benzene to various N-alkylated indoles at the electron deficient C2 position in good selectivity using a

$Pd(OAc)_2/PPh_3$ catalytic system. Interestingly, this was somewhat counterintuitive, as the coupling of N-indoles with electrophiles traditionally occurs at C3, the position at which indole is most electron rich. Activation at the less reactive C2 position is generally affected via a base-promoted lithiation (due to the acidic nature of the C2 proton). However, Sames' method afforded C2 arylation with exclusivity, providing moderate to good yields for all studied N-substituted indoles (**Figure 6**).

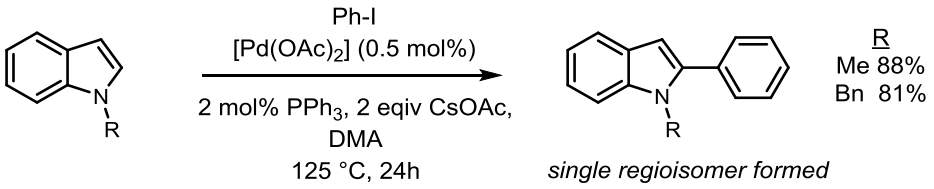

Figure 6. Sames' direct arylation of N-alkylated indoles at the C2 position

Further examples displaying C2 alternative direct arylation reactions using Pd(II) were forthcoming. Many variations on the chemical methodology provided a wide array of synthetic procedures for arylation at the C2 position. Sanford[56] arylated exclusively at the C2 position employing milder conditions which excluded the need for any phosphine ligands using hypervalent aryliodonium to engage functionalization and subsequent arylation (**Figure 7**).

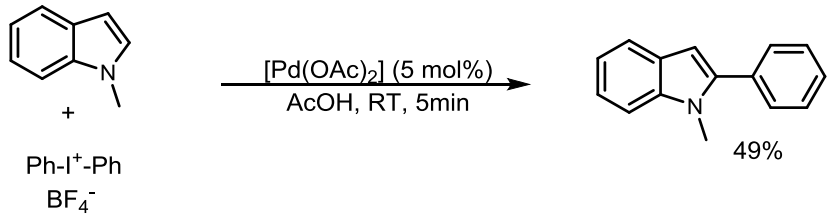

Figure 7. Sanford's direct arylation of N-methyl indole at C-2 using hypervalent iodine salts

The authors proposed that a 12 electron catalytic $Pd(OAc)_2$ species would be more electron deficient (i.e. 'ligandless'), hence palladating faster to N-alkylated indoles relative to a bulkier electron rich $Pd(OAc)_2(PPh_3)_2$ catalyst which is traditionally used in Pd C-C bond formation. Hence omitting electron rich, bulky triphenylphosphine ligands would therefore lead to the palladated indole intermediate at C2 (presumably through palladation at C3). The mechanism of arylation was proposed to proceed through an alternative Pd(II)/Pd(IV) catalytic cycle, where the oxidative addition of the Ar-X species occurs on Pd(II) prior to reductive elimination. The traditional Pd(0)/(II)

cycle observed in most palladium catalyzed cross couplings was claimed to be slower due to the electron rich nature of the Pd(0) catalyst (**Figure 8**).

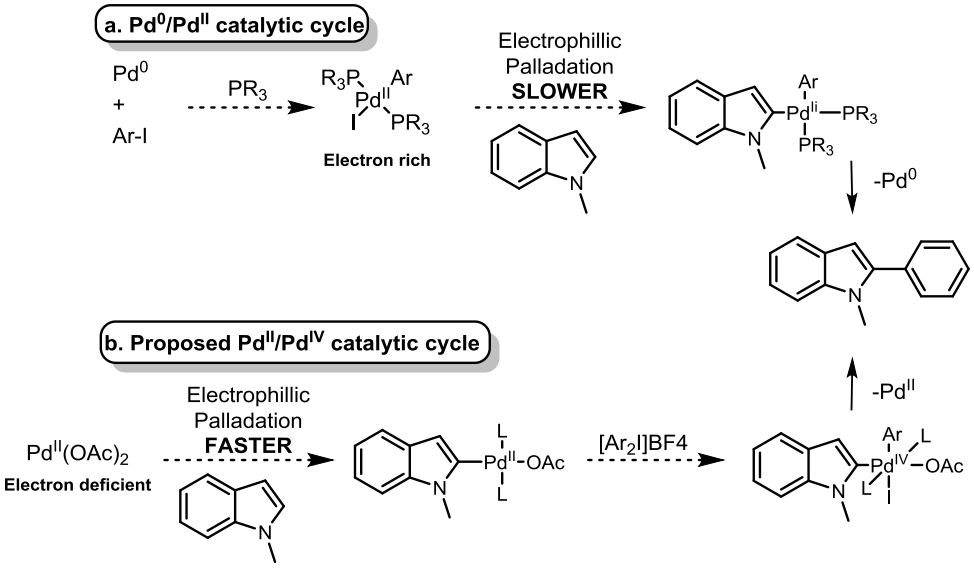

Figure 8. Proposed catalytic species in direct arylation of room-temperature catalyzed direct arylation by Sanford and coworkers

Larossa[57] used $Pd(OAc)_2$ in room temperature catalyzed C-2 arylation of N-methlyindole employing iodoarenes as the coupling partner (**Figure 9**). This avoided hypervalent iodine (III) arylating agents and extended the scope of the functionality on the iodoarene species, supporting both electron withdrawing and electron donating substituents on the arene coupling partner. The reaction also benefited from ligandless (i.e. phosphine free) conditions, citing the ability of an electron deficient Pd species to elicit faster palladation, akin to Sanford.[56] The authors suggested that cationic Pd^+ could be produced through ligand substitution, where an iodine ligand on Ar-Pd-I is replaced by either coordinating solvent (DMF) or acid to create an electron deficient, cationic species more susceptible to a palladation event.

Recent work exhibiting advances on this reaction by the same group illustrated the ability to conduct the reaction "on water" without the need for acid (e.g. AcOH) or polar solvent (DMA/DMF).[58] The ligand free methodology has gained prominence and has been utilized in the C2 arylation of N-indoles by Bellina[59] and Sames.[60]

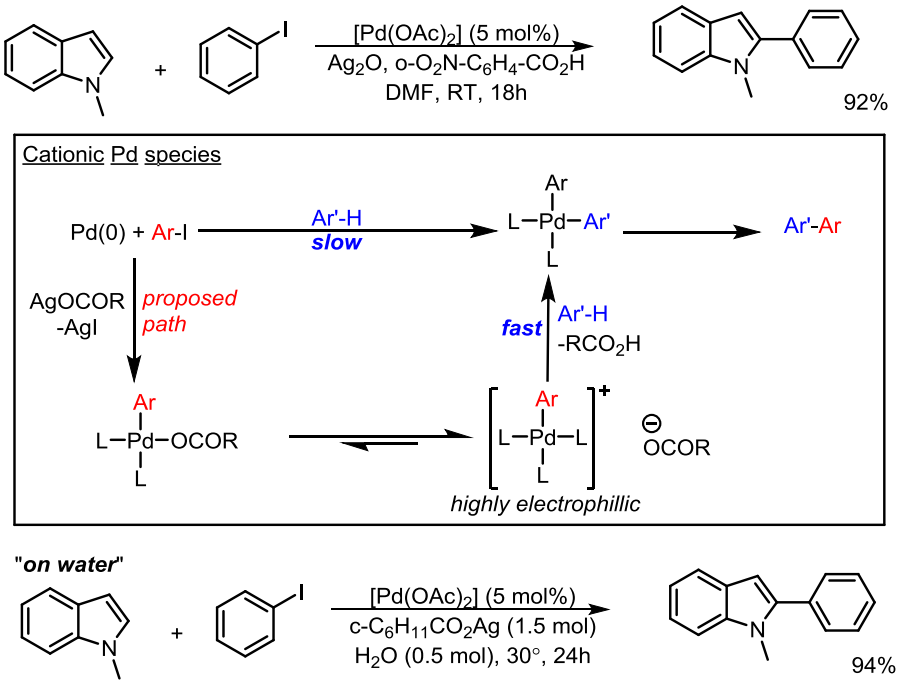

Figure 9. Larossa's direct arylation of N-methyl indole at C2 (top) with related cationic Pd catalyst mechanistic scheme. Later work examined the reaction "on water" at the C2 position of N-methyl indole.

Alternative methodologies employing aryl boronic acids have emerged as the synthetic diversity in utilizing direct arylation has evolved. These methods are prone to extending the synthetic steps required, due to the preparation of the aryl boron reagent, however, the increase in step economy by generally offset by lower reaction temperatures. A co-oxidant (usually $Cu(OAc)_2$) is used with Pd(II) catalysts in order to arylate various (hetero)arene motifs, including benzothiazoles[61], thiophenes, thiazoles[62] and indoles. Exclusive regioselectivity for the C2 position of n-alkylated indoles can be attained without the need for metallic co-oxidants, as recently reported by Shi and coworkers.[63] The coupling of N- methyl indole to benzene when utilizing aryl boronic acids was achieved in good to excellent yields (**Figure 10**). Notably, the oxidant used is O_2 – illustrating the benign conditions in which the reaction can take place, avoiding the inevitable waste byproduct associated with using metallic co-oxidants.

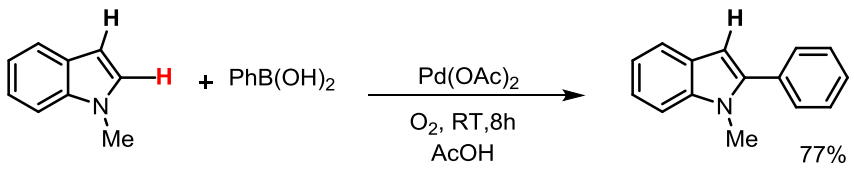

Figure 10. Shi's indole arylation with phenyl boronic acid through direct arylation.

Many direct arylation methodologies have emerged in recent years signifying the growing popularity and significance of the method within the synthetic community. However, one major drawback still remains – the need to prefunctionalize one of the substrates, which in turn must also be performed with the desired regioselectivity. The noble aim of achieving 'waste-free' arylation of heteroarenes is therefore unfulfilled.

1.2.4. Oxidative arylation

The ability to construct biaryls without the need to prefunctionalize at a C-H bond (i.e. without C-X) is a synthetic challenge. The benefits of such C-C bond couplings include the marked reduction in step economy (no need to prefunctionalize), substantial reduction in cost (halide/pseudohalide not required) and importantly, atom economy (limited to no toxic waste halide byproduct) and thus have become an attractive synthetic route to the construction of new C-C bonds.[64] However, the inherent challenge of reactivity and regioselectivity is still a major issue that needs to be overcome. Conducting two separate C-H activation events sequentially without encouraging homocoupling of either substrate is in itself a challenge. The absence of directing, protecting, activating groups increases the probability of such events. Therefore the synthetic methodology has to ensure the ability to conduct the reaction of two tandem C-H activations leading to eventual Pd C-C bond formation (**Figure 11**).

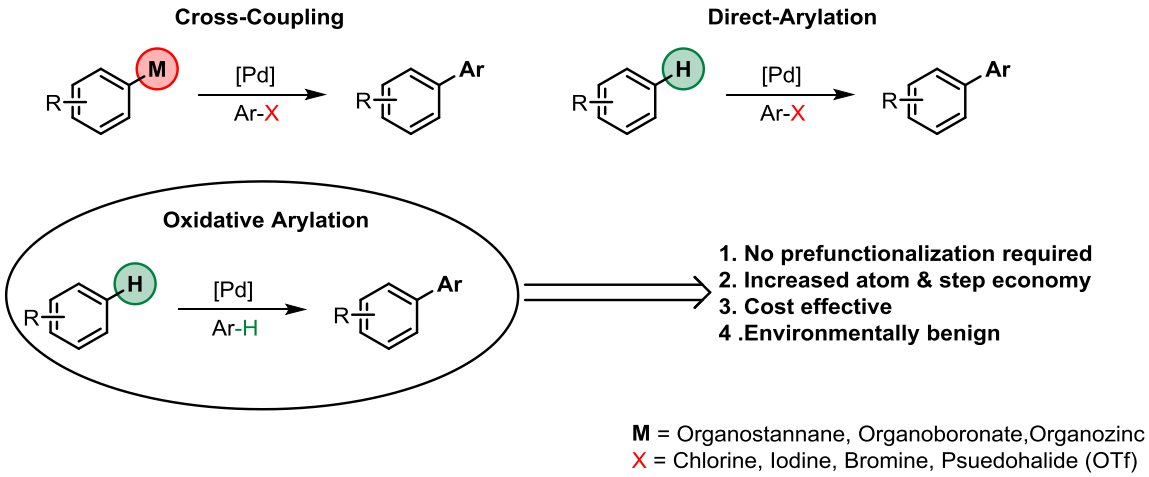

Figure 11. Traditional cross-coupling, direct arylation and oxidative arylation methods.

Seminal oxidative cross couplings with Pd(II) catalysts can be attributed to work from Van Helden's synthesis of biphenyl, where $PdCl_2$ was employed to create biphenyl.[65] The oxidative cross-coupling of indoles and pyrroles with benzene in AcOH was

reported by Ithara[66] in 1981, where stoichiometric $Pd(OAc)_2$ was used as the catalyst (**Figure 12**).

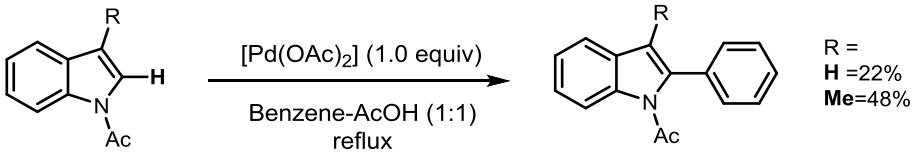

Figure 12. Ithara's seminal oxidative cross coupling N-acetyl indole and benzene.

Despite these seminal C-H activations, few examples of (hetero)arene – (hetero)arene cross coupling were forthcoming until recently. There has been a noticeable increase in the application of the method, with the complexity of substrates ranging from unsymmetrical biaryls, polycyclic aromatic hydrocarbons and other pharmaceutically relevant biaryl products such as fluorobiphenyl. Itami's work utilizing Pd cross-couplings in the arylation of polycyclic aromatic hydrocarbons (PAHs) is an illustration of an oxidative arylation reaction where the synthetic usefulness extends to materials science (**Figure 13**). Fluoroanthene and pyrene were both coupled with mesitylene using $Pd(OAc)_2$/*o*-chloronil/AgOTf producing arylated products with desired regioselectivity.[67] Furthermore, the authors extended the approach to coupling electron rich naphthalene with fluoroanthene with the same optimized catalytic conditions, again coupling with excellent regioselectivity.

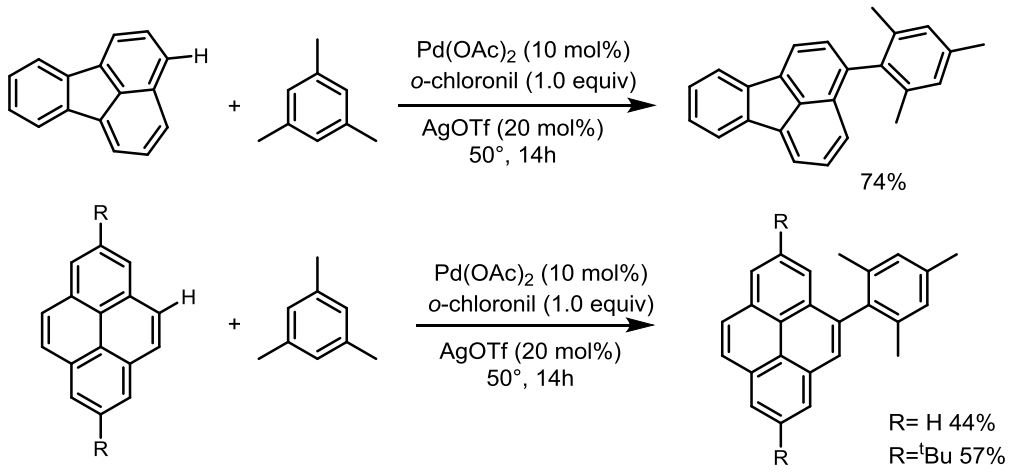

Figure 13. Itami's C-H/C-H cross coupling between flouroanthene and mesitylene at the 3-position (*top*) and pyrene and mesitylene (*bottom*) via oxidative arylation methodology.

The significance of fluorobiphenyl made it a privileged synthetic target with Su and coworkers elaborately expanding the oxidative arylation methodology to cross-couple

electron deficient polyfluoroarenes to substituted benzenes illustrating the tolerance of their oxidative arylation protocol to unfunctionalized arene-arene C-H/C-H bond formation.[68]

1.2.5. Oxidative arylation of indoles

The cross coupling of arenes to electron-rich indole is a relatively difficult procedure, plagued with the susceptibility of indoles to undergo significant oxidative decomposition in oxidative arylation procedures.[69] However, recent advances have resulted in many elegant examples of cross-coupling of indoles with various arenes, most notably work conducted within the Fagnou group offering the most prominent examples of oxidative arylation of N-substituted indoles.

In 2007, the oxidative cross coupling of N-Pivaloyl (N-Piv) indole with various substituted benzenes was reported where neither substrate was prefunctionalized and dimerization of both arenes were avoided. The reaction used $Pd(TFA)_2$ /AgOAc/PivOH, however the authors did speculate that $Pd(OPiv)_2$ could rapidly interconvert (from $Pd(TFA)_2$) in the reaction.[70] The ability to couple at the C2 position was observed in excellent selectivity (25:1) and tolerated a range of substituted benzenes. Interestingly, upon changing the heteroarene from N-Piv to N-acetyl indole and substituting the terminal oxidant, AgOAc with $Cu(OAc)_2$, a switch in selectivity could be observed (Figure 14).[71] The C3 arylation product was significantly favoured (8.9:1) in high yield (84%).

The authors proposed that the terminal oxidant itself could lead to the formation of bimetallic clusters which could play a role in the selectivity. For $Cu(OAc)_2$, it was suggested that this could form bimetallic clusters with Pd (e.g. $PdCu(OPiv)_4$) which would exert C3 selectivity in the arylation of N-acetyl indole, whereas the acetate anion in AgOAc was assumed to cleave tri or bimetallic aggregated Pd to monomeric Pd which would lead to experimentally observed C2 selectivity. Experimental work exhibiting similar oxidant-related selectivity and the importance of AgOAc in C2 arylation (of N-acetyl indole) was subsequently reported by the DeBoef group.[72]

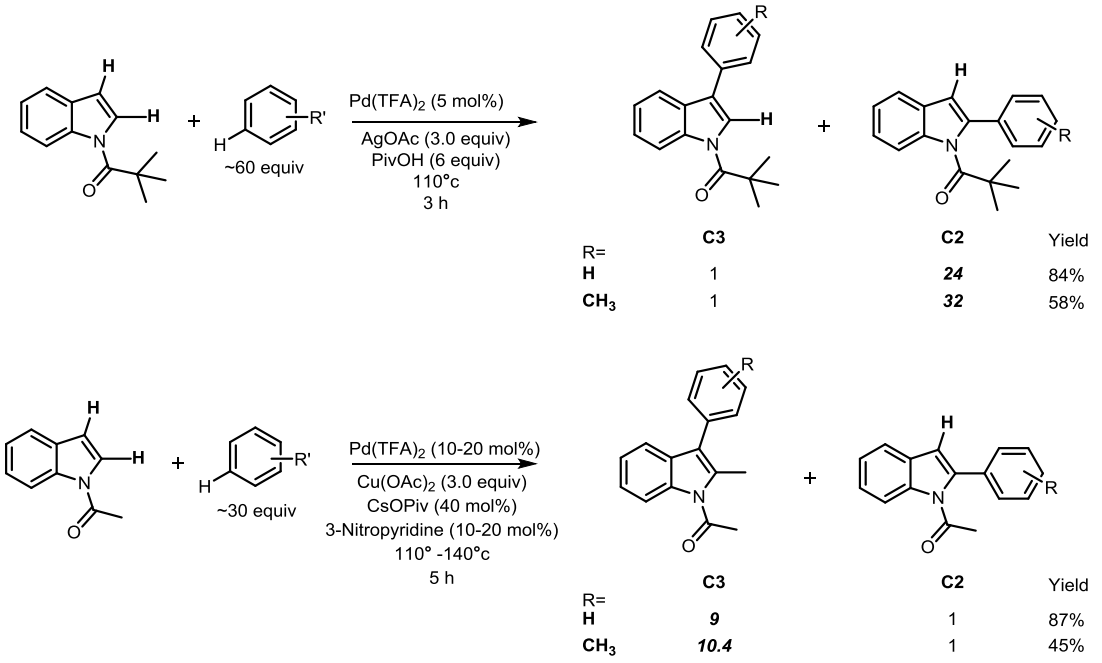

Figure 14. Fagnou's oxidative arylation of N-Piv Indole (*top*) and N-Ac indole (*bottom*) with benzene. Selectivity is favoured for C2 arylation of N-Piv indole using AgOAc as terminal oxidant whereas C3 selectivity observed for N-Ac indole using $Cu(OAc)_2$.

Furthermore, DeBoef and coworkers illustrated the C2 oxidative arylation of N-alkylated indoles where once again C2 selectivity was favoured with AgOAc as the terminal oxidant in buffered conditions (with PivOH). Good selectivity was once again observed for the C2 position with N-alkyl, N-methyl and N-[2-(Trimethylsilyl)ethoxy]methyl acetal (N-SEM) indole albeit in low to moderate yields, with no homodimerization of N-methyl indole observed (**Figure 15**).

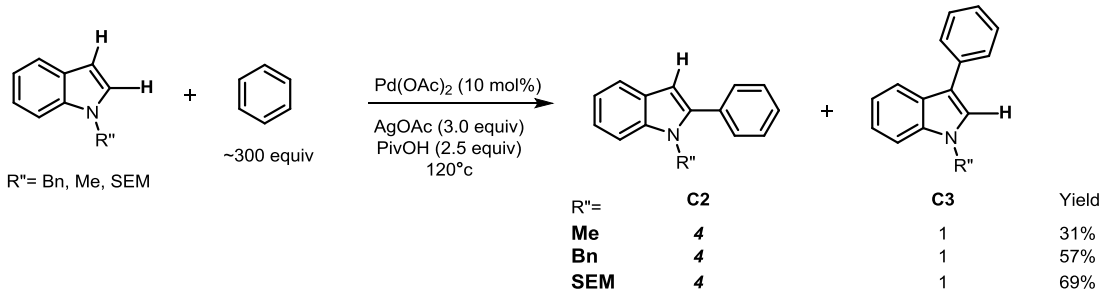

Figure 15. Deboef's C2 arylation of N-alkylated indoles via Pd-catalyzed oxidative arylation.

With the advent of oxidative arylation reactions becoming more prominent in the formation of (hetero)arene-(hetero)arene formation the reaction scope has extended to a variety of heteroarenes. However, the oxidative arylation reaction for indoles (and other heteroarenes) is still hindered by large requirement of excess of the arene coupling

partner (>30 equivalents), high catalytic loadings and the recovery of waste byproduct in the form of Ag. Nevertheless, the scope of such C-C bond forming strategy has provided an exceptionally elegant route to producing complex and synthetically relevant molecules.

1.3 C-H activation

1.3.1. Mechanisms of C-H activation

Coupling of (hetero)arenes via direct or oxidative arylation requires an activation of the rather inert C-H bond. The ubiquity of the C-H bond creates its own inherent problems, especially in (hetero)arenes, *vida supra*. Synthetic methods using Pd catalyzed activation have largely addressed the issue of activation and cleavage of the C-H bond, however, the problem of controlling selectivity (chemo-, enantio-, regio-) is more challenging. In fact, many methods using Pd catalyzed activation can lead to unwanted multi-functionalization of C-H bonds, creating a variety of (unwanted) isomers.

To date, the methods that are employed to impart C-H activation with Pd catalysis in direct and oxidative arylation reactions can be summarized in **Figure 16**, illustrating a model system of biphenyl formation. For direct arylation reactions C-H activation events are necessary in the second activation leading to biaryl formation. This proceeds from the initial oxidative insertion of a Pd(0) species into the aryl halide species. For oxidative insertion – the initial activation can proceed via three proposed mechanistic pathways for a Pd(II) species. Pathway **1** is the traditional electrophilic aromatic substitution (EAS) or S_EAr mechanism where the π-bond of the arene reacts in a nucleophilic sense with the electron deficient Pd species (acting as the 'electrophile') generating a Wheland intermediate, which is possible with Pd catalysts in the C-H activation of heteroarenes.[73] Rearomatization and reductive elimination complete the pathway – generating the biphenyl product. Pathway **2** is the intermolecular base-assisted deprotonation pathway, more commonly known as S_E3. This is a concerted intermolecular deprotonation–palladation pathway which would require a suitable amount of free base, however, is noted to be a competitive pathway in the arylation of arenes.[74] Pathway **3** is a concerted intramolecular deprotonation-palladation pathway (CMD) where deprotonation of the arene is undertaken by a carboxylate ligand on the Pd species which coordinates to the arene π system. This carboxylate ligand is usually an OAc, OTFA or OPiv anion, and is referred to as the intramolecular base or

ambiphillic ligand. Following the activation and cleavage of the C-H bond, the reaction can proceed through reductive elimination resulting in coupled product. This pathway has gained significant prominence as a mechanistic route to Pd-catalyzed C-H activation of (hetero)arenes.[75]

Pathway **4** is a Heck-type carbopalladation/carbometalation where the Ph-Pd-X species undergoes syn-type palladation across the π-bond of the arene.[76] This is followed by isomerization to permit β-hydride elimination. However, it is usually disfavoured due to the high energetic cost to isomerize. Alternatively, in basic conditions, the reaction may start with the initial Heck—type carbopalladation and rearomatize through a base-promoted E2 *antiperiplanar* deprotonation leading to expulsion of Pd.

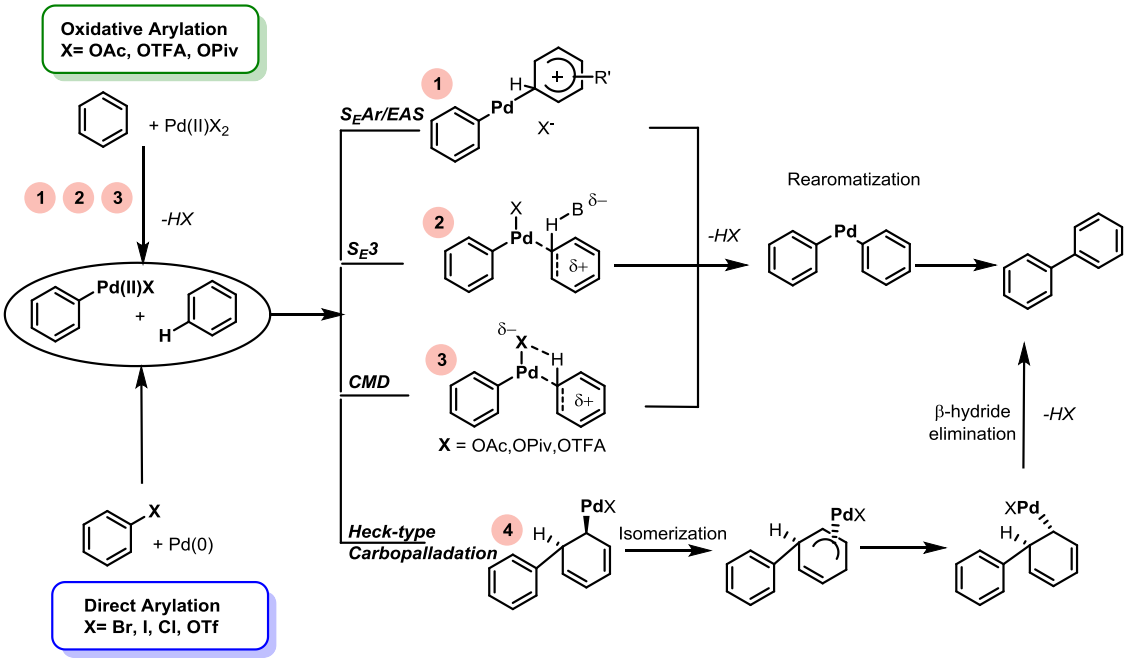

Figure 16. Mechanistic routes for C-H activation in a model coupling of biphenyl.

With a multitude of mechanistic possibilities, it is evident that Pd catalyzed C-H activation is a complex and diverse experimental topic. The work in this thesis aims to investigate the inherent mechanism behind the arylation of both simple arenes and N-substituted indoles, where the underlying mechanism is yet to be elucidated. This thesis will examine the C-C bond formation via Pd catalyzed C-H activation of indoles (chapter 2, 3 and 4) and arenes (chapter 5 and 6) examining mechanism, regio- and chemoselectivity (as appropriate) with DFT and transition state modelling (**Figure 17**).

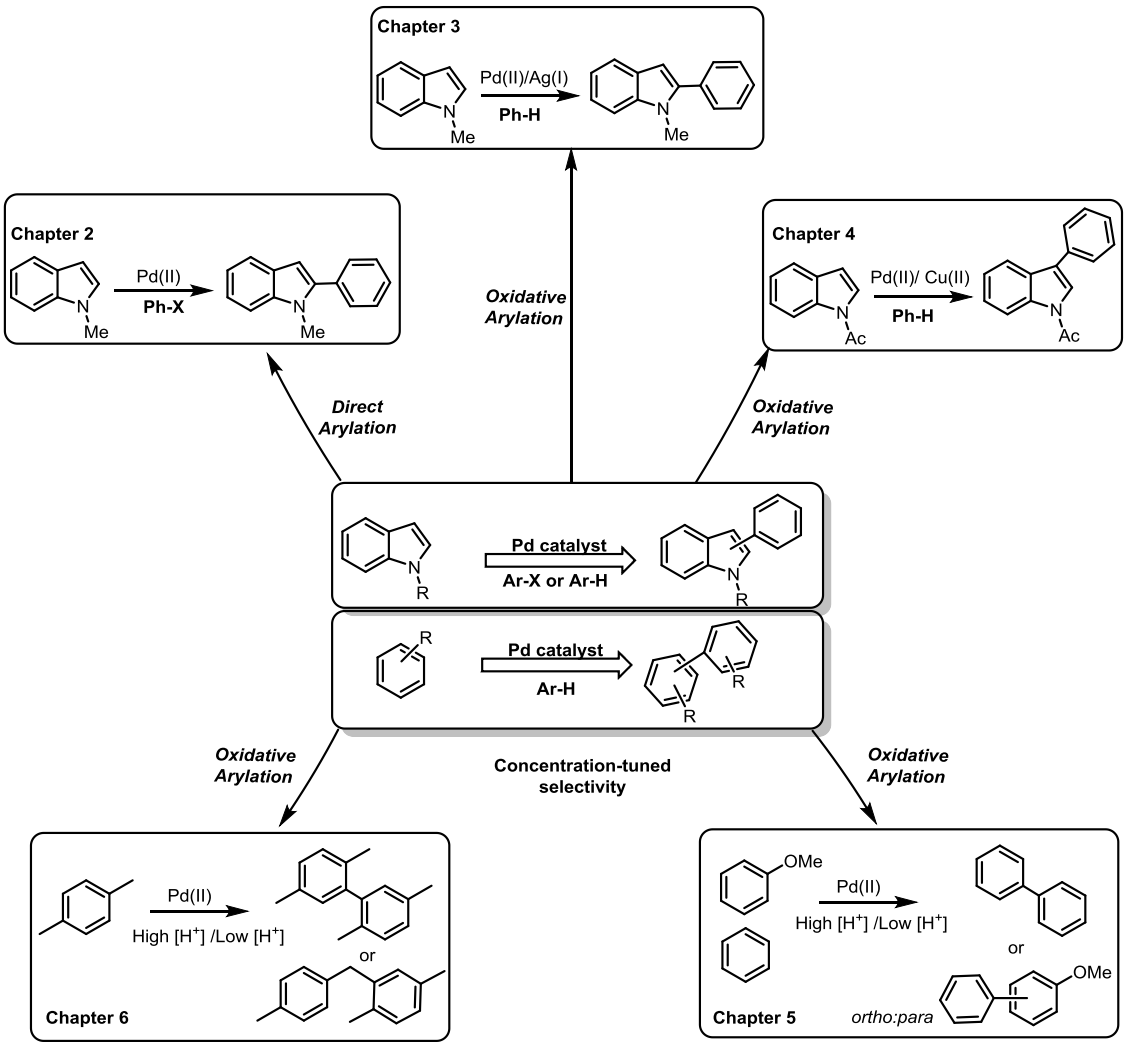

Figure 17. Work examined in this thesis including DFT investigation into mechanism of Pd-catalyzed arylation of N-indoles with direct (chapter 2) and oxidative arylation (chapters 3 and 4) and the coupling of simple arenes with Pd catalysis via acid-concentration selectivity (chapters 5 and 6).

Chapter 1 *References*

[1] Born, M.; Oppenheimer, R. *Ann. Phys.* **1927**, *84*, 457.
[2] Pauli, W. *Z. Phys.* **1925**, *31*, 765.
[3] Fock, V. *Z. Phys.* **1930**, *62*, 795.
[4] Fock, V. *Z. Phys*. **1930**, *61*, 126.
[5] Slater, J. C. *Phys. Rev.* **1929**, *34*, 1293.
[6] (a) Atkins, P.; Friedman, R. *Molecular Quantum Mechanics*; Oxford University Press, **2005**; (b) Leach, A. R. *Molecular Modelling: Principles and Applications*;Prentice Hall; 2nd edition, **2001**; (c) Cramer, C. J. *Essential of Computational Chemistry: Theories and Models*; John Wiley & Sons: New York, **2002**.
[7] Hehre, W. J.; Radom, L.; Schleyer, P. von R.; Pople, J. A. *Ab Initio Molecular Orbital Theory*; John Wiley and Sons, New York, **1986**.
[8] Slater, J. C. *Phys. Rev.* **1930**, *36*, 57.
[9] Ditchfield, R.; Hehre, W. J.; Pople, J. A. *J. Chem. Phys.* **1971**, *54*, 724.
[10] Hehre, W. J.; Ditchfield, R.; Pople, J. A. *J. Chem. Phys.* **1972**, *56*, 2257.
[11] Møller, C.; Plesset, M. S. *Phys. Rev.* **1934**, *46*, 618.
[12] Grimme, S. *J. Chem. Phys.* **2003**, *118*, 9095.
[13] Schwabe, T.; Grimme, S. *Acc. Chem. Res.* **2008**, *41*, 569. (b) Grimme, S.; Goerigk, L.; Fink, R. F. *WIREs Comput. Mol. Sci.* **2012**, *2*, 886.
[14] Cizek, J. *J. Chem. Phys.* **1966**, *45*, 4256.
[15] Hohenberg, P.; Kohn, W. *Phys. Rev. A* **1964**, *136*, 864.
[16] Kohn, W.; Sham, L. J. *Phys. Rev. A* **1965**, *140*, 1133.
[17] Perdew, J. P.; Schmidt, K. Jacob's Ladder of Density Functional Approximations for the Exchange-Correlation Energy. In *Density Functional Theory and Its Application to Materials*; Van Doren, V.; Van Alsenoy, C.;Geerlings, P. Eds.; AIP, Melville, NY, **2001**; pp. 1-20.
[18] Perdew, J. P.; Ruzsinszky, A.; Tao, J.; Staroverov, V. N.; Scuseria, G. E.; Csonka, G. I. *J. Chem. Phys.* **2005**, *123*, 622.
[19] Zhao, Y.; Truhlar, D. *Theor. Chem. Acc.* **2008**, *120*, 215.
[20] Zhao, Y.; Schultz, N. E.; Truhlar, D. G. *J. Chem. Theory Comput.* **2006**, *2*, 364.
[21] Evans, D. A.; Siska, S. J.; Cee, V. J. *Angew. Chem. Int. Ed.* **2003**, *42*, 1761.
[22] Cee, V. J.; Cramer, C. J.; Evans, D. A. *J. Am. Chem. Soc.* **2006**, *128*, 2920.
[23] Schwabe, T.; Grimme, S. *Phys. Chem. Chem. Phys.* **2006**, *8*, 4398.
[24] Steinmetz, M.; Grimme, S. *ChemistryOpen*, **2013**, *2*, 115.
[25] Laury, L. M.; Wilson, A. K. *J. Chem. Theory. Comput*. **2013**, *9*, 3939.
[26] Ehrlich S.; Moellmann, J.; Grimme, S. *Acc Chem Res.* **2013**, *46*, 916.
[27] Grimme, S. *WIREs Comput. Mol. Sci.* **2011**, *1*, 211.
[28] Grimme, S. *J. Comput. Chem.* **2004**, *25*, 1463.
[29] Chai, J.-D.; Head-Gordon, M. *Phys. Chem. Chem. Phys.* **2008**, *10*, 6615.
[30] Minenkov, Y.; Singstad, A.; Occhipinti, G.; Jensen, V.R. *Dalton Trans.* **2012**,*41*, 5526
[31] Marenich, A. V.; Cramer, C. J.; Truhlar, D. G. *J. Phys. Chem. B*. **2009**, *113*, 6378.
[32] Miertus, S.; Scrocco, E.; Tomasi, J. *Chem. Phys.* **1981**, *55*, 117.
[33] Takano, Y.; Houk, K. N. *J. Chem. Theory. Comput.* **2005**, *1*, 70.
[34] Ortuno, M.A.; Lledos, A.; Maseras, F.; Ujague, G. *ChemCatChem*, **2014**, *6*, 3132. (b) Anand, M.; Sunoj, R. *Organometallics* **2012**, *17*, 6486.
[35] Baker, J. *J. Comput. Chem.* **1986**, *7*, 385.
[36] Schlegel, H. B. *Theor. Chim. Acta*. **1984**, *66*, 333.
[37] Godula, K.; Sames, D. *Science*. **2006**, *312*, 67.
[38] (a) Stille, J. K. *Angew. Chem.* **1986**, *98*, 504; (b) Stille, J. K. *Angew. Chem. Int. Ed.* **1986**, *25*, 508; (c) Miyaura, N.; Suzuki, A. *Chem. Rev*. **1995**, *95*, 2457; (d) Luh, T-Y.; Leung M-K.; Wong, K.-T. *Chem. Rev*. **2000**, *100*, 3187. (e) Hiyama, T. *J. Organomet. Chem*. **2002**, *653*, 58; (f) Negishi, E.I. Hu, Q.; Huang, Z.; Qian, M.; Wang G. *Aldrichimica. Acta.* **2005**, *38*, 71; (h) Trost, B. M.; Crawley, M. L. *Chem. Rev.* **2003**, *103*, 2921; (i) Nicolaou, K. C.; Bulger, P. G.; Sarlah, D. *Angew. Chem.* **2005**, *117*, 4516; *Angew. Chem. Int. Ed*. **2005**, *44*, 4442; (j) Surry, D. S.; Buchwald, S. L. *Angew. Chem.* **2008**, *120*, 6438; (k) Surry, D. S.; Buchwald, S. L. *Angew. Chem. Int. Ed.* **2008**, *47*, 6338; (l) Hartwig, J. F. *Nature*, **2008**, *455*, 314; (l) Denmark, S. E.; Regens, C. S. *Acc. Chem. Res*. **2008**, *41*, 1486.
[39] Heck, R. F. *J. Am. Chem. Soc.* **1968**, *90*, 5518.
[40] Heck, R. F.; Nolley, J. P. *J. Org. Chem.* **1972**, *37*, 2329.

[41] Dieck, H. A.; Heck, R. F. *J. Am. Chem. Soc.* **1974**, *96*, 1133.
[42] Tamao, K.; Sumitani, K.; Kumada, M. *J. Am. Chem. Soc.* **1972**, *94*, 4374.
[43] King, A. O.; Okukado, N.; Negishi, E. *J. Chem. Soc., Chem. Commun.* **1977**, 683.
[44] Milstein, D.; Stille, J. K. *J. Am. Chem. Soc.* **1978**, *100*, 3636; (b) Milstein, D.; Stille, J. K. *J. Am. Chem. Soc.* **1979**, *101*, 4992.
[45] Miyaura, N.; Yamada, K.; Suzuki, A. *Tetrahedron Letters* **1979**, *20*, 3437.
[46] Ames**,** D. E.; Bull, D. *Tetrahedron* **1982**, *38*, 383.
[47] Akita, Y.; Inoue, A.; Yamamonto, K.; Ohta, A.; Kurihara, T.; Shimizu, M. *Heterocycles*, **1985**, *23*, 2327.
[48] Akita, Y.; Itagaki, Y.; Takizawa, S.; Ohta, *A. Chem. Pharm. Bull.* **1989**, *37*, 1477.
[49] Dyker,G.; Borowski, S.; Heiermaan, J.; Korning, J.; Opwis, K.; Henkel, G.; Kockerling, M. *J. Organomet. Chem.* **2000**, *606*, 108.
[50] Lafrance, M.; Fagnou, K. *J. Am. Chem. Soc.* **2006**, *128*, 16496.
[51] Qin, C.; Lu, W. *J. Org. Chem.* **2008**, *73*, 7424.
[52] Mosseau, J. J.; Vallee, F.; Lorioin, M. M.; Charlette, A. B. *J. Am. Chem. Soc.* **2010**, *132*, 14412.
[53] (a) Cacchi, S.; Fabrizi, G. *Chem. Rev*. **2005**, *105*, 2873; (b) Humphrey, G. R.; Kuethe, J. T. *Chem. Rev*. **2006**, *106*, 2875; (c) Brancale, A.; Silvestri, R. *Med. Res. Rev*. **2007**, *27*, 209; (d) Thansandote, P.; Lautens, M. *Chem. Eur. J.* **2009**, *15*, 5874; (e) Bandini, M.; Eichholzer, A. *Angew. Chem.* **2009**, *121*, 9786; (f) Kochanowska-Karamyan, A. J.; Hamann, M. T. *Chem. Rev*. **2010**, *110*, 4489; (g) Cacchi, S. Fabrizi, G. *Chem. Rev*. **2011**, *111*, 215; (h) Vicente, R. *Org. Biomol. Chem.* **2011**, *9*, 6469; (i) Shiri, M. *Chem. Rev.* **2012**, *112*, 3508.
[54] (a) Seregin, I. V.; Gevorgyan. V. *Chem. Soc. Rev*. **2007**, *36*, 1173; (b) Sun, C. L.; Li, B. J.; Shi, Z. J.; *Chem. Commun.* **2010**, *46*, 677; (c) Ackermann, L. *Chem. Commun*. **2010**, *46*, 4866; (d) Smith, A. M. R.; Hii, K. K. *Chem. Rev*. **2011**, *111*, 1637; (e) Krause, N.; Winter, C. *Chem. Rev*. **2011**, *111*, 1994; (f) Arockiam, P. B.; Bruneau, C.; Dixneuf, P. H. *Chem. Rev*. **2012**, *112*, 5879.
[55] Wang, X. S.; Lane, B. S.; Sames, D. *J. Am. Chem. Soc.* **2005,** *127*, 8050.
[56] Deprez, N. R.; Kalyani, D.; Krause, A.; Sanford, M. S. *J. Am. Chem. Soc.* **2006**, *128*, 4972.
[57] Lebrasseur, N.; Larrosa, I. *J. Am. Chem. Soc.* **2008**, *130*, 2926.
[58] Islam, S.; Larrosa, I. *Chem. Eur. J.* **2013**, *19*, 15093.
[59] Bellina, F. ; Cauteruccio, S.; Rossi, R. *Eur. J. Org. Chem*. **2006**, *6*, 1379.
[60] Wang, X.; Gribkov, V. D.; Sames, D. *J. Org. Chem*. **2007**, *72*, 1476.
[61] Ranjit, S.; Liu, X. *Chem. Eur. J*. **2011**, *17*, 1105.
[62] Kirchberg, S.; Tani, S.; Ueda, K.; Yamaguchi, J.; Studer, A.; Itami, K. *Angew. Chem. Int. Ed.* **2011**, *50*, 2387.
[63] Yang, S-D.; Sun, C-L.; Fang, Z.; Li, B.J.; Li, Y. Z.; Shi, Z-J. *Angew. Chem. Int. Ed*. **2008,** *120*, 1495.
[64] (a) Chen, X.; Engle, K. M.; Wang, D.; Yu, J. Q. *Angew. Chem., Int. Ed.* **2009**, *48*, 5094; (b) Lyons, T. W.; Sanford, M. S. *Chem. Rev*. **2010**, *110*, 1147; (c) Ackermann, L. *Chem. Rev*. **2011**, *111*, 1315; (d) Neufeldt S. R.; Sanford, M. S. *Acc. Chem. Res*. **2012**, *45*, 936.
[65] Van Helden, R.; Verberg, G. *Recl. Trav. Chim. Pays-Bas.* **1965**, *84*, 1263.
[66] Itahara, T. *J. Chem. Soc*. *Chem. Commun.* **1981,** 254.
[67] Kawasumi, K.; Mochida, K.; Kajino, T.; Segawa, Y.; Itami, K. *Org. Lett.* **2012,** *14*, 418.
[68] Wei, Y.; Su, W. *J. Am. Chem. Soc.* **2010**, *132*, 16377.
[69] Ferreira, E.M.; Stoltz, B.M. *J. Am. Chem. Soc.* **2003**, *125*, 9578.
[70] Stuart, D.R.; Fagnou, K. *Science*. **2007**, *316*, 1172.
[71] Stuart, D.R.; Villemure, E.; Fagnou, K. *J. Am. Chem. Soc.* **2007**, *129*, 12072.
[72] Dwight, T.A.; Rue, N. R.; Charyk, D.; Joeslyn, R.; DeBoef, B. *Org. Lett*. **2007**, *9*, 3137.
[73] (a) Martín-Matute, B.; Mateo, C.; Cárdenas, D. J.; Echavarren, A. M. *Chem. Eur. J.*, **2001,** *7*, 2341. (b) Park, C-H.; Ryabova, V.; Seregin, I.V.; Sromek, A.W.; Gevorgyan, V. *Org. Lett.* **2004**, *6*, 1159.
[74] Flegeau, E. F.; Bruneau, C.; Dixnuef, P. H.; Jutand, A. *J. Am. Chem. Soc.* **2012**, *133*, 10161.
[75] Gorelsky, S.I.; Lapointe, D.; Fagnou, K. *J. Am. Chem. Soc.* **2008**, *130*, 10848.
[76] Glover, B.; Harvey, K. A.; Lui, B.; Sharp, M. J.; Tymoschenko, M. F. *Org. Lett*. **2003**, *5*, 301.

Chapter 2

DFT studies into the mechanism of Pd-catalyzed direct arylation of N-methyl indole with phenyl boronic acid [$PhB(OH)_2$]

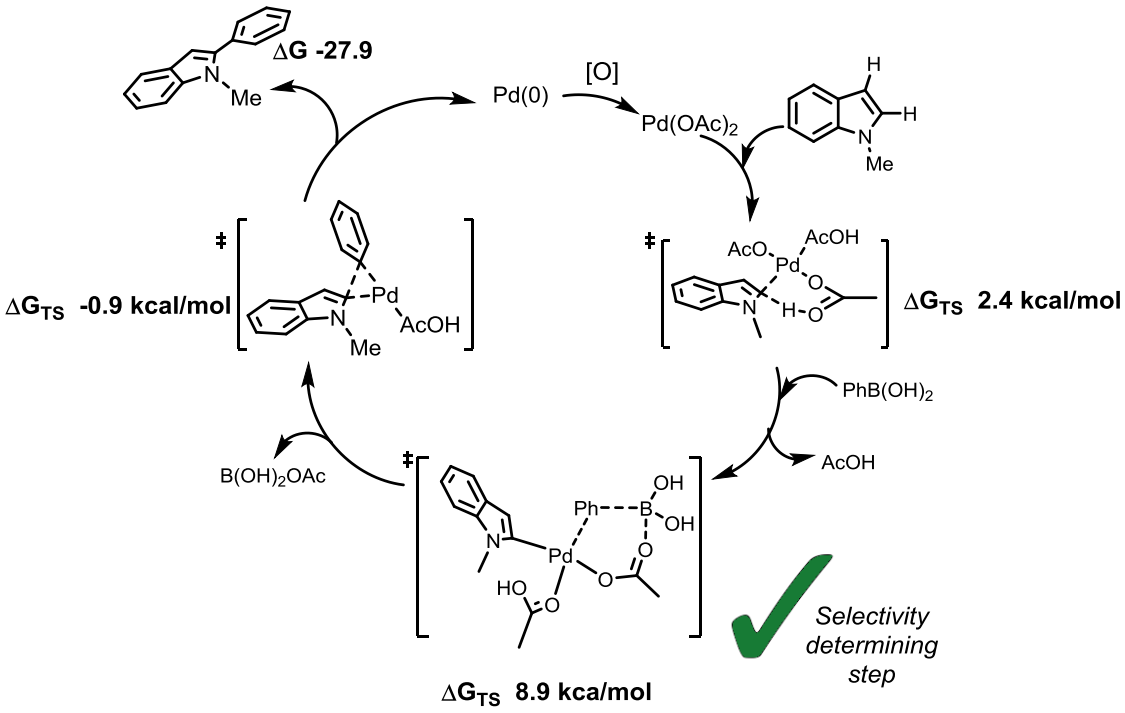

2.1. Introduction

Using organoboron reagents in transition metal-catalyzed cross coupling reactions is an extremely powerful method to construct new C-C bonds, for example in the Suzuki-Miyuara reaction.[1] In Suzuki-Miyuara cross-coupling a prefunctionalized aryl C-X species (where X is a suitable leaving group such as halide or OTf) undergoes a coupling reaction with boronic-esters or aryl boronic acids. The synthesis of numerous drugs and natural products has been achieved via Suzuki-Miyaura cross couplings highlighting its utility and significance in contemporary synthetic applications.[2] However, with the advent of the direct arylation mechanistic manifold, much focus has now centred on eliminating waste by-products and increasing efficiency. Recently, elegant methodology has emerged where aryl boronic acids have found favour as a coupling partner with unfunctionalized arenes or heteroarenes, replacing aryl halides as the traditional coupling partner (**Figure 1**).

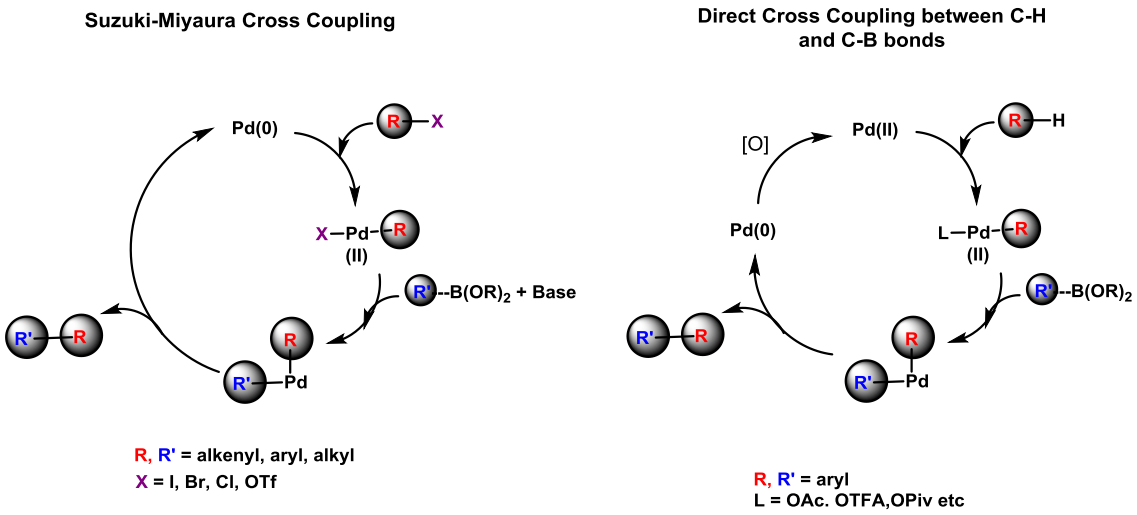

Figure 1. *Left:* Traditional Suzuki-Miyaura aryl cross coupling. *Right:* Direct C-H activated cross coupling using aryl boronic acids, R-B(OH)$_2$.

Direct arylation reactions where the functionalized aryl boronic acid can participate as an aryl donor to indoles has been recently reported by Studer and coworkers, where both N-H and N-Me indoles were arylated at the C2 position.[3] Here the authors proposed initial activation occurred via transmetalation of ArB(OH)$_2$ with Pd(OAc)$_2$ species to generate AcO-PdAr species, followed by electrophilic activation at the C3 position, followed by a 1,2-migration and subsequent reductive elimination to give 1-methyl-2-phenylindole (**Figure 2**).

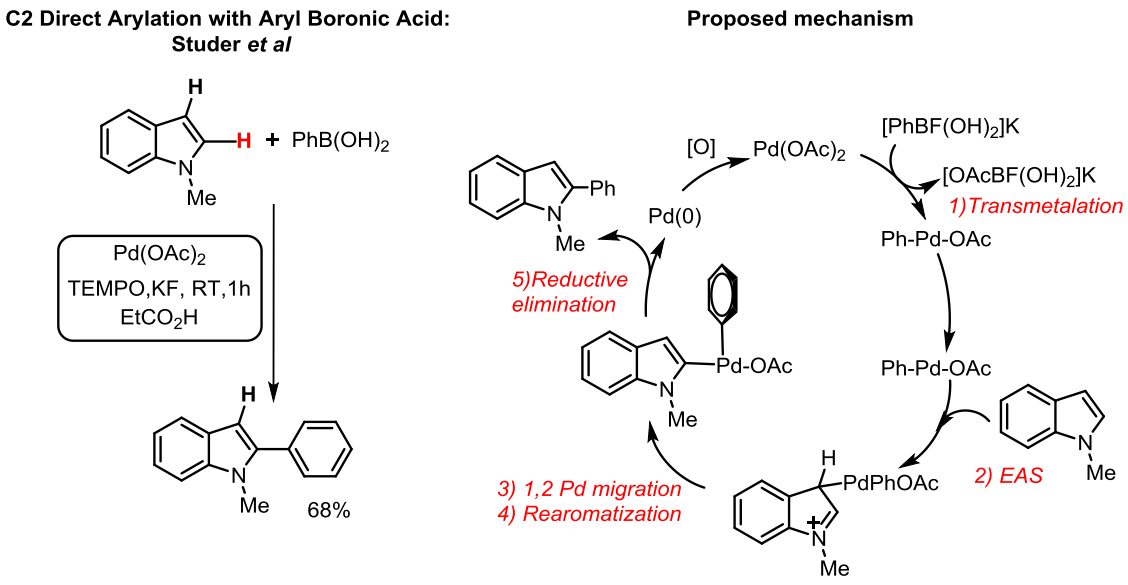

Figure 2. Studer's direct arylation of N- methyl indole. Proposed mechanism proceeding with transmetalation of aryl boronic acid with Pd(II).

Shi and coworkers reported the coupling of N-methyl indole, which was found to occur exclusively at the C2 position, using $PhB(OH)_2$ as reagent and $Pd(OAc)_2$ as the catalyst, applying the direct arylation mechanistic manifold.[4] Their methodology allowed mild conditions and occurred without the need for additives or co-catalysts, with O_2 acting as the oxidant at room temperature. Excellent selectivity was observed and the C2 product was obtained in good yields for a variety of N-substituted indoles and other electron rich arenes. In this direct arylation, the active catalyst is Pd(II) as opposed to traditional phosphine based $Pd(0)PPh_3$ used in Suzuki-Miyaura cross-couplings (which itself is generated from the reduction of a stable Pd(II) precursor to the active zero-valent Pd catalyst).[5] However, the relatively benign reaction conditions (i.e. RT, using O_2 as oxidant, and absence of halide) provide a distinct advantage in providing environmentally friendly, regioselective, high yielding couplings of various N-alkylated indoles. Mechanistic proposals were similar to Studer's catalytic cycle, whereby initial transmetalation occurs at Pd(II), before activation of the indole species (**Figure 3**).

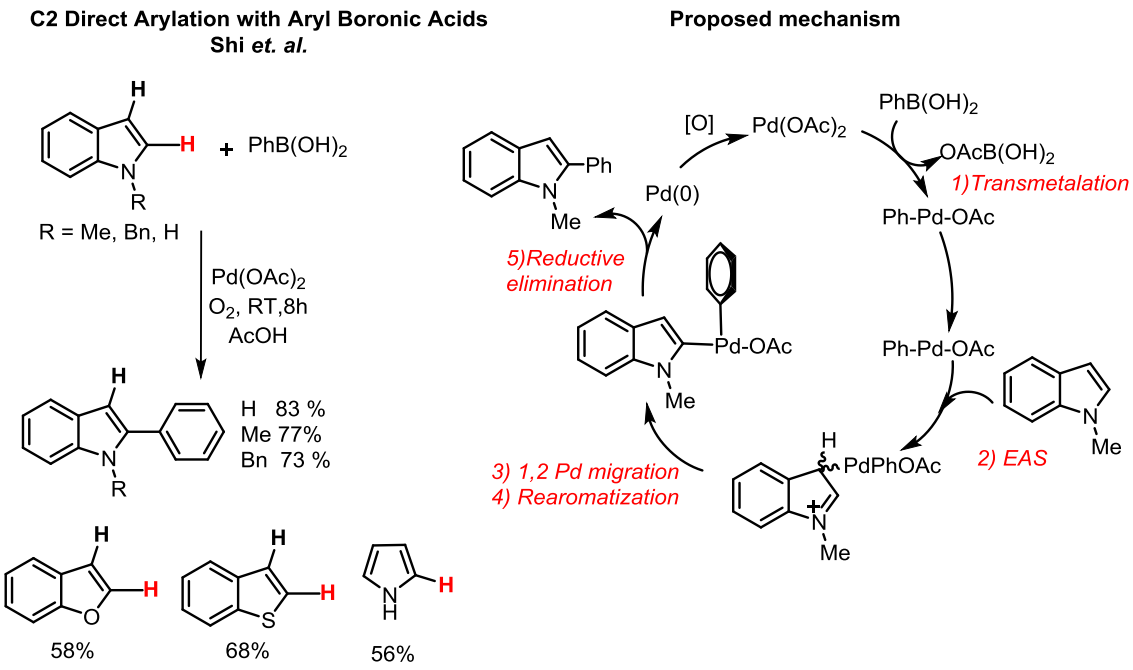

Figure 3. Shi and coworkers direct arylation of N-methyl indole using $PhB(OH)_2$ and $Pd(OAc)_2$. Exclusive regioselectivity is inferred at the C2 position with a wide range of electron-rich (hetero)arenes.

Shi and coworkers[6] extended the direct arylation methodology to the *ortho* arylation of N,N-dimethyl-1-(o-tolyl)methanamine with various aryl boronic acids and $Pd(OAc)_2$ (**Figure 4**). Interestingly, the mechanistic proposal in this direct arylation is for an initial C-H activation event (as opposed to transmetalation) creating *ortho* palladated N,N-dimethyl-1-(o-tolyl)methanamine, which is assisted by chelation of the Pd catalytic species with the lone pair on the neighbouring nitrogen group. Subsequent transmetalation with $PhB(OH)_2$ and reductive elimination yield the arylated product.

Thus, the opposite order of C-H activation and transmetalation has been proposed in the literature, for direct arylation with boronic acids (in **Figure 3** and **4**). Therefore, the direct arylation mechanism of N-methyl indole can proceed via two different catalytic cycles, which involve either C-H activation or transmetalation as the initial step. Therefore establishing the sequence of events, and thus characterizing the catalytic cycles with computation will provide a more thorough understanding.

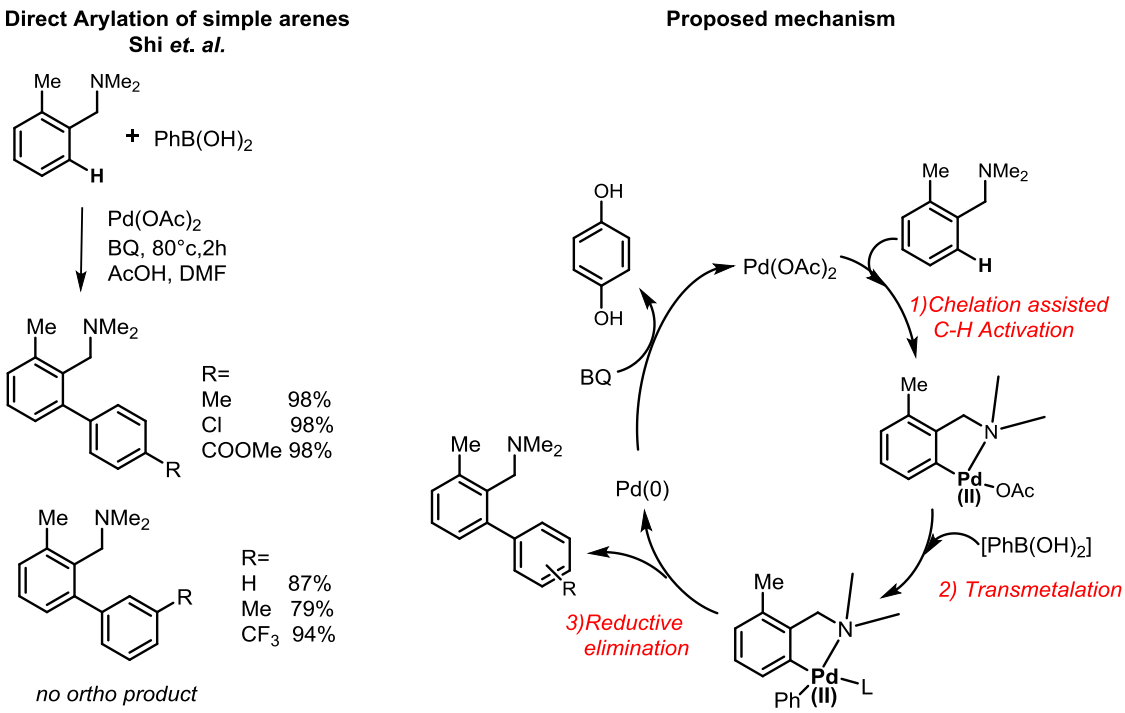

Figure 4. Direct arylation of N,N-dimethyl-1-(o-tolyl)methanamine with aryl boronic acids. A variety of electron withdrawing and donating substituents were tolerated with coupling not occurring at the ortho position of the substituted aryl coupling partner.

Boronic acids and their derivatives are relatively attractive cross-coupling partners in transition-metal catalyzed cross-couplings and C-H activations.[7] Pd(II) catalyzed C-H arylations have appeared more frequently in recent times, notably Buchwald's cross-coupling of unprotected, nitrogen-rich heterocycles employing SPhos:Pd(II) catalysts and aryl boronic acid.[8] Surprisingly, to our knowledge, minimal computational investigation has been conducted to seek the mechanistic rationale behind many of these Pd catalyzed aryl-boronic C-H arylation reactions. Maseras[9] has investigated the classical Suzuki-Miyaura coupling computationally while experimental studies of of this reaction through experimental physical organic (Jutand[10], Lloyd-Jones[11], Hartwig[12]) and more recently with computation (Ujaque)[13] illustrate that there is considerable interest in the nature of the species undergoing transmetalation.

Our investigation therefore seeks to rationalize the mechanism behind the regioselectivity of direct arylation of N-methyl indole, establishing the catalytic cycle that results in the arylation at C2 and in doing so elucidating the sequence of mechanistic events.

2.2. Computational methods

DFT calculations were performed using the *Gaussian 09*[14] package using the dispersion corrected range-separated hybrid **ω**B97XD functional. **ω**B97XD is a long-range corrected (LC) hybrid density functional with damped atom-atom dispersion corrections that has shown to be effective at describing thermochemistry, kinetics and non-covalent interactions which included the study of aromatic systems and C-H-π interactions against the CCSD(T)/Complete basis (CBS) set limit.[15] **ω**B97XD addresses deficiencies in errors related to correlation, dispersion and the self-interaction, which are common in many hybrid density functionals. This provides a lower mean absolute error (MAE) against conventional GGA (BLYP) and hybrid (B3LYP) functionals in describing atomization energies (in the 48 reactions comprising the G3/05 test set) and weak interactions (25 intermolecular-complex binding energies).[16] The addition of Grimme's D2 dispersion correction corrects for the $-C_6/R^6$ dependence of the dispersion interaction energy of the interatomic (molecular) distances for DFT functionals lacking adequate long-range dispersion interactions.[17] It has accurately described the geometry of transition metal compounds[18] and outperforms a variety of other hybrid and non-hybrid functionals employing the generalized gradient approximation (GGA) in a study of Bond Dissociation Energies (BDE) of Pd-L complexes where **ω**B97XD BDE calculations are shown to be within 1.0 kcal/mol of CCSD(T)/aug-cc-pVTZ benchmarks.[19] The results of our own benchmarking studies with this functional are described in chapter 3, where a good description of X-ray crystal structures is obtained.

Initial geometry optimizations were performed with the **ω**B97XD functional and split-valance polarized 6-31G(d) basis set for C, N, O, B and H atoms, whilst the LANL2DZ double-zeta valence basis set and associated effective core potential (ECP) were used to describe Pd.[20] ECPs treat only the valence electrons and replace the inner, core electrons with an effective potential which reduces the computational cost of quantum mechanical calculations of transition metal complexes and provides efficient treatment of relativistic effects. Single point energies were computed on all optimized geometries with the larger valence triple-zeta 6-311+G(d,p) and LANL2TZ basis set obtained from the EMSL Basis Set Exchange which include f polarization.[21,22] A fine grid density was used for numerical integration in all DFT calculations.

Harmonic vibrational frequencies were computed for all optimized structures at the same level as the optimization to verify that they were either minima or transition structures, possessing zero imaginary frequencies and one imaginary frequency, respectively. Each TS was connected to the corresponding minima on either side of the PES to confirm that corresponds to the reaction of interest by calculation of the Intrinsic Reaction Coordinate (IRC). Free energies were evaluated at 298K including zero point vibrational energies. The effects of solvent (acetic acid ε= 6.2528) were incorporated through the use of a conductor-like polarizable continuum model (CPCM), defining the solute cavity with UFF radii[23] by conducting single point calculations on optimized geometries. A smooth damping function centred about a frequency of 100 cm^{-1} was used to switch between the harmonic approximation for vibrations above this value and the free-rotor approximation below.[24]

A conventional standard state of 1 mol/l in solution for all species was employed in calculating the translational entropies via the Sackur-Tetrode expression. In effect this adds a correction of 1.89 kcal/mol to all species relative to the default standard state in Gaussian of 1 atm. All structures are depicted with CYLview [25] or ChemDraw. All energies presented within this work are Gibbs (ΔG) free energies (calculated against separated reactants) and calculated via the following method:

$$\Delta G_{solv} = \Delta E_{solv} + (\Delta G_{gas} - \Delta E_{gas})$$

The NBO program [26] analyses the many-electron molecular wavefunction in regards to localized electron-pair bonding units. The program carries out the determination of natural atomic orbitals (NAOs), natural bond orbitals (NBOs), and natural localized molecular orbitals (NLMOs), and uses these to perform natural population analysis (NPA) which is used in this chapter to describe the charge present on individual atoms.

2.3. Results

2.3.1. Electrophilic Aromatic Substitution

Our mechanistic investigations probing direct arylation of N-methyl indole and $PhB(OH)_2$ focused on the effects of explicit solvation (acetic acid) and the exact sequence of mechanistic events. The computed mechanism must also rationalize exclusive formation of the C2 arylated species, observed experimentally. Shi proposed a catalytic cycle whereby the initial Pd (II) species undertakes C-H activation on N-methyl indole at the C2 position, which is then followed by transmetalation with $PhB(OH)_2$. The resultant species is then proposed to be a diarlylated Pd(II) species, which can undergo reductive elimination to afford the C2 product and regenerate the Pd(0) catalyst. The proposal advocated an electrophilic mechanism for the aromatic C-H activation via the Pd(II), although the authors do not speculate as to the turnover or selectivity determining steps.[27]

Our initial calculations focused on examining this mechanistic rationale with DFT calculations. Calculations seeking to locate the intermediate or transition structure on the (3N-*6*) PES corresponding to such an electrophilic activation were unsuccessful – unable to characterize the arenium ("Wheland") metalated intermediate associated with S_NAr reactions irrespective of density functional or basis set used (**Figure 5**).

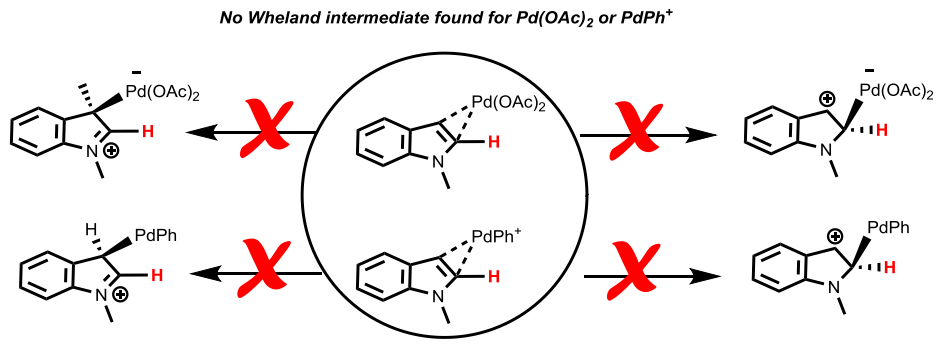

Figure 5. Potential energy scans at wB97XD and B3LYP level of theory for N-methyl indole and $Pd(OAc)_2$ and $PdPh^+$ yielded ground states.

In fact, potential energy scans yielded only ground state species, where the Pd (II) was now η^2 with the π-system of both N-methyl indole. Clearly in both cases the Pd(II) species was not nearly as electrophilic/positive as required to elicit an electrophilic addition. We postulated that perhaps a cationic Pd species, $PhPd^+L$ (where L=AcOH)

could perhaps induce the nucleophilic character of N-methyl indole leading to an electrophilic addition. Calculations confirmed that only a ground state can be located on the PES for this particular mechanistic manifold, thus ruling out the absence of the proposed initial activation (i.e. C-H activation) proceeding via EAS.

Stahl recently reported construction of biaryls through Pd(II) catalyzed oxidative arylation.[28] It was shown that two independent C-H activation events create two distinct aryl-palladium species, which can couple through a bimetallic Pd transmetalation event, followed by reductive elimination. Although computational studies looking into bimetallic Pd(II) based arylations have been reported,[29] none to our knowledge have computed a bimetallic Pd(II) transmetalation despite transmetalation events of aryl-Pd(II) being thoroughly experimentally investigated.[30] Calculations were unable to locate a transmetalation between N-methyl indole and phenyl on distinct Pd centres via this proposed mechanism (**Figure 6**). Potential energy scans located a ground state structure where the phenyl resided on the Pd centre, but not a transmetalation type TS geometry where an imaginary frequency associated with the Ph transfer could be observed. Additionally, the sub-stoichiometric quantity of catalyst used (2 mol%) means that a bimetallic mechanism is disfavoured based on the low concentration of any putative intermediate along such a pathway.

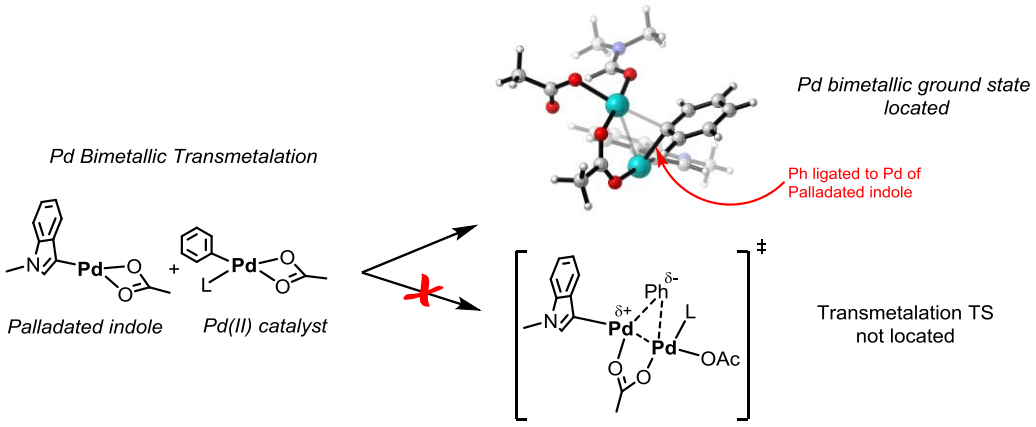

Figure 6. Proposed bimetallic transmetalation not located. Scans found only the ground state structure. PES scans conducted at M06-2X/6-31G(d)/LANL2DZ and ωB97XD/6-31G(d)/LANL2DZ level of theory.

Alternative mechanistic rationale to account for the initial C-H activation led us to propose two different catalytic cycles which proceeded through C-H activation of the electron rich N-methyl indole at the C2 position via the CMD mechanism, which has

garnered support as a favoured mechanism for a wide variety of aromatic C-H activations using Pd(II) catalysts (**Figure 7**).

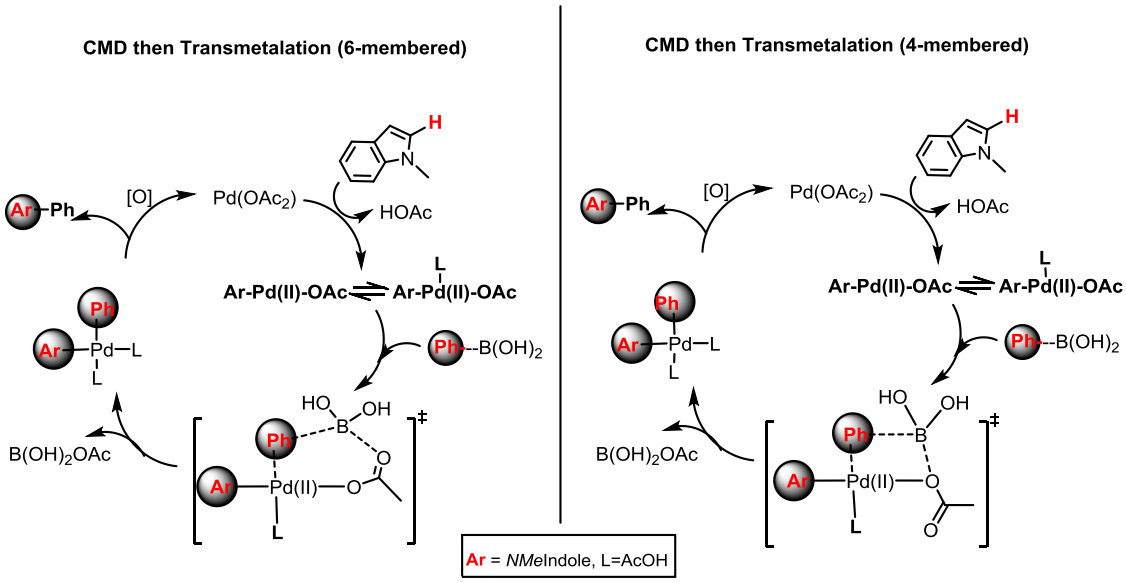

Figure 7. Possible catalytic cycles for C2 arylation reaction of N-methyl indole.

This initial C-H activation would lead to the palladated C2 species Ar-Pd(II)-OAc. We acknowledged that due to the nature of the reaction medium, the coordination of acetic acid will cause a variation in valence electron count of the catalytic Pd species. Whilst the oxidation state will remain Pd(II), hence adhering to the Pd(0)/(II) manifold - the palladated indole species may now reside as either 14 electron Ar-Pd(II)-OAc, or 16 electron Ar-Pd(II)L-OAc (where L=acetic acid). It is reasonable to expect the 14 electron Pd species to be more electron deficient, thus palladation to occur with relative urgency as compared with its 16 electron, solvated counterpart, however, it is not entirely unfeasible that in the reaction conditions acetic acid can ligate as a neutral two electron donor to a vacant site of Pd. Therefore, both scenarios must be considered in any computational investigation.

Once transmetalation has occurred, dissociation of the organoborane species $B(OH)_2OAc$ leads to a diarylated species Ar-Pd(II)-Ph. Subsequent reductive elimination which leads to arylation at C2. The effects of solvation will be examined throughout the cycle via explicit modelling of acetic acid. Within both aforementioned catalytic cycles, it is noteworthy that the transmetalation with $PhB(OH)_2$ can be

undertaken via a 6-membered or 4-membered transition state. Both these possibilities have been considered, and are precedented within transition-metal catalyzed transmetalation reactions.[31,32,33]

It is indeed possible to initiate the sequence of mechanistic events with the transmetalation first, proceeding once again via the 4 or 6 membered transmetalation, this time on $Pd(OAc)_2$ (**Figure 8**) and therefore we intend to investigate which catalytic cycle results in predicted selectivities in agreement with experiment.

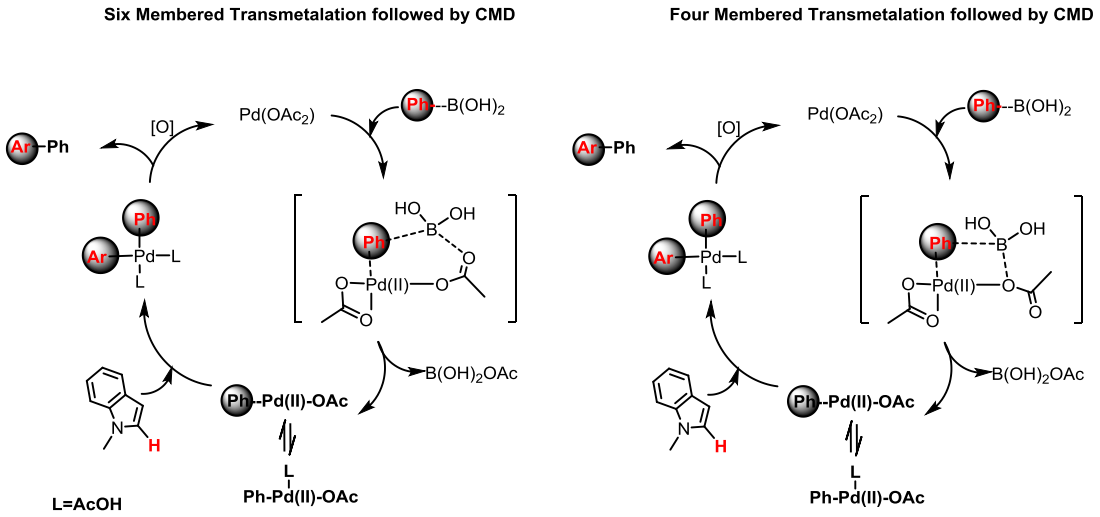

Figure 8. Alternative catalytic cycles for C2-arylation. Six or four membered transmetalation on $Pd(OAc)_2$ provide the catalytic species which initiate C-H activation. Reductive elimination yields the new arylated species, with Pd(0) regenerated and oxidized to Pd(II).

2.3.2. Transmetalation of $Pd(OAc)_2$ with $PhB(OH)_2$

2.3.2.1. Four vs six membered transmetalation

We computed the transmetalation of $Pd(OAc)_2$ with $PhB(OH)_2$ (**Figure 8**). Following geometry optimization, TSs were located for both the four (**CB)** and six membered transmetalation (**CC**) pathway.

The initial precomplex for both pathways differ in geometry (**Figure 9**). The four membered precomplex **CB1** displays initial η^2 coordination of Pd to the benzene π-system, which is also exhibited in the six membered precomplex **CC1**. This initial pre-coordination allows stabilization of the electron deficient Pd(II) species to the π-system. The shortest C(Ph)-Pd optimized bond length is placed at 2.32 Å for **CB1** and 2.29 Å for **CC1** leading to the eventual C(Ph)-Pd bond formation in corresponding transition states, **CB2** and **CC2**. Distinct geometrical variation is illustrated in the orientation of the monodentate OAc ligand on the Pd(II) species in both pathways. In **CB1**, the OAc ligand has the dihedral of O-Pd-O-C of 105°, whereas this angle is exaggerated in **CC1** to 170°, due to the rotation of the ligand in order to facilitate coordination with the boron species.

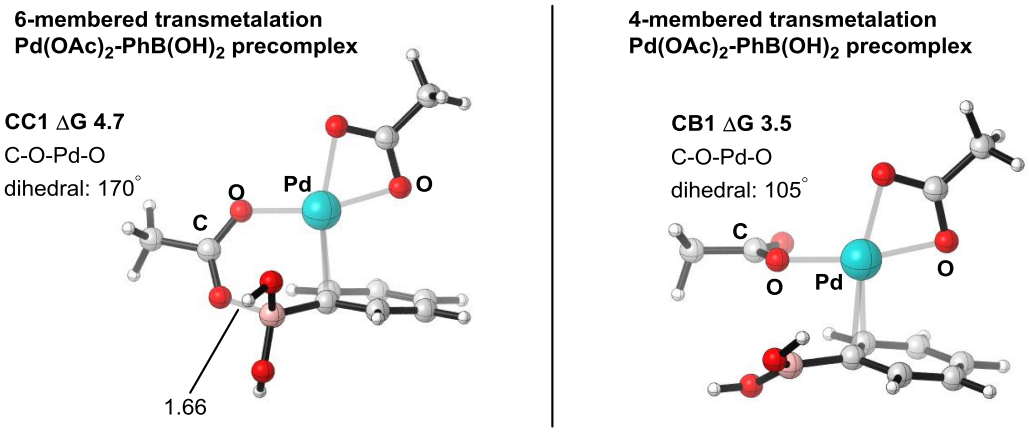

Figure 9. Precomplexes for both the 6-membered transmetalation and 4-membered transmetalation. Energies given in kcal/mol. Bond distances in Å. Coordination of interaction between lone pair on OAc and B in the six membered precomplex shown.

However, the acetoxy OB coordination is less favourable, proving to be energetically costly, causing the **CC1** (4.7 kcal/mol) to be 1.2 kcal/mol higher in energy than **CB1** (3.5 kcal/mol), relative to the separated reactants. Thus, the creation of a new σ bond

does not compensate for the distortion in geometry of both the $Pd(OAc)_2$ species or the $PhB(OH)_2$ species which has to rotate around the C(Ph)-B bond in order to distort from its coplanar arrangement with benzene and facilitate coordination with the acetate ligand.

The four membered transmetalation transition state **CB2** exhibits Pd-C(Ph) bond formation (2.11 Å), whereby a new sigma donor ligand has now coordinated to the Pd centre. This is furthermore exemplified by the bond length of the C(Ph)-B on $PhB(OH)_2$. **CB1** has a C(Ph)-B distance of 1.59 Å, which elongates to 1.85 Å in **CB2** illustrating the transfer of Pd from the $PhB(OH)_2$ species (**Figure 10**).

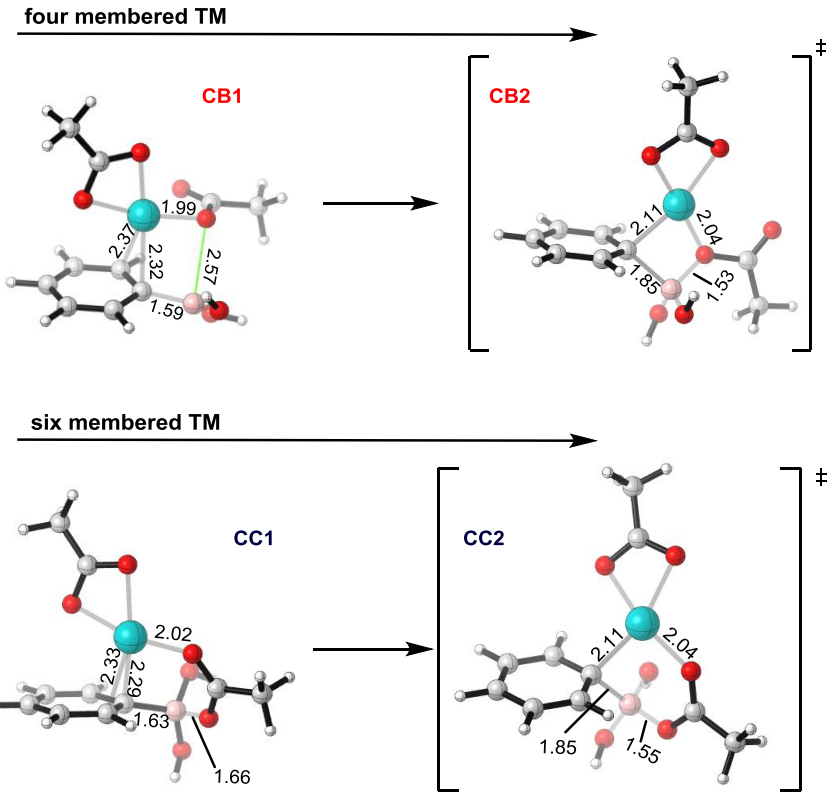

Figure 10. Optimized precomplex and transition state geometries for the four membered (*top*) and six membered pathway (*bottom*). All bond distances in Å.

Dissociation of the $B(OH)_2OAc$ species in the six membered species occurs through lengthening of the C(Ph)-B bond from **CC1** (1.63 Å) to **CC2** (1.85 Å) with bond formation now occurring between the oxygen lone pair and the p-orbital of $B(OH)_2$. This is signified by the acetoxy OB bond length shortening from **CC1** (**1.66 Å**) to **CC2** (**1.55 Å**). The six membered TS, **CC2** (ΔG 11.6 kcal/mol) is energetically favoured in comparison to the four membered TS, **CB2** (ΔG 16.9kcal/mol). A plausible explanation

for this is the greater strain in the four membered transition state. Additionally, in the six membered TS the acetate ligand interacts with the two Pd and B (electron deficient) centres in a bidentate fashion, while in the four membered TS bonding is via a single oxygen atom. The basicity of the lone pair *trans* to the carbonyl is expected to be reduced via anomeric-type hyperconjugation, diminishing the donating strength. These calculations show that if transmetalation is to occur first, the reaction is kinetically and thermodynamically favoured to proceed via the six membered transition state through an exergonic process of -12.0 kcal/mol (**Figure 11**). We therefore concentrated on transmetalation occurring via a six membered TS, and discarded the four membered pathway.

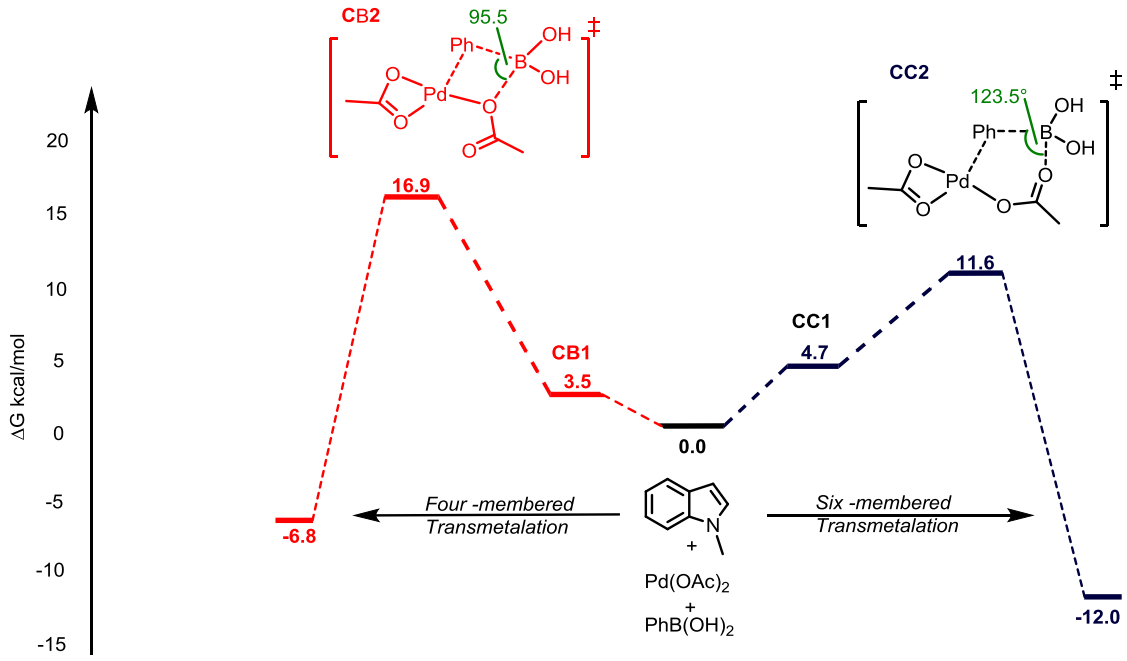

Figure 11. ωB97XD/6-31G(d)//6-311+G(d,p) free energy profile for the four membered (*red*) and six membered (*navy*) transmetalation of $Pd(OAc)_2$ with $PhB(OH)_2$ where six membered transmetalation is favoured and proceeds through a lower TS. All values are in kcal/mol.

2.3.2.2. CMD of N-methyl indole following six membered transmetalation

The CMD mechanism (following transmetalation) was investigated to compare the computed and experimental regioselectivity. The catalytic species, Ph-Pd(II)-OAc, would result from dissociation of the $AcOB(OH)_2$ species from the initial six membered transmetalation product (**Figure 12**). The dissociation of $AcOB(OH)_2$ requires 6.5 kcal/mol, however is necessary to provide the Ph-Pd-OAc catalytic species **CD1** (-5.5 kcal/mol), which then proceeds to the precomplex **CD2**.[I]

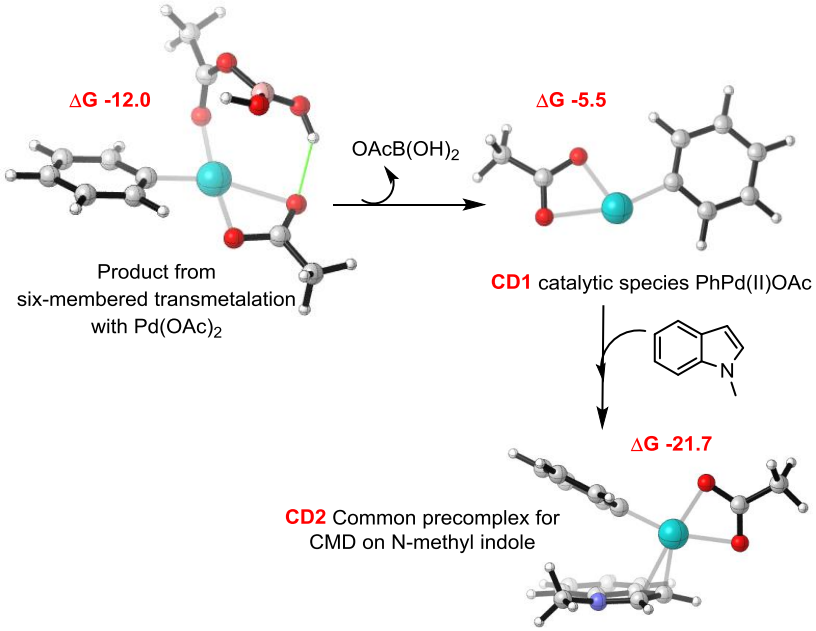

Figure 12. Dissociation of $AcOB(OH)_2$ species is favourable enroute to forming the CMD precomplex, CD2.

The electron density in N-alkylated indoles is predominantly localized on nitrogen and the C3 position. As such, metalation would be expected to occur preferentially at either position, while C-C formation is only possible at the C3 position. Our computational investigation supports this hypothesis. Proceeding from **CD1**, insertion of N-methyl indole leads to η^2 coordinated complex to the π system of the indole, where the coordinated acetate ligand changes its coordination to monodentate from bidentate. The precomplex **CD2** is a highly exergonic process at ΔG -21.7 kcal/mol (relative to the separated reactants). Subsequent six membered CMD transition states were attained for both C2 C-H activation, **D1**, and C3 C-H activation, **F1**, where simultaneous

[I] This value is relative to the substrates and subsequent removal of $PhB(OH)_2OAc$ generated from the six membered transmetalation transition state.

palladation and C-H activation occurs via the monodentate OAc ligand, which functions as an intramolecular 'proton shuttle' or 'ambiphilic' intramolecular base through a six membered palladacycle (**Figure 13**). The Gibbs free energy for this process is calculated at ΔG 4.8 kcal/mol for C2 and ΔG 0.9 kcal/mol for C3 for the CMD process, favouring activation at the C3 position. The reductive elimination is a relatively facile process – the TS involves Ph transfer on to indole via a three-centred, non-polar TS in a C-C bond forming reaction. In this step, the calculated selectivity is reversed, where C2 (**D2) =** ΔG 2.2 kcal/mol and C3 (**F2**) = ΔG 4.4 kcal/mol, (**Figure 14**).

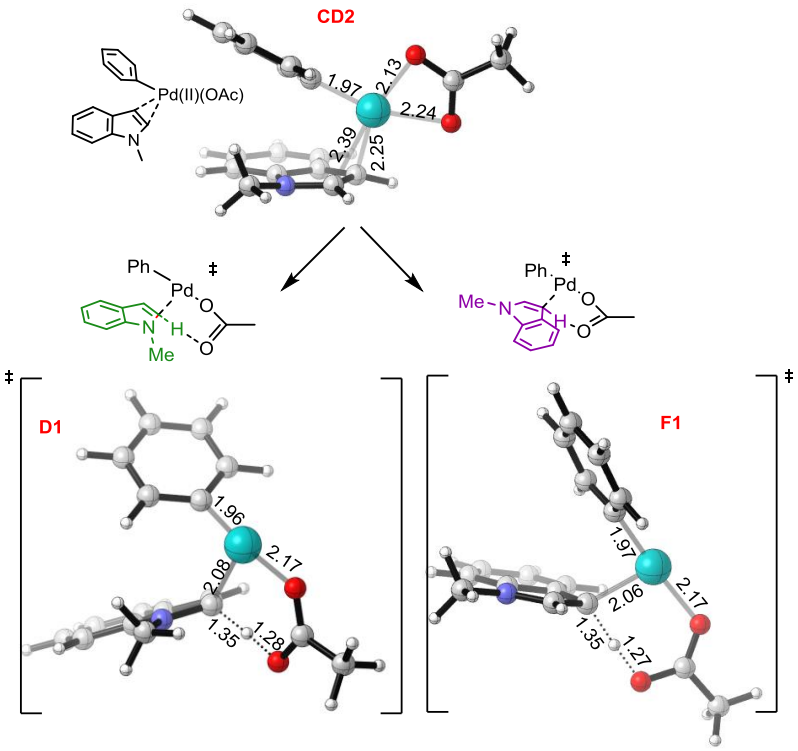

Figure 13. Optimized geometries of PhPd(II)OAc based CMD C-H activation. The precursor for CMD is the precomplex CD2, followed by C2 (D1) or C3 (F1) C-H activation through a six membered palladacycle. All bond lengths are given in Å. Calculations were conducted at ωB97XD/6-31G(d)//6-311+G(d,p).

The "energetic span" as defined by Kozuch and Shaik[34] (of the computed catalytic cycle) is the free energy gap between the most stable intermediate and the highest transition structure and gives an indication of the overall rate (or equivalently, turnover frequency) for the formation of C2 and C3 adducts. The activation energy of the

reaction based on this model depends on the largest energetic gap between any given transition state and any given intermediate, regardless of which occurs first.

Since both pathways proceed from the common intermediate **CD2**, which is the lowest intermediate, there is a predicted (marginal) selectivity in favour of the C3 adduct since the highest TS (F2) lies ΔG 0.4 kcal/mol below that for the C2 pathway (D1), with an energetic span of ΔG 26.1 kcal/mol. In this mechanism the formation of the C2 isomer is disfavoured due to the high energy of the CMD TS, **D1**, and the computed selectivity is therefore in the opposite sense to experiment. Computations therefore do not support this as the operative mechanism.

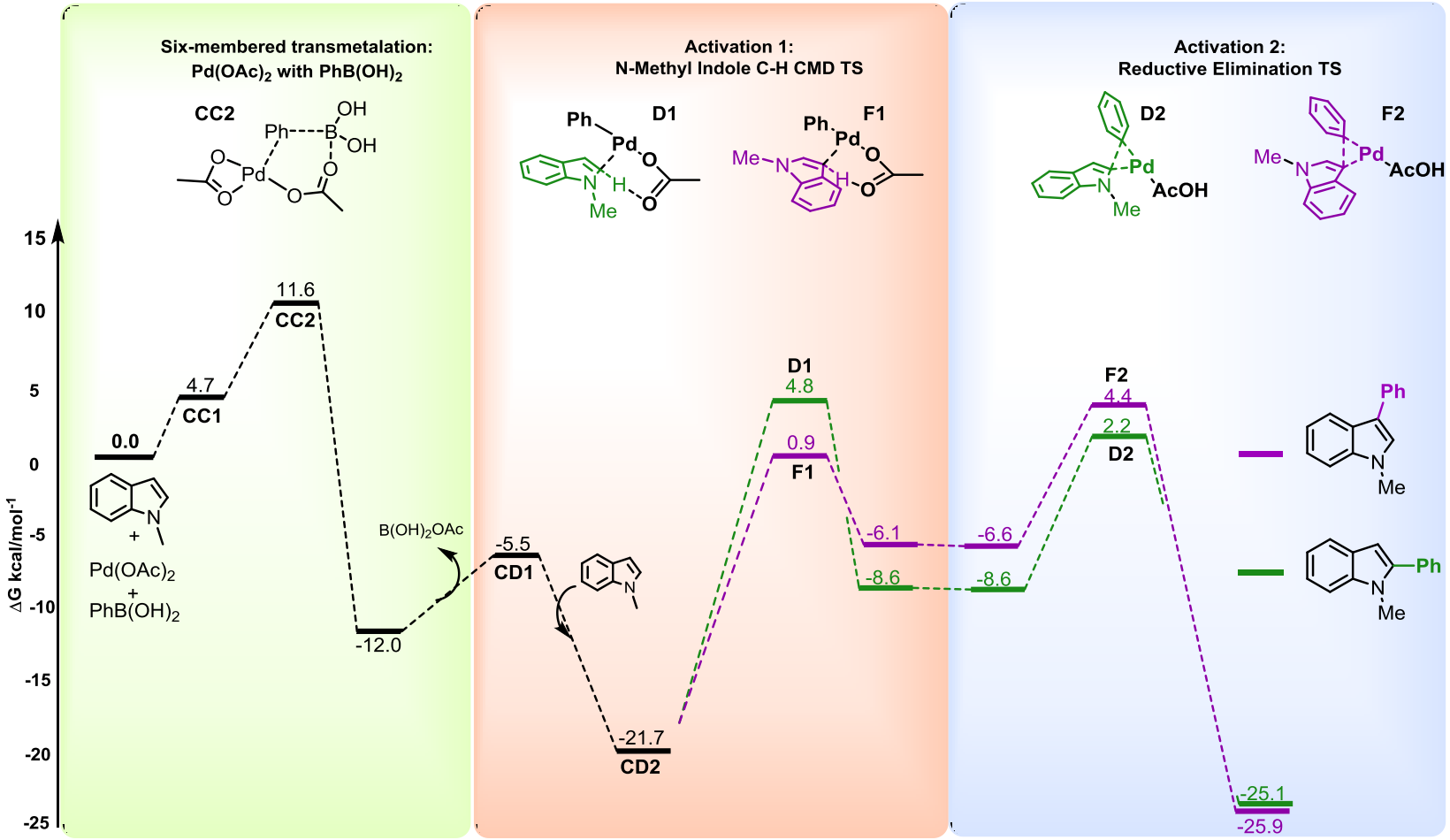

Figure 14. Gibbs free energy profile (in kcal/mol) depicting the mechanistic pathway for (**1**) six membered transmetalation followed by (**2**) CMD for arylation at C3 and C2 on N-methyl indole and completed by (**3**) reductive elimination. All values in kcal/mol. Calculations conducted at ωB97XD/6-31G(d)//6-311+G(d,p).

2.3.2.3. Six membered transmetalation on $Pd(OAc)_2$: Solvent coordination

The reaction is conducted in a medium of acetic acid. Therefore the vacant coordination sites on the Pd(II) species in the catalytic cycle can be fully saturated (in terms of coordination number) if AcOH acts as a neutral two-electron donor ligand. We investigated whether this apolar protic solvent is able to affect the catalytic cycle through coordination, and more importantly, assist in determining regioselectivity.

Initial calculations yielded a solvent-coordinated six membered transition state where the addition of AcOH acid created an energetically stable, competitive precomplex, **T1** (ΔG -4.1 kcal/mol). Square planar coordination geometry is maintained with two new distinct intramolecular hydrogen bonding interactions and a hapticity change of Pd, coordinating η^1 on Ph, as opposed to η^2 in precomplex **CC1 (Figure 15)**.

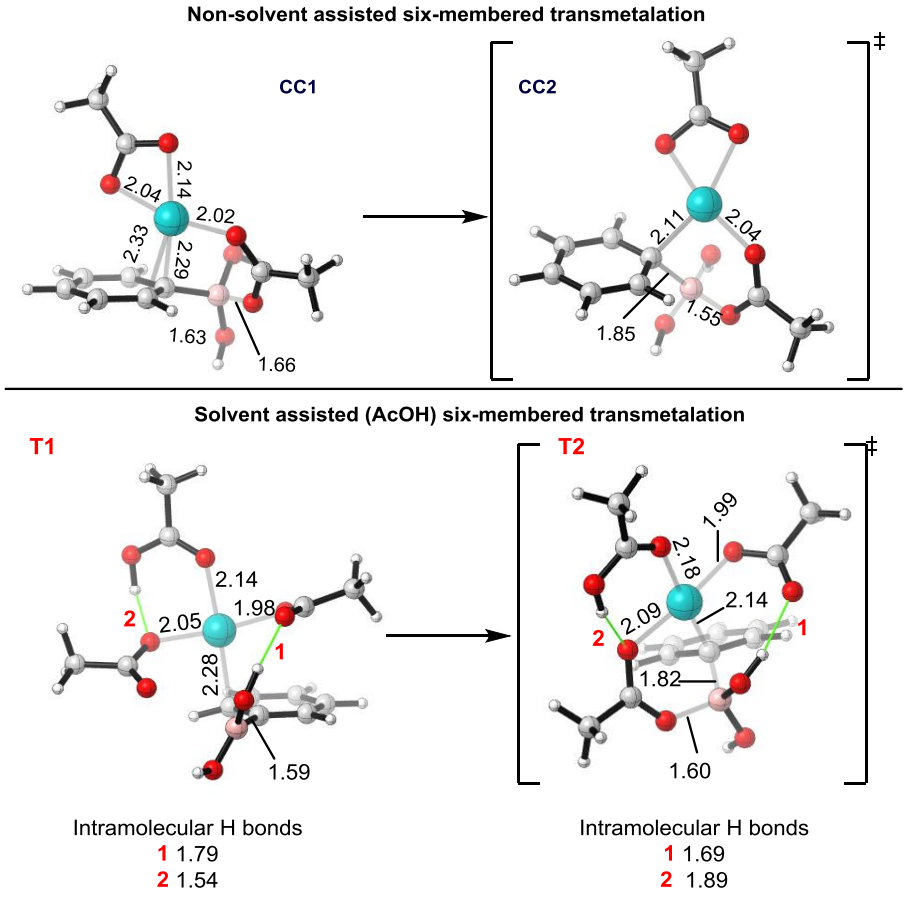

Figure 15. Optimized geometries of six membered transmetalation of $Pd(OAc)_2$ and $PhB(OH)_2$ in both a non-solvent (top) and solvent-assisted (AcOH) pathway. All bond lengths in Å.

Hydrogen bonding (O---H-O) is observed between the acetic acid ligand (O-H) and oxygen on the coordinating acetate ligand and also between the OH group on

$PhB(OH)_2$, which twists out of the plane to create a H-bond with the monodentate acetate ligand. The monodentate acetate ligand is able to do this as it is now displaced from previous bidentate coordination to Pd in **CC1** (due to the explicit coordination of AcOH). Overall this leads to a favourable solvent-coordinated precomplex where the intramolecular H bonding network assists in augmenting the stability of the precomplex, T1 (ΔG -4.1 kcal/mol), whereas the non-solvent coordinated precomplex, **CC1**, is substantially higher at ΔG 4.7 kcal/mol (**Figure 16**). These interactions are maintained in **T2** transmetalation transition state. **T2** (ΔG 9.1 kcal/mol) has a lower Gibbs free energy to separated reactants against **CC2** (ΔG 11.6 kcal/mol).

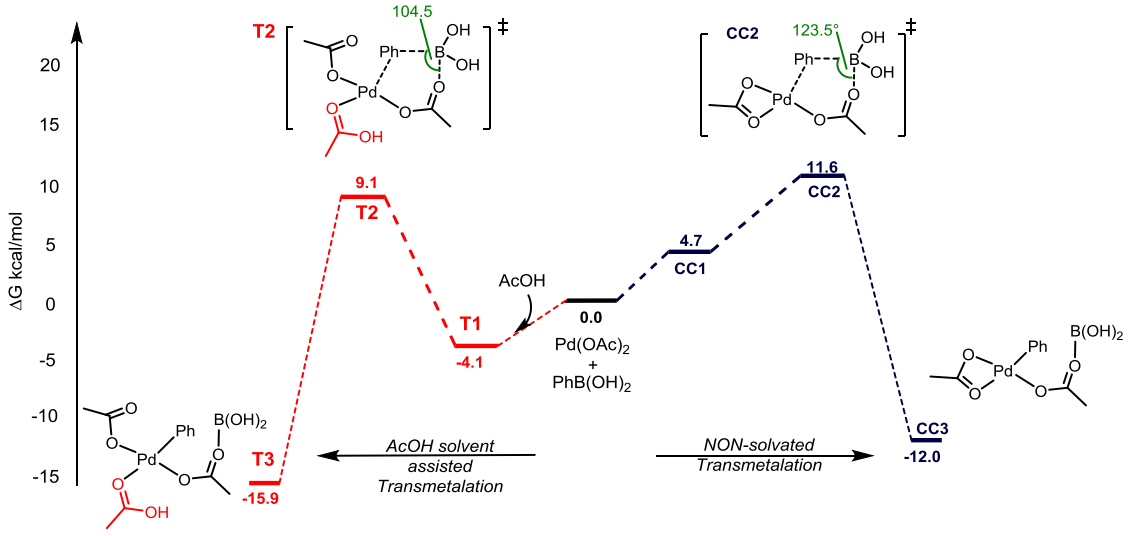

Figure 16. ωB97XD/6-31G(d)//6-311+G(d,p) free energy profile for the non-solvated six membered (*navy*) and solvated six membered (*red*) transmetalation of $Pd(OAc)_2$ with $PhB(OH)_2$. All values are in kcal/mol. Relative TS are shown as T2 (solvated) and CC2 (non-solvated).

This decrease in energy barrier is assisted through the introduction of two intramolecular hydrogen-bonds in the precomplex, TS and product. There is marked reduction of the O—B—Ph angle in **T2**, to 104.5º from 123.5º in **CC2**. The addition of the acetic acid ligand creates a more congested Pd-L geometry, presumably accelerating the reaction. Therefore addition of another σ-donor in AcOH creates a 16 electron Pd centre, **T2**, which is more susceptible to Ph addition, compared with the 14 electron Pd centre in **CC2**. Overall, solvent-assisted transmetalation is highly exergonic at ΔG -15.9 kcal/mol. The resulting transmetalation product is also more stable for the acetic acid coordinated pathway at ΔG -15.9 kcal/mol, as opposed to the non-solvated pathway at ΔG -12.0 kcal/mol.

Next we examined solvation effects on the CMD mechanism. As seen in the previous section, upon expulsion of the boron-acetate species post transmetalation, a new catalytic species can be formed. Here the species is Pd-PhOAc-AcOH, **DA1** (ΔG -14.7 kcal/mol), which is stable relative to the reactants, and even more so than Pd(II)PhOAc, (or **CD1,** seen in the previous section) and is calculated to exist as the catalytic resting state. Following the addition of N-methyl indole, precomplex **CE** (ΔG -27.1 kcal/mol) is formed. This species sees **DA1** complexed η^2 to the π-system of N-methyl indole. The acetate ligand has reverted from bidentate to monodentate coordination, with the lone pair of electrons retaining a hydrogen bonding network with the acetic acid ligand *cis* to it (**Figure 17**).

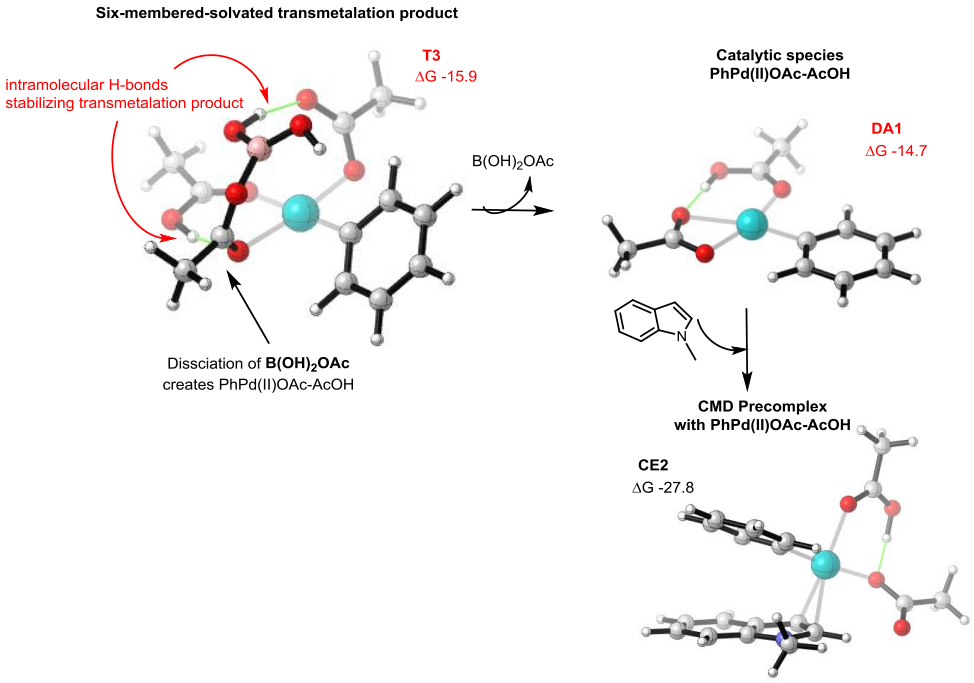

Figure 17. Products **T3** and **CC3** resulting from *solvated* and *non-solvated* six membered TM TS, respectively. **DA1** is the catalytic species formed upon expulsion of $B(OH)_2OAc$ which forms a energetically favourable precomplex with N-methyl indole, **DA1**. All values in kcal/mol.

Transition states for both C2 and C3 were located, the C-H activation barrier notably lowered in both instances. C2, **DB1**, ΔG -5.7 kcal/mol and C3, **FB1,** ΔG -9.0 kcal/mol. Post C-H activation, the palladated aryl species are favourable energetically with C3(ΔG -12.4 kcal/mol) and C2 (ΔG -15.8 kcal/mol) being precursors to the subsequent reductive elimination.

The effect of explicit solvation is to stabilize the Pd(II) species. Relative to the most stable intermediate, **CE2**, the barrier to reductive elimination is higher and the thermodynamic favourability of C-C formation is reduced. Presumably this is due to the stable 16 electron, square planar Pd(II) having preferential binding as opposed to Pd(0). The effect of explicit solvent on the computed reaction coordinate is therefore a relative increase in the reductive elimination barrier making it the highest, selectivity determining point. Comparing these TSs for C3, **DB2,** (ΔG 1.4 kcal/mol) and C2, **FB2**, (ΔG -0.9 kcal/mol) leads to a prediction of 49:1 regioselectivity (C2:C3) (**Figure 18**). Experimentally, none of the C3 product is detected so this mechanism underestimates the level of selectivity, although yields the correct major product. In our calculations, the C3-favourability of C-H activation, and the C2-favourability of reductive elimination is a common feature for both solvated and non-solvated cases. Therefore, contrasting selectivity can result depending on which of these two steps is higher in free energy. Based on the observed preference for exclusive C2 arylation, we exclude those mechanisms in which the CMD activation of indole is the slowest step, since this leads to a kinetic preference for the incorrect regioisomer. We now explore the mechanism in which transmetalation occurs after C-H activation of indole.

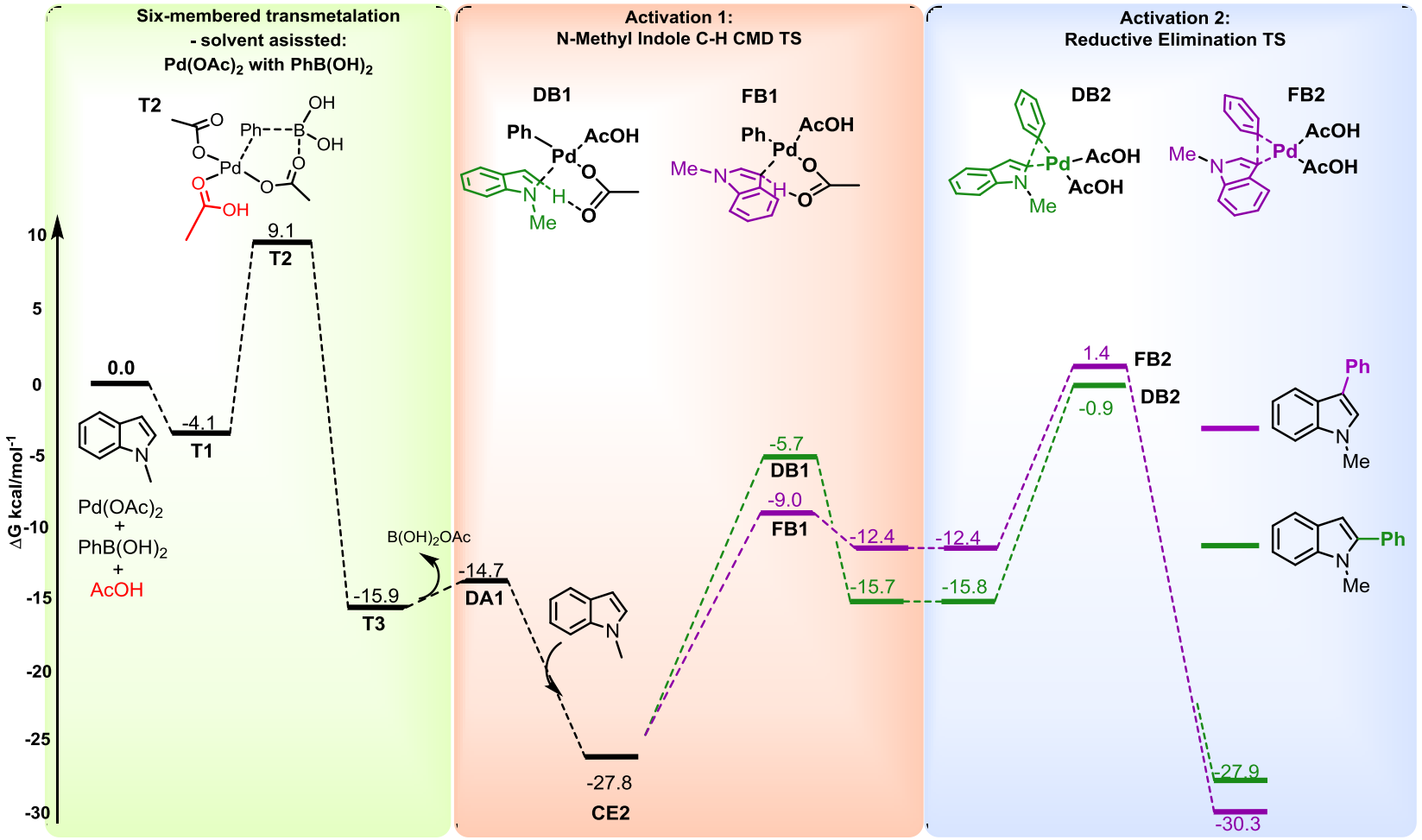

Figure 18. Gibbs free energy profile (in kcal/mol) depicting the mechanistic pathway for (**1**) solvent-assisted transmetalation followed by (**2**) CMD C-H activation (Activation 1) and (**3**) subsequent reductive elimination (Activation 2). Calculations conducted at ωB97XD/6-31G(d)//6-311+G(d,p).

2.3.3 The CMD-Transmetalation pathway

2.3.3.1. CMD of N-methyl indole with $Pd(OAc)_2$: solvated and non-solvated

Our computational investigation sought to characterize an alternative series of mechanistic events that would explain C2 selectivity. This begins with (**1**) the initial C-H activation of N-methyl indole with $Pd(OAc)_2$, (**2**) followed by four or six membered transmetalation with $PhB(OH)_2$, and culminates in (**3**) a C-C bond forming reductive elimination, where the arylated product is created and Pd(0) expelled.

Transition states for both regioisomers were located, with low energy precomplex (**A1**), a common precursor to C2 and C3 TS. In this common precomplex (ΔG -8.9 kcal/mol), $Pd(OAc)_2$ is bound η^2 to N-methyl indole with an acetate ligand monodentate to Pd. This coordination allows an 'ambiphilic' acetate ligand to initiate proton transfer in non-solvated TS, **A2** and **AA3**, and solvated TS (i.e. AcOH coordinated) TS, **A2-AcOH** and **A3-AcOH** (**Figure 19**).

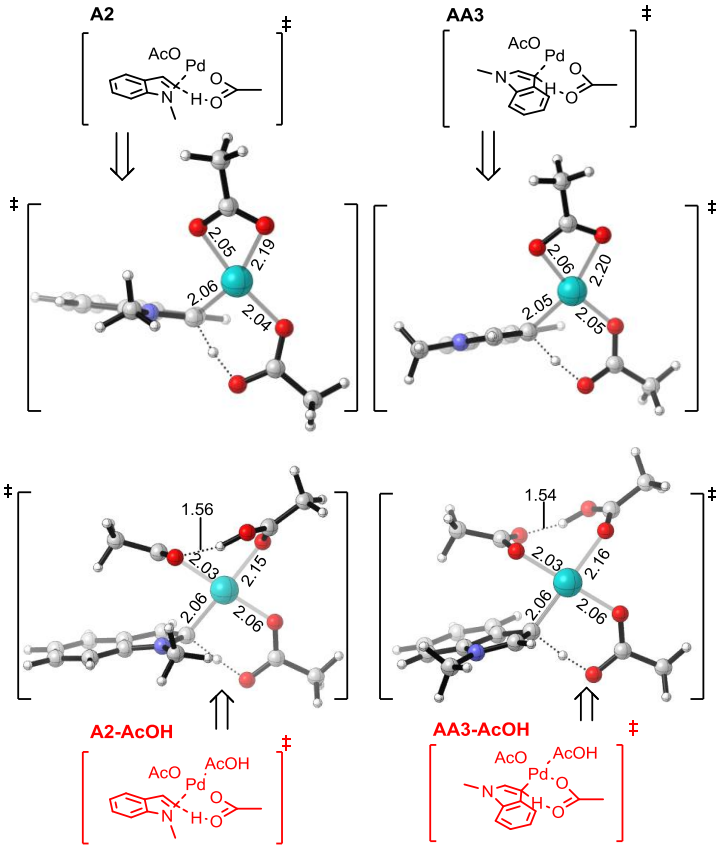

Figure 19. Initial C-H activation of N-methyl indole at C2 and C3, with and without explicit coordination of AcOH. All bond lengths are given in Å. Calculations were conducted at ωB97XD/6-31G(d)//6-311+G(d,p).

As expected, it was noted that C-3 C-H activation is favoured, with **AA3** (ΔG 7.8 kcal/mol) having a lower Gibbs free energy barrier (relative to separated reactants) than **A2** (ΔG 11.9 kcal/mol). Corresponding TS for the solvent assisted CMD, C2 (**A2-AcOH**) and C3 (**A3-AcOH**), were located, with the calculated activation energies for both C-H activation processes lowered as a result of the coordination of acetic acid (**Figure 20**).

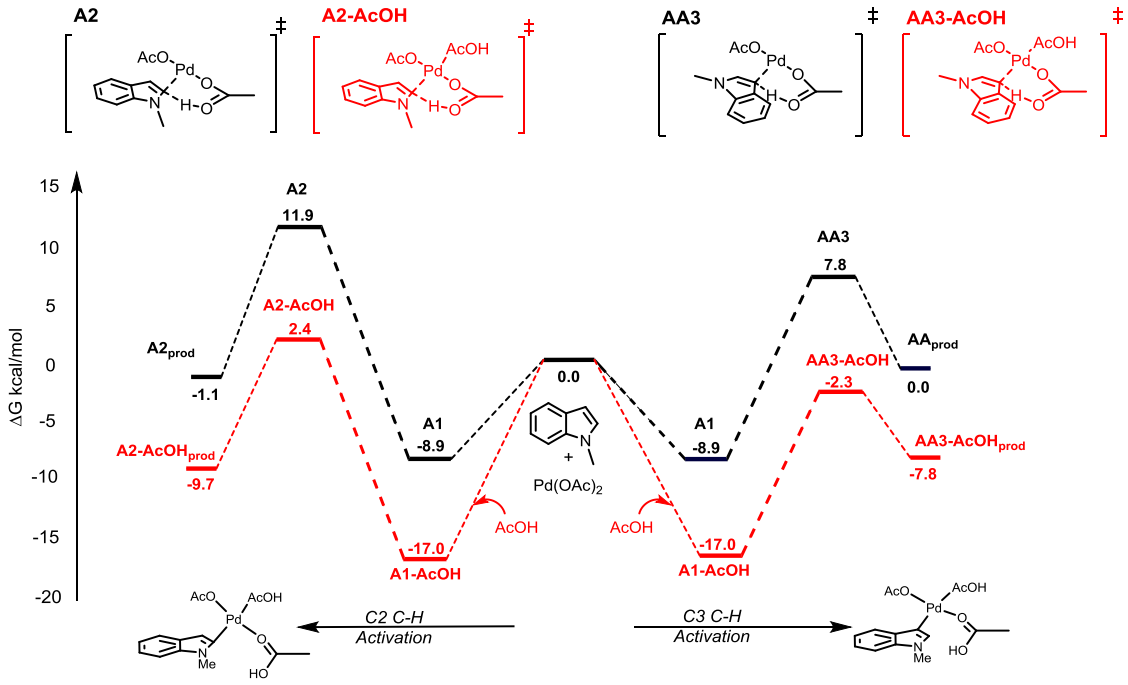

Figure 20. ωB97XD/6-31G(d)//6-311+G(d,p) free energy profile for the non-solvated CMD pathway (navy) and solvated CMD C-H activation (red) of N-methyl indole. C2 C-H activation is shown on the left and C3 C-H activation on the right. All values are in kcal/mol.

The solvated catalyst (i.e. $Pd(OAc)_2$-AcOH) assists in creating a CMD TS where the geometry is distinctly square planar, as opposed to the 14 electron $Pd(OAc)_2$ which is calculated as a 3-coordinate Pd(II) TS. The coordination geometry of the AcOH ligand is *trans* to indole and therefore it acts a H-bond donor in O--H-O bonding interaction with the coordinated acetate ligand *cis* to it, which uses a lone pair as a H-bond acceptor. Ligand coordination of this acetate switches from bidentate to monodentate (as opposed to non-solvated Pd species where it remains bidentate) to accommodate the σ-donor coordination of AcOH. Thus it has a spectator role in the CMD TS, and now it can rotate to form an intramolecular hydrogen bonding network to stabilize the solvated TS (as seen in **Figure 19**).

For the subsequent transmetalation to elicit regioselectivity, this C-H activation would have to occur reversibly. It has been noted in the Pd(II) catalyzed oxidative arylation of N-indoles at C2 that initial deuteration is observed at the C3 position even though regioselectivity for C-C formation is exclusively attained at the C2 position.[35] Recent experimental and computational studies by Ibanez also showed Pd(II) catalyzed arylation of amino acid derivatives proceed with a reversible CMD step and therefore this is not an irreversible procedure.[36] This would be even more accentuated if the PES for the arylation of indole shows a high energy selectivity determining step. Our calculations show that the C-H activation is theoretically reversible – for all of the CMD transition structures computed, the reverse reaction (i.e. reprotonation) has a lower barrier than the forward (i.e. C-H activation) process. This step would therefore be reversible, provided the barrier of the next step, the intermolecular transmetalation with the boronic acid is relatively slow in comparison.

Post CMD, the resulting Pd-Aryl intermediates ($A2_{prod}$/A2-$AcOH_{prod}$/$AA3_{prod}$/AA3-$AcOH_{prod}$) are now susceptible to subsequent transmetalation with $PhB(OH)_2$. Having characterized the C-H activation step, investigations focused on examining solvation effects (modelled via an explicit atomistic manner in combination with the CPCM solvation model). Acetic acid is a non-charged, two-electron ligand that coordinates *trans* to N-methyl indole, creating a low-energy η^2 precomplex that is -17.0 kcal/mol relative to reactants (**A1-AcOH**). The trend in computed thermochemistry and kinetics remains essentially identical to the case without explicit solvation – the C2 pathway is kinetically disfavoured relative to C3, while the C2 arylpalladium species is the more stable intermediate. Again, however, the C-H activation step is predicted to be disfavoured for both regioisomeric pathways.

It is evident that regioselectivity is still calculated to be prevalent for the C3 C-H activation (ΔG -2.3 kcal/mol) rather than C2 (ΔG 2.4 kcal/mol), with both processes benefitting from explicit solvent association.

2.3.3.2. Four vs six membered transmetalation post CMD

Initial geometry optimizations were successful in yielding four and six membered transmetalation transition states for both C2 and C3. We postulated that perhaps a 'naked' Pd, i.e. electron deficient Pd intermediate, may experience transmetalation faster than a species with an extra two-electron donor. This is due to the nature of the Ph(δ^-)--Pd(δ^+) transfer in the transition state, presumably accentuated by an electron deficient Pd. Thus, our initial calculation focused on the transmetalation of $PhB(OH)_2$ with the 14 electron Indole-Pd-OAc species. Calculated four membered TS for C2 (**FM-TS2)** and C3 (**FM-TS3)** were found on the PES with the transmetalation favouring C2 selectivity. **FM-TS2** (ΔG 23.4 kcal/mol) was shown to be 2.4 kcal/mol lower than **FM-TS3** (ΔG 25.6 kcal/mol) compared to the relative reactants. However, enhanced C2 selectivity was observed through six membered transition states **SM-TS2** and **SM-TS3 (Figure 21)**.

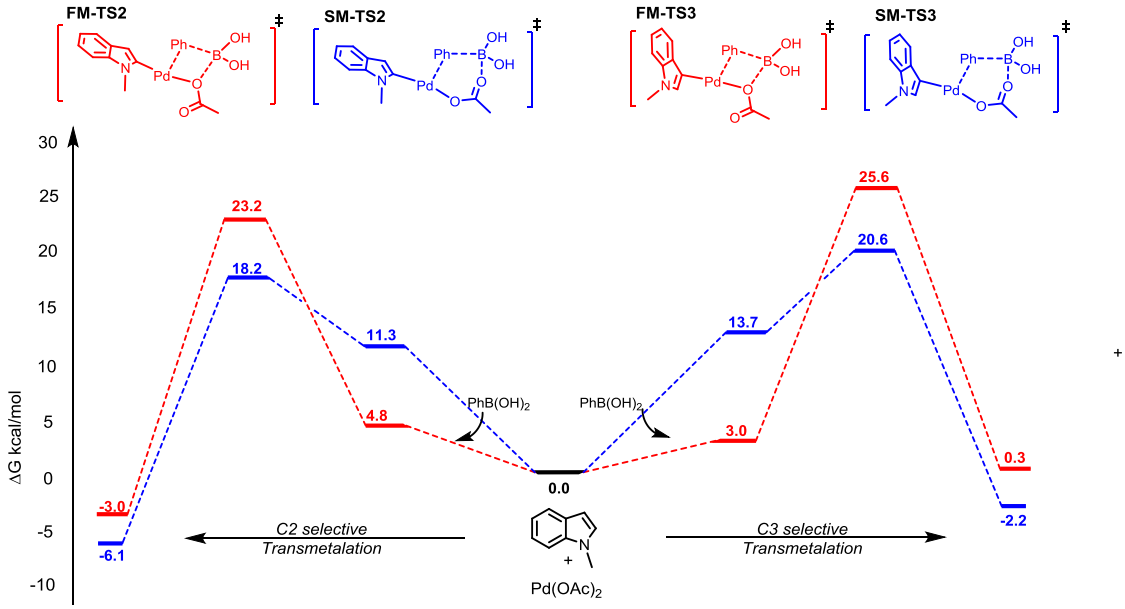

Figure 21. ωB97XD/6-31G(d)//6-311+G(d,p) free energy profile for the four membered transmetalation (*red*) and six membered transmetalation (*blue*) post CMD. C2 transmetalation shown on the left and C3 transmetalation on the right. All values are in kcal/mol.

As seen previously with the transmetalation of $Pd(OAc)_2$, the six membered transmetalation has a lower overall energy barrier compared with the four membered. Energies of six membered precomplex relative to **SM-TS2** and **SM-TS3** are higher than their four membered counterparts. In C3 this phenomenon is the most striking, creating a ~10 kcal/mol difference between six and four membered pre-complex. In

addition to the distortion of planarity of $B(OH)_2$ moiety of $PhB(OH)_2$ in the six membered species, there is an additional hydrogen bond featured in the 4-membered species which contributes to this stability.

Comparing **SM-TS3** and **SM-TS2** selectivity towards C2 transmetalation is observed. C2 based transmetalation is favoured by 2.4 kcal/mol (**SM-TS2 vs SM-TS3)**. Using NBO calculations, Natural Population Analysis[37] (NPA) charges were calculated (**Figure 22**) which incorporates atomic charges and orbital populations of molecular wave functions in general atomic orbital basis sets. This method is known to improve stability and accuracy compared to Mulliken population analysis, which is sensitive to basis set variation. In **SM-TS2/3** the bond is polarized $C(\delta^-)$--$Pd(\delta^+)$. The incoming Ph (δ^-) ligand *cis* to the indole will transmetalate faster at Pd centre bearing higher positive charge. **SM-TS2** shows a slightly higher positive atomic charge on Pd (0.68) compared to **SM-TS3** (0.66), thus explaining why transmetalation may occur faster for the C2 arylpalladium species.

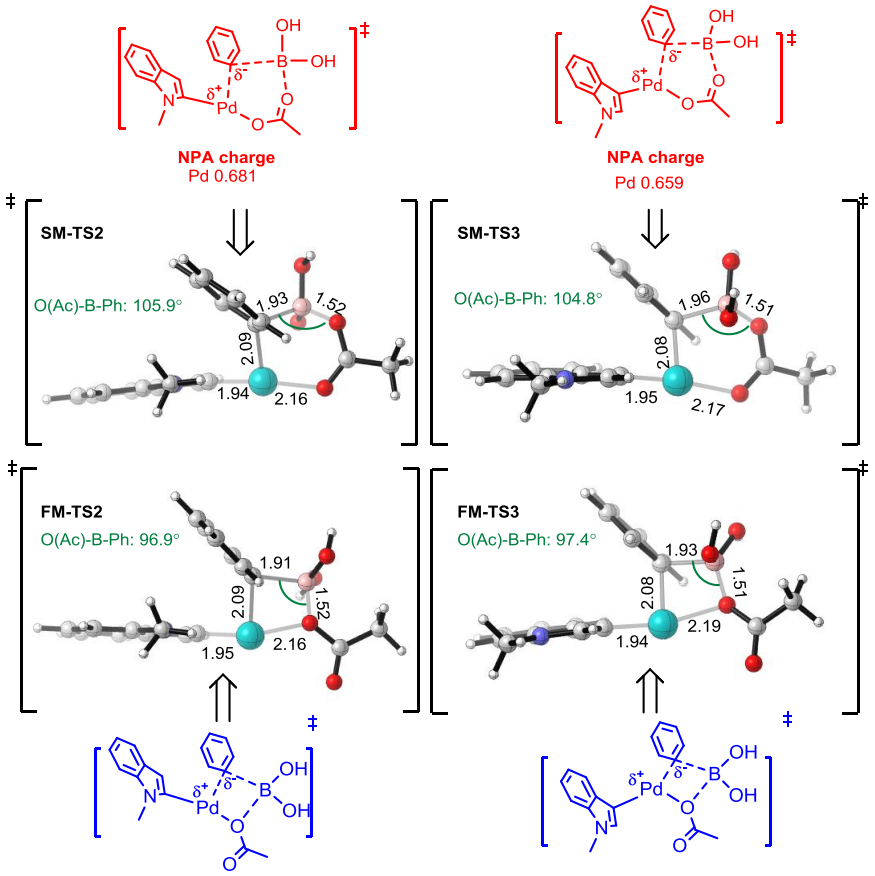

Figure 22. Optimized geometries of four membered (FM) and six membered (SM) transmetalation transition states. All bond lengths are given in Å. NPA charge of Pd in six membered TS is shown.

2.3.3.3. Six membered transmetalation post CMD: solvent effects

Having established the preferred transmetalation pathway to initiate via a six membered fashion we examined whether AcOH solvation would assist in the Gibbs energy profile for six membered transmetalation as seen previously with the CMD based process. Here we rationalized that solvation could assist via two potential interactions.

Firstly, the possibility of O---H-O hydrogen bonding interaction with acetic acid (*cis* to indole) and the coordinating acetate ligand (*trans* to indole) could exist. The second interaction that is viable occurs via a polar-π interaction between the solvent molecule (O-H on acetic acid with the indole C2-C3 π-system) and N-methyl indole (**Figure 23**). Polar-π interactions (or π hydrogen bonds) occur with molecules with a permanent dipole moment (acetic acid) interacting with the quadrupole moment of a π-system (N-methyl indole) and are known to have a stabilizing effect of ~1-2 kcal/mol.[38]

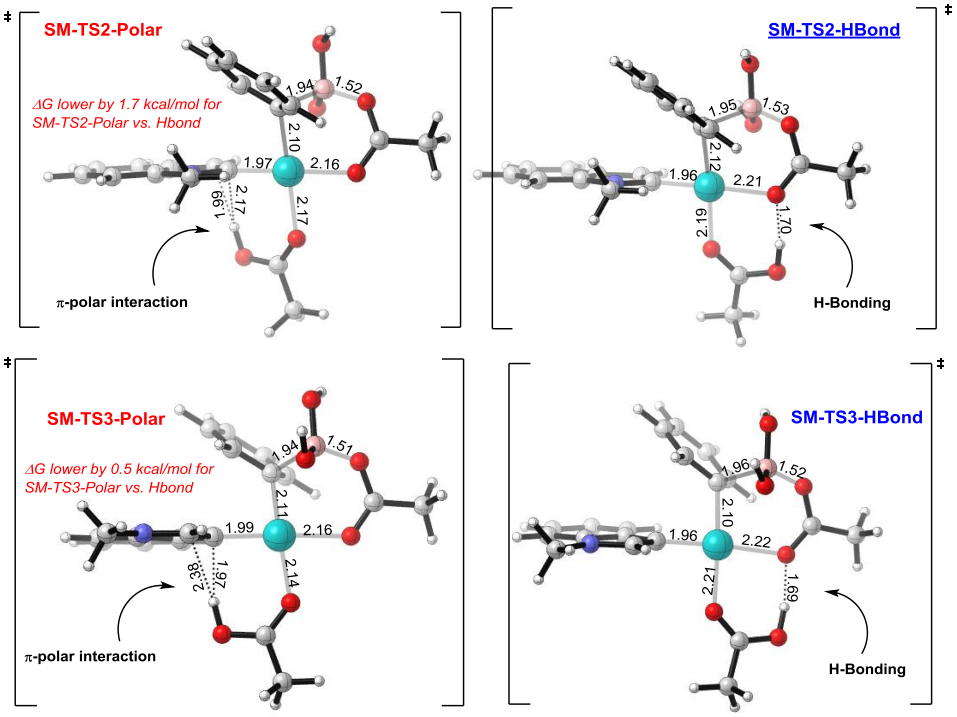

Figure 23. Optimized geometries of solvated six membered TS. Hydrogen bonding and π-polar bonding rotation are shown for C2 (*top)* and C3 (*bottom*) All bond lengths are given in Å. Calculations were conducted at ωB97XD/6-31G(d)//6-311+G(d,p).

Both interactions can be achieved through 180° rotations of the solvent ligand about its axis. Upon optimization, both C2 and C3 six membered solvated transition states energetically favoured the polar-π orientation with the C2 TS (**SM-TS2-Polar**)

energetically preferred by 1.7 kcal/mol. Interestingly, our calculations showed that hydrogen bonding assists in stabilizing the precomplex. Therefore the acetic acid may act as a rotational "switch", adopting hydrogen bonding in the precomplex and the polar-π interaction in the TS to lower the global energy barrier. C2 selectivity is retained in the solvent assisted transmetalation, indicating once the initial CMD step is undertaken; C2 transmetalation is preferred via this route, with the TS lower at ΔG 8.9 kcal/mol as opposed to C3 TS ΔG 12.4 kcal/mol (**Figure 24**).

In **TS SM-TS3-Polar** and **TS SM-TS2-Polar** the 14 electron Pd species displays increased positive character as compared to non-solvated species according to NPA charges. In **TS SM-TS3-Polar** (+0.71) the charge is lower than **TS SM-TS2-Polar** (+0.72), thus suggesting that the C2 species is marginally more electrophilic and thus receptive to transmetalation than the C3 species.

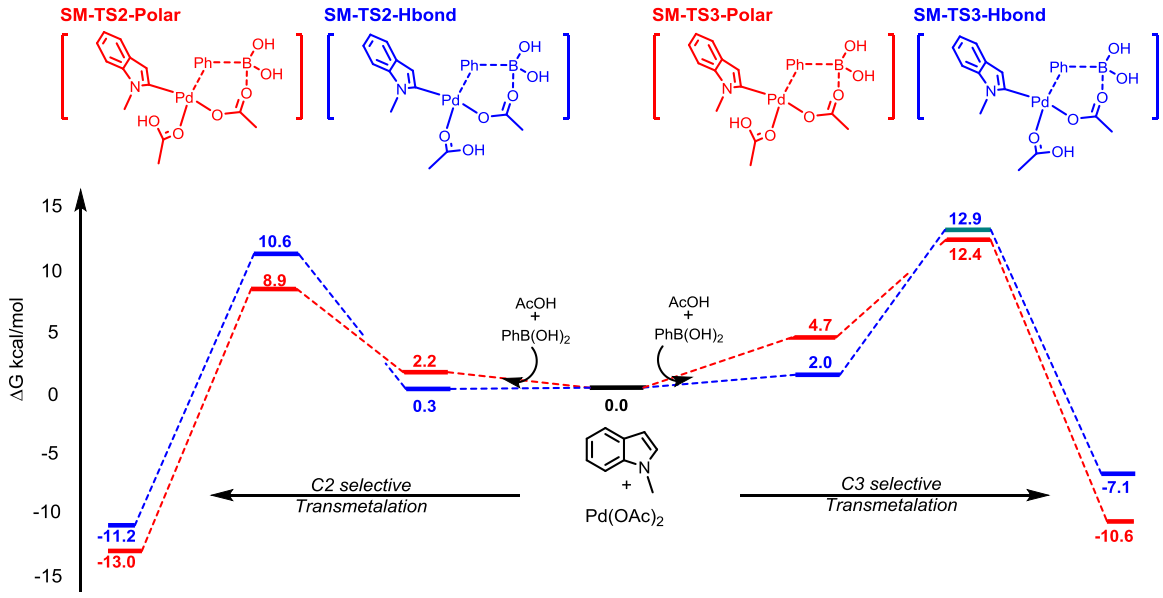

Figure 24. ωB97XD/6-31G(d)/LANL2DZ free energy profile for the solvated six membered transmetalation (post CMD). The polar-π interaction pathway is displayed in *red* and the hydrogen bonding interaction pathway in *blue*. Solvent-assisted C2 transmetalation shown on the *left* and C3 transmetalation on the *right*. Corresponding six membered TS are illustrated above the relative free energy pathway. All values in kcal/mol

2.3.3.4. Reductive elimination: “Non”, “mono “or “bis” ligated Pd

Arylation of C2 is completed via the three-centred reductive elimination after the solvent assisted polar-π six membered transmetalation (seen in **Figure 24**). Solvation effects were accounted for in addition to the PCM solvation method by atomistic modelling of acetic acid as previously described. This could create three different pre-reductive elimination intermediates, each capable of transferring electron density to the metal centre via a concerted-three centred mechanism with Ph and N-methyl indole residing in required *cis* disposition relative to each other (**Figure 25**).

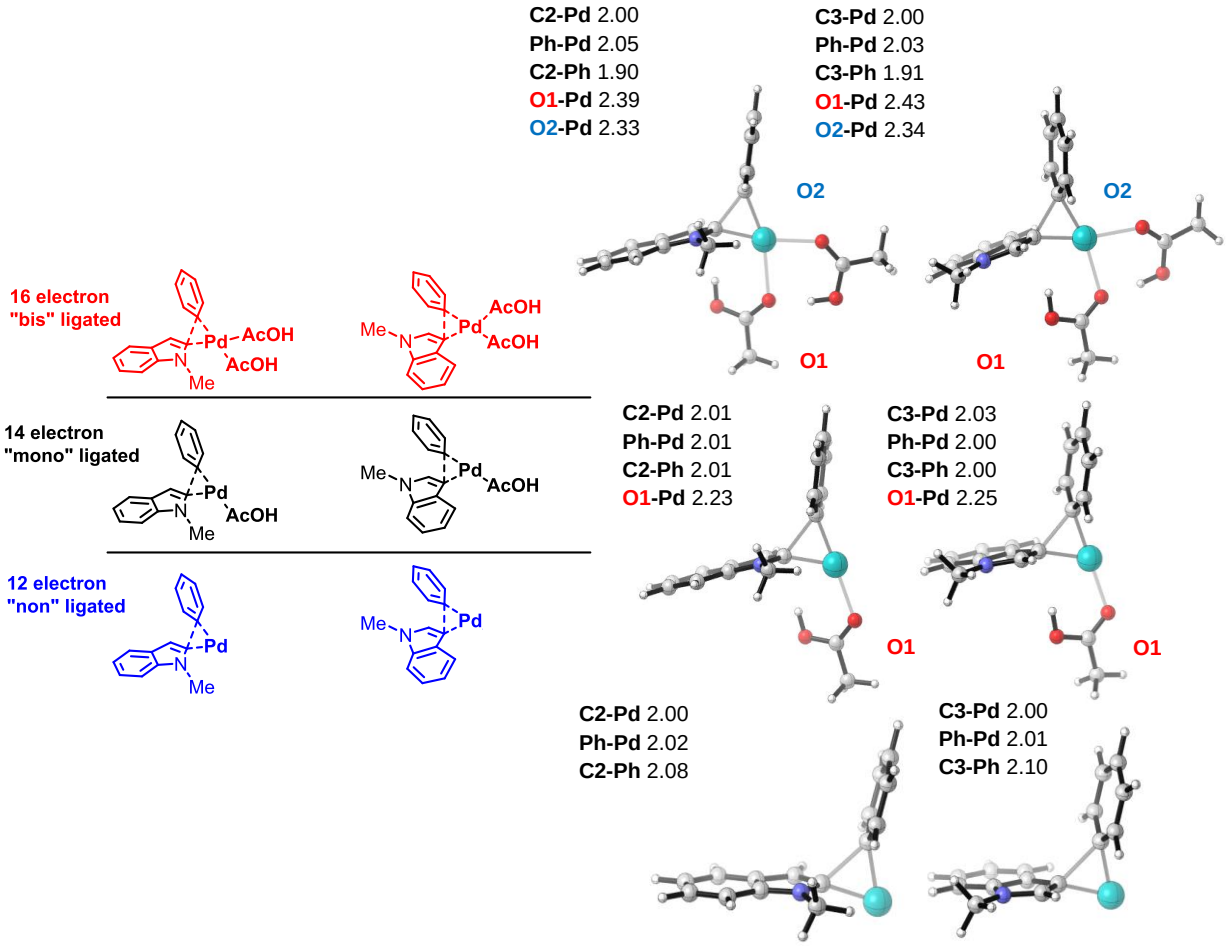

Figure 25. “Non”, “mono”, and “bis” ligated transition states depicted on the *left*. Optimized (ωB97XD/6-31G(d,p) transition state geometries of corresponding reductive elimination geometries displayed on the *right*. Key bond lengths are included (in Å).

Therefore three possibilities were examined. A 12 electron (non-ligated), 14 electron (mono-ligated) and 16 electron (bis-ligated) reductive elimination transition state where the additional 2-electron donor in each consecutive TS is courtesy of acetic acid.

Additionally, intramolecular polar-π and hydrogen bonding networks were considered through rotations in the bis-ligated TS. Computed Gibbs energy profiles display selectivity preferences towards C2 in all studied species i.e. (12, 14 and 16 electron reductive elimination TS) (**Figure 26**).

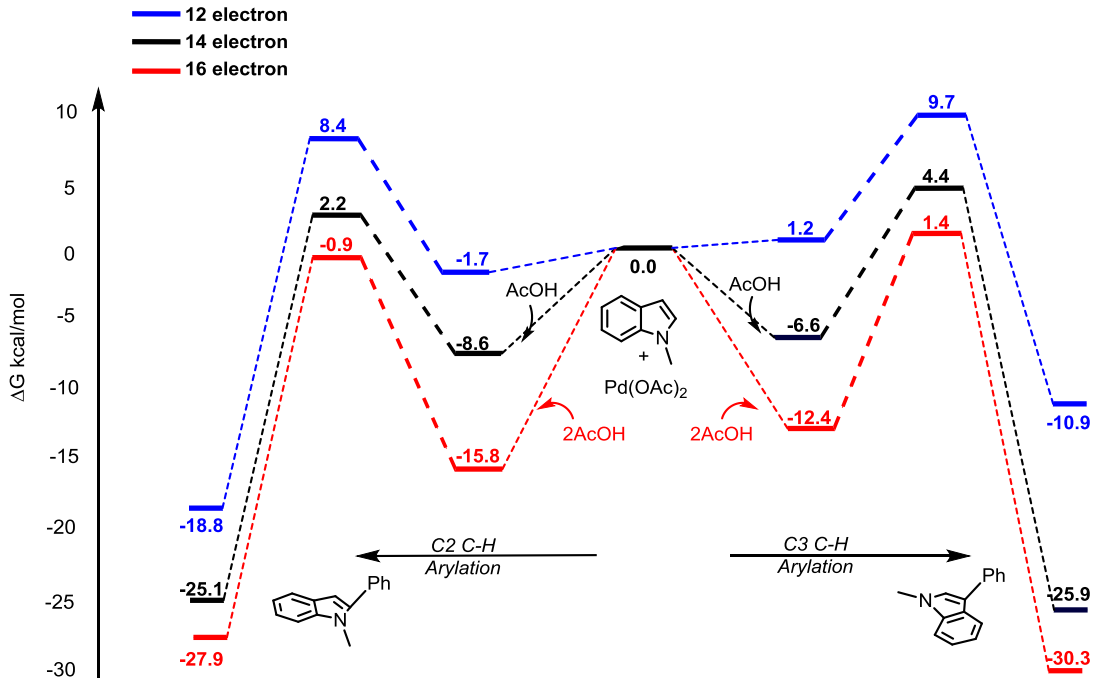

Figure 26. ωB97XD/6-31G(d)//6-311+G(d,p) free energy profile for the non (blue), mono (black), bis (blue) ligated reductive elimination pathway. C2 arylation is shown to the left with C3 arylation on the right. All values in kcal/mol.

All pathways of reductive elimination leading to both C2 and C3 products were seen to be exergonic and the C2 precomplex displayed superior stability relative to its C3 counterpart. Increased electron density on the Pd centre was noted to decrease Gibbs energies of activation in both C3 and C2, with the most stable being the 16 electron reductive elimination transition state, adopting favoured Pd(II) square planar symmetry with all coordination sites saturated. The ability of *trans* influence in the Pd(II) reductive elimination species can also be ruled out as AcOH was seen to be inadequate at exerting sufficient σ-donor character. This is signified by Ph and N-methyl indole retaining consistent C-Pd bond lengths across the mono and bis-ligated species, when AcOH was placed *trans* to both aryl groups respectively.

2.4. Summary

2.4.1. Calculated pathway for arylation of N-methyl indole at C2

Four membered transmetalation is deemed to be less competitive than six membered and crucially solvation on the Pd centre (with AcOH) helps to form polar-π interaction between solvent molecule and π system of indole to stabilize six membered transition states, precomplexes and products. The favoured mechanism proceeds via CMD (solvent-assisted) which is a reversible reaction. Following reprotonation and eventual C-H activation at C2, the reaction can accumulate at the low-energy, stable C2 aryl-palladium intermediate. The dissociation of the AcOH *cis* to C2 on the arylpalladium intermediate opens a coordination site on the square planar Pd, presenting ideal coordination geometry for incoming $PhB(OH)_2$.

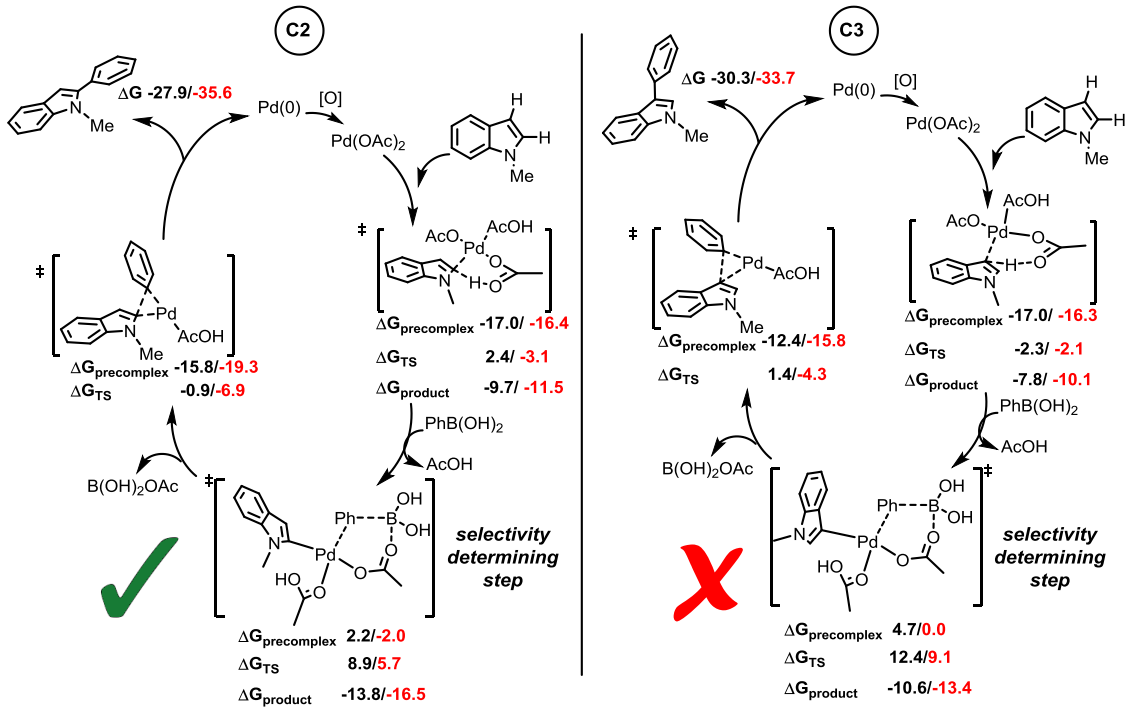

Figure 27. Computed catalytic cycles for the direct arylation at C2 and C3 of N-methyl indole. Selectivity is determined through a six membered solvent assisted transmetalation TS. All values in kcal/mol. Calculations conducted at ωB97XD/6-31g(d)/LANL2DZ//6-311+G(d,p)/LANL3TZ (black) and ωB97xd/6-31G(d)//M062x/6-311+G(d,p)/LANLTZ (red).

The transmetalation event with $PhB(OH)_2$ occurs via a six membered solvated transition state which is more competitive in energy than the C3 regioisomer. Through calculation this is the shown to be the rate and selectivity determining step. The catalytic cycle concludes through a facile bis-ligated C2 reductive elimination TS that

undergoes concerted three centred elimination to form a new C-C bond between N-methyl indole and phenyl, expelling Pd(0) and producing the C2 arylated product (**Figure 28**).

2.5. Conclusions

As with previous computational work, Pd catalyzed aromatic C-H activation is found not to occur via electrophilic aromatic substitution but via CMD. Our DFT treatment of this step is the first to compare the relative ease of C2 and C3 C-H activation of N-methyl indole. We find the computed selectivity of this activation step universally shows C-3 selectivity for this substrate with a number of different Pd(II) catalytic species, which corresponds to the more electron rich position of the indole substrate. Interestingly, given the experimental results, it is clear that the kinetically preferred site of C-H activation cannot account for the C2 selectivity of arylation. Significant effort has been focused in the literature upon comparing the relative rates of CMD C-H activations. However, our results demonstrate the need for consideration of the complete PES.

Our calculations show that four membered transmetalation is disfavoured, and the reaction is more favourable by six membered transmetalation mechanism. Indeed, the C2-selectivity is predicted to emerge in the six membered solvent assisted transmetalation to the Pd-indole complex, which is calculated to be the slowest (i.e. rate determining) step in the catalytic cycle due to the increased electropositive character of Pd. Overall, our favoured mechanism (**Figure 28**) provides an overall barrier (observing the energetic span model) of ΔG 25.9 kcal/mol and a $\Delta\Delta G^{\ddagger}$ of 3.5 kcal/mol in the selectivity determining transmetalation step, which corresponds to exclusive formation (i.e. 100:0, C2:C3) of the C2 product. This is in excellent agreement with experimental observation as no C3 regioisomer was observed. Reversible C-H activation occurs as a first step in the mechanism, and is favoured over transmetalation.

Furthermore, our prediction remains consistent across the M06-2X functional of Truhlar **Figure 28**, *red*) providing agreement across two popular DFT functionals for the treatment of Pd based systems, predicting $\Delta\Delta G^{\ddagger}$ of 3.4 kcal/mol in the selectivity determining transmetalation step which once again confirms predicted exclusive regioselectivity of the C2 isomer.

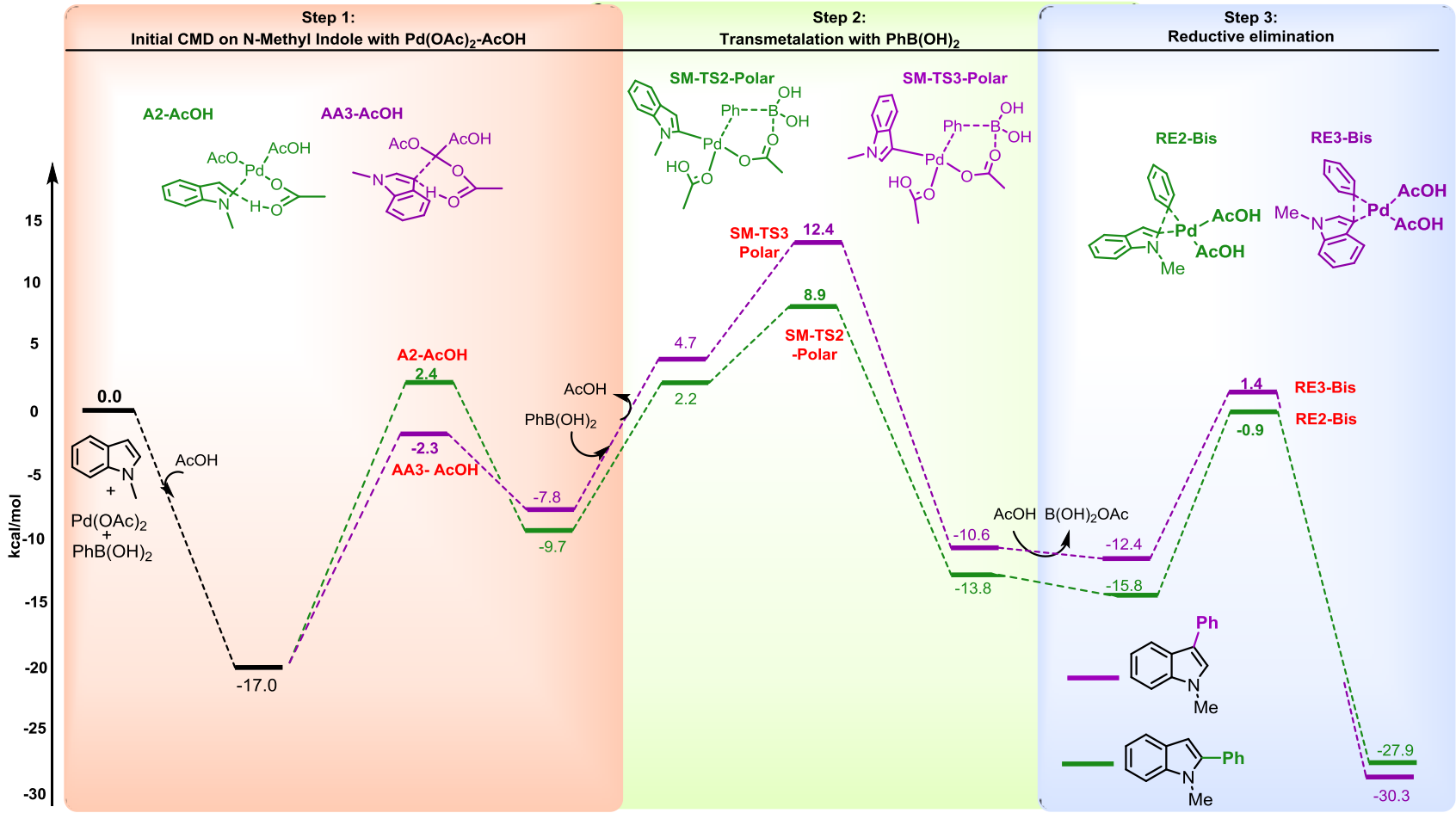

Figure 28. Gibbs free energy profile depicting the proposed mechanistic pathway for arylation at C2. This proceeds via (1) initial CMD on N-methyl indole, (2) A six membered, solvent-assisted transmetalation allows the creation of a biaryl-Pd complex, which proceeds to a (3) 'mono'-ligated reductive elimination. Optimizations were conducted at ωB97XD/6-31G(d)/6-311+G(d,p). All values are in kcal/mol.

Chapter 2 *References*

[1] Miyaura, N.; Yamada, K.; Suzuki, A. *Tetrahedron Letters*, **1979**, *20*, 3437.

[2] (a) Suzuki, A. *Angew. Chem. Int. Ed.* **2011**, *50*, 6722; (b) Miyaura, N.; Suzuki, A. *Chem. Rev*. **1995**, *95*, 2457; (c) Martin, R.; Buchwald, S. L. *Acc. Chem. Res*. **2008**, *41*, 1461; (d) Fu, G. *C. Acc. Chem. Res*. **2008**, *41*, 1555; (e) Valente, C.; Çalimsiz, S.; Hoi, K. H.; Mallik, D.; Sayah, M.; Organ, M. G. *Angew. Chem., Int. Ed.* **2012**, *51*, 3314.

[3] Kirchberg, S.; Frohlich, R.; Studer, A. *Angew. Chem., Int. Ed*. **2009**, *48*, 4235.

[4] Yang, S.-D.; Sun, C.-L.; Fang, Z.; Li, B.-J;, Li, Y.-Z.; Shi, Z.-J. *Angew. Chem. Int. Ed*. **2008,** *120*, 1495.

[5] Wei, C. S., Davies, G. H. M., Soltani, O., Albrecht, J., Gao, Q., Pathirana, C. Eastgate, M. D. *Angew. Chem. Int. Ed*. **2013**, *52*, 5822.

[6] Zhang, J. C. ;Shi, J.L.; Wang, B.Q.; Hu, P.; Zhao, K.Q.; Shi, Z. J. *Chem. Asian. J*. **2015**, *10*, 840.

[7] (a) Kakiuchi, F.; Usui, M.; Ueno, S.; Chatani, N.; Murai, S. *J. Am. Chem. Soc*. **2004**, *126*, 2706; (b) Kakiuchi, F.; Kan, S.; Igi, K.; Chatani, N.; Murai, S. *J. Am. Chem. Soc*. **2003**, *125*, 1698; (c) Pastine, S. J.; Gribkov, D. V.; Sames D. *J. Am. Chem. Soc*. **2006**, *128*, 14220; (d) Fujiwara, Y.; Domingo, V.; Seiple, I. B.; Gianatassio, R.; Bel, M. D.; Baran, P. S. *J. Am. Chem. Soc*. **2011,** *133*, 3292; (e) Seiple, I. B.; Rodriguez, S. S. R. A.; Gianatassio, R.; Fujiwara, Y.; Sobel, A. L.; Baran, P. S. *J. Am. Chem. Soc*. **2010,** *134* , 13194.

[8] Düfert, M. A.; Billingsley, K. L.; Buchwald, S. L. *J. Am. Chem. Soc.*, **2013**, *135*, 12877.

[9] Braga, A.A.C.; Ujaque, G.; Maseras, F. *Organometallics.* **2006**, *25*, 3647.

[10] Amatore, C.; Le-Duc, G.; Jutand, A. *Chem. Eur. J*. **2013**, *19*, 10082.

[11] Butters, M.; Harvey, J. N.; Jover, J.; Lennox, A. J. J.; Lloyd-Jones, G.C.; Murray, M. *Angew. Chem. Int. Ed.* **2010**, *49*, 5156.

[12] Carrow, B.P.; Hartwig, J. F. *J. Am. Chem. Soc.* **2011**, *133*, 2116.

[13] Ortuno, M. A.; Lledos, A.; Maseras, F.; Ujaque, G. *Chem. Cat. Chem.* **2014**, *6*, 3132.

[14] Frisch, M. J.; et al. *Gaussian 09*, revision A.02; Gaussian, Inc.: Wallingford, CT, **2009**

[15] (a) Mishra, B. K.; Karthikeyan, S.; Ramanathan, V. *J. Chem. Theory Comput.*, **2012,** *8*, 1935; (b) Fokin, A. A.; Chernish, L.;Gunchenko, V. P. A.; Tikhonchuk, E.Y.; Hausmann, H.; Serafin, M.;.Dahl, J E. P.; Carlson, R. M. K.; Schreiner, P.R. *J. Am. Chem. Soc*. **2012**, *134*, 13641; (c) Chudzinski, M.; Taylor, M. S. *J. Org. Chem.* **2012**, *77*, 3483.

[16] Bell, A. T.; Head-Gordon, *M. Annu. Rev. Chem. Biomol. Eng*. **2011**, *2*, 453.

[17] Grimme, S. *J. Comput. Chem.* **2004**, *25*, 1463.

[18] (a) Minenkov, Y.; Singstad, A.; Occhipinti, G.; Jensen, V. R. *Dalton Trans.*, **2012**, *41*, 5526; (b) Dang, l. Yang, X.; Zhou, J.; Brothers, E. N.; Hall, M. B. *J. Phys. Chem. A*. **2012,** *116*, 476; (c) Powers, D. C.; Lee, E.; Ariafard, A.; Sanford, M. S.; Yates, B. F.; Canty, A. J.; Ritter, T. *J. Am. Chem. Soc.* **2012**, *134*, 12002.

[19] Chen, M.; Cracuin, R.; Hoffman, N.; Dixon, D. A.; *Inorg. Chem.* **2012**, *51*, 13195..

[20] (a) Kitahama, K.; Frech, R. *J. Chem. Phys.* **1985**, *82*, 720; (b) Wadt, W. R.; Hay, P. J.; *J. Chem. Phys.* **1985**, *82*, 284.

[21] Feller, D. *J. Comp. Chem.* **1996,** *17*, 1571.

[22] Roy, E. L.; Hay, J.; Martin, R. L. *J. Chem. Theory. Comput.* **2008**, *4*, 1029.

[23] (a) Barone, C.; Cossi, M. *J. Phys. Chem. A.* **1998**, *102*, 1995; (b) Barone, C.; Rega, N.; Schimani, G.; Cossi, M. *J. Comput. Chem.* **2003**, *24*, 669.

[24] (a) Ribeiro, R. F.; Marenich, A. V.; Cramer, C. J.; Truhlar D. G. *J. Phys. Chem. B*, **2011**, *115*, 14556; (b) Grimme, S. *Chem. Eur. J.* **2012**, *18*, 9955.

[25] Legault, C. Y. *CYLView*, version 1.0b. http://www.cylview.org, (accessed Aug 1 2012).

[26] NBO 6.0. E. D. Glendening, J. K. Badenhoop, A. E. Reed, J. E. Carpenter, J. A. Bohmann, C. M. Morales, C. R. Landis, and F. Weinhold, Theoretical Chemistry Institute, University of Wisconsin, Madison (2013).

[27] Martinez, R.;Chevalier, R.; Darses, S.; Genet, J. P. *Angew. Chem. Int. Ed*. **2006,** *45*, 8232.

[28] Wang, D.; Izawa, Y.; Stahl, S. S. *J. Am. Chem. Soc.* **2014**, *136*, 9914.

[29] Canty, A. J.; Ariafard, A.; Sanford M. S.; Yates, B. F. *Organometallics*, **2013**, *32*, 544.

[30] (a) Ozawa, F.; Fujimori, M.; Yamamoto, T.; Yamamoto, A. *Organometallics* **1986**, *5*, 2144; (b) Casado, A. L.; Caseras, J. A.; Espinet, P. *Organometallics* **1997**, *16*, 5730; (c) Tan, Y.; Barrios-Landeros, F.; Hartwig, J. F. *J. Am. Chem. Soc.* **2012**, *134*, 3683.

[31] Levin, M. D.; Toste, F. D. *Angew. Chem., Int. Ed*., **2014**, *53*, 6211.

[32] Smith, D. A.; Rosca D. A.; Bochmann, M. *Organometallics*, **2012**, *31*, 5998.

[33] Rosca, D. A.; Smith D. A.; Bochmann, M. *Chem.Commun*. **2012**, *48*, 7247.
[34] Kozuch, S.; Shaik, S. *Chem. Eur. J*. **2011**, *17*, 7623.
[35] Campbell, A. N.; Meyer, E. B.; Stahl, S. S. *Chem. Commun.* **2011**, *47*, 10257.
[36] Poveda, A.; Alonso, I.; Angeles-Fernandez-Ibaanez, M; *Chem. Sci*., **2014**, *5*, 3873.
[37] Reed, A. E.; Weinstock, R. B.; Weinhold, F. *J. Chem. Phys.* **1985,** *83*, 735.
[38] Anslyn, Eric (2004). *Modern Physical Organic Chemistry*. Sausalito, CA: University Science

Chapter 3

DFT studies of the mechanism of '*ligandless*' Pd(II) arylation of N-methyl indole

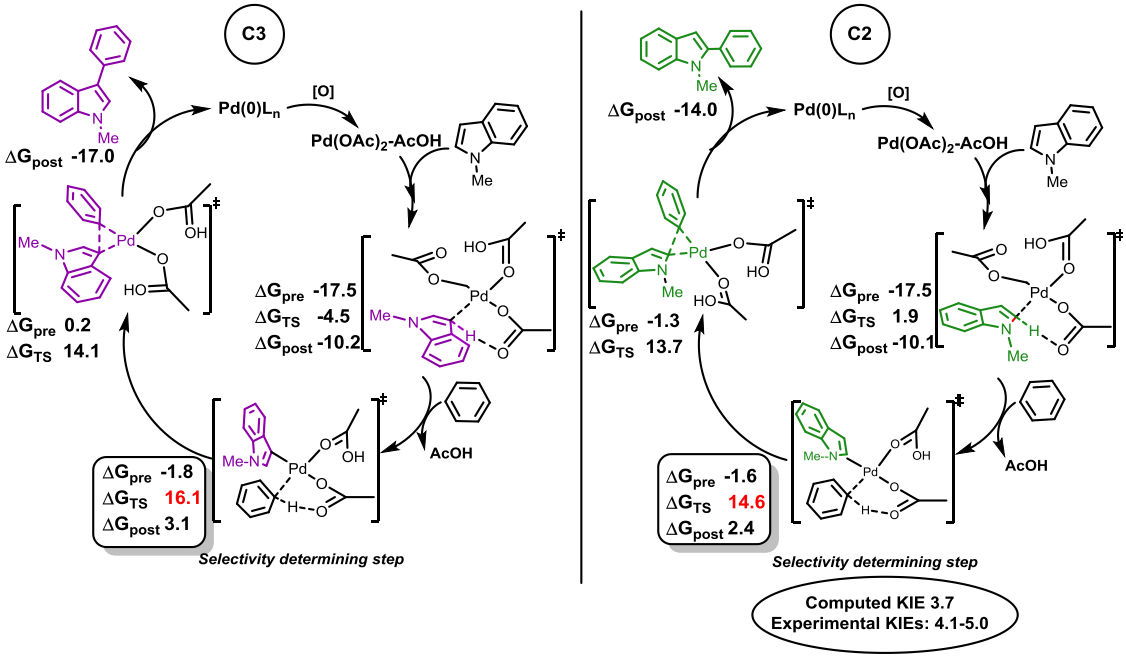

3.1. Introduction

Conventional Pd-catalyzed cross-coupling reactions are widely applied in synthesis to achieve biaryl C-C bond formation. Recent advances in transition metal catalyzed C-H activation[1] reactions have addressed the inherent problems associated with having to pre-functionalize C-H bonds[2] (e.g. by prior halogenation), and have led to the advent of so-called "oxidative" Pd-catalyzed arylation reactions where neither substrate involved in the coupling requires prefunctionalization.

Indole is an important biological motif and is termed as being a 'privileged' scaffold by Evans, signifying its ability to serve as a ligand for different classes of biological receptor.[3] This has further enhanced its role in pharmaceutical drugs which span a wide variety of drug targets including anti-migraine, hypertensive, statins and β-blockers (**Figure 1**). Seven of such indole based FDA approved small molecule drugs appear in the top 200 annual sales/grossing drugs of 2014.[4]

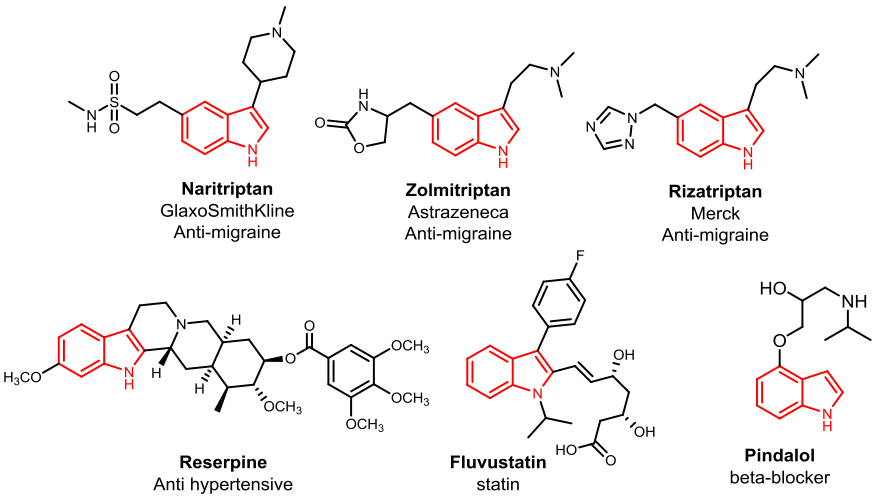

Figure 1. Pharmaceutical drugs with the indole motif.

Thus, functionalization of the indole motif is essential for structural diversification and addition of bioactive functional groups. For N-substituted indoles, the major challenge of such an approach is not just one of reactivity but also the ability to control (or induce) regioselective C-H bond activation. Managing to functionalize this motif in the most benign fashion possible (with respect to temperature and ligands used) allows for numerable benefits (as mentioned in Chapter 1).

Pd-catalyzed direct (with one substrate prefunctionalized, C-X/C-H) and oxidative (neither substrate prefunctionalized, C-H/C-H) arylation of N-substituted indoles in

phosphine free (i.e. 'ligandless') conditions is a topic which has stoked significant interest.[5] Given that functionalization at C2 and C3 positions of indoles is possible and precedented, understanding the factors and the mechanisms which dictate and underpin such regioselectivity is important.

One of the first examples indole C–H bond functionalization was reported by Trost, using stoichiometric Pd(II)-salts in combination with silver(I) tetrafluoroborate to achieve alkenylation.[6] Following Ohta's[7] seminal work on Pd-catalyzed indole arylation, efforts have refocused on refining Pd catalyzed synthetic methods for C2/C3 regioselective arylation. More recently, Sames[8] developed a methodology resulting in preferential C2 arylation of N-methyl indole using $Pd(OAc)_2$ as catalyst (**Figure 2**). The lack of a measured primary C-H kinetic isotope effect (KIE) for this reaction seemed to support a traditional mechanistic view of an electrophilic aromatic substitution (EAS) pathway; the unexpected C2 product was proposed to arise via initial attack at C3, followed by a 1,2 migration of ArPd(II)X. At the same time the authors acknowledged that their data did not preclude the involvement of 'Heck-type' carbopalladation.

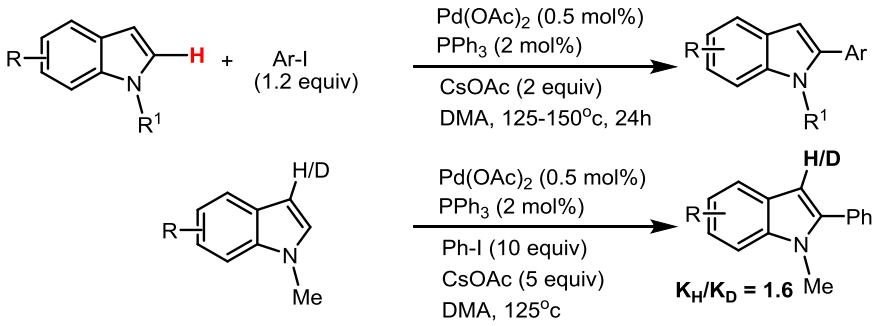

Figure 2. Sames' arylation using direct arylation conditions. A secondary kinetic isotope (KIE) effect was observed.

Subsequently, Gaunt[9] has shown that regioselectivity in Heck reactions of indole may be modulated by altering the solvent used, whilst Larossa[10] and Sanford[11] have now developed milder phosphine free conditions in which C2 arylation occurs at RT. In fact, Hartwig has suggested that Pd:phosphine complexes are not themselves catalytically active in the C-H activations of arenes, and the use of high temperatures may be to necessary to induce dissociation of phosphine to the "ligand-free" or "ligandless" Pd catalyst[12] which may have a broader implication with regards to C-H activation of arenes.

Aromatic C-H activation via a metal promoted transformation is an important step in the functionalization of (hetero)arenes. Experimental and computation has provided insights into Pd catalyzed mechanisms, where simultaneous metalation and intramolecular deprotonation lead to cleavage of an aromatic C-H bond. This mechanism is known commonly as concerted metalation-deprotonation, although some authors have used other names, such as ambiphilic metal-ligand activation (AMLA)[13,23] and internal electrophilic substitution (IES).[14] Davies and Macgregor[15] have provided computational insights with BP86/6-31G(d) into the cyclometallation of DMBA-H by $Pd(OAc)_2$ to show that the reaction proceeds via a three centred agostic M-C-H complex, rather than an expected Wheland Intermediate, thus computation would seem to discount a traditional EAS mechanism (**Figure 3**). This is followed by facile intramolecular H-transfer via a six membered transition state to coordinated acetate acting as intramolecular base, ultimately presenting a picture of ambiphilic palladium acetate. Additional DFT studies have now shown that for many, mostly electron deficient arenes, sp^2 C-H bond functionalization by $Pd(OAc)_2$ occurs via this pathway, now termed Concerted Metalation Deprotonation (CMD). [16,17]

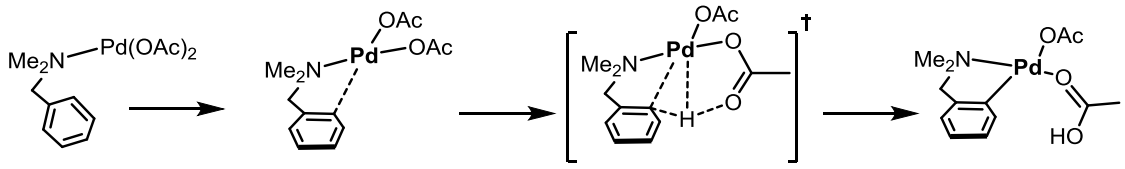

Figure 3. Macgregor's computational insights into the cyclometallation of DMBA-H by $Pd(OAc)_2$. A six membered transition state where palladation and deprotonation occur were found to computationally favoured.

The CMD mechanism is commonly noted as the established route of C-H activation with (Pd catalysts) in (hetero)arenes[45], proceeding via a palladacyclic transition state as proposed by MacGregor. Examples utilizing oxidative arylation techniques have been forthcoming (**Figure 4**). DeBoef has shown that both free indole (i.e. NH-indole) and N-methyl indole can be arylated at C2 in good selectivity using buffered conditions with $Pd(OAc)_2$ as the catalyst and Ag(I)OAc as the terminal oxidant.[18] Similar experimental results illustrating arylation at the C2 position were reported by the Fagnou group, where N-Piv indole coupled selectively at C2 (24:1) in the presence of $AgOAc/Pd(TFA)_2/PivOH$.[19]

It has been suggested (by both Fagnou and DeBoef), that the oxidant (i.e. AgOAc) could partake in the metalation event through a bimetallic Pd-Ag catalytic species.[20] Such precedence for heterometallic dimers is supported by Myers *et al* utilizing Pd-based bimetallic catalytic systems in Heck-type couplings.[21] However, this does not eliminate the possibility of silver acetate acting a reservoir for acetate anions, which could cleave aggregated Pd clusters (e.g. $Pd_3(OAc)_6$ → $Pd_2(OAc)_4$ → $Pd(OAc)_2$), a possibility acknowledged by Fagnou and DeBoef.

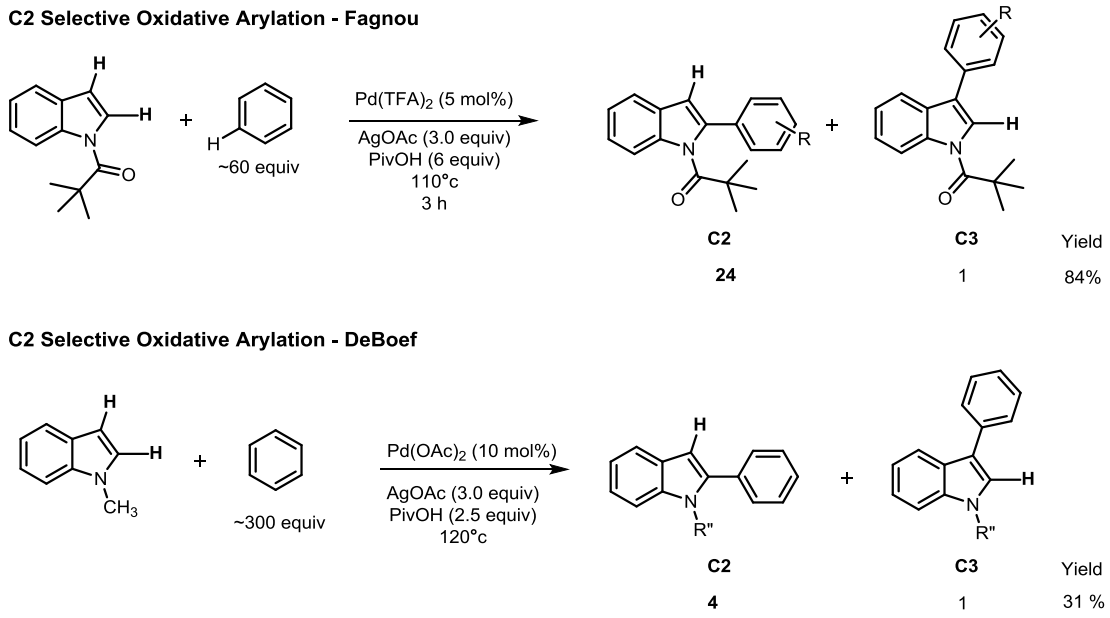

Figure 4. Arylation of C2 position in N-alkylated indoles by the Fagnou and DeBoef.

The mechanistic rationale behind arylation at the C2 position in oxidative arylation reactions is yet to be fully elucidated. However, both authors (in **Figure 4**) have proposed CMD to be important in the activation of the indole. The mechanistic possibilities for activation and arylation at C2 cannot exclude a Heck-type carbopalladation mechanism or an intermolecular S_E3 mechanism, which we have considered in this chapter (**Figure 5**).

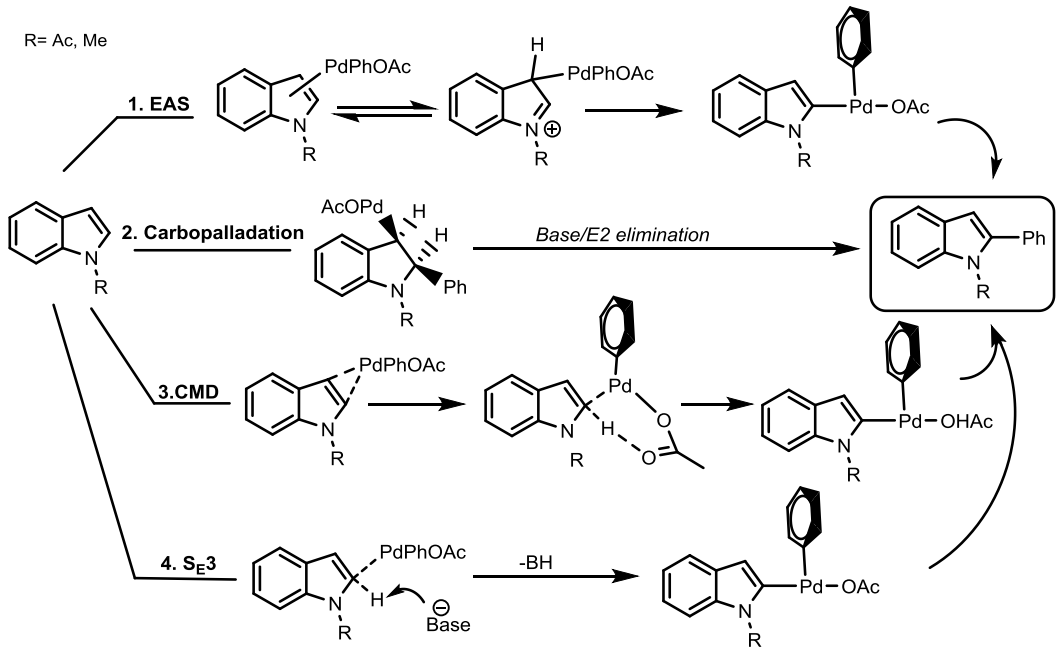

Figure 5. Postulated mechanistic pathways for the arylation of N-methyl indole at C2 using Pd(II)ArX catalytic species.

Despite the importance of indole functionalization, we are unaware of any computational studies rationalizing the C2 regioselectivity observed in Pd-catalyzed C-H functionalization of indoles, and there have been no systematic comparisons of all possible pathways including all steps.[22,23] We have performed this analysis for the steps shown for N-methyl indole in the classically invoked Pd (0)/(II) catalytic cycle for the mechanisms shown (**Figure 6)**.

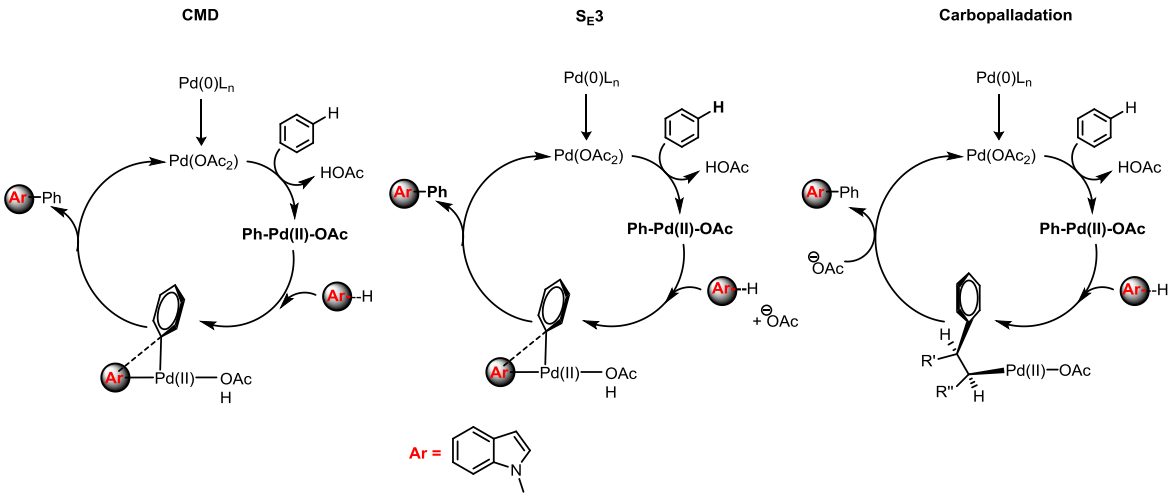

Figure 6. Pd (0)/(II) catalytic cycles investigated computationally in this chapter for N-methyl indole. An alternative set of events where indole is activated first is also examined (not shown). Oxidation from Pd (0) to Pd (II) is not computed.

3.2. Computational methods

The computational protocol used for this chapter follows the methodology presented in section 2.2., Chapter 2. Modifications made to the methodology (for work presented in this chapter) are mentioned herein.

Initial geometry optimizations were performed with the **ω**B97XD functional and split-valance polarized 6-31G(d) basis set for C, N, O and H atoms, whilst the LANL2DZ double-Zeta valence basis set and associated effective core potential (ECP) were used to describe Pd and Ag. Single point energies were computed on all optimized geometries with the larger valence triple-zeta 6-311+G(d,p) and LANL2TZ basis set obtained for Ag and Pd from the EMSL Basis Set Exchange [24,25] A fine grid density was used for numerical integration in all DFT calculations.

The effects of solvent (N,N-dimethlyformamide ε= 37.22 or acetic acid ε= 6.25) were incorporated through the use of a conductor-like polarizable continuum model (CPCM), defining the solute cavity with UFF radii [26] by conducting single point calculations on optimized geometries. Higher level *ab initio* single point calculations (CEPA and SCS-MP2) conducted with the *Orca*[27] program. The CEPA method has been shown to reproduce CCSD benchmarks within a tenth of a kcal/mol[28] whilst improving computational efficiency by up to three orders of magnitude and maintaining high accuracy in calculations of large-scale chemical systems.[29]

All energies presented within this work are Gibbs (ΔG) free energies (calculated against separated reactants unless mentioned otherwise) and calculated via:

$$\Delta G_{solv} = \Delta E_{solv} + (\Delta G_{gas} - \Delta E_{gas})$$

3.3. Results

3.3.1. DFT Benchmarking

Preliminary benchmarking studies were conducted to assess the accuracy of available computational (DFT) methods. Crystallographic data of representative Pd(II) complexes were acquired from the Cambridge Structural Database (CSD).[30] Bond lengths were optimized with B3LYP[31] and the more recently developed **ω**B97XD[32] and functionals were assessed against experimental values (Å) by evaluating Mean Squared Error (MSE) and Maximum Error (Max) (**Figure 7**). Both functionals treat electronic correlation differently. In B3LYP, the Becke 3-term correlation functional is applied to describe correlation, whereas in **ω**B97XD the B97[33] correlation functional treats short range interactions and long range correlation is treated solely with empirical dispersion. Therefore validation of both functionals against experimental data is essential.

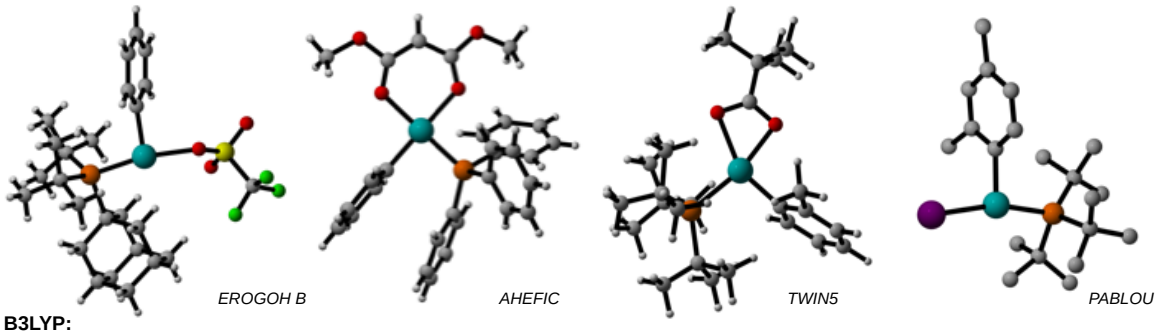

	EROGOH B	*AHEFIC*	*TWIN5*	*PABLOU*
B3LYP:				
MSE	0.083	0.058	0.048	0.079
Max Error	0.10	0.09	0.09	0.12
wB97XD:				
MSE	0.065	0.034	0.033	0.048
Max Error	0.08	0.06	0.05	0.08

Figure 7. Benchmarking structural data against crystallized structures (from CCSD, ID shown) shows ωB97XD is superior to B3LYP is reproducing geometry of various Pd(II) species.

The superior performance by **ω**B97XD over B3LYP can be attributed to the implementation of a long-range dispersion correction in this functional, thus accounting for van der Waals interactions. Norrby[34] showed recently that dispersion is critical to accurately compute the structure of $Pd(PPh_3)_n$, where *n*=1-4 and Dixon has shown dispersion corrected **ω**B97XD to give Bond Dissociation Energies (BDE) within 1.0 kcal/mol of CCSD(T) benchmarks for Pd(II) complexes.[35] All subsequent calculations were thus performed with the **ω**B97XD functional.

Further work to establish $C(sp^2)$-H bond strength in N-methyl indole through calculations applying the composite *ab initio* G3B3 (or G3//B3LYP) computational

method was conducted. We calculated the BDEs for the C-H bonds around the 6,5 ring system (**Figure 8**). Probing the structure, it was evident that there was little disparity between C2 or C3 in terms of bond strength. Notably, the C-H bonds of the C6 ring were predicted to be more amenable thermodynamically to cleavage. Presumably they are less likely to undergo cleavage due to potential loss of aromaticity in the CMD TS. The computed electrostatic potential map (ESP) of N-methyl indole also exhibited large electron localization over the benzene ring and markedly at the C3 position (as expected). Therefore it is evident that the C2 C-H activation is counter intuitive, based on a presumed election deficient Pd(II) catalyst and the inherent electronics of the indole substrate. However, activation and arylation at the C2 position does occur and there is active debate on the factors which influence the mechanism and subsequent arylation at this position.

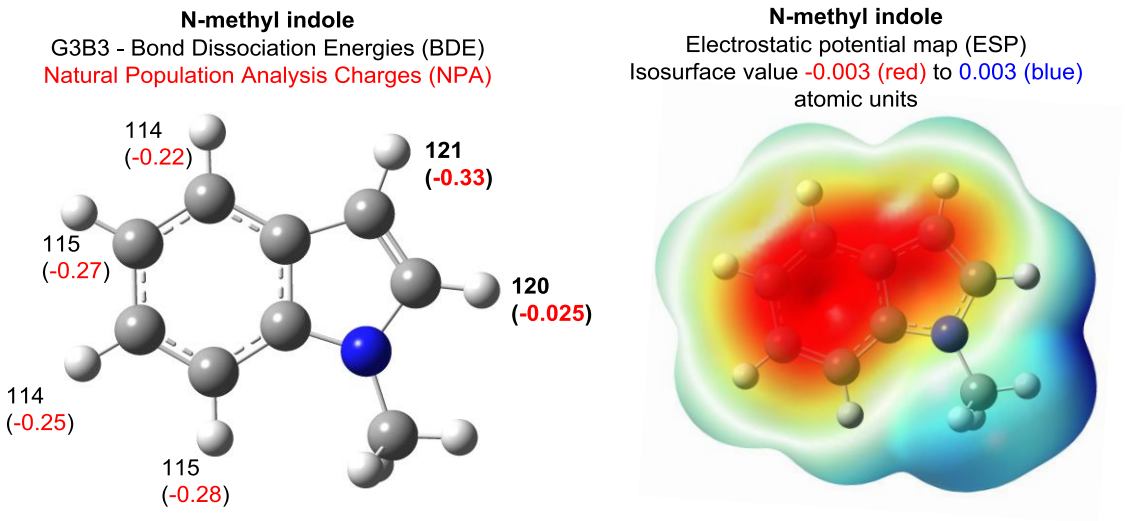

Figure 8. Bond dissociation enthalpies (BDE) displaying the strength of C-H bond (*black*, kcal/mol) and the associated computed natural charge of corresponding C atom (*red*). Electrostatic Potential Map (ESP) exhibiting the electrostatics of N-methyl indole where electron rich regions (*red*) and electron deficient regions (*blue*) are shown.

3.3.2. Model studies: benzene as a prototypical arene

Hartwig's recent experimental work on 'ligandless' 12-electron ArPd(II)X (Ar=Tol, X = OAc, OPiv) and its role in C-H bond activation suggests phosphine dissociation is necessary to form a catalytically competent organopalladium species.[12] This work also discussed the possibility of the phosphine ligand being replaced by a molecule of coordinating solvent; typically N,N'-dimethylformamide (DMF) or N,N'-

dimethylacetamide (DMA) are used experimentally, however, this could extend to other coordinating solvents. Based on these findings, we designed a suitable model system, examining the biaryl coupling of benzene with PhPd(II)OAc under phosphine-free conditions which modelled the reaction via the proposed CMD mechanism supported by Hartwig. Explicit solvent coordination to catalytic arylpalladium species (in this case DMF) was also examined (**Figure 9**). Previous computational work by Fagnou,[36] Maseras[37] and others[38] has suggested that the benzene C-H activation step involves simultaneous cleavage of the C-H bond and formation of a Pd-aryl bond with the catalytic species[1]. This is reflected in **TS_1** where the square planar d^8-Pd catalyst simultaneously forms a Pd–C bond with benzene and the ligated OAc acts as the proton shuttle. **TS_1** ΔG (kcal/mol) of **23.0** for the non-solvated and **25.2** for DMF coordinated Ph-Pd(OAc)-DMF species were obtained, indicating a slight preference for a non-solvated 'ligandless' species to undertake the initial C-H activation step in the CMD mechanism.

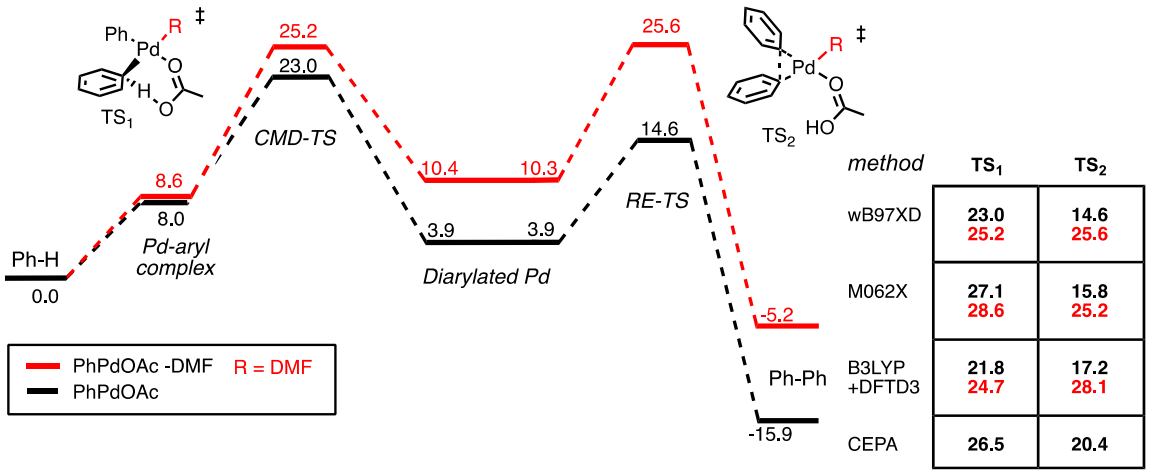

method	TS_1	TS_2
wB97XD	**23.0** **25.2**	**14.6** **25.6**
M062X	**27.1** **28.6**	**15.8** **25.2**
B3LYP +DFTD3	**21.8** **24.7**	**17.2** **28.1**
CEPA	**26.5**	**20.4**

Figure 9. Optimized geometries with the ωB97XD/6-311+G(d,p)/LANL2TZ(f). Single point energies obtained with other functionals are tabulated. All values in kcal/mol. Energies calculated against Ph-H and PdPhOAc, and PdPhOAc-DMF.

Interestingly, for the reductive elimination step there was a sizeable difference in energy between the two proposed catalytic species. The solvent-coordinated species in **TS_2** was unfavourable at 25.6 kcal/mol, in contrast to the non-coordinated alternative,

[1] All previous computational work regarding CMD mechanism regarding indole arylation has been conducted predominantly with B3LYP or equivalent methodology. No literature examples have yet applied the wB97XD functional.

which is kinetically more favourable at 14.6 kcal/mol. Generation of the biaryl product occurs readily from **TS_2**. The process is exergonic (i.e. negative ΔG_{rxn}) thus thermodynamically favourable. Our calculations showed that this 'ligandless' biaryl coupling of benzene via a non-solvated palladium catalyst is faster, with the rate-limiting step being the initial C-H activation consistent with a KIE studies. Hartwig determined experimentally a primary C-H kinetic isotope effect of 5.6 in the closely related reaction of benzene with TolPd(OPiv), suggesting CMD is rate limiting. Similarly Fagnou observed a pronounced KIE for the intramolecular direct arylation of perfluorobenzene.[39] From our calculations only the solvent-free pathway is consistent with this result suggesting that ligandless Pd(II) is capable of being energetically competitive in the cross coupling of arenes. Other DFT methods (M06-2X [40] and B3LYP+DFT-D3[41] dispersion correction) give comparable quantitative and qualitative results. The more demanding coupled pair (CEPA)[42] *ab initio* method of Neese was also examined, which suggests that ωB97XD underestimates the CMD step by 3.5 kcal/mol and the reductive elimination step by 5.8 kcal/mol The CEPA results in particular suggest that the reductive elimination step cannot be neglected completely; with different substrates and conditions it may be possible that this step becomes rate-limiting.

Our computed results are consistent with a primary KIE observed for benzene homocoupling, since the C-H activation step is rate-limiting. Particularly, for more electron rich substrates, such as indoles, we reasoned that a more facile C-H activation could change the relative barrier heights of these two steps.

3.3.3. Catalytic cycle 1: Initial C-H activation of benzene

The presence of 'ligandless' $Pd(OAc)_2$ species in direct arylation reactions is known.[43] Our initial work examined the C-H activation of both benzene and N-methyl indole with a $Pd(OAc)_2$ species (**Figure 10**), more notably, investigating the C-H palladation-insertion step implicit in oxidative C-H cross-couplings as opposed to the traditionally invoked C-X species where the halogenated arene would be the activated species Ar-Pd-X (X= halide).

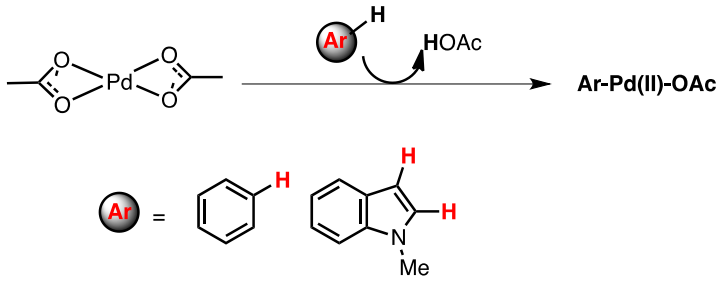

Figure 10. Putative C-H activation with ligandless palladium (II) diacetate resulting in heteroatomic oxidative arylation of benzene and N-methyl indole.

We examined Pd catalyzed activation of indole/benzene in a competitive energy profile. The initial C-H activation/palladation can theoretically occur at either of the two substrates in a one-pot experiment, with both substrates undergoing successive palladation/C-H activation events at the same palladium centre.[44] Our attempts to locate an EAS TS for both benzene and N-Me indole through PES geometry scans resulted in stable ground state structure, presumably as the $Pd(OAc)_2$ catalyst was unable to exert enough electrophilic character in order to produce a Wheland intermediate (**Figure 11**). Similar results were attained with cationic species Ar-Pd^+, thus claims of a cationic species incurring a faster palladation (via EAS mechanism) could not be substantiated by DFT.

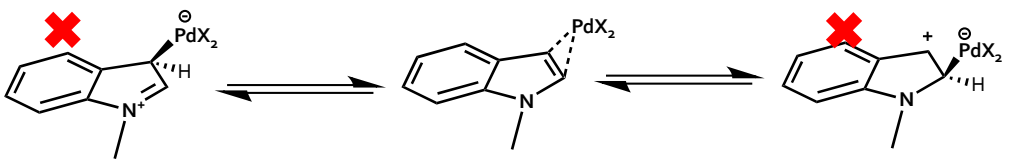

Figure 11. DFT calculations disfavoured Wheland type intermediates and instead produced a stable Pd-indole/ Pd-benzene ground state complex.

Recently, Gorelsky has studied the CMD mechanism computationally for a multitude of heteroarenes as an alternative mechanism for C-H activation.[45] The CMD mechanism is a unimolecular process, proceeding via η^2 coordination of Pd(II) with the π system of benzene. This step is subsequently followed by the simultaneous palladation and proton abstraction from the arene/aryl species facilitated by the acetate ligand. The carboxylate ligand switches from bidentate to monodentate coordination on the Pd centre, reorienting itself to form a six membered palladacyclic transition state, capable of behaving as a proton shuttle. We examined the mechanism (**Figure 12**) for the C-H activation of benzene (**1**) followed by C-H activation at N-methyl indole (**2**) and the creation of the arylated indole through a reductive elimination (**3**) mechanism which completes the catalytic cycle.

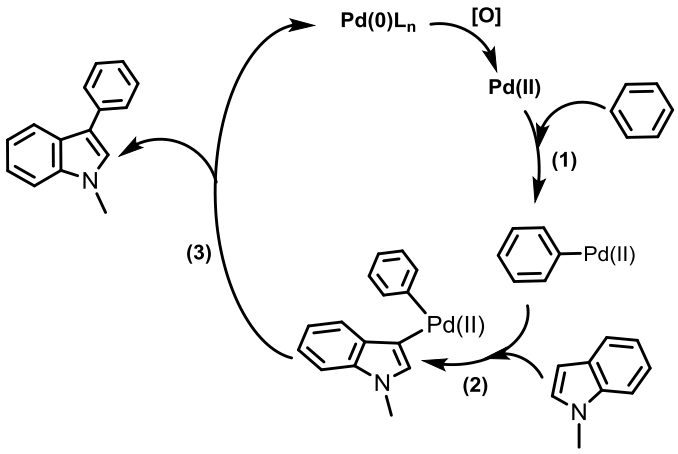

Figure 12. Calculated catalytic cycle via CMD mechanism. Oxidation of Pd(0) to Pd(II) was not modelled. Cleavage of the C-H bond in benzene (**1**) is calculated with a variety of Pd(II) catalysts in this section.

Our investigation assessed a variety of Pd(II) species as possible catalytic species (in a CMD mechanism) including both bimetallic and monomeric Pd species, thus examining which would be the most favourable at initiating C-H activation of benzene (**Figure 13**). A $Pd_2(OAc)_4$ and $PdAg(OAc)_3$ dimer were also calculated as potential catalytic species, to examine the possibility of such dimers undertaking C-H activation (as suggested by Fagnou and DeBoef). Recent computational work by Schaefer and Sunoj[46] has shown that silver(I) acetate (AgOAc) is non-innocent in the Pd catalyzed activation of arenes and assists in lowering C-H activation energy via a co-operative Pd-Ag catalyst (via CMD) and therefore this possibility cannot be ignored.

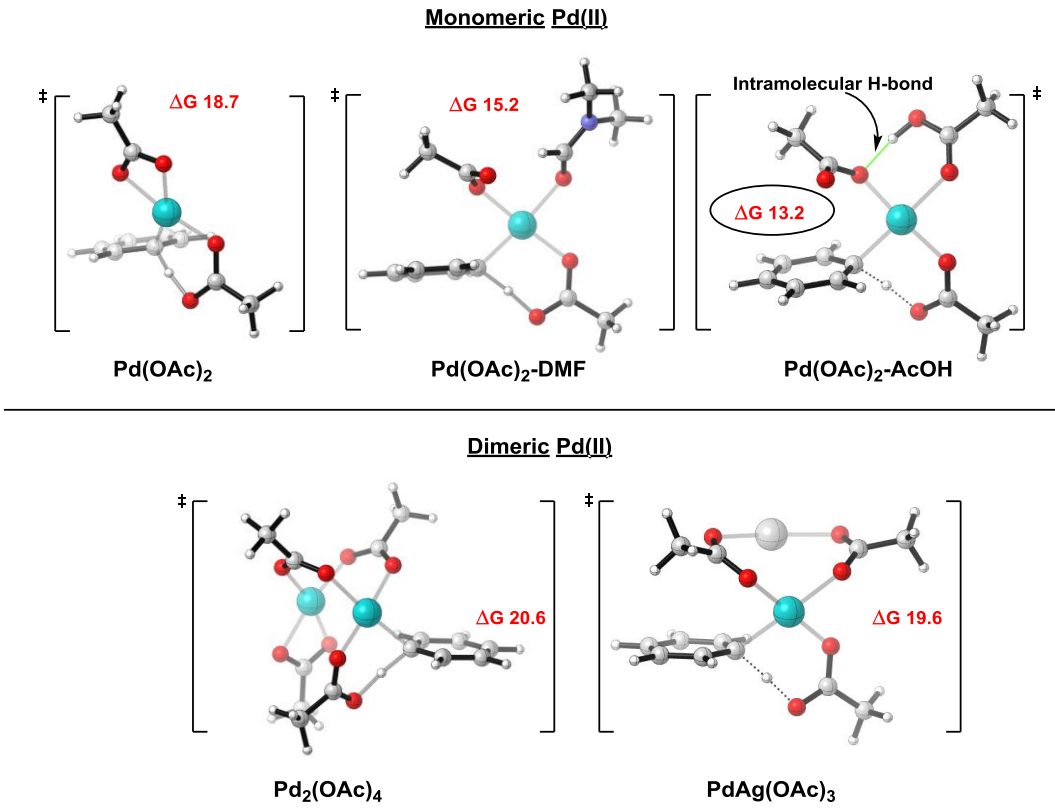

Figure 13. Intramolecular deprotonation (CMD) mechanism for benzene with monomeric Pd catalyst (*top*) and bimetallic Pd catalyst (*bottom*). Geometry optimizations conducted at ωB97XD/6-31G(d)/LANL2DZ, which is consistent in all cases within Chapter 3 (unless otherwise stated). All values in kcal/mol and relative to separated reactants.

Within the studied catalytic species, $Pd(OAc)_2$-AcOH (model system for PivOH) gave the lowest C-H activation energy (i.e. Gibbs free energy against separated reactants) at ΔG 13.2 kcal/mol and exhibited an intramolecular H-bonding network between the AcOH and OAc^- ligand. Acetic acid coordination also lowered the Gibbs free energy compared to $Pd(OAc)_2$ (Δ18.7 kcal/mol) by 5.5 kcal/mol.

$Pd(OAc)_2$-DMF(ΔG 15.2 kcal/mol) is calculated to be 3.5 kcal/mol lower in the C-H activation of benzene versus the C-H activation of benzene with $Pd(OAc)_2$. This is in agreement with a recent computational study examining the solvent-assisted $Pd(OAc)_2$ catalyzed CMD step of arene alkoxylation, where polar solvent coordination (methanol) to Pd proved important in creating a favourable TS for intramolecular C-H cleavage through a monomeric $Pd(OAc)_2$ species.[47]

Dimeric $Pd_2(OAc)_4$ (ΔG 20.4 kcal/mol) produced a higher TS for C-H bond cleavage of benzene compared to all monomeric Pd(II) species (solvated and ligandless). The

possibility of a heterometallic dimer - in the form of $PdAg(OAc)_3$ was also calculated to be higher in energy for the C-H activation step than monomeric catalytic species. Bimetallic C-H activation of benzene with $PdAg(OAc)_3$ (ΔG 19.6 kcal/mol) was located on the PES, however, the Ag(I)OAc is unlikely to participate directly in the activation of benzene through a bimetallic catalyst according to our calculations, where monomeric species are more competitive. As such, dimeric/bimetallic catalysts are unlikely to be favoured in the initial C-H activation of benzene and calculations suggest that monomeric Pd species are more likely to elicit C-H bond cleavage, with $Pd(OAc)_2$-AcOH giving the lowest energy for C-H activation, suggesting that in buffered conditions the association of acid may stabilize the TS through an intramolecular H-bonding network (as seen in **Figure 13**). Furthermore, the experimental conditions may disfavour initial aggregation of Pd species due to concentration effects associated with low catalytic loadings.

3.3.4. Catalytic cycle 1: Oxidative arylation of N-methyl indole

3.3.4.1. 'Ligandless' $Pd(OAc)_2$

From initial calculations it is observed that C-H activation of benzene is likely to occur via a monomeric Pd catalyst. We chose to compute both 'ligandless' $Pd(OAc)_2$ and 'ligated' (i.e. $Pd(OAc)_2$-DMF or $Pd(OAc)_2$-AcOH) pathways as a route to C-H activation of benzene and subsequent arylation of indole. Our initial calculations focus on a ligandless pathway where initial benzene activation occurs with $Pd(OAc)_2$.

Our calculations show that an indole-Pd(II) complex (**IL_1**) would be more stable (ΔG -8.8 kcal/mol) as a precomplex than a competing benzene-Pd(II) precomplex (**BL_1**) within the reaction (**Figure 14**), where the Pd catalyst is η^2 to the π bond in the 5-membered pyrrole ring in indole. This is presumably due to the electron rich nature of the indole stabilizing the Pd-Ar complex more than benzene.

Thus, we predict that the indole-Pd(II) complex (**IL_1**) is the resting state of the catalyst and in order to activate benzene two preliminary steps are a requisite, (1) dissociation of indole from the stable precomplex, **IL_1** (2) Association of Pd catalyst to π system of benzene, **BL_1**. This is an energetically intensive process (ΔG 8.7 kcal/mol). However, it is required to be, in order to create **BL_1**, which is the precursor to the C-H activation TS, **BL_TS** (ΔG 18.7 kcal/mol).

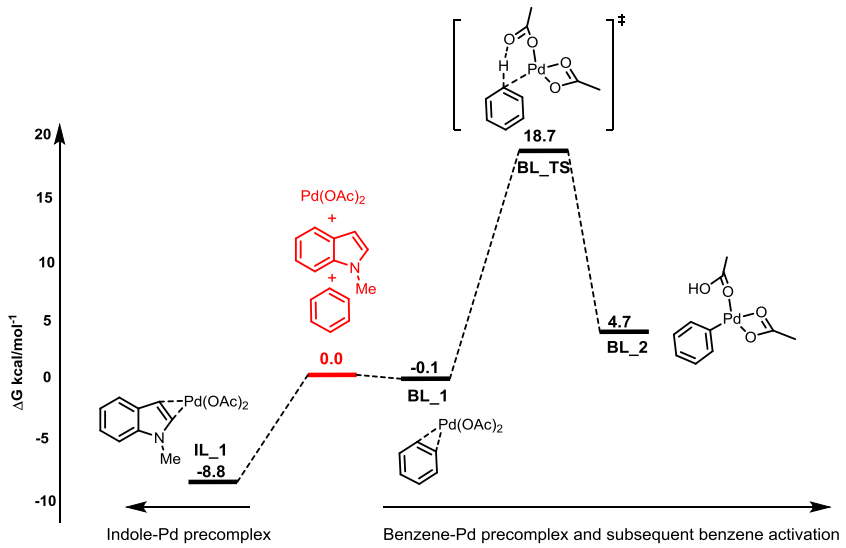

Figure 14. Initial $Pd(OAc)_2$ precomplex is shown to be more favourable for indole, however for benzene activation precomplex **BL_1** must be formed, which requires energy from the resting state, **IL_1**. All values in kcal/mol.

The TS (**BL_TS**) proceeds through a six membered CMD mechanism described in the previous section. Upon deprotonation a new square planar, Pd(II) species is generated, **BL_2** (ΔG 4.7 kcal/mol) which will act as the catalytic species in the activation of indole in the next step of the reaction. Following the initial CMD activation, a new Pd-aryl catalytic species of the form Ph-Pd(II)-OAc can be created via dissociation of acetic acid from **BL_2**. A vacant coordination site on Pd for the coordination of N-methyl indole is now available, proceeding via a kinetically favourable pre-complex **Pre_1** (ΔG -6.7 kcal/mol) where η^2 coordination of PhPd(II)OAc with the C2-C3 π system is observed (**Figure 15**). Subsequent palladation/C-H activation is significantly more favoured for C3 (**C3_CMD1**: ΔG 15.8 kcal/mol) as opposed to C2 (**C2_CMD1**: ΔG 20.0 kcal/mol).

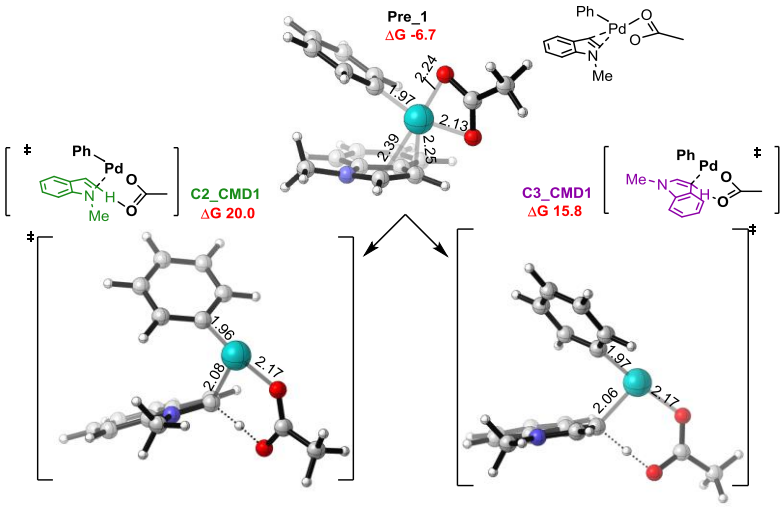

Figure 15. C-H bond cleavage of C2 (*left*) and C3 (*right*) positions on N-methyl indole. Activation is favoured at the electron rich C3 position. All values in kcal/mol. All bond lengths in Å.

A reversal in kinetic preference is observed in the reductive elimination event, where the reaction proceeds via a three coordinate, three centred non-polar, non-radical mechanism (**Figure 16**). The Ph group and N-methyl indole assume *cis* coordination on the Pd(II) centre, concomitant to the RE TS, which proceeds via a tricoordinate 14 electron Pd species. The C-C bond forming reaction for C2 (ΔG 17.4) proceeds with a more favourable Gibbs free energy profile than C3 (ΔG 19.6) thus providing the C2 and C3 arylated N-indole products, with the C3 product thermodynamically preferred (C3:ΔG -10.9 kcal/mol, C2: ΔG -9.8 kcal/mol). Interestingly if the mechanism was to proceed via a selectivity determining reductive elimination, the initial C-H activation of N-methyl indole (i.e. Activation 2) would be required to be reversible.

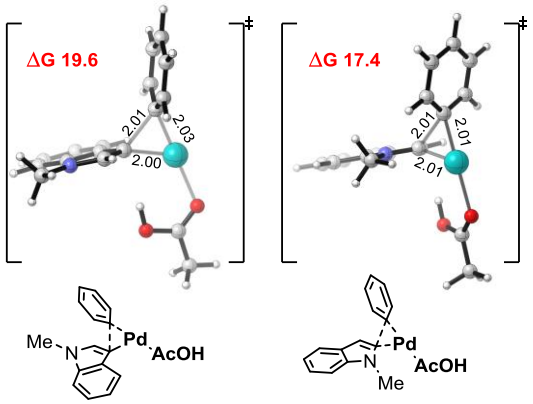

Figure 16. Reductive elimination TS for the C-C bond formation of arylation at C2 (*right*) and C3 (*left*). All values in kcal/mol. All bond lengths in Å.

Through this set of mechanistic events, C2 selectivity is observed in the reductive elimination TS. However, the steps preceding reductive elimination in the reaction for C2 arylation are slower (observing the energetic span model) giving an overall ΔG of 28.8 kcal/mol (from **IL_1** to **C2_CMD1**). It is therefore unlikely that C2 arylation would be imparted via this pathway (**Figure 17**).

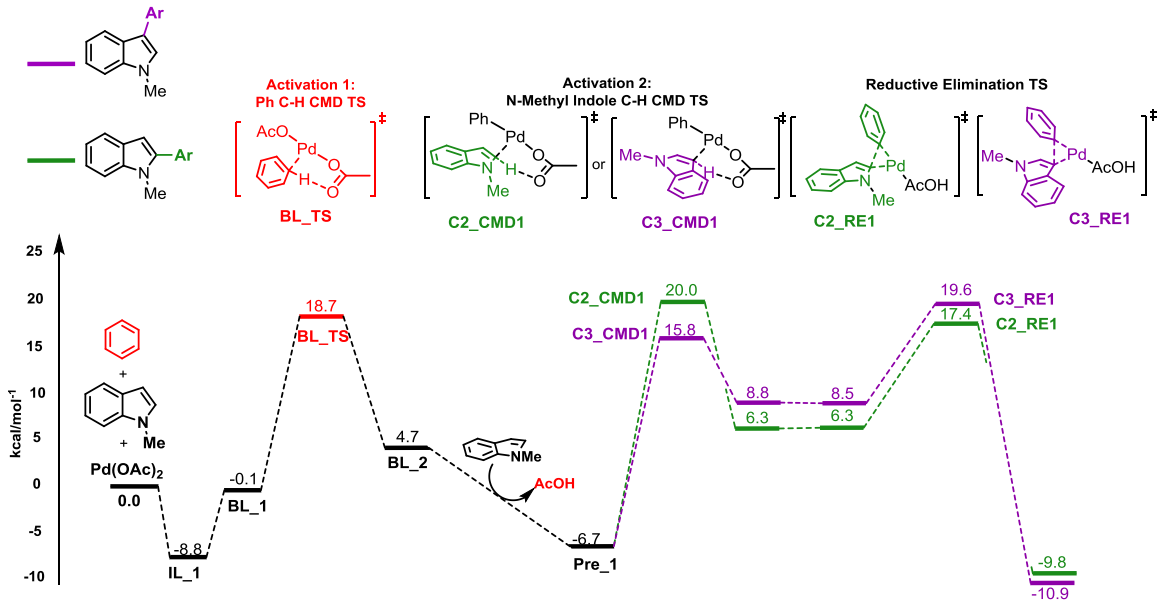

Figure 17. ωB97XD/6-311+G(d,p) computed free energy profile (kcal/mol) for the initial C-H activation of benzene followed by C-H activation on N-methyl indole. All values in kcal/mol.

3.3.4 2. $Pd(OAc)_2$-DMF

The active Pd (II) catalytic species can be susceptible to solvent coordination and therefore this cannot be completely neglected. Solvent molecules can potentially coordinate to a vacant coordination site on $Pd(OAc)_2$ (this would involve one acetate ligand to change coordination from bidentate to monodentate), thus saturating all coordination sites on square planar Pd and creating a four coordinate, 16 electron Pd(II) species. Coordination with DMF can occur through the in-plane lone pair which is *trans* to the NMe_2 group. Therefore we focused on determining the energy profile using $Pd(OAc)_2$-DMF as the catalytic species.

As in the previous section, the catalytic resting state with $Pd(OAc)_2$-DMF favours an indole-Pd species, **IP_1** (ΔG -10.5 kcal/mol) which is predicted to be the resting state via this pathway (**Figure 18**). The benzene precomplex, **BP1,** which is concomitant to the C-H activation TS, **BP_TS**, requires 11.0 kcal/mol from **IP_1** to **BP_1** to affect dissociation of indole and coordination of benzene. This creates **BP1** (ΔG 0.5 kcal/mol) where the Pd(II) species coordinates to the π system of benzene. The C-H activation of benzene occurs through the CMD mechanism proceeding via a six membered palladacyclic transition state, **BP_TS** (ΔG 15.2 kcal/mol). In order to elicit C-H activation of benzene the energetic span from resting state, **IP_1,** to C-H activation TS **BP_TS,** is calculated at 25.7 kcal/mol.

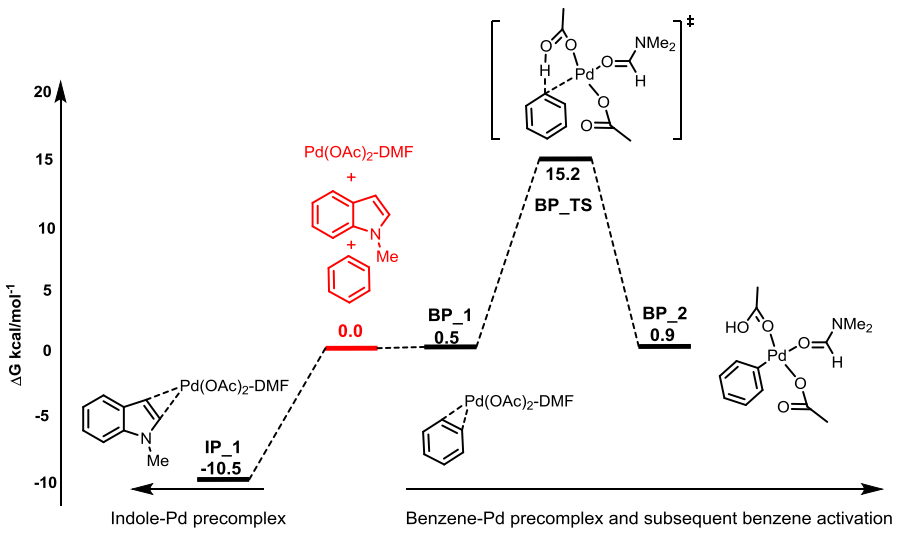

Figure 18. Initial $Pd(OAc)_2$-DMF precomplex is shown to be favourable for indole. **IP_1** is the calculated resting state. All values in kcal/mol.

Following the activation of benzene, a 16 electron square planar complex, **BP_2** (ΔG 0.9 kcal/mol) is created. The dissociation of a neutral ligand is required in order to open a coordination site on Pd(II) for the subsequent C-H activation event on N-methyl indole (Activation 2). Either DMF or AcOH could dissociate from **BP_2**. As we are examining the effect of DMF, AcOH dissociation was assumed, producing the active catalytic species PhPd(II)OAc-DMF. This coordinates to N-methyl indole in precomplex **Pre_2** (ΔG -7.7 kcal/mol) (**Figure 19**), where PhPd(II)OAc-DMF catalyst coordinates η^2 with the C2-C3 π system of N-methyl indole. In **Pre_2**, the C(3)-Pd bond distance (2.22Å) is shorter than the C(2)-Pd bond distance (2.39 Å), signifying preference of Pd coordination at the C3-position due to the electron localization inherent to C3. The C-H activation of N-methyl indole results in a markedly lower energy (compared with $Pd(OAc)_2$) for both C2 TS, **C2_CMD_P** (ΔG 12.7 kcal/mol) and C3 TS, **C3_CMD_P** (ΔG 10.1 kcal/mol).

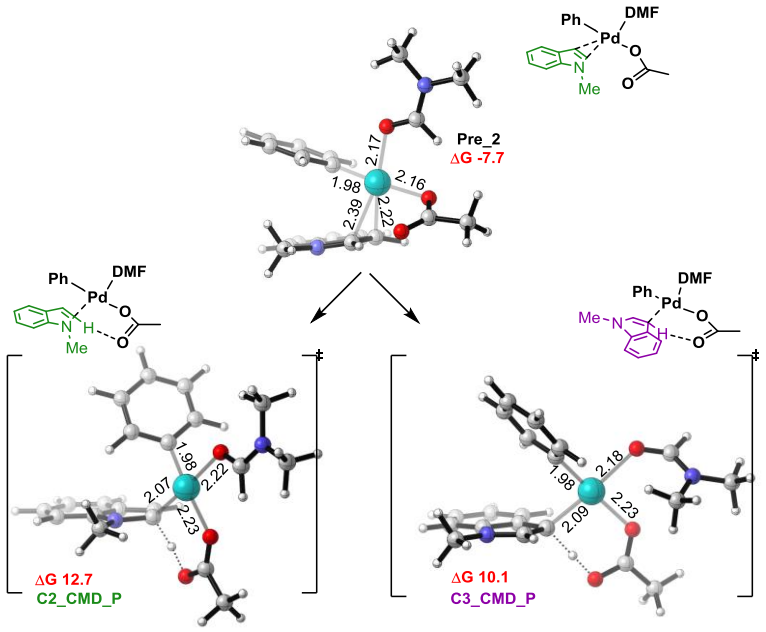

Figure 19. Initial C-H activation of N-methyl indole with DMF solvent coordination of Pd(II) catalyst. All values in kcal/mol. All bond lengths in Å

In both cases however, ($Pd(OAc)_2$-DMF and $Pd(OAc)_2$), the initial activation of N-methyl indole is favoured at C3. This activation proceeds via an endergonic reaction profile for both C2 and C3, with an energetically stable intermediate produced for C2 (ΔG 0.5 kcal/mol) post CMD, whereas the intermediate at C3 is relatively higher in energy (ΔG 4.5 kcal/mol). These intermediates are the precursor to the reductive elimination TS (**Figure 20**). Reductive elimination TS energies for C2, **C2_RE_P** (ΔG

17.4 kcal/mol) and C3, **C3_RE_P** (ΔG 19.4 kcal/mol) show minimal change in Gibbs free energy from the tricoordinated, non-solvated RE TS energy (observed in $Pd(OAc)_2$). Coordination of DMF to create four-coordinate 16 electron arylpalladium(II) RE TSs (i.e. **C2_RE_P** and **C3_RE_P)** are almost equally as competitive as 14 electron, three coordinate counterpart observed in the ligandless $Pd(OAc)_2$ system. This is noteworthy, as a square planar 16 electron Pd species would likely be more stable of the two, and presumably require more energy to lose a two electron σ donor, than a three coordinate 14 electron species.

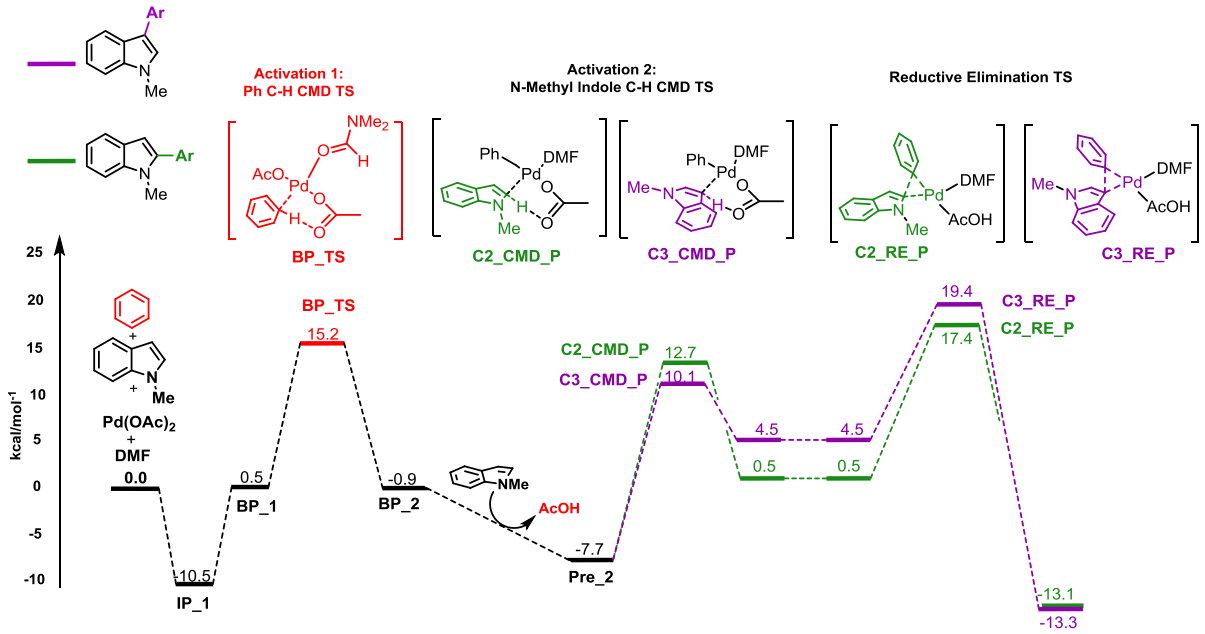

Figure 20. ωB97XD/6-311+G(d,p) computed free energy profile (kcal/mol) for the initial C-H activation of benzene followed by C-H activation of N-methyl indole with explicit solvation of (DMF). All values in kcal/mol

Regardless, both solvated/non-solvated systems where benzene activation occurs first display experimentally observed C2 selectivity to be imparted via the reductive elimination TS. In this reaction pathway, the energetic span from precomplex to the highest energy TS (for C2) is calculated to be 27.9 kcal/mol, from **IP_1** (ΔG -10.5 kcal/mol) to **C2_RE_P** (ΔG 17.4 kcal/mol), which is also the slow step in this pathway.

The calculated selectivity via this slow, selectivity determining reductive elimination step is calculated to be 97:3 (C2:C3), with the calculated $\Delta\Delta G^{\ddagger}$ between reductive elimination TSs of 2.0 kcal/mol. This computed selectivity is similar to that observed experimentally by Fagnou of 24:1. (i.e. 96:4 between C2:C3). The experimentally observed selectivity of Deboef (4:1) would require $\Delta\Delta G^{\ddagger}$ barrier to be 1.2 kcal/mol.

3.3.4.3. $Pd(OAc)_2$-AcOH

Oxidative arylation reactions of N-indoles are commonly conducted in acidic conditions (i.e. PivOH or AcOH is used). Therefore we examined an AcOH explicit coordination pathway where a molecule of acetic acid could coordinate to the vacant site of Pd. Our initial calculations (earlier in section 4.1) suggested that C-H activation of benzene with $Pd(OAc)_2$-AcOH is the most energetically preferred TS of all Pd(II) species studied. The resting state of the catalytic system was calculated to favour an indole-Pd complex (**INP_1**). The span between the low energy resting state at **IP_1** (ΔG -17.5 kcal/mol) to benzene activation, **BNP_TS** (ΔG 13.2 kcal/mol) suggests activation of benzene maybe difficult with an energetic span of 30.7 kcal/mol (**Figure 21**).

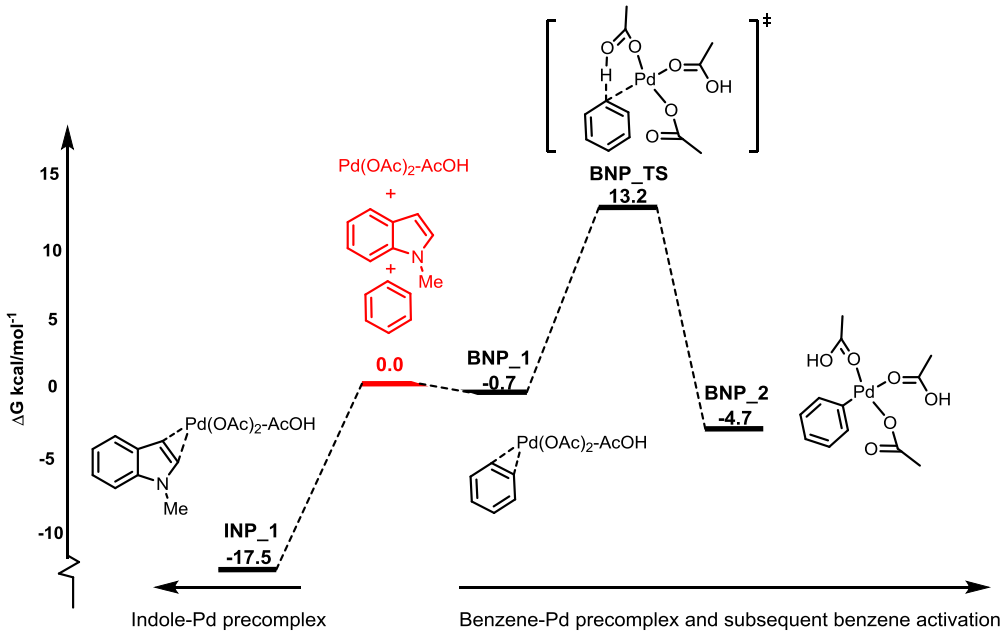

Figure 21. Initial $Pd(OAc)_2$-AcOH precomplex is shown to be more favourable for indole, however for benzene activation precomplex BNP_2 is required to be formed. All values in kcal/mol

If the initial barrier to activation of benzene is surmounted, the reaction proceeds through a kinetically favoured pre-complex, where the coordination of AcOH produces an energetically stable precomplex, **Pre_3** (ΔG -13.0 kcal/mol). The precomplex benefits from an intramolecular hydrogen bond (O-H---O), between the hydrogen on AcOH and a lone pair on oxygen of the OAc ligand *cis* to it. The C-H bond cleavage of the C3 position, **C3_CMD_NP** (ΔG 5.5 kcal/mol) is energetically favoured opposed to C2, **C2_CMD_NP** (ΔG 9.0 kcal/mol). The reaction profile therefore displays the same

trend as ligandless and polar solvent coordinated reaction pathways for the C-H activation of N-methyl indole (**Figure 22**).

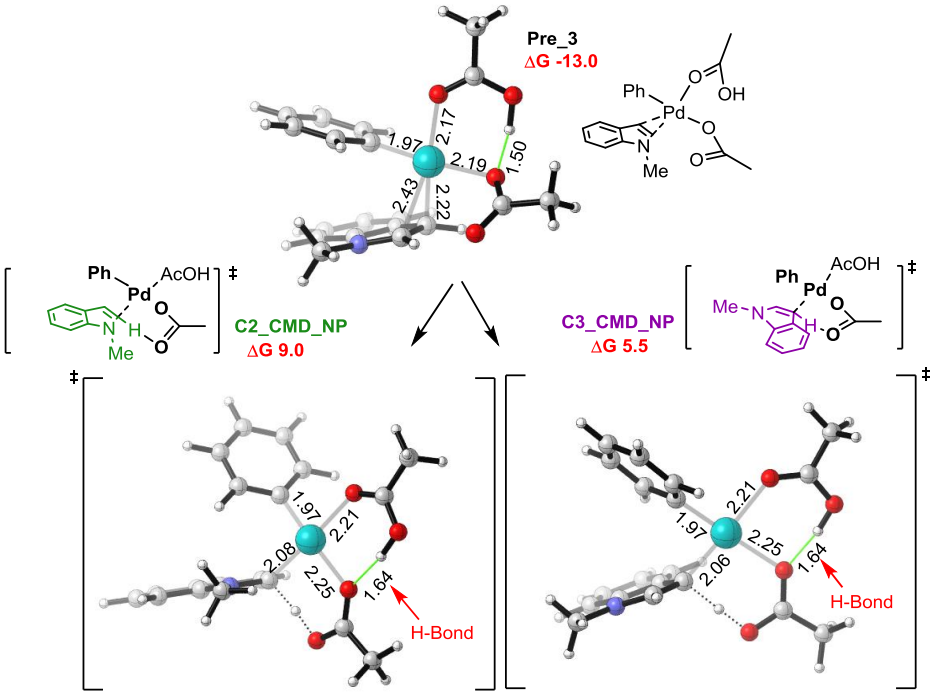

Figure 22. Initial C-H activation of N-methyl indole with AcOH- solvated Pd(II) catalyst. In **Pre_3**, there is a shorter bond distance for C-3 coordination. All values in kcal/mol

Therefore, irrespective of catalytic species, the initial C-H activation is calculated to be preferred at C3. Interestingly, a selectivity determining C2 selective reductive elimination TS is also evident in all three pathways studied. Here the $\Delta\Delta G^{\ddagger}$ between C2 and C3 RE TS is 0.4 kcal/mol in the AcOH assisted pathway, 2.0 kcal/mol in DMF assisted pathway, and 2.2 kcal/mol for the ligandless pathway in favour of C2 selectivity. Reductive elimination at C3 (ΔG 14.1 kcal/mol) is calculated to be difficult to surmount if observing the energetic span model (**Figure 23**). This would require 31.6 kcal/mol to proceed from resting state **INP_1** to reductive elimination **C3_RE_NP**. The span is lower for C2 (i.e. **INP_1** to **C2_RE_NP**) at 31.2 kcal/mol.

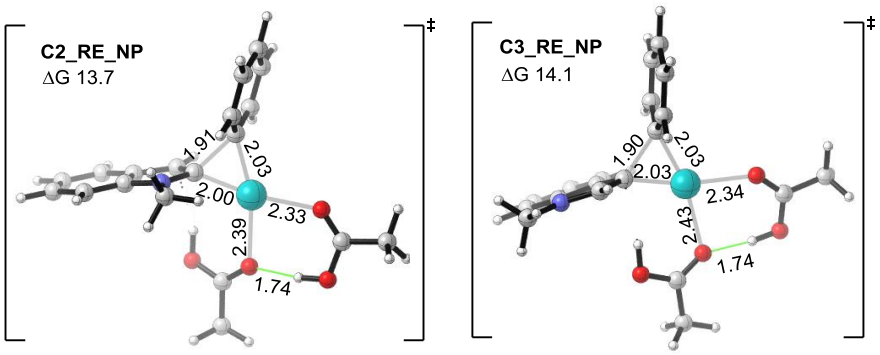

Figure 23. Reductive elimination TSs for AcOH assisted pathway at C2 and C3. Energies in kcal/mol. Bond lengths in Å

Fagnou's oxidative arylation of N-Piv indole displayed 24:1 selectivity to C2:C3 arylation (i.e. 96:4). This selectivity is not mirrored in our calculations (modelling reductive elimination as the selectivity determining step) as the $\Delta\Delta G^{\ddagger}$ between C3 and C2 of 0.4 kcal/mol results in selectivity for C2:C3 product at 67:33. To replicate the selectivity observed by DeBoef *et. al*. of 4:1 (C2:C3) the $\Delta\Delta G^{\ddagger}$ would have to be 1.2 kcal/mol. The pathway displays better agreement with DeBoef's oxidative arylation; however the energetic span between the resting state, **INP_1**, and selectivity determining TS, **C2_RE_NP** of 31.2 suggests that this pathway would be rather sluggish.

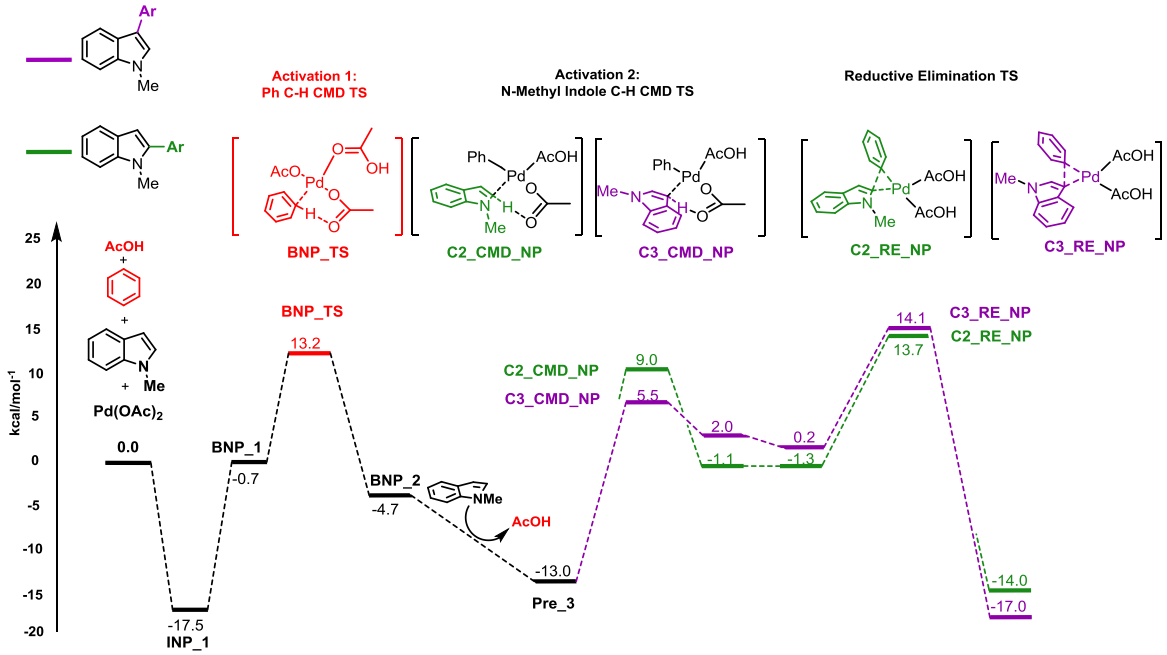

Figure 24. ωB97XD/6-311+G(d,p) computed free energy profile (kcal/mol) for the initial C-H activation of benzene followed by C-H activation of N-methyl indole incorporating the explicit solvation of acetic acid (AcOH).

3.3.5. Summary of catalytic cycle 1

According to our calculated catalytic cycles, the explicitly solvated pathways (i.e. DMF or AcOH assisted) display C2 selectivity as a result of a selectivity determining reductive elimination step. This reductive elimination step is also calculated to be the slowest step (observing the energetic span model). Inclusion of solvent molecules is important in the reproduction of experiment selectivities. Further examination reveals that enhanced stability of the intermediate (or precursor) species prior to the reductive elimination TS assists in producing a lower energy reductive elimination TS. To understand why this is the case we have considered the relative stabilities and the bonding in the palladated indole intermediates. In Figure 25, we show that the greater stability of palladated C2-intermediate is a result of a stronger C-Pd bond. This is supported by BDE calculations showing larger (i.e. stronger) values for the C2 intermediates, with the difference in BDE values resulting from stronger C-Pd bond strengths by 1.4 to 1.9 kcal/mol (**Figure 25**).

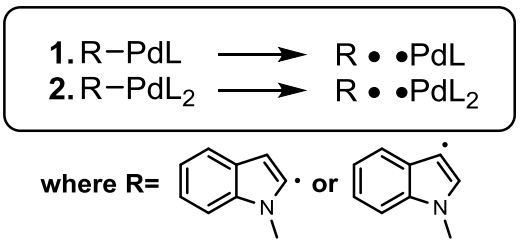

Species	ΔG(kcal/mol)	BDE radical stability
1.C2 RE precursor $Pd(OAc)_2$	6.3	**72.6**
1.C3 RE precursor $Pd(OAc)_2$	8.5	71.2
2.C2 RE precursor $Pd(OAc)_2$-DMF	0.5	**89.4**
2.C3 RE precursor $Pd(OAc)_2$-DMF	4.5	87.5

Figure 25. Radical stability of pre-reductive elimination intermediates of N-methyl indole conducted through homolytic bond cleavage. The radical is more stable at the C2 intermediate. All values in kcal/mol. Calculations conducted at uωB97XD/6-31G(d)/LANL2DZ.

To further understand this difference in bond strengths we considered the intrinsic electronic polarization of the C-Pd bond and that in other metalated indoles. A broader study of substituted indoles, spanning electron donating and electron withdrawing

groups (substituents analyzed include Ag, Au, Cu, K, Li, Na, Cs and PdCl) was conducted to assess the energy difference between C3 and C2 substituted indoles. We find that the preference for the C2-metalated isomer over the C3-form increases as the electronegativity of the metal decreases (and indeed is linearly correlated, R2 = 0.89). This trend reflects the greater ability for the C2-position of indole to stabilize a partial negative charge. (**Figure 26**). In the case of palladation, polarization in the sense C(δ^-)--Pd(δ^+) drives the preference for the formation of the more stable C2 intermediate. Inductive electron withdrawal by the adjacent nitrogen atom is the likely cause. Thus, in respect of C-H activation, N-Me indole displays a *kinetic* preference for C3 reactivity due to greater π-electron density, and a thermodynamic preference for the C2-palladated intermediate (leading to preferential reductive elimination of this isomer). The contrasting kinetic and thermodynamic preference towards palladation seen in our calculations demonstrates the importance of understanding mechanism to account for and predict regioselectivity.

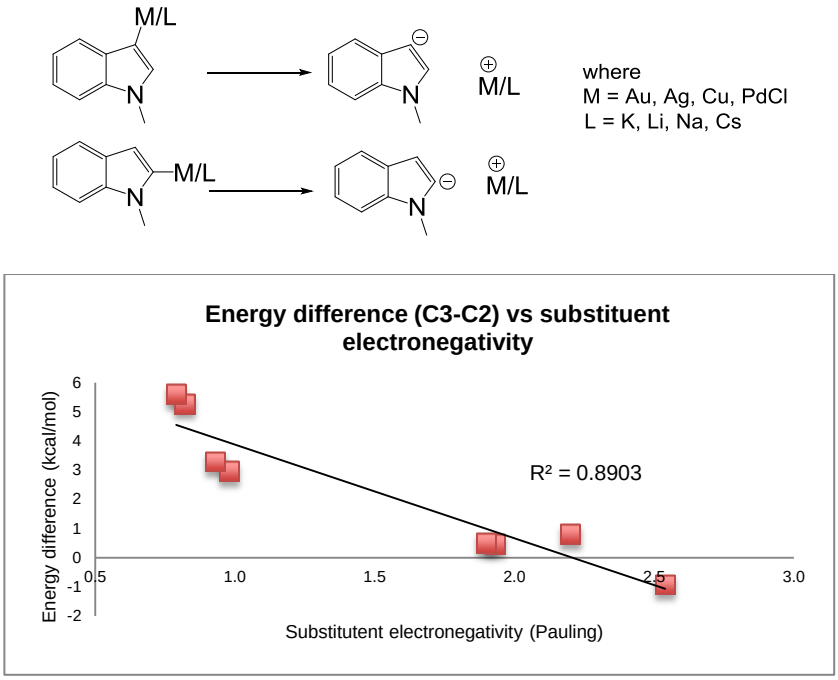

Figure 26. Correlation of energy difference (kcal/mol) and the substituent electronegativity in the stabilizing of C3 and C2 substituted N-methyl indole.

Our calculations indicate oxidative arylations are C2 selective as a result of the reductive elimination TSs, where experimentally observed selectivity is calculated to be corroborated in good agreement with Fagnou's arylation in the DMF and ligandless

mechanism. The selectivity in $Pd(OAc)_2$-AcOH mechanism via the reductive elimination TS is more akin to that observed by DeBoef, where calculated selectivity (C2:C3, 67:33) is close to experimentally observed selectivity of (C2:C3 80:20).

It is known that C-H activation can be reversible (as noted in chapter 2), therefore this proposed catalytic cycle is feasible. The energetic span for the DMF ligated mechanism is 27.9 kcal/mol for the major product; at the typical reaction temperature of 120ºC this correlates to a reaction half-life (TST) on the order of 5 minutes demonstrating the feasibility of this mechanism. We acknowledge that the reductive elimination transition state maybe overstated by the ωB97XD functional by ~5 kcal/mol when compared to higher level *ab-initio* methods (seen in the model system in section 3.3.2.). Nonetheless, the selectivity predicted would be expected to be similar since this would affect C2 and C3 pathways to a similar degree.

3.3.6. Catalytic cycle 2: Initial C-H activation of N-methyl indole

Our calculations focused on examining the alternative catalytic cycle (**Figure 27**), where initial activation of N-methyl indole (**1**) occurs prior to subsequent benzene C-H activation (**2**) in the presence of a Pd(II) catalyst. The cycle is completed via a reductive elimination C-C bond forming event (**3**).

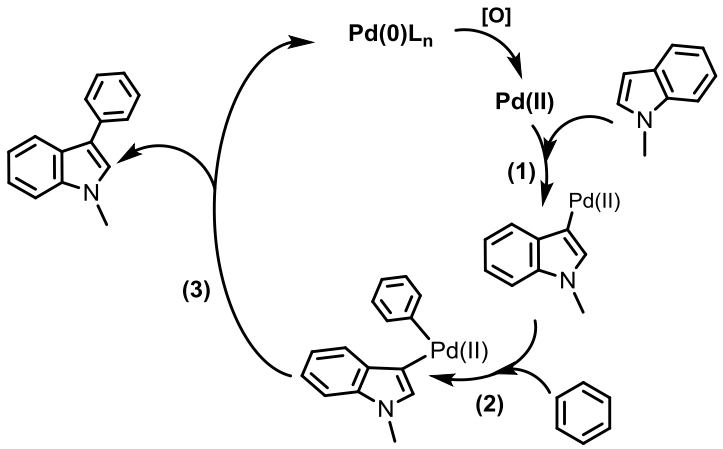

Figure 27. Calculated catalytic cycle via CMD mechanism. Oxidation of Pd(0) to Pd(II) was not modelled. Cleavage of the C-H bond in N-methyl indole (1) is calculated with a variety of Pd(II) catalysts in this section.

Our computational work focused on bimetallic, dimeric and mixed-ligand Pd catalysts (i.e. Ph-Pd-OAc) in the initial C-H activation event of N-methyl indole (as opposed to benzene activation seen in the previous section) to examine if these Pd catalysts could elicit regioselectivity for C2 in the C-H activation step of N-methyl indole. However, all calculations predict C-H activation to be preferred at C3 rather than C2 (**Figure 28**), therefore it is unlikely that C2 selectivity is results from the kinetics of C-H activation of N-methyl indole. This is line with our results obtained in chapter 2.

Dimeric $Pd_2(OAc)_4$ displayed selectivity for C3 (ΔG 15.1) with C2 C-H activation 3.4 kcal/mol higher in energy (ΔG 18.4). Bimetallic species, $PdAg(OAc)_3$ and $PdCu(OAc)_4$ were also studied. Selectivity for the C2 regioisomer was not forthcoming in the initial C-H activation step with both bimetallic species. C3 was favoured for $PdCu(OAc)_4$ (ΔG **C3**: 1.5 kcal/mol **C2**: 6.3 kcal/mol) and $PdAg(OAc)_3$ (ΔG **C3**: 5.3 kcal/mol **C2**: 8.0 kcal/mol) . In fact, through the study, all catalytic species studied displayed an overall preference for activation at C3, thus indicating that observed selectivity is unlikely to

be imparted in the initial C-H activation of indole, or when indole is activated second (as seen in the previous section).

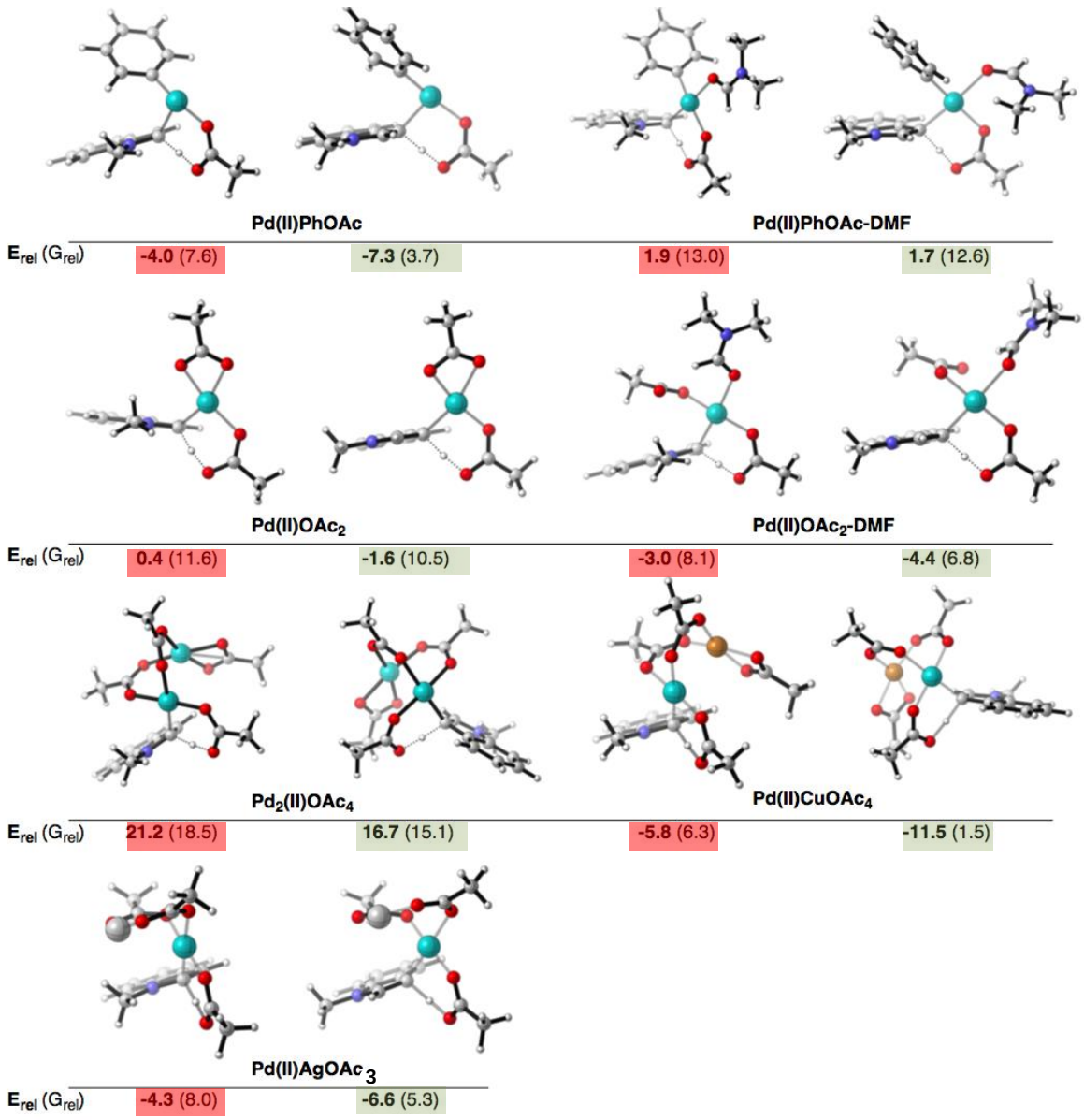

Figure 28. C-H activation of N-methyl indole with different Pd catalytic species, with the C2 (red) and C3 (green) C-H activation energies. Gibbs free energy of the TS is given in brackets. All values in kcal/mol. Energies given relative to separated indole and catalyst.

Further work studied whether 'switch' coordination – where Cu or Ag coordinate to indole as opposed to Pd (in a bimetallic catalytic species) in the C-H activation step (**Figure 29**). Coordination of Ag (in $PdAg(OAc)_3$) as opposed to Pd resulted in a steep increase in Gibbs free energy for C2 TS (ΔG 49.7 kcal/mol) rendering it highly unlikely to be implicit in the C-H activation of N-methyl indole. The C3 TS was not located for

the coordination at C3. Despite higher activation barriers obtained for C-H activation of N-methyl indole, the kinetic selectivity for the C3 product is maintained when metalation is by Cu rather than Pd in the mixed heterometallic catalytic species, $PdCu(OAc)_4$. Activation at C3 is preferred (ΔG 31.1 kcal/mol) to C2 (ΔG 33.7 kcal/mol), however, the high energy required for activation render this mechanistic scenario unlikely, with C2 selectivity not displayed in any of the studied Pd species including other indoles such as N-Piv indole with $Pd_2(OAc)_4$ (C2: ΔG 17.3 kcal/mol, C3: ΔG 12.4 kcal/mol) or with $PdCu(OAc)_4$ (C2: ΔG 9.9 kcal/mol, C3: ΔG 4.4. kcal/mol).

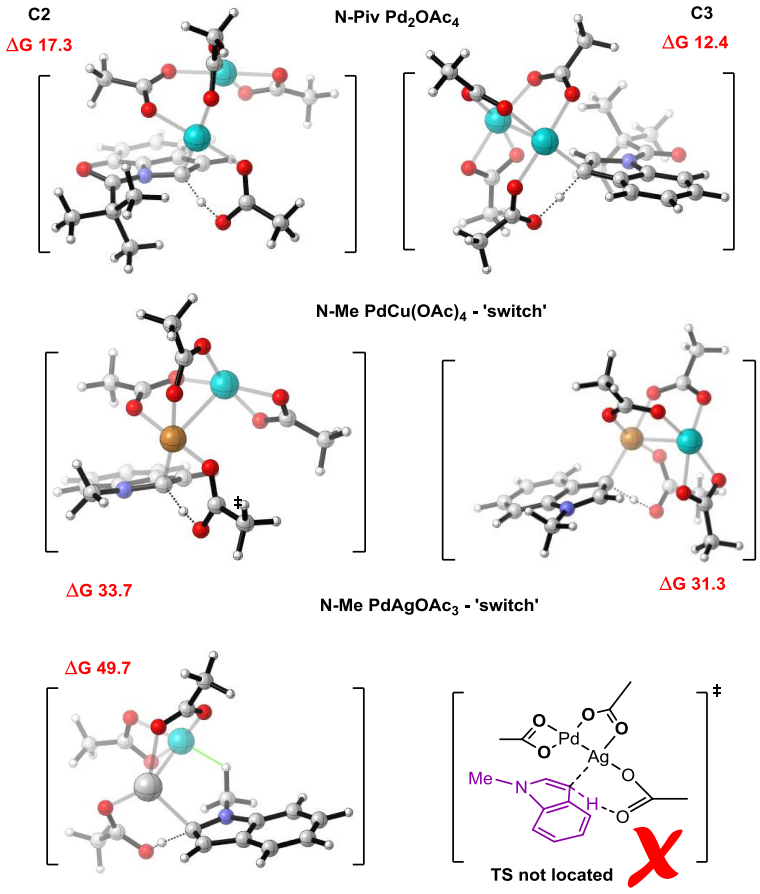

Figure 29. 'Switch' dimers in N-methyl indole and N-Piv indole in C-H activation. All values in kcal/mol

The roles of dimeric or higher order aggregates has been speculated in the chemistry of palladium(II)diacetate, however, as we have shown, the innate regioselectivity is unaffected relative to the monomeric species. Furthermore, low catalytic loadings, and

coordinating solvent act to favour lower aggregation states. We therefore focused on monomeric Pd(II) catalysts with respect to C-H activation of N-methyl indole.

3.3.6.1. $Pd(OAc)_2$ catalyzed C-H activation of N-methyl indole

The alternative catalytic cycle for indole arylation, where indole C-H activation is successively followed by benzene C-H activation was studied. As we saw in section 4, the initial resting state proceeds through coordination with indole and therefore this precomplex will be concomitant to C-H activation TS on N-methyl indole (**Figure 30**).

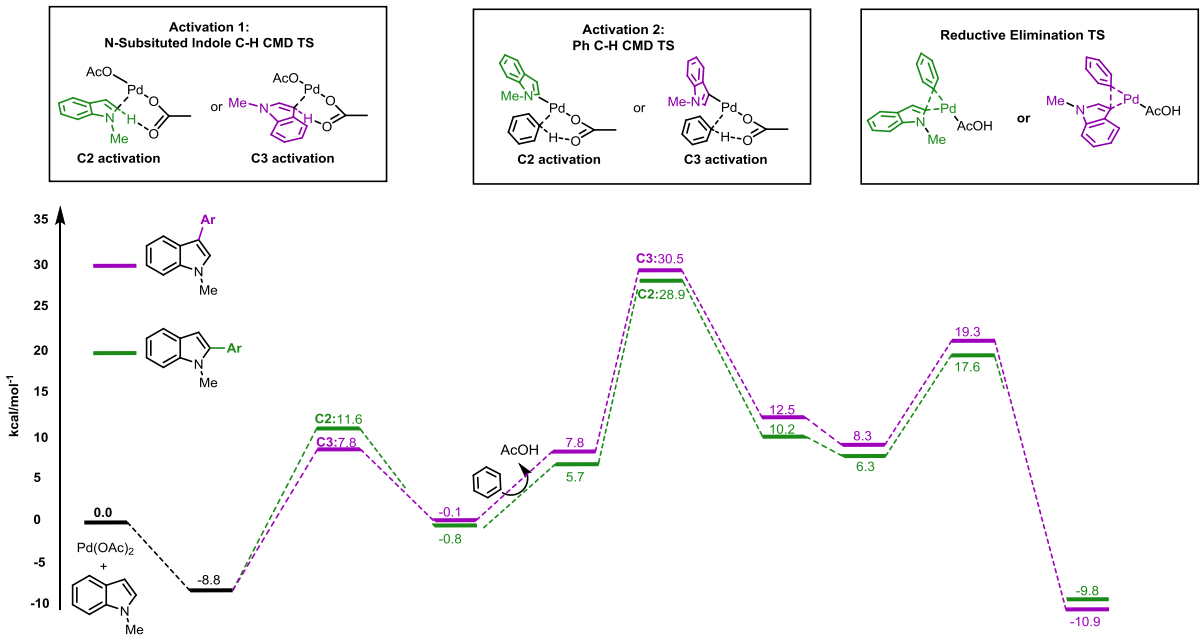

Figure 30. ωB97XD/6-311+G(d,p) computed free energy profile (kcal/mol) for the initial C-H activation of N-methyl indole (Activation 1) followed by C-H activation of benzene (Activation 2)

The initial C-H activation of N-methyl indole with $Pd(OAc)_2$ through a CMD mechanism (Activation 1) is indeed energetically feasible with C3 activation (ΔG 7.8 kcal/mol) preferred to C2 (ΔG 11.6 kcal/mol), with both regioisomers displaying an exergonic reaction profile (relative to reactants). Activation 1 proceeds initially through a stable precomplex (ΔG -8.8 kcal/mol), where the Pd(II) catalytic species coordinates η^2 to the indole C2-C3 π system. Subsequent C-H bond cleavage is undertaken through six membered TS, and favours C3 due to this position being significantly more electron rich than C2, thus preferential for palladation. The activation of the relatively electron poor benzene is far higher in energy as opposed to the activation of indole (Activation 2). However, it is evident that there is change in selectivity displayed in this step – with the C2Indole-Pd-OAc TS (ΔG 28.9 kcal/mol) marginally preferred over the C3Indole-Pd-OAc TS (ΔG 30.5 kcal/mol). This is calculated to be the selectivity and rate

determining step within this reaction profile (**Figure 31**). The subsequent reductive elimination occurs preferentially for C2 (ΔG 17.6 kcal/mol) over C3 (ΔG 19.3 kcal/mol), where the new C-C bond is formed and Pd(0) is expelled providing the C2 and C3 product. The C3 product is calculated to be thermodynamically more stable (ΔG -10.9 kcal/mol) than C2 product (ΔG -9.8 kcal/mol).

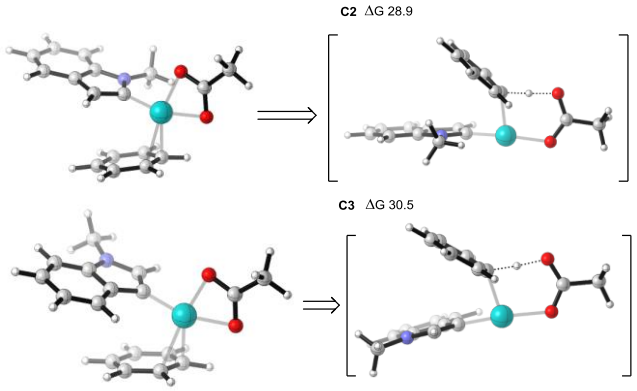

Figure 31. Precomplex and corresponding C-H activation of benzene with both C2 palladated (*top*) and C3 (*bottom*) palladated catalytic species (Indole-Pd(II)-OAc). All values in kcal/mol

Selectivity calculated from the C-H activation of benzene (the selectivity determining slow step) gives 9:1 selectivity for the C2 product with a $\Delta\Delta G^{\ddagger}$ of 1.6 kcal/mol (C3:C2) in Activation 2. This selectivity ratio is similar to the experimental ratio in DeBoef's oxidative arylation of 4:1 (80:20) where a $\Delta\Delta G^{\ddagger}$ of 1.1 kcal/mol would replicate observed selectivity. The calculated selectivity is more in tune with the Fagnou conditions, where selectivity was 24:1 (96:4) for C2 arylation, corresponding to $\Delta\Delta G^{\ddagger}$ of 1.5 kcal/mol. The Gibbs free energy of rate-determining TS (for both regioisomers) is high and if observing the energetic span model[48] it is unlikely that the observed experimental selectivity would occur, as 37.7 kcal/mol would be required in order to cleave the C-H bond of benzene with an Pd-Ar-OAc (where Ar=N-methyl indole palladated at the C2 position) from the lowest energy resting state (ΔG -8.8 kcal/mol) to the C2 TS (ΔG 28.9 kcal/mol).

3.3.6.2. $Pd(OAc)_2$-DMF catalyzed C-H activation of N-methyl indole

Our calculations sought to characterize a solvent coordinated pathway activation occurring at indole first with $Pd(OAc)_2$ (**Figure 32**). In the presence of polar solvent it is likely that DMF/DMA coordination can occur, as seen in section 3, and such solvent systems are utilized by Sames[8] and Larossa[10] and based on Hartwig's[12] recent findings where phosphine complexes play little or no role in direct arylation reactions, we modelled the pathway in the form of a ligandless $Pd(OAc)_2$ catalyst, which may undergo solvent coordination to give $Pd(OAc)_2$-DMF.

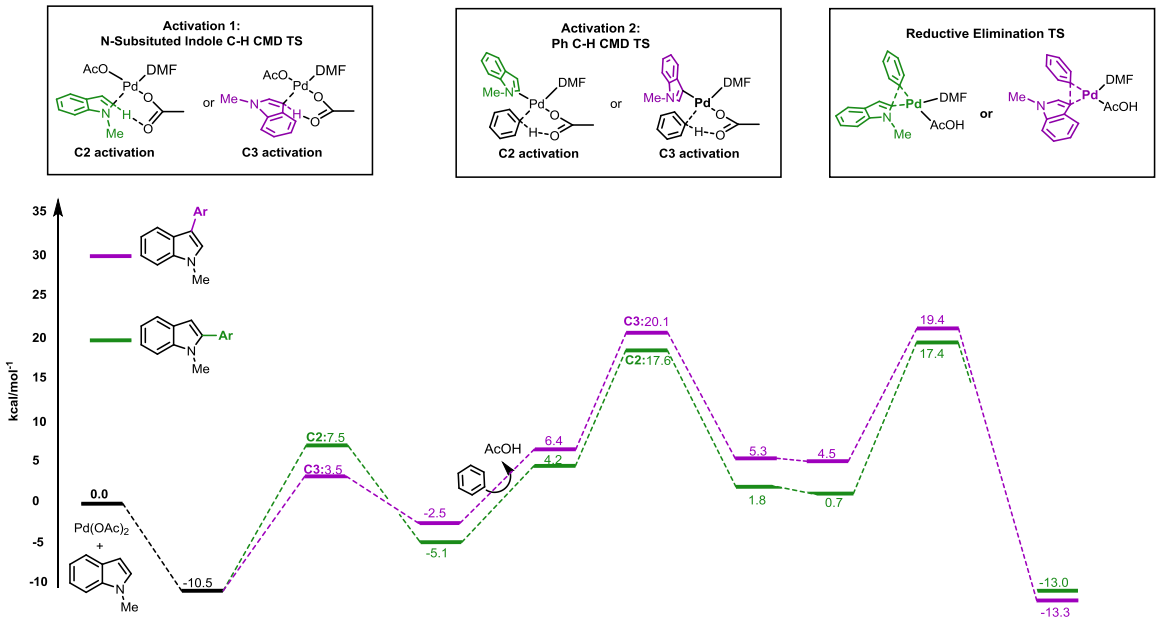

Figure 32. ωB97XD/6-311+G(d,p) computed free energy profile (kcal/mol) for the initial C-H activation of N-methyl indole (Activation 1) followed by C-H activation of benzene (Activation 2)

The reaction proceeds through a common precomplex, where $Pd(OAc)_2$-DMF catalytic species coordinates to the π system of indole. This requires the acetate ligand on Pd, which is bidentate, to switch coordination to monodentate in order to allow for coordination to occur. This provides a kinetically favoured resting state (ΔG -10.5 kcal/mol) which leads to the subsequent CMD TS at C2 (ΔG 7.5 kcal/mol) and C3 (ΔG 3.5 kcal/mol). As seen previously, the CMD event is favoured heavily for C3, however, the C3 palladated intermediate (post C-H abstraction) is higher in energy (ΔG -2.5 kcal/mol) than the resulting C2 intermediate (ΔG -5.1 kcal/mol) post CMD.

In order to facilitate the C-H activation of benzene (which is the rate determining and selectivity determining step), dissociation of AcOH must occur from Pd – this allows for coordination of benzene. This process requires 8.9 kcal/mol for C3 and 9.3 kcal/mol for C2 (i.e. from post C-H intermediate in Activation 1 to pre C-H activation precomplex in Activation 2).

In Activation 2, the C-H activation TS of benzene has lower Gibbs free energy than that of analogous ligandless C-H activation for both C2 and C3, signifying the benefit of solvent coordination on Pd, however, this step is still the highest energy step within the profile, and ultimately selectivity determining. Through the C-H activation of benzene selectivity is favoured at the C2 position, where C-H activation is calculated to occur much more readily than C3 (C2: ΔG 17.6 kcal/mol, C3: ΔG 20.1 kcal/mol). The reaction is completed via reductive elimination of a four coordinate species, where the C2 arylation is once again favoured (ΔG 17.4 kcal/mol) over C3 (ΔG 19.4 kcal/mol).

The selectivity calculated through the rate and selectivity determining C-H activation of benzene (Activation 2) provides a ratio of 49:1 (98:2) favouring C2:C3 arylation. This predicts almost exclusive C2 selectivity, with a $\Delta\Delta G^{\ddagger}$ of 2.5 kcal/mol between the two TS. The calculated selectivity is in good agreement with experimentally observed selectivity in the reaction of Fagnou, where the C2 product was attained in 24:1 (96:4). In order to replicate the DeBoef conditions $\Delta\Delta G^{\ddagger}$ of 1.1. kcal/mol is required The energetic span from the resting state to the C2 TS in the selectivity determining step is calculated at 28.1 kcal/mol which is far more favourable than the energetic span predicted by the ligandless pathway of 37.7 kcal/mol.

3.3.6.3. $Pd(OAc)_2$-AcOH catalyzed C-H activation of N-methyl indole

Modelling the reaction with AcOH as explicit coordinating solvent describes a comparative system for oxidative arylation reactions, where buffered conditions are employed such as work on arylation at C2 by DeBoef[18], Fagnou[19] and Sanford.[11]. We modelled the coordination of AcOH (as a model system for PivOH) to examine the PES of C-H/C-H activation and arylation of N- methyl indole in acidic medium.

The PES is strikingly similar to that calculated of $Pd(OAc)_2$ and $Pd(OAc)_2$-DMF in the previous sections. The resting state of the system is predicted to be the initial precomplex; where Pd(II) is coordinated to the C2-C3 π bond of N-methyl indole. This coordinated species is kinetically stable (ΔG -17.5 kcal/mol) and is concomitant to the subsequent C-H bond cleavage CMD TS (**Figure 33**), where a six membered CMD TS is favoured at the C3 position of N-methyl indole (ΔG -4.5 kcal/mol) as opposed to C2 C-H activation (ΔG 1.9 kcal/mol). Activation of indole is favoured at the C3 position of N-methyl indole irrespective of catalytic species used in our studies. Also, the sequence of events (i.e. activation of indole first or second) results in C3 C-H activation as the favoured TS.

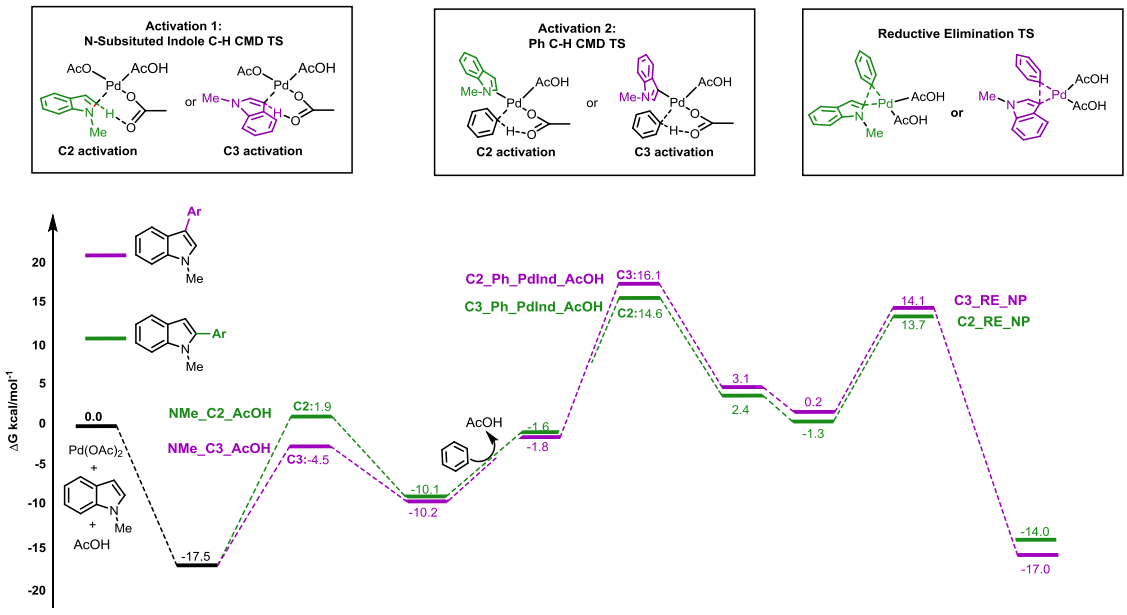

Figure 33. Free energy profile for the C-H activation of N-methyl indole and benzene. C2 selectivity is observed through a selectivity determining second activation of benzene. All values in kcal/mol.

After the initial activation of N-methyl indole (Activation 1), the reaction continues with the dissociation of an AcOH ligand from Pd and to accommodate the coordination and C-H activation of benzene with the indole-Pd-OAc catalyst (Activation 2). The calculated Gibbs free energy is more favourable to cleavage at the C2 position (ΔG 14.6 kcal/mol) whereas C-H activation at C3 is disfavoured (ΔG 16.1 kcal/mol). This is also the highest energy step calculated this set of mechanistic events, with a calculated $\Delta\Delta G^{\ddagger}$ of 1.5 kcal/mol in favour of the C2 TS (**Figure 34**).

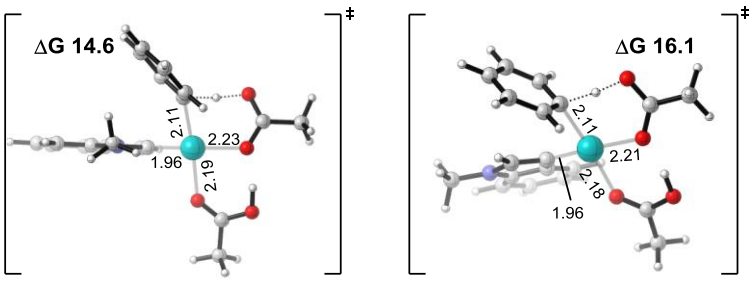

Figure 34. Optimized geometry of benzene C-H activation (Activation 2) with C2Indole-PdOAcAcOH (*left*) and C3Indole-PdOAcAcOH (*right*). All energies in kcal/mol. All bond lengths in Å.

Proceeding from the second TS (i.e. Activation 2), the C2 diarylated species (resulting from benzene C-H activation) is calculated as the more stable of the two diarylated products (C2: 2.4 kcal/mol, C3: 3.1 kcal/mol). Rotation of one of the AcOH ligands on the Pd centre (*cis* to Ph) in the precursor to reductive elimination TS, creates a new intramolecular O—H-O bond, in addition to the polar-π interaction between AcOH and the π system of the indole (**Figure 35**), which helps stabilize the precursor to reductive elimination TS further. This is evident in both C2 and C3 pre-reductive elimination intermediates. The C3 pre-reductive elimination intermediate is higher (ΔG 2.3 kcal/mol), whereas the C2 pre-reductive elimination intermediate resides at ΔG -0.8 kcal/mol. Reductive elimination proceeds via a three-centre, four-coordinate Pd(II) transition state, which is calculated to be favourable for the formation of a new C-C bond at C2 (ΔG 14.2 kcal/mol) as opposed to C3 (Δ16.2 kcal/mol). Upon reductive elimination Pd(0) is expelled and both arylated regioisomers produced.

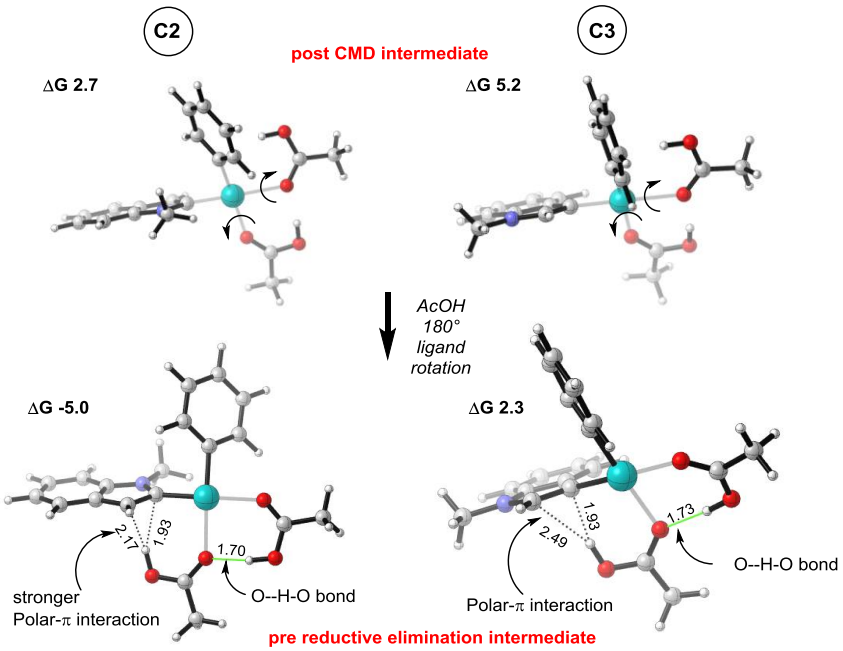

Figure 35. The C2 intermediate is calculated to be more stable than C3. This is in part due to stronger polar-π bonding in C2. All values in kcal/mol. All bond lengths in Å.

Examining the rate and selectivity determining C-H activation of benzene predicts the C2 regioisomer to be produced in a selectivity of 93:7 (C2:C3) through $\Delta\Delta G^{\ddagger}$ of 1.5 kcal/mol.

3.3.7. Kinetic Isotope Effects

Through DFT optimizations it is possible that both sets of events are possible (i.e. activation of either benzene or N-methyl indole first). According the calculated selectivity from $\Delta\Delta G^{\ddagger}$ barriers (kcal/mol) from both reactions it is evident that selectivity determining steps for C2 arylation do replicate experimental selectivity of Fagnou (24:1) or DeBoef (4:1). Where benzene undergoes C-H activation first, this is observed in reductive elimination TSs, and where indole is activated first, this is displayed in the second C-H activation of benzene. Therefore, we computed the kinetic isotope effect (KIE) of both selectivity determining steps resulting from replacing benzene with perdeuterated benzene (C_6D_6) in the arylation of N-methyl indole to see if either corroborated with experimentally observed KIEs. The computed KIE (neglecting contributions from tunneling) was calculated via:

$$\frac{K_H}{K_D} = exp^{\frac{\Delta\Delta G^{\ddagger}}{RT}}$$

Where $\Delta\Delta G^{\ddagger}$ refers to difference in overall activation barriers of arylation at the C2 position by C_6D_6 and C_6H_6. T= 383K, R=8.314 J/K mol.

Experimentally, Sames[8] observed a small KIE of 1.2 upon deuteration of the indole substrate at the C2 position for arylation with benzene. DeBoef[18] used equimolar amounts of perdeuterated benzene and benzene (**Figure 36**), observing a large KIE between 4.1-5.0 (depending on the indole substrate used). Taken together these two results suggest that indole C-H activation is not involved in the rate-determining step of the mechanism, while benzene C-H activation is involved in the slow step. From our calculations, the computed isotope effect for the arylation proceeding through the activation of benzene second (i.e. following indole palladation) was calculated to be $K_H/K_{D=}$ **3.4, 3.5, 3.7** for our studied reactions (i.e. ligandless, DMF and AcOH solvent respectively).

With benzene activation taking place first the values were calculated as **3.3, 3.7, 3.6** (ligandless, DMF, and AcOH respectively) – this could arise if the subsequent steps are comparatively fast compared to an initial (slow) benzene activation, which is not the case in any of the studied mechanisms. In the ligandless mechanism, the subsequent C-

H of N-methyl indole (with PhPdOAc) is higher in energy for C2 than the initial activation of benzene. In the solvated mechanisms, the reductive elimination is higher in energy than the initial C-H activation of benzene, thus ruling out this scenario of events.

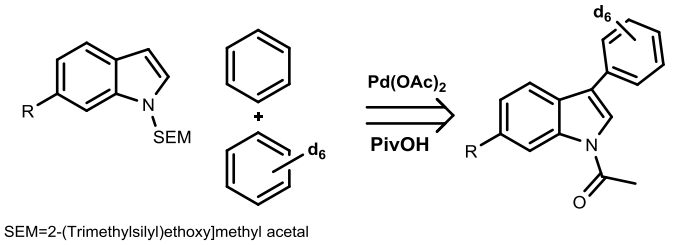

SEM=2-(Trimethylsilyl)ethoxy]methyl acetal

Experimental KIE of C2 arylation = 4.1- 5.0

R	PivOH	KIE
NO_2	0 equiv	**4.5**
NO_2	2.5 equiv	**5.0**
NO_2	30 equiv	**4.9**
OMe	0 eqiv	**4.6**
OMe	2.5 equiv	**4.1**
OMe	30 equiv	**5.0**

Figure 36. KIE experiments conducted by DeBoef with perdeuterated benzene. Large kinetic isotope effects were observed in varying concentration of PivOH and electron withdrawing/donating groups on indole, suggesting the mechanism is consistent.

We also considered the possibility of whether a large effect due to benzene deuteration could arise if the C-H activation occurs before the slow step in the mechanism – i.e. as could be the case if the final reductive elimination becomes turnover-limiting. Any difference in relative rate would then correspond to an equilibrium isotope effect (EIE) due to the loss of C-H/C-D and the gain of O-H/O-D, and a secondary KIE resulting from the remaining 5 deuterium atoms in the aryl-Pd intermediates. We computed an equilibrium isotope effect associated with reductive elimination of **0.8, 0.9, 1.0** for the reactions studied (ligandless, polar, non-polar respectively), which is not consistent with result of DeBoef and thus reductive elimination is unlikely to be rate-determining.

Thus, mechanistic possibilities which satisfy both a predicted selectivity for the major C2-product, and would account for a primary KIE with C_6D_6 are the pathways in which benzene is activated second after indole (**Figure 30**, **Figure 32**, **Figure 33**) however it must be noted that the energetic span for these pathways is relatively high. With the ligandless pathway it is >37.0 kcal/mol, with AcOH assisted pathway it is 32.1 kcal/mol and with DMF it is 28.1 kcal/mol for C2 selectivity. From TST at the reaction temperature of 120º C, a free energy span of 30 kcal/mol corresponds to a reaction half-

life of 68 minutes. Experimental rate constants are not reported, however, the reaction time of 3 hours is used. As the reaction is conducted in acidic medium (PivOH) it is likely that AcOH assisted modelled pathway is likely to be most competitive (**Section 3.7.4.**), however, our calculations suggest that using a more polar solvent in the form of DMF may assist in lowering the overall energy profile of N-methyl indole arylation at the C2 position.

3.3.8. Summary of the CMD mechanism

Through computed kinetic isotope calculations, predictions of selectivity and observing the energetic span of the reaction we favour a mechanism where (**1**) C-H activation occurs on N-methyl indole with a solvated $Pd(OAc)_2$-AcOH catalyst. This C-H activation is preferred at C3 (vs C2) and is reversible as the next step is the selectivity and rate determining slow step (**2**) which favours C-H activation of benzene with a Pd-C2Indole species as opposed to Pd-C3Indole species. The bond formation of the phenyl ring to indole (**3**) is relatively facile in comparison, and also favours the C2 position through reductive elimination (**Figure 37**), which leads to the arylated indole product and regenerates Pd(0). The AcOH ligand will now presumably stabilize Pd(0) before reoxidation to Pd(II). This mechanistic profile shows good agreement with experimental selectivity of Fagnou and DeBoef. Kinetic isotope experiment data also predicts a primary KIE (of benzene/ C_6D_6) as observed by DeBoef.

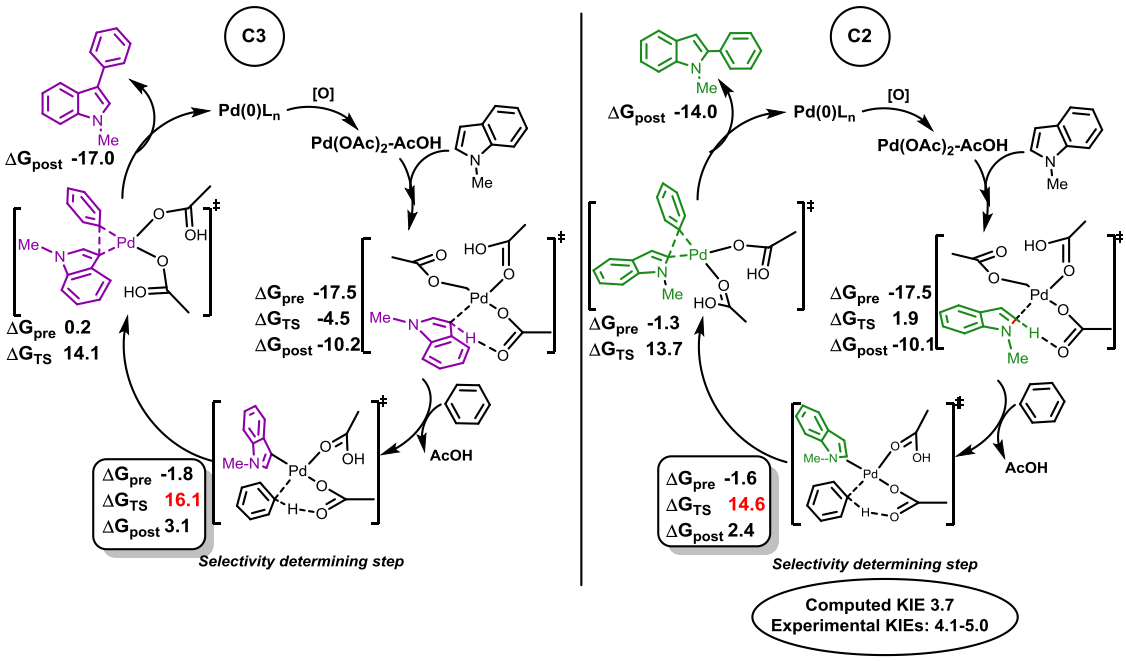

Figure 37. Computed catalytic cycle for the arylation of N-methyl indole at C2 and C3. All values in kcal/mol. All values against separated reactants.

Why are C2 TSs energetically more favourable for the second C-H activation step? Partly this is due to the greater stability of the C2 palladated indole intermediate which has a stronger C-Pd bond as discussed earlier. Additionally the Pd centre is more electrophilic; analyzing the unit charge (**Figure 38**) of the incoming benzene (essentially the polarization of benzene as a sum of individual NPA charges on C and H atoms), it was observed that Ph-H carried a higher charge in TS for C2 (+0.13) as compared to C3 (+0.11), providing a more electron deficient Ph-H for C-H cleavage by the ambiphilic acetate ligand. Higher charge on Ph-H with the Pd catalysts containing C2-palladated indole was evident amongst all studied catalytic species. There is greater charger transfer from benzene to the catalyst in the more stable TS.

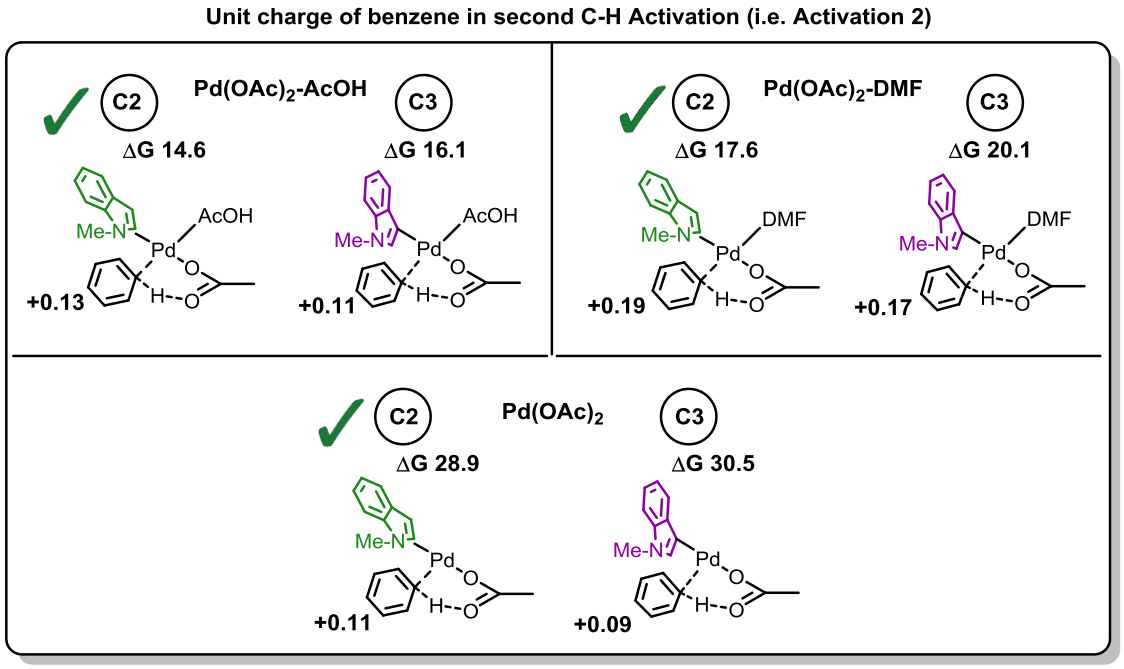

Figure 38. Unit charge of Ph-H in C-H activation TS with various Indole-Pd(II) catalytic species. The charge carried on Ph-H in C2 TS is higher in across all studied systems. Energy values in kcal/mol.

3.9 Alternative mechanistic pathways

3.9.1. S_E3

Whilst the CMD mechanism has garnered much support from computation concentrating on Pd-catalyzed direct arylations of electron deficient aromatics and unfunctionalized arenes, a variety of pathways are potentially viable for indole by virtue of its nucleophilicity, and the fact that C2/C3 often display alkene-type reactivity. Our initial mechanistic investigation into arylation of N-methyl indole began with addressing the conventional picture of S_EAr reactivity between indole and electrophile, which has also been invoked in Pd-catalyzed arylation. The mechanism should proceed via the initial rate-limiting generation of an Indole-ArPd(OAc) intermediate followed by deprotonation to regain aromaticity of the 6,5 ring system and the arylated product. The inherent electronic bias of indoles should usually lead to selectivity at C3.[49,50,51] Geometry optimizations did not yield either C2 or C3 metalated intermediates (as mentioned previously). Clearly, ArPdX is not electrophilic enough to induce the formation of the highly unstable dearomatized Wheland intermediate.

Recent work investigating $Pd(OAc)_2$ catalyzed direct arylation of an electron deficient arene has also found that no complex containing arene cationic character, invoked in S_EAr mechanism could be found computationally.[52] Experimentally, DeBoef and coworkers have shown the mechanism to be unlikely in the C-H palladation step of N-indoles.[53] Thus discussions in the literature of C3-attack followed by migration to C2 in the context of Pd catalysis are not supported by theory. However, we were able to locate TSs and intermediates for the intermolecular electrophilic substitution pathway.

The S_E3 pathway is known to exist for arenes[54,55,56] whereby the concerted process is facilitated by base (in our system, OAc^-). Occasionally this may also be termed as an outer sphere CMD mechanism – where carboxylate ligand dissociates and act as an intermolecular anionic base. Recently Jutand and coworkers have shown experimentally that intermolecular deprotonation mechanism is favoured over intramolecular acetate/pivalate deprotonation for Rh (II) C-H activation of arenes.[57] We characterized the activation and arylation at C2 and C3 of N-methyl indole for $Pd(OAc)_2$ (**Figure 39**).

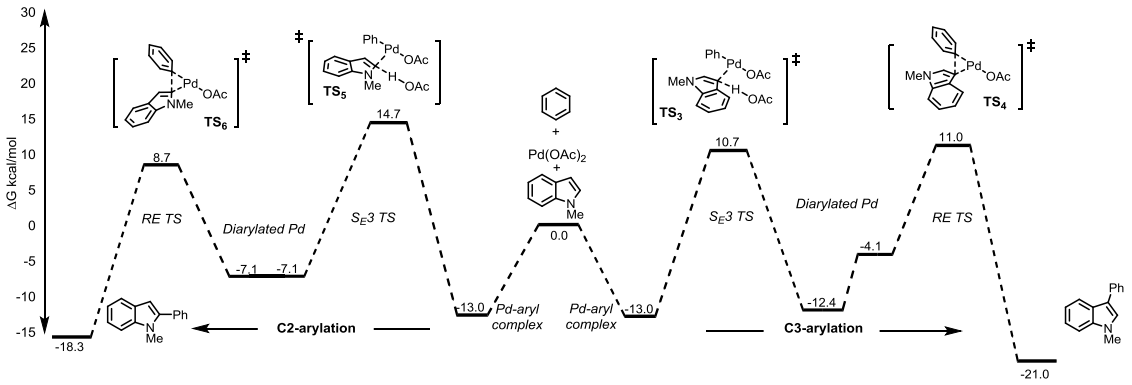

Figure 39. Intermolecular C-H activation for C3 arylation of N-methyl indole with solvated Pd(II) catalysts. C2 arylation was not located via solvated Pd(II). Initial activation of benzene with Pd(OAc)2-DMF and $Pd(OAc)_2$-AcOH shown in section 4.2-4.4. All values in kcal/mol

Calculations show the reaction proceeds through an initial energetically favourable Pd-aryl precomplex (ΔG -13.0 kcal/mol) where the catalytic species is η^2 to C2-C3 π system. This is a precursor to the subsequent intermolecular C-H activation and palladation step (shown here as **TS_3** and **TS_5).** Intermolecular deprotonation prefers C3 C-H activation - **TS_3** (ΔG 10.7 kcal/mol) over C2 **TS_5** (ΔG 14.7 kcal/mol). The reaction continues through an exergonic reaction profile, with both C2 and C3 TS producing stable post abstraction intermediates. Subsequent reductive elimination in **TS_4** (11.0 kcal/mol) and **TS_6** (8.7 kcal/mol) imparts preference for the C2 C-C bond forming reaction. This mirrors the trend in the CMD C-H activation of N-methyl indole with $Pd(OAc)_2$, where C2 selectivity is favoured in reductive elimination TSs. However, overall C3 arylation is predicted to be favourable via this pathway and therefore experimental selectivity where the C2 regioisomer is the major product is not replicated.

We could only locate C-H activation of N-methyl indole at C3 with solvated $Pd(OAc)_2$-DMF and $Pd(OAc)_2$-AcOH as the catalytic species in the S_E3 mechanism (**Figure 40**). Despite efforts in trying to locate analogous TS for C2, we could not locate an intermolecular C-H activation with either $Pd(OAc)_2$-AcOH or $Pd(OAc)_2$-DMF. Therefore the solvated and non-solvate pathway both predict selectivity for C3 arylation and thus, according to our calculations, it seems unlikely that the S_E3 mechanism would be responsible for arylation at C2.

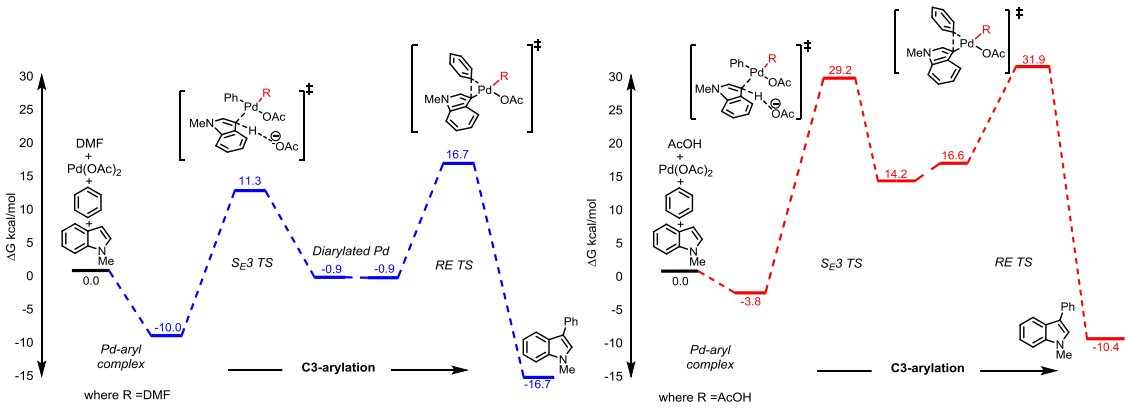

Figure 40. Computed free energy profile (kcal/mol) for Pd-catalyzed indole arylation via an S_E3 pathway. The DMF assisted pathway is shown in *red*, the AcOH assisted in *blue* and the ligandless pathway in *black*. Arylation at C2 was only located via a ligandless mechanism. All values in kcal/mol.

3.9.2. Heck-type Carbopalladation

The carbopalladation/'Heck' type pathway has been proposed as a feasible mechanism in Pd-catalyzed functionalization of heteroarenes [58] although synthetic efforts to intercept the postulated Heck-type intermediate in the arylation of indolizines (through a subsequent intramolecular carbopalladation onto an internal alkene) have been unsuccessful. [59] However, computational studies into the Pd catalyzed arylation of thiophene[60] and pyridine[61] have suggested that Heck-type carbopalladation could be theoretically favourable. Our work examined direct indole arylation via initial carbopalladation followed by *anti*-periplanar E2 elimination by acetate (as base) leading to desired product and releasing Pd (0) catalyst (**Figure 41**).

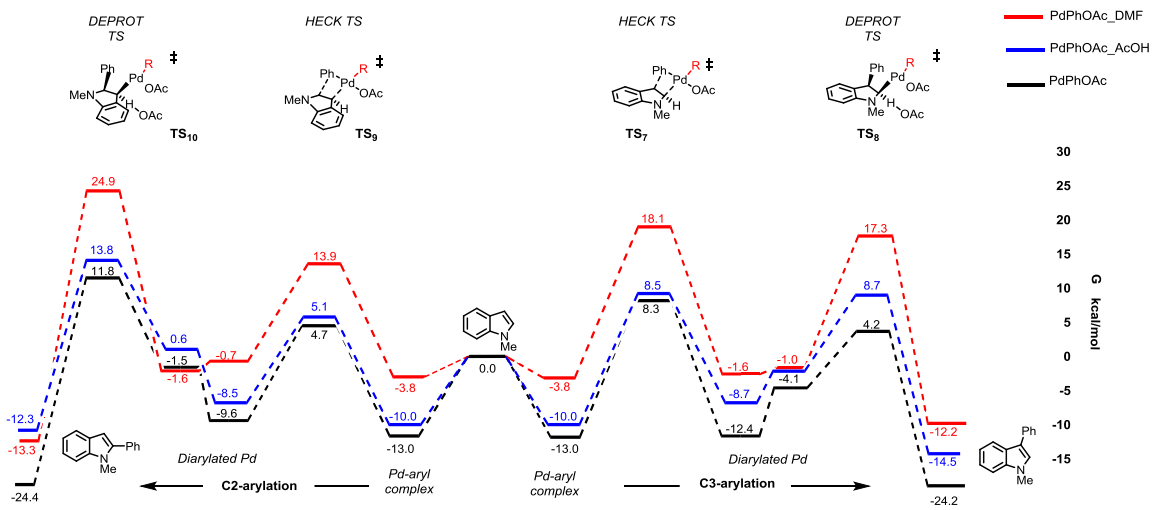

Figure 41. ωB97XD/6-311+G(d,p) computed free energy profile (kcal/mol) for Pd-catalyzed indole arylation via a 'Heck-type'/Carbopalladation pathway. Energy values relative to separated reactants.

For this mechanism to be viable, the initial step would need to be C-H activation of benzene with Pd(II). This could potentially result in either PhPdOAc (*black*), PhPdOAc-AcOH (*blue)* or PhPdOAc-DMF(*red*) as the species which would undergo palladation to indole, at either C2 or C3. All these scenarios were modelled in a competitive energy profile

Palladation at C3, and arylation at C2 is more favourable amongst all studied species. With PhPdOAc, C2 arylation is favoured via **TS_9** =17.7 kcal/mol, whereas C3 arylation

is shown to be less preferable, **TS_7** =19.3 kcal/mol. This bias for C2 regioselectivity may arise due to the effect of higher electron density at the C3 position, thus favouring electrophilic palladation preferentially at C3. Rearomatization is thermodynamically downhill, however in this step a strong C-H bond must be broken and so this step is by no means a facile process, with comparable barriers to the first. Solvation again increases TS energies, with C2 (**TS_{10}**) E2 elimination (an intermolecular β–Hydride elimination – the intramolecular version is prohibited by geometry) exhibiting higher energetic cost than initial palladation, at 11.8 kcal/mol (ligandless). For C3 E2 elimination this process is slightly more facile with the **TS_8** 4.2 kcal/mol (ligandless). Here it is the second step that requires an external molecule of base and in both cases it seems the non-solvated, i.e. ligandless pathway is more likely to be active in a heck-type carbopalladation mechanism.

Similar energetic trends are observed with the AcOH assisted pathway where the initial palladation is favoured at C2 (5.1 kcal/mol) but the C3 product is predicted to be favoured through a lower energy rearomatization step for C3 (8.7 kcal/mol) as opposed to C2 (13.8 kcal/mol). As before, observing the energetic span model, C3 regioselectivity is predicted to occur by this pathway and therefore does not account for C2 selectivity observed in experiment. Polar solvent coordination (in the form of DMF on Pd) creates a high energy profile, with respect to its non-solvated counterpart. The deprotonation step (which is the slow step in solvent assisted pathway) in C2 arylation is 13.1 kcal/mol higher than then non-solvated $Pd(OAc)_2$ pathway. Our calculations predict selectivity to favour C3 arylation via the DMF assisted method.

Similarly, the $Pd(OAc)_2$-AcOH pathway displays preference for C3 arylation, with the deprotonation/rearomatization step calculated as the slow step in this pathway. The C3 deprotonation (ΔG 8.7 kcal/mol) is significantly lower than C2 (13.8 kcal/mol) and thus experimental selectivity (i.e. C2 selectivity) is not calculated to be favoured by the Heck-type carbopalladation pathway. Therefore, our calculations predict that the carbopalladation pathway is unlikely to account for experimentally observed selectivity.

3.4. Conclusions

A comparison of activation free energy barriers from the three postulated mechanisms, S_E3, Heck and CMD suggests that all are thermally accessible; however, the first two of these mechanisms involve bimolecular steps where the concentration of free base is important. Thus, where oxidative arylation conditions are buffered or acidic the CMD pathway is likely to be favoured. Nevertheless, the characteristic C2 selectivity observed in oxidative arylations of N-alkylated indoles does not seem to arise in the C-H activation step and is predicted to be unfavourable in the S_E3 or Heck-type carbopalladation mechanism. Suggestions of catalytic bimetallic/heterometallic Pd clusters undertaking C-H activation are not supported by our calculations. Instead we favour monomeric Pd species which provide lower energy for the C-H activation step of N-methyl indole. The role of Ag(I)OAc is likely to assist in disaggregation of Pd clusters.

Previous literature reports a primary KIE for the benzene coupling partner which we are able to correctly reproduce in the favoured mechanism where C-H activation of benzene occurs subsequent to N-methyl indole. This observation means indole activation occurs reversibly, and so regioselectivity does not result from the kinetic preference to undergo C-H activation at C2 and C3 positions. We have determined that for N-methyl indole kinetics favour C3 activation via the CMD pathway but in fact C2 palladation forms a more stable intermediate. Our calculations show that the selectivity determining step in the C2-arylation of N-methyl indole is the activation of the electron poor benzene in the second activation via a CMD mechanism where AcOH plays a role as a coordinating solvent to a vacant site on Pd. The initial C-H activation of N-methyl indole is predicted to be reversible (**Figure 42**).

The energy span for the favoured computed cycle is 32.1 kcal/mol for C2 which is close to that expected from the elevated reaction temperatures. Alternative catalytic cycles where benzene is activated first and the energy span is lower (sections 3.5.1→ 3.5.3.) predict C2 selectivity in the reductive elimination step. In the mechanism where benzene is activated first, the observed equilibrium KIE for the reductive elimination TS does not corroborate with experimental KIE's for competitive intermolecular KIE's with perdeuterated benzene and indole as performed by DeBoef.

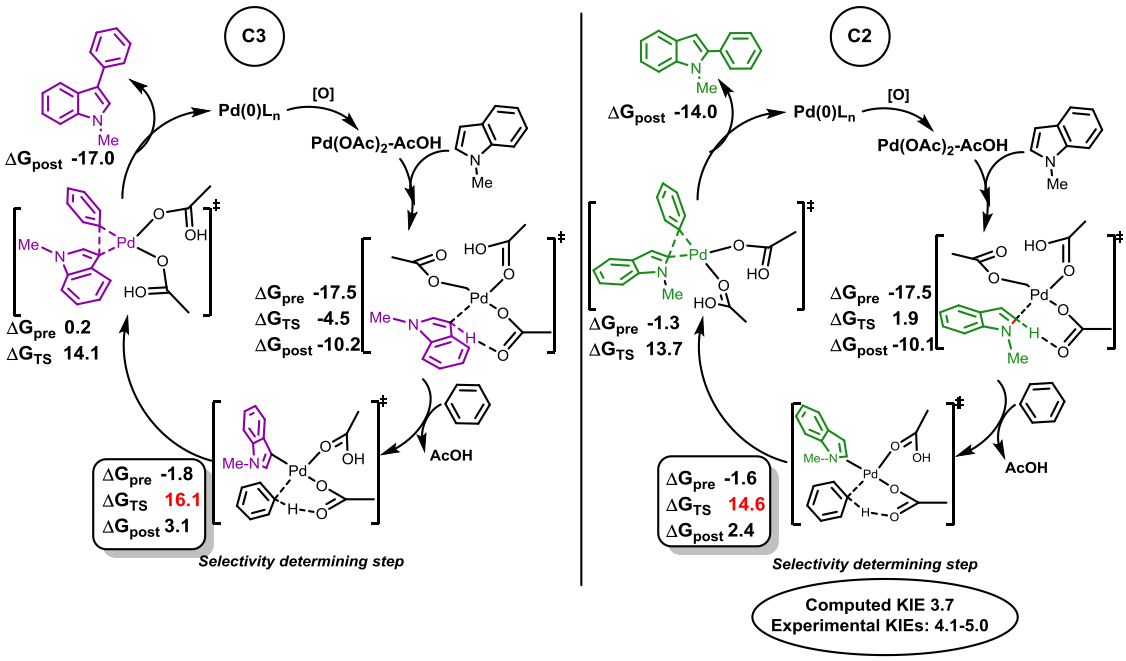

Figure 42. Favoured catalytic cycle in the C2 C-H activation and arylation of N-methyl indole. All energies given in kcal/mol.

The mechanistic scenario seen in **Figure 42** corroborates experimental observations in predicting favourable C2 selectivity for oxidative arylation of N-methyl indole. Overall selectivity is predicted at 97:3 (C2:C3) which is in excellent agreement with Fagnou's observed selectivity of 96:4 (C2:C3). If $\Delta\Delta G^{\ddagger}$ between the selectivity determining TSs in **Figure 42** were to reduce by 1.1 kcal/mol, this would correspond to the selectivity observed by DeBoef. There is also good agreement between calculated KIE (3.7) of the deprotonation of benzene via this mechanism and the competition KIE experiments with perdeuterated benzene (of DeBoef), where a KIE of 4.1 and above is observed.

Thus, the examination of mechanistic pathways, and a combination of computed selectivity and corroborating computed KIE provide a degree of confidence in our favoured mechanistic pathway, where greater charge transfer between benzene and Pd in the C2 pathway (as seen in **Figure 38**) allow C-H activation of benzene to occur more readily in the selectivity determining TS, thus leading to the major product, 1-Methyl-2-phenylindole.

Chapter 3 *References*

[1] (a) Alberico, D.; Scott, M. E.; Lautens, M. *Chem. Rev.* **2007**, *107*, 174; (b) Seregin, I.V.; Gevorgyan, V. *Chem. Soc. Rev.* **2007**, *36*, 1173; (c) Satoh, T.; Miura, M. *Chem Lett.* **2007**, *36*, 200; (d) Campeau, L. C.; Stuart, D. R; Fagnou, K. *Aldrichim Acta*, **2007**, *40*, 35; (e) McGlacken, G. P.; Bateman, L. M. *Chem. Soc. Rev.* **2009**, *38*, 2447; (f) Chen, X.; Engle, K. M.; Wang, D. H.; Yu, J. Q. *Angew. Chem. Int. Ed.* **2009,** *48*, 5094; (g) Hartwig, J. F. *Nature*. **2008**, *455*, 314; (h) Joucla, L.; Djakovitich, L. *Adv. Synth. Catal.* **2009**, *351*, 673; (i) Lyons, T. W.; Sanford, M. S. *Chem. Rev.* **2010**, *110*, 1147; (j) Ackermann, L. *Chem. Rev.* **2011**, *111*, 1315; (k) Fabrizi, G.; Cacchi, S. *Chem. Rev.* **2011**, *111*, PR215; (l) Cho, S. E.; Kim, J Y.; Kwak, J.; Chang, S. *Chem. Soc. Rev.* **2011**, *40*, 5068; (m) Yamaguchi, J.; Yamguchi, A. D.; Itami, K. *Angew. Chem. Int. Ed.* **2012**, *51*, 8960; (n) Neufeldt, S.R.; Sanford, M. *S. Acc. Chem. Res.* **2012**, *45*, 936; (p) Kapdi, A. R.; Vicente, R.; Ackermann, L. *Angew. Chem. Int. Ed.* **2009**, *48*, 9792.

[2] (a) J.A. Ellman, *Science,* **2007,** *316*, 1131; (b) Liu, Y.-J.; Xu, H.; Kong, W.-J.; Shang, M.; Dai, H.-X.;Yu, J. Q. *Nature.* **2014**, *515*, 389.

[3] Evans, B. E.; Rittle, K. E.; Bock, M. G.; DiPardo, R. M.; Freidinger, R. M.; Whitter, W. L.; Lundell, G. F.; Veber, D. F.; Anderson, P. S.; Chang, R. S.; Lotti, V. J.; Cerino, D. J.; Chen, T. B.; Kling, P. J.; Kunkel, K. A.; Springer, J. P.; Hirshfield, J. *J. Med. Chem.* **1988**, *31*, 2235; (b) Welsch, M. E.; Snyder, S. A.; Stockwell, B. R. *Curr. Opin. Chem. Biol.* **2010,** *14*, 347.

[4] Zhang, M-Z.; Chen, Q.; Yang, G-F. *Eur. J. Med. Chem.* **2015**, *89*, 421.

[5] (a) Lebrassuer, N.; Larossa, I. *Advances in Heterocyclic Chemistry*, **2012**, *105*, 309 ; (b) Boorman, T.; Larossa, I. *Progress in Heterocyclic Chemistry*, **2010**, *22*, 1.

[6] Trost B. M.; Godleski, S. A.; Genet, J. P. *J. Am. Chem. Soc.* **1978**, *100*, 3930.

[7] Ohta, A.; Inoue, A.; Ohtsuka, A.; Wantanbe, T. *Heterocycles* **1985**, *23*, 133.

[8] Wang, X. S.; Lane, B. S.; Sames, D. *J. Am. Chem. Soc.* **2005,** *127*, 8050.

[9] Grimster, N. P.; Gauntlett, C.; Godfrey, C.; Gaunt, M. J. *Angew. Chem. Int. Ed.* **2005**, *44*, 3125.

[10] Lebrasseur, N.; Larrosa, I. *J. Am. Chem. Soc.* **2008**, *130*, 2926.

[11] Deprez, N.R.; Kalyani, D.; Krause, A.; Sanford, M.S. *J. Am. Chem. Soc.* **2006**, *128*, 4972.

[12] Tan, T.; Hartwig, J. F. *J. Am. Chem. Soc*. **2010**, *133*, 3308.

[13] Boutadla, Y.; Davies, D. L.; Macgregor, S. A.; Poblador-Bahamonde, A.I. *Dalton Trans*. **2009**, *30*, 5887.

[14] Jazzar, R.; Hitce, J.; Renaudat, A.; Sofack-Kreutzer, J.; Baudoin, O. *Chem. Eur. J*. **2010**, *16*, 2654.

[15] Davies, D. L.; Donald, S.; Macgregor, S.A. *J. Am. Chem. Soc*. **2005**, *127*, 13754.

[16] Gorelsky, S. I.; Lapointe, D.; Fagnou, K. *J. Am. Chem. Soc* **2008**, *130*, 10848.

[17] Garcia-Cuadrado, D.; Mendoza, P.; Braga, A. A. C.; Maseras, F.; Echavarran, A. M. *J. Am. Chem. Soc.* **2006**, *128*, 1066.

[18] Potavathri, S.; Pereira, K. C.; Gorelsky, S. I.; Pike, A.; LeBris, A. P.; DeBoef, B. *J. Am. Chem. Soc*. **2010**, *132*, 14676.

[19] Stuart, D.R.; Villemure, E.; Fagnou, K. *J. Am. Chem. Soc*. **2007**, *129*, 12072.

[20] Cornella, J.; Lu, Pengfei.; Larrosa, Igor. *Org. Lett.* **2009,** *11*, 5506. (b) Pérez-Temprano, M. H., Casares, J. A. and Espinet, P. *Chem. Eur. J.* **2012**, *18*, 1864.

[21] (a) Tanaka, D.; Romeril, A. S. P.; Myers, A. G. *J. Am. Chem. Soc.* **2005**, *127*, 10323; (b) Tanaka, D.; Myers, A. G. *Org. Lett.* **2004**, *6*, 433; (c) Myers, A. G.; Tanaka, D.; Mannion, M. R. *J. Am. Chem. Soc*. **2002**, *124*, 11250.

[22] Balcells, D.; Clot, E.; Eisenstein, O. *Chem. Rev*. **2010**, *110*, 749.

[23] Boutadla, Y.; Davies, D.L.; Macgregor, S. A.; Poblador-Bahamonde, A. I. *Dalton. Trans.*, **2009**, *30*, 5820.

[24] Feller, D. *J. Comp. Chem*. **1996**, *13*, 1571.

[25] Roy, E. L.; Hay, J.; Martin, R. L. *J. Chem. Theory. Comput.* **2008**, *4*, 1029.

[26] (a) Barone, C.; Cossi, M.; *J. Phys. Chem. A*, **1998**, *102*, 1995; (b) Barone, Rega, N.; Schimani, G.; Cossi, M. *J. Comput. Chem.* **2003**, *24*, 669.

[27] Neese, F. *et. al*. Orca, *Version 1.0* Max-Planck-Institute for Chemical Energy Conversion Stiftstr. 34-36, 45470 Mulheim a. d. Ruhr, Germany , **2011**

[28] Meyer, W. *J. Chem. Phys*. **1973**, *58*, 1017.

[29] (a) Neese, F.; Wennmohs, F.; Hansen, A. *J Chem Phys* **2009**, *130*, 114108; (b) Neese, F.; Liakos, D.; Hansen, A. *J Chem Phys* **2009**, *131*, 103.

[30] Allen, F. H. *Acta Cryst*. **2002**, B58, 380.

[31] (a) Becke, A.D. *J. Chem. Phys.* **1993**, *98*, 5648; (b) Lee, C.; Yang, W.; Parr, R. G. *Phys. Rev. B.* **1988**, *37*, 785; (c) Vosko, S. H.; Wilk, L.; Nusair, M. *Can. J. Phys.* **1980**, *58*, 1200; (d) Stephens, P. J.; Devlin, F. J.; Chabalowski, C. F.; Frisch, M. J. *J.Phys.Chem.* **1994**, *98*, 11623.
[32] Chai, J. D.; Head-Gordon, M. *Phys. Chem. Chem. Phys.* **2008**, *10*, 6615.
[33] A. D. Becke, *J. Chem. Phys*., **1997**, *107*, 8554.
[34] Ahlquist, M. S. G.; Norrby, P.O. *Angew. Chem. Int. Ed.* **2011**, *50*, 11794.
[35] Chen, M.; Cracuin, R.; Hoffman, N.; Dixon, D. A. *Inorg. Chem.* **2012**, *51*, 13195.
[36] Lafrance, M.; Fagnou, K. *J. Am. Chem. Soc*. **2006**, *128*, 16496.
[37] Garcia-Cuadrado, D.; Mendoza, P.; Braga, A. A. C.; Maseras, F.; Echavarran, A. M. *J. Am. Chem. Soc*. **2007**, *129*, 6880.
[38] Zhang, S.; Shi, L.; Ding, Y. *J. Am. Chem. Soc*. **2011,** *133*, 20218.
[39] Lafrance, M.; Rowley, C. N.; Woo, T. K.; Fagnou, K. *J. Am. Chem. Soc*. **2006**, *128*, 8754.
[40] Zhao, Y.; Truhlar, D. G. *Theor. Chem. Acc.* **2008**, *120*, 215.
[41] Grimme, S.; Antony, J.; Ehrlich, S.; Krieg, H. *J. Chem. Phys*. **2010**, *132*, 154104; (b) Grimme, S.; Ehrlich, S.; Georigk, L. *J. Comp. Chem.* **2011**, *32*, 1456.
[42] Neese, F.; Wennmohs, F.; Hansen, A. *J. Chem. Phys.* **2009**, *130*, 114108.
[43] (a) Roger, J.; Doucet, H. *Tetrahedron*. **2009**, *65*, 9772; (b) Churruca, F.; Hernandez, S.; Perea, M.; San Martin, R.; Dominguez, E. *Chem Commun.* **2013**, *49*, 1413; (c) Roger, J.; Doucet, H. *Adv. Synth. Catal.* **2009**, *351*, 1977; (d) Bellina, F.; Benelli, F.; Rossi, R. *J. Org. Chem.* **2008**, *73*, 5529; (e) Bheeter, C. B.; Bera, J. K.; Doucet, H. *J. Org. Chem.* **2011**, *76*, 6407; (f) Yan, G.; Kuang, C.; Zhang, Y.; Wang, J. *Org. Lett.* **2010**, *12*, 1052.
[44] Meir, R.; Kozuch, S.; Uhe, A.; Shaik, S. *Chem. Eur. J*. **2011**, *17*, 7623.
[45] Gorelsky S. I.; Lapointe D.; Fagnou, K. *J. Org. Chem.* **2012**, *77*, 658.
[46] Anand, M.; Sunoj, R. B.;.Schaefer, III., H.F. *J. Am. Chem. Soc.*, **2014**, *136*, 5535.
[47] Anand, M.; Sunoj, R. B. *Org. Lett.* **2011**, *13*, 4802.
[48] Kozuch, S.;Shaik, S. *Acc. Chem. Res.* **2011,** *44*, 101.
[49] Mandal, D.; Yamguchi, A. D.; Yamaguchi, J.; Itami, K. *J. Am. Chem. Soc.* **2011**, *133*, 19660.
[50] Gong, X.; Song, G.; Zhang, H.; Li, X. *Org. Lett.* **2011**, *13*, 1766.
[51] Wang, Z.; Li, K.; Zhao, D.; Lan, J.; You. J.; *Angew. Chem. Int. Ed*. **2011**, *50*, 5365.
[52] Sun, Y. H.; Gorelsky, S. I.; Stuart, D. R.; Fagnou, K.; Campeau, L. C. *J. Org. Chem*, **2010**, *75*, 8180.
[53] Potavathri, S.; Pereira, K. C.; Gorelsky, S. I.; Pike, A.; LeBris, A. P.; DeBoef, B. *J. Am. Chem. Soc*. **2010**, *132*, 14676.
[54] Glover, B.; Harvey, K. A.; Lui, B.; Sharp, M. J.; Tymoschenko, M. F. *Org.Lett*. **2003**, *5*, 301.
[55] Lafrance, M.; Lapointe, D.; Fagnou, K. *Tetrahedron*. **2008**, *64*, 6015.
[56] Pascaul, S.; Mendoza, P. D.; Braga, A. A. C.; Maseras, F.; Echavarren, A. M. *Tetrahedron*, **2008**, *64*, 6021.
[57] Flegeau, E. F.; Bruneau, C.; Dixnuef, P. H.; Jutand, A. *J. Am. Chem. Soc.* **2012**, *133*, 10161.
[58] Hughes, C. C.; Trauner, D. *Angew. Chem. Int. Ed.* **2002**, *41*, 1569.
[59] Park, C.-H.; Ryabova, V.; Seregin, I. V.; Sromek, A. W.; Gevorgyan, G. *Org. Lett.* **2004**, *6*, 1159.
[60] Steinmetz, M.; Ueda, K.; Grimme, S.; Yamaguchi, J.; Kirchberg, S.; Itami, K.; Studer, A. *Chem. Asian J*. **2012,** 7, 1256.
[61] Tang, S.Y.; Guo, Q.X.; Fu, Y. *Chem. Eur. J*. **2011**, *17*, 13866.

Chapter 4

DFT studies of the mechanism and regioselectivity of '*ligandless*' Pd(II) arylation of N-acetyl indole

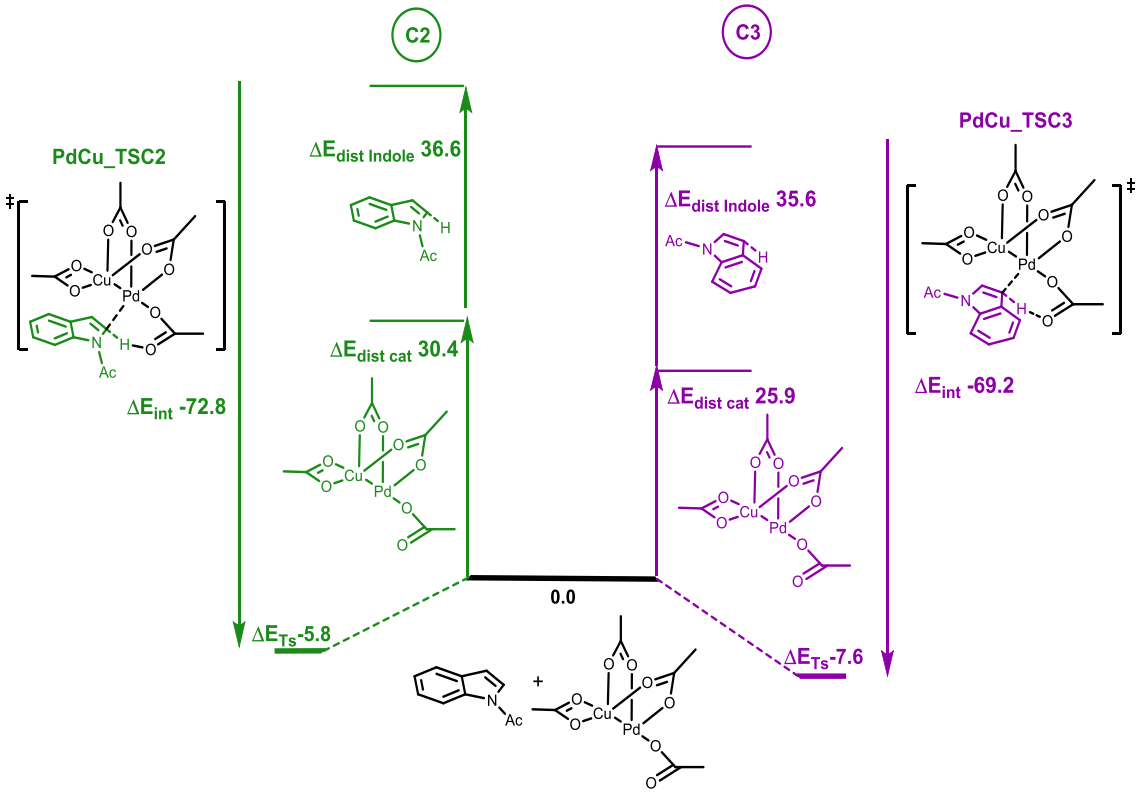

4.1. Introduction

The importance of functionalization of indole's C3 position is illustrated by the inclusion of twenty-eight C3 aryl indole in the World Drug Index[1], with twelve of these drugs established as important FDA approved pharmaceuticals.[2] Arylation of indoles has been the focus of synthetic endeavours since Ithara's novel arylation of N-acetyl indole using a $Pd(OAc_2)$ catalyst.[3,4] More recently, development in synthetic methodology has allowed for relatively benign conditions to be employed to initiate C-H functionalization of indoles and other heteroarenes in an oxidative (i.e. non-functionalized C-H/C-H manifold).[5] The N-acetyl indole motif has benefitted from advances in synthetic methodology, with arylation at the C3 position via oxidative arylation methodology now possible via Pd(II) catalysts.[6,7,8]

One of the most prominent examples of oxidative arylation of N-acetyl indole originates from the Fagnou group.[9] Here, the electron rich C3 position is cleaved and arylated in good selectivity (9:1, C3:C2) through successive oxidative C-H/C-H activations with a $Pd(OTFA)_2$ catalyst. Interestingly, the reaction conditions are similar to those utilized to activate and arylate at the C2 position (as seen in Chapter 3). However, judicious choice of oxidant is shown influence regioselectivity, where Ag(I)OAc produces the C2 regioisomer and switching to $Cu(OAc)_2$ results in the C3 arylated regioisomer (**Figure 1**).

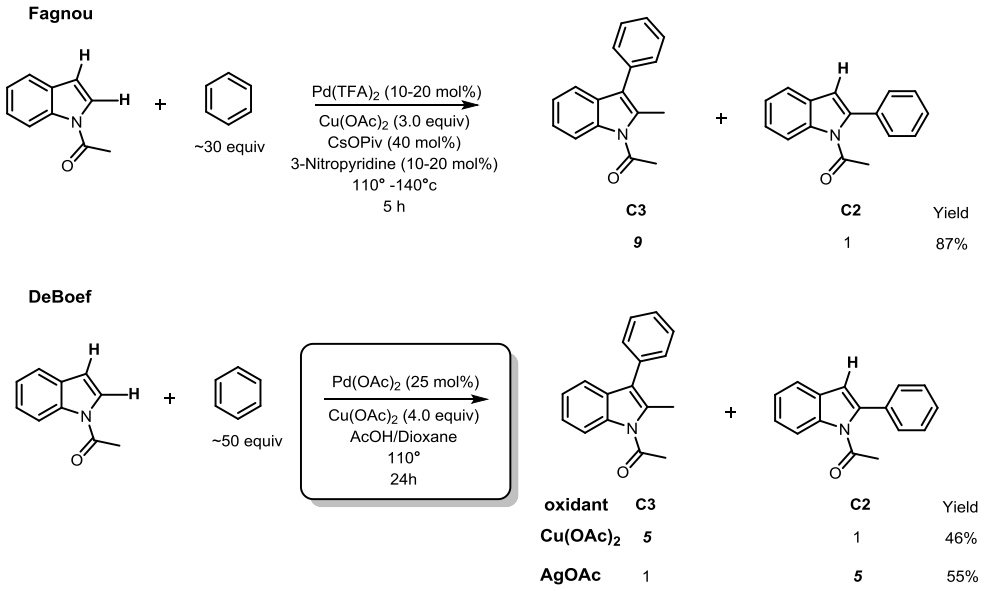

Figure 1. Fagnou and DeBoef's C3 arylation of N-acetyl indole under oxidative arylation conditions.

The choice of additives in the reaction (i.e. 3-Nitropyradine and CsOPiv) does not seem to alter experimental selectivity; however, turnover was accentuated with the use of these additives, with Fagnou suggesting that the stabilization of Pd(0) could be achieved through coordination with these additives.

Subsequently, DeBoef and coworkers[6] employed $Pd(OAc)_2$ with $Cu(OAc)_2$ to provide the C3 regioisomer in good selectivity (5:1). When AgOAc was used, a switch in regioselectivity occurred, favouring the C2 isomer in good selectivity (5:1). This observation of "oxidant-related" selectivity led the authors to speculate on the involvement of Pd-Cu clusters/ polymetallic catalysts in the C-H activation step. Similar selectivity for the C3 position of N-acetyl indole has been achieved by Gaunt[10] utilizing a Cu(II) catalytic system, however, under the conditions used by DeBoef using $Cu(OAc)_2$ alone results in no conversion . Similarly, if $Cu(OAc)_2$ is excluded from the reaction, $Pd(OAc)_2$ has to be increased to 100 mol% from 25 mol% (i.e. stoichiometric rather than catalytic) to elicit a reaction where a mixture of 1:1 is achieved for C2 and C3 regioisomers in low yield (40%). Therefore, there is a strong indication both reactivity and selectivity for the C3 position is reliant upon the cooperation of both Pd and Cu in the arylation of N-acetyl indole.

Both DeBoef and Fagnou have acknowledged the potential of a catalytic Pd-Cu species eliciting regioselectivity through C-H activation on N-acetyl indole, however no computational work examining this step has been presented. Previously, work from Houk[11] and Sunoj[12] has detailed the involvement of bimetallic catalysts in the C-H activation of aromatic systems illustrating the possibility of a cooperative (i.e. Pd-M, where M=copper, silver) CMD mechanism. Shaik[13] has examined the activation and homocoupling of benzene and N-acetyl indole respectively, however, for Pd catalyzed oxidative arylation of N-acetyl indole (or for that matter or any indole substrates prior to this work) there is to the best of our knowledge no known computational investigation into factors behind observed regioselectivity.

The mechanistic manifold follows from the previous chapter, with the CMD mechanism garnering much traction as the proposed mechanistic route to activation of heteroarenes.[14] We focused on examining the CMD mechanism as a route to arylation in N-acetyl indoles. In particular, we examined the catalytic cycles

possible for the oxidative arylation of N-acetyl indole at C3 and C2. The effect of the $Cu(OAc)_2$ in the CMD C-H activation step was also investigated to establish whether the possibility of a heterometallic dimer is supported by DFT calculations.

4.2. Computational methods

The computational protocol used for this chapter follows the methodology presented in section 2.2., Chapter 2. Modifications made to the methodology (for work presented in this chapter) are mentioned herein.

Initial geometry optimizations were performed with the **ω**B97XD functional and split-valance polarized 6-31G(d) basis set for C, N, O and H atoms, whilst the LANL2DZ double-zeta valence basis set and associated effective core potential (ECP) were used to describe Pd, Ag and Cu.[15] Single point energies were computed on all optimized geometries with the larger valence triple-zeta 6-311+G(d,p) and LANL2TZ basis set obtained from the EMSL Basis Set Exchange[16,17] A fine grid density was used for numerical integration in all DFT calculations.

The effects of solvent (acetic acid ε= 6.2528) were incorporated through the use of a conductor-like polarizable continuum model (CPCM), defining the solute cavity with UFF radii[18] by conducting single point calculations on optimized geometries. A smooth damping function centred about a frequency of 100 cm^{-1} was used to switch between the harmonic approximation for vibrations above this value and the free-rotor approximation below.[19] Bond dissociation energies (BDE) were calculated through enthalpy calculations using the G3B3 composite method, where structures and zero point vibrational energies are calculated at the B3LYP/6-31g(d) level of theory.[20]

A conventional standard state of 1 mol/l in solution for all species was employed in calculating the translational entropies via the Sackur-Tetrode expression. All structures are depicted with CYLview [21] or ChemDraw. All energies presented within this work are Gibbs (ΔG) free energies calculated via:

$$\Delta G_{solv} = \Delta E_{solv} + (\Delta G_{gas} - \Delta E_{gas})$$

Natural Population Analysis (NPA)[22] was performed using the NBO 6.0 program[23] to evaluate the natural atomic charge on individual atoms.

4.3. Results

Previous work (Chapter 2 & 3) provided computational evidence against the EAS mechanism in indoles. However, the electronic character of N-acetyl indole differs from N-methyl indole due to the electron withdrawing effect of the attached N-acetyl moiety (as opposed to the electron donating nature in N-methyl). Therefore, we calculated the ESP map for N-acetyl indole (**Figure 2**). The electron density in N-acetyl indole is focused predominantly within the C6 benzene ring; however, activation is favoured at C3, which is counter intuitive to the electrostatics of the substrate. This is similar to N-methyl indole where the electron density resides predominantly in C6 ring and the C3 position and arylation is can be observed at the C2 position (as seen in the previous chapter).

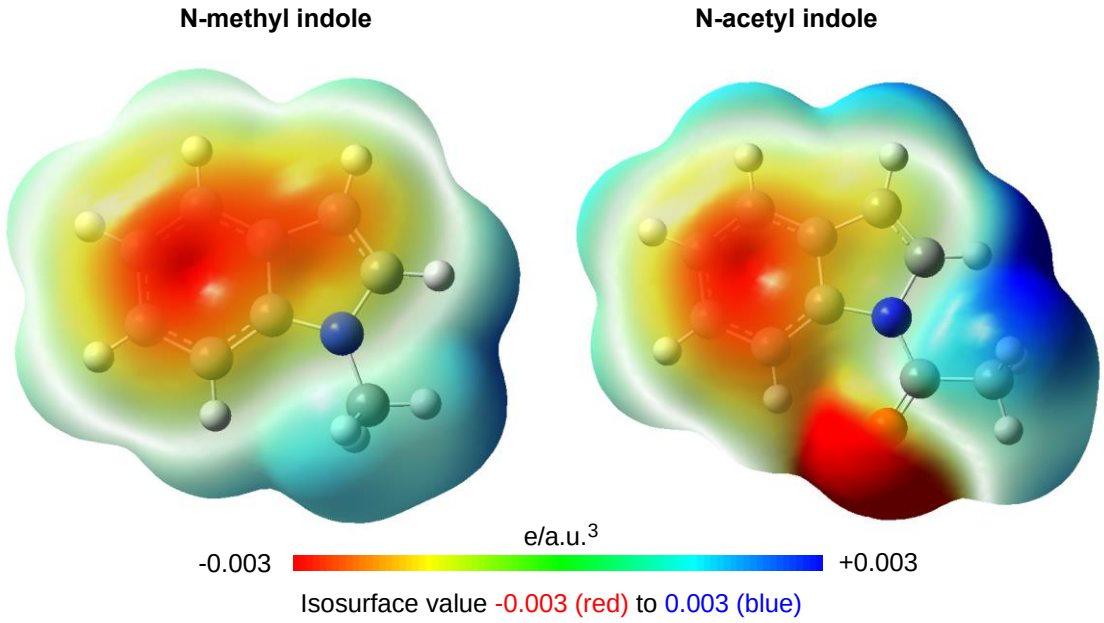

Figure 2. Electrostatic Potential Map (ESP) exhibiting the electrostatics of N-methyl indole and N-acetyl indole where electronegative regions (blue) and electropositive regions (red) are shown.

For completeness potential energy scans (focussing on the bond distance between Ph-H and the C2-C3 bond) using cationic $PhPd^{+}$ catalyst and N-acetyl indole were conducted at the **ω**B97XD and MO6-2X[24] level of theory in order to examine the nucleophilic character of N-acetyl indole. Potential energy surface scans yielded ground states for the indole-Pd species and as before no EAS TS was located (**Figure 3**).

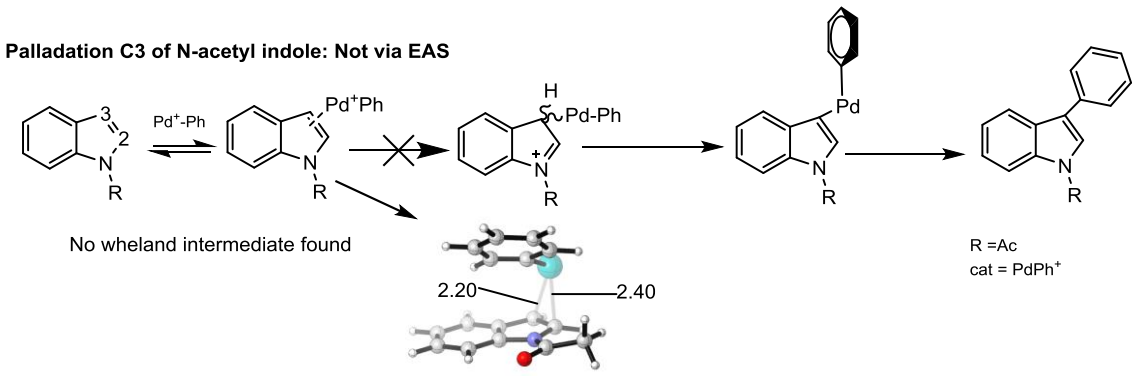

Figure 3. Wheland intermediate associated with EAS not located with potential energy scans of N-acetyl indole and Pd(II). Instead, ground state structure of Pd(II) η^2 to N-acetyl indole was located.

Therefore, our calculations focused on examining the C-3 arylation of N-acetyl indole with initial C-H activation occurring via CMD (**Figure 4**), where C-H activation of N-acetyl indole occurs with Pd(II) catalyst (**1**), followed by subsequent C-H activation of benzene with a Pd(II)-indole species (**2**) and arylation is completed through (**3**) a C-C bond forming reductive elimination through a three centred transition state. Oxidation of Pd(0) to the active catalytic species Pd(II) is independent of substrate and so it is unlikely to be involved in imparting regioselectivity and was therefore not calculated explicitly.

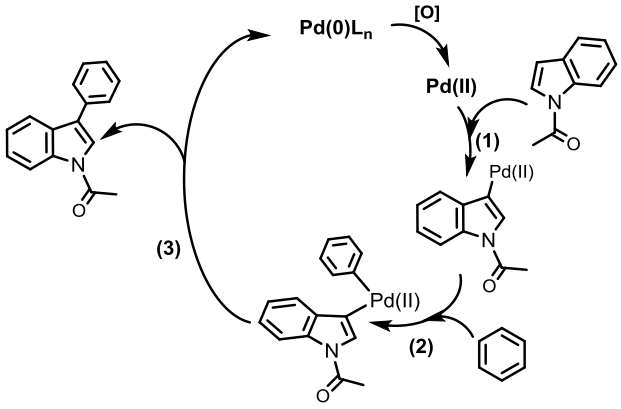

Figure 4. Initial calculation of CMD mechanism with activation of N-acetyl indole first. Hydrogens are omitted for clarity and L (in Pd(0)L) is presumed to be AcOH.

4.3.1. Initial C-H activation of N-acetyl indole

We investigated the role of Cu in the initial C-H activation step of N-acetyl indole. It has been suggested that Pd-Cu dimers may play a role in providing favourable activation at C3. In fact, it is presumed that C3 would be the naturally reactive position for N-acetyl indole due to the higher electron density located there (compared to C2). Our calculations characterized the transition state of the CMD C-H activation (step **1** of catalytic cycle in **Figure 4**) at the C2 and C3 positions with $Pd(OAc)_2$, $Pd(OAc)_2$-DMF, $Pd(OAc)_2$-AcOH and $PdCu(OAc)_4$ (**Figure 5**).

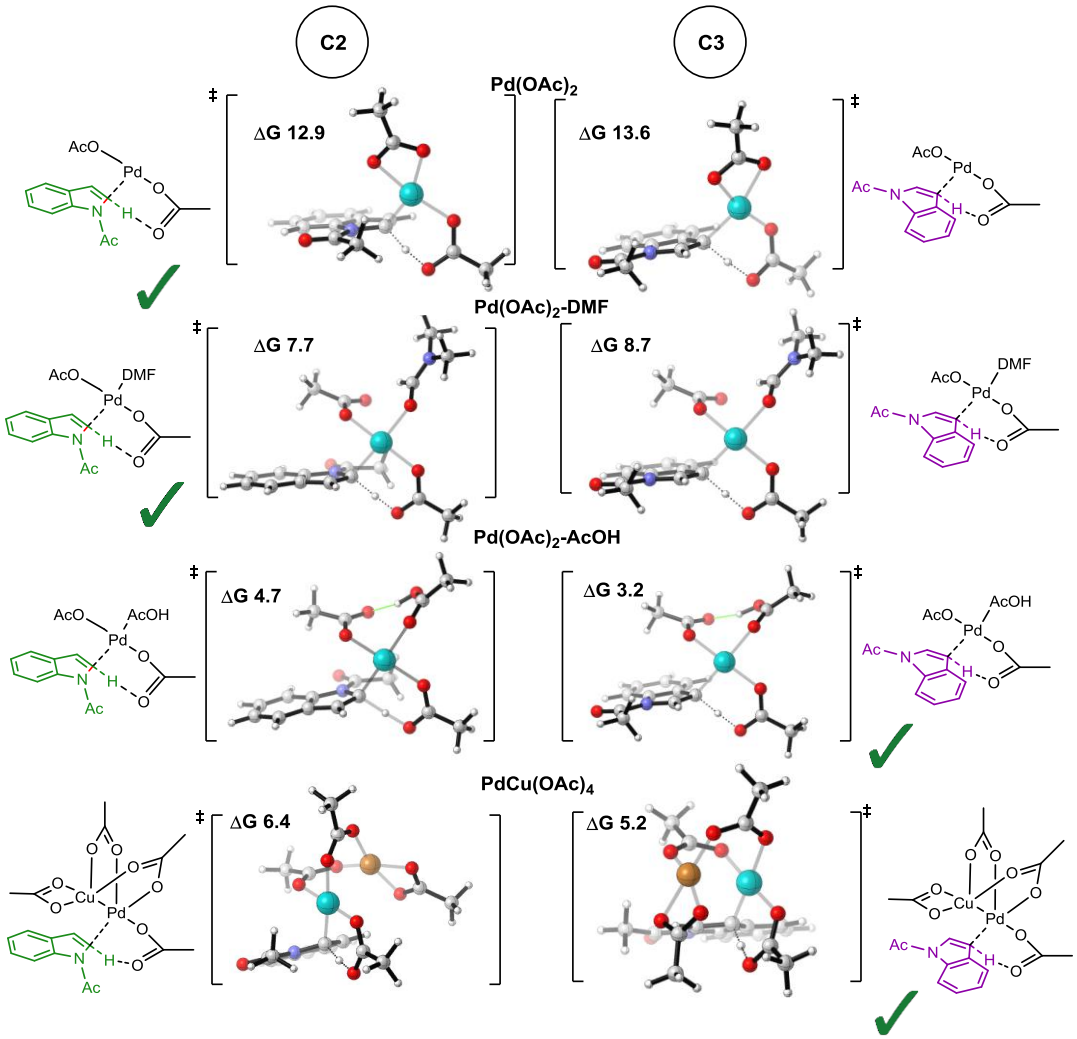

Figure 5. Calculated TS geometries of Pd(II) species for the initial C-H activation step of N-acetyl indole at C2 (LHS) and C3 (RHS). All values given in kcal/mol.

Upon calculation of the six membered intramolecular deprotonation TS (facilitated by the OAc^- ligand on Pd) it was noted that C-H activation of N-acetyl indole was favoured for the C2 position with $Pd(OAc)_2$(C3: ΔG 13.6 kcal/mol; C2: ΔG 12.9

kcal/mol) and $Pd(OAc)_2$-DMF (C3: ΔG 8.7 kcal/mol; C2: ΔG 7.7 kcal/mol) as the catalytic species.

However, using $Pd(OAc)_2$-AcOH and $PdCu(OAc)_4$ – the selectivity for the CMD step changes to give the C3 position as the favoured site for deprotonation, $Pd(OAc)_2$-AcOH (C3: ΔG 3.2 kcal/mol; C2: ΔG 4.7 kcal/mol) and $PdCu(OAc)_4$ (C3: ΔG 5.2 kcal/mol; C2: ΔG 6.4 kcal/mol). This is also observed in $Pd_2(OAc)_4$ where C3 (ΔG 13.8 kcal/mol) is favoured over C2 deprotonation (ΔG 15.6 kcal/mol). However, the dimeric Pd species, $Pd_2(OAc)_4$ is not as competitive as the monomeric Pd species, $Pd(OAc)_2$-AcOH in the C-H activation step, which is be consistent for both N-methyl indole (chapter 3) and N-acetyl indole.

Calculations using $PdAg(OAc)_3$ as a catalytic species favoured activation at C3 (ΔG 8.9 kcal/mol) over C2 (ΔG 9.3 kcal/mol), where a rotation of N-acetyl group on indole provides a weak electrostatic interaction with Ag through coordination, however, this does not influence selectivity, as selectivity is still favoured at C3 whereas in experiment, upon changing oxidant from Cu to Ag, the favoured regioisomer is the C2 product (**Figure 6**).

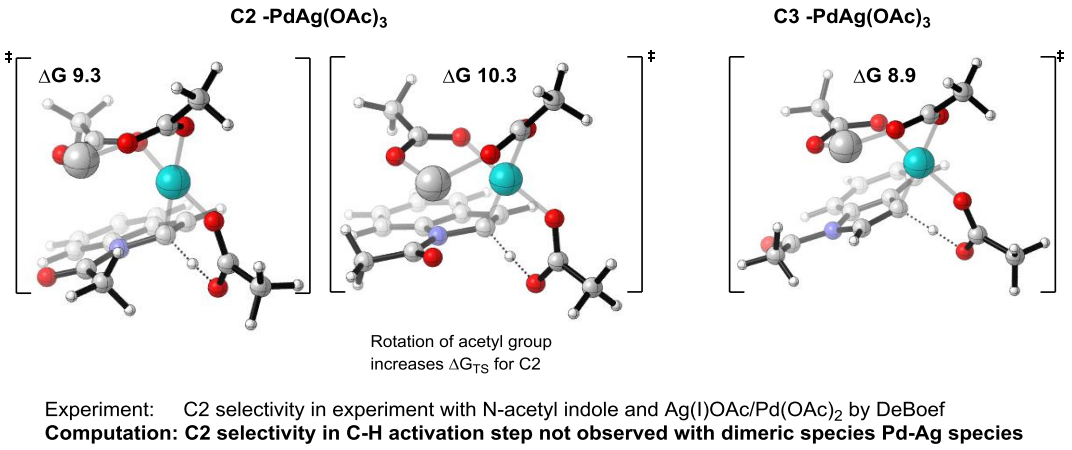

Figure 6. CMD C-H activation TSs for Pd-Ag dimer and N-acetyl indole. Calculations predict C-H activation to be favoured at the C3 position. All energies in kcal/mol.

Proposals by both Fagnou and DeBoef have hypothesized that mixed Pd-Cu species are catalytically active, while the role of AgOAc is to disrupt $Pd_x(OAc)_{2x}$ clusters to form monomeric $Pd(OAc)_2$ species.[9] Here we gain some support for this argument in observing that the Pd/Cu catalyst gives lower activation barriers by around 4 kcal/mol than the Pd/Ag catalyst examined above. More compelling

support of this hypothesis comes from DFT calculations examining the thermodynamics of forming such mixed metal clusters, which show that creating a Pd-Ag dimer from aggregated $Pd_3(OAc)_6$ and $Ag_2(OAc)_2$ is an extremely energeticallly unfavourable process (**Figure 7**), since E_{rxn}=62.6 kcal/mol. In contrast the creation of a mixed $PdCu(OAc)_4$ cluster is relatively more favourable (E_{rxn}=46.4 kcal/mol). However, it must be acknowledged that the creation of the Pd-Cu dimer requires a substantial amount of energy (according to our calculations). Experimentally, the existence of Pd-Cu polymetallic catalytic clusters (e.g. $CuPd(OAc)_4$ and $CuPd_2(OAc)_6$) has been determined through infra-red and ultra-violet spectroscopy, and within the same study it was noted that in the presence of alkali metal acetates (e.g. KOAc), these clusters did not aggregate.[25] Therefore, it is likely that AgOAc provides the anionic OAc^- to disrupt aggregated $Pd_x(OAc)_{2x}$ clusters creating monomeric $Pd(OAc)_2$, which is more likely to be involved in the C-H activation of N-acetyl indole where C2 regioselectivity is observed (as shown by calculations in **Figure 5**).

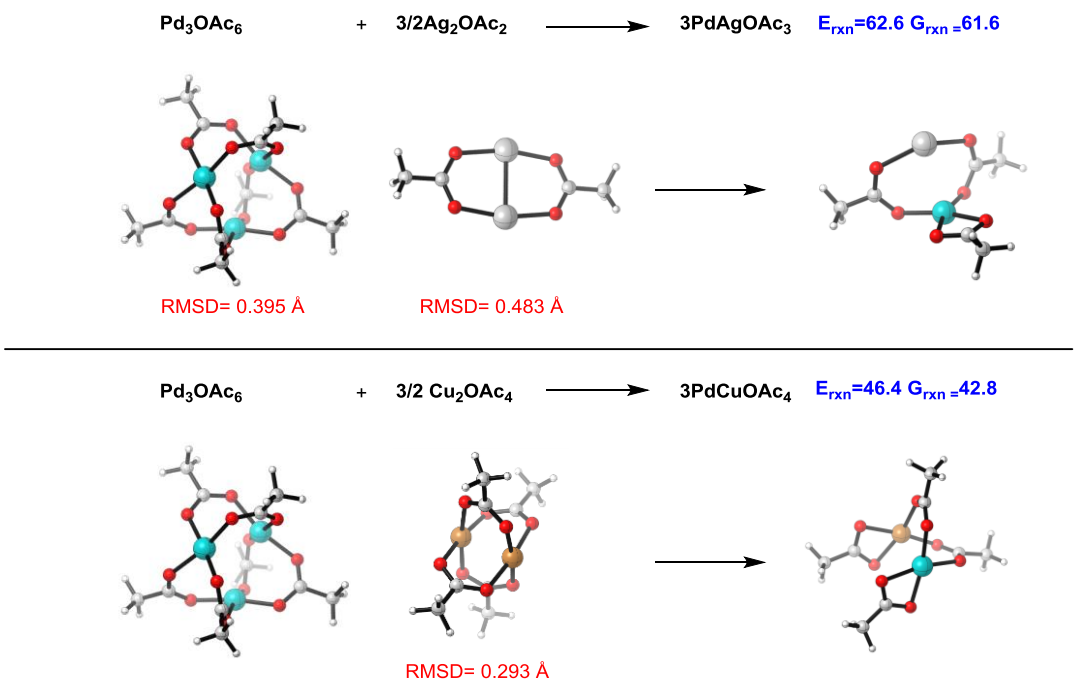

Figure 7. Optimizations at ωB97XD/6-31G(d)/LANL2DZ. RMSD calculated against crystal structures. All values in kcal/mol.

We therefore suggest that the initial C-H activation is more likely to occur via Pd-Cu dimer as the catalytic species, which prefers coordination with Pd as opposed to Cu to C2 or C3 of N-acetyl indole. Work investigating a switch in coordination (i.e.

where Cu coordinates to C3 or C2 instead of Pd in the CMD C-H activation TS) resulted in higher TS energies for the C-H activation of C2 and C3 and produced the C2 regioisomer as the favoured regioisomer for C-H activation (C3: ΔG 21.8 kcal/mol; C2: ΔG 20.8 kcal/mol). This is contrary to observed experimental results of DeBoef and Fagnou, and thus, our calculations favour a picture where the palladation and deprotonation occurs via a CMD mechanism, as part of a dimeric Pd-Cu catalytic species (**Figure 8**).

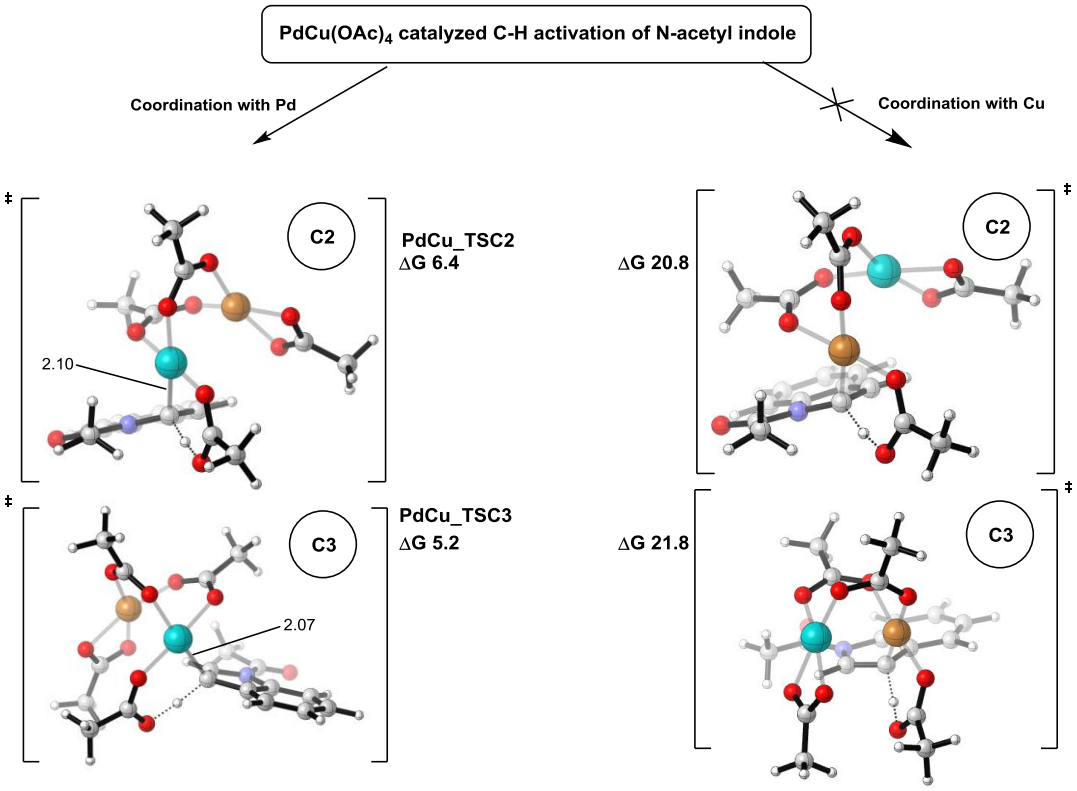

Figure 8. Different methods of C-H activation with N-acetyl indole and Pd-Cu catalytic species. Activation at C2 with Pd coordination as opposed to Cu coordination gives the lowest ΔG_{TS}. All values in kcal/mol.

Distortion-Interaction Energy Analysis

No significant difference in the computed NPA charge of Pd was seen amongst all calculated TSs, therefore the regioselectivity of N-acetyl indole C-H activation is not simply the result of charge differences between the various Pd catalysts considered. To more fully understand the energy difference between the two dimeric Pd-Cu TSs (i.e. C2 and C3), a distortion interaction analysis was performed (**Figure 9**).[26,27] This analysis separates and quantifies the energy cost for distorting the substrate and catalyst from their minimum energy geometry to the geometry adopted in CMD TS (ΔE_{dist}) and the energy released in their associated interaction (ΔE_{int}). The ΔE_{dist} (cat) is the energy associated with distorting the Pd-Cu catalyst and its ligands to the TS geometry, similarly, ΔE_{dist} (indole) is the energy associated with distorting N-acetyl substrate to the TS geometry.

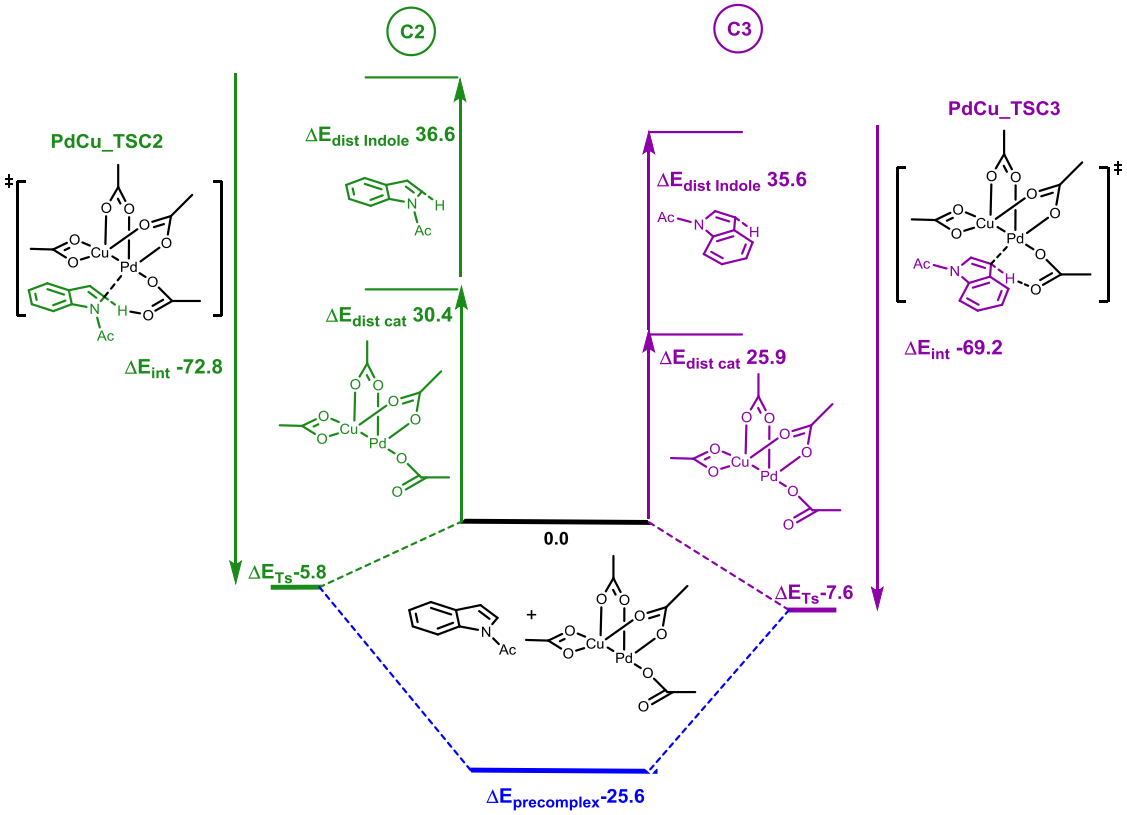

Figure 9. Distortion-Interaction Analysis (ΔE kcal/mol) for Pd-Cu CMD TSs of N-acetyl indole. Less distortion of the Pd-Cu catalyst in the CMD TS is observed for C3 C-H activation (*purple*). All values in kcal/mol.

While **PdCu_TSC2** has slightly more favourable interaction energy (E_{int}) than **PdCu_TSC3**, the unfavourable distortion term ($\Delta E_{dist\ cat}$) of the Pd-Cu catalyst is

more significant in C2 (by 5.5 kcal/mol) and ultimately this outweighs the benefit of the interaction energy. The indole substrate experiences almost identical variation of distortion for both regioisomers and the computed distortion of the Pd-Cu catalyst creates the distinct preference for C3. The differential catalyst distortion in the two TS structures was traced to geometric differences: in the higher energy, more distorted/strained catalyst the distance between Pd and Cu centres is increased (2.87 Å) relative to the less distorted structure (2.77Å). While it is tempting to speculate on the role of a Cu-Pd bonding interaction in this energy difference, computed bond orders are small and differ by an even smaller amount (0.02 vs. 0.01, for C3 and C2, respectively).

In addition to the geometrical analysis, a charge transfer analysis, where the cumulative charge of the indole and catalyst in the TS was calculated via NBO calculations in order to quantify the charge separation in the TS between the two regioisomers for the Pd-Cu species.[28,29] However, this charge transfer was always more prominent for the C3 TS, irrespective of the relative stabilities of the two regioisomers, signifying the inability of a charge transfer argument to explain observed regioselectivity.

Studying the four catalytic species which provided regioselectivity at C3 (in the C-H activation step) for N-acetyl indole – $Pd(OTFA)_2$, $Pd(OAc)_2$-AcOH, $Pd_2(OAc)_4$ and $PdCu(OAc)_4$ – the six TS (i.e. C2 and C3 for all three species) studied provided a good correlation (R^2=0.874) between distortion of the catalyst in the TS ($\Delta E_{dist\ cat}$) and ΔG TS. Therefore, increased structural distortion of the catalyst in the TS provides a higher ΔG TS for the species, with $\Delta E_{dist\ cat}$ always higher for the C2 TS. No correlation was observed between the distortion of the indole substrate (ΔE_{indole}) and ΔG, or between the interaction energy (Δ_{int}) and ΔG. This emphasises the identity of the catalyst in controlling the site of activation (A).

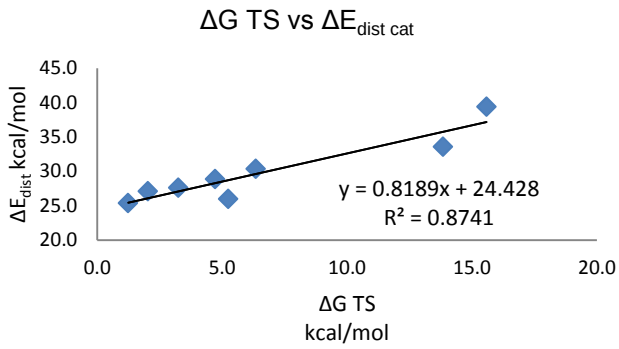

Species	ΔG TS	$\Delta E_{dist\ cat}$
$Pd(OAc)_2$-AcOH – C2	4.7	28.9
$Pd(OAc)_2$-AcOH – C3	3.2	27.6
$Pd(OTFA)_2$ – C2	2.0	27.1
$Pd(OTFA)_2$ – C3	1.2	25.4
$Pd_2(OAc)_4$ –C2	15.6	39.4
$Pd_2(OAc)_4$ –C3	13.8	33.6
$PdCu(OAc)_4$-C2	6.4	30.4
$PdCu(OAc)_4$-C3	5.2	25.9

Figure 10. Relationship between ΔG_{TS} and $\Delta E_{dist\ cat}$ indicating distortion in TS of catalyst leads to disfavourable ΔG_{TS}, with the C2 $\Delta E_{dist\ cat}$ experiencing higher distortion in C-H bond cleavage of N-acetyl indole. All values in kcal/mol.

4.3.2. C-H activation of benzene with Ar-Pd(II)-OAc

Following the initial C-H activation of N-acetyl indole, the second C-H activation of benzene must occur in order to produce the diarylated Pd species required for reductive elimination. In order for coordination of benzene to occur (to Pd), a coordination site has to become available on the metal centre.

Post abstraction, the reaction can proceed through the dissociation of $Cu(OAc)_2$ as a stable species (ΔG -5.7 kcal/mol), thus opening a coordination site *cis* to the indole species. Activation and palladation of benzene can therefore occur through the CMD mechanism, where an acetate ligand affixed to the Pd centre, *cis* to the incoming benzene can undertake proton abstraction. The dissociation of AcOH (produced from the first activation of N-acetyl indole) is disfavoured, and the reaction is calculated to proceed through a four coordinate, square planar Pd CMD transition state (**Figure 11**).

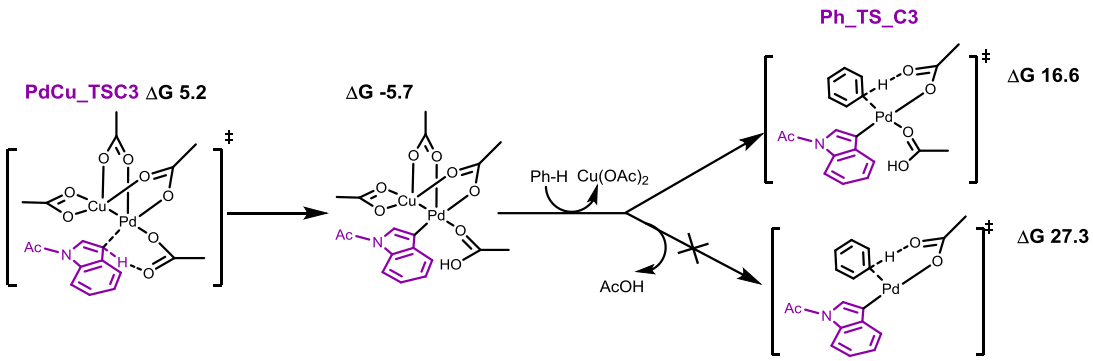

Figure 11. The initial C-H activation of N-acetyl indole (**PdCu_TSC3)** at the C3 position followed by dissociation of $Cu(OAc)_2$ and coordination/deprotonation of benzene in **Ph_TS_C3**. Dissociation of AcOH is disfavoured. All values in kcal/mol.

The activation of benzene was calculated to be lower for C3-coordinated N-acetyl indole species (**Ph_NAc_C3**: ΔG 16.6 kcal/mol) as opposed to C2 (**Ph_NAc_C2**: ΔG 18.1 kcal/mol). The reaction proceeds through initial η^2 coordination of the benzene π system with Pd, followed by deprotonation initiated by the acetate ligand *cis* to benzene through a six membered transition state (**Figure 12)**.

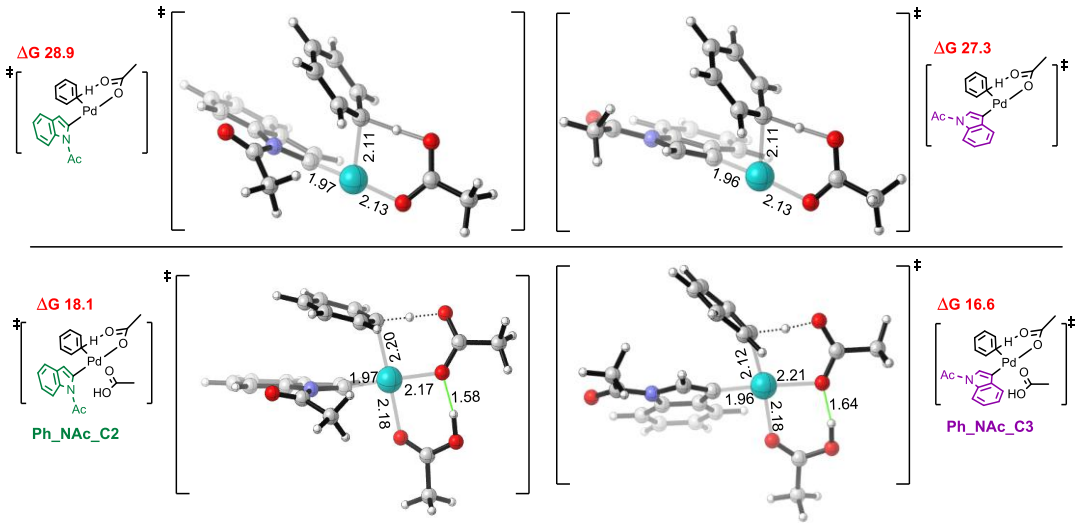

Figure 12. Optimized geometries of C-H activation of benzene through (*top*) tri coordinate Pd(II) and (*bottom*) four coordinate Pd(II) species. All values in kcal/mol. All bond lengths in Å

An intramolecular hydrogen bond is present in both precomplexes, between the AcOH ligand *cis* to the OAc ligand (C2 O-H—O: 1.58Å; C3 O-H—O: 1.64Å). In the activation of **Ph_TS_C2**, the acetyl group is not co-planar with the indole ring and there is noticeable out of plane bending. Presumably this is due to the steric interaction between the adjacent benzene ring and the CH_3 groups on acetyl, which

is avoided in **Ph_TS_C3**. The precomplex for the C3 coordinated Pd species is lower (ΔG -2.6 kcal/mol) compared with C2 (ΔG 1.9 kcal/mol). Upon deprotonation, the Ph species coordinates to the metal centre, in *cis* conformation to N-acetyl indole thus providing ideal coordination for the subsequent reductive elimination step. The C-H activation of benzene is calculated as the selectivity determining slow step of the catalytic cycle (as seen in the final energy profile, **Figure 15**).

4.3.3 Reductive elimination of N-acetyl indole and Ph

The new C-C bond is formed through a reductive elimination step. For the RE pathway we calculated two potential RE TSs, with a variety of coordinated AcOH ligands. Calculations focused on tri coordinate Pd(II) (i.e. Ar-Pd(II)AcOH-Ar') and four-coordinate RE TS (Ar-Pd(II)$AcOH_2$-Ar') RE TSs. The square planar 16 electron Pd(II) RE TS were calculated with lower Gibbs free energy and are more favourable than their 14 electron counterpart (**Figure 13**).

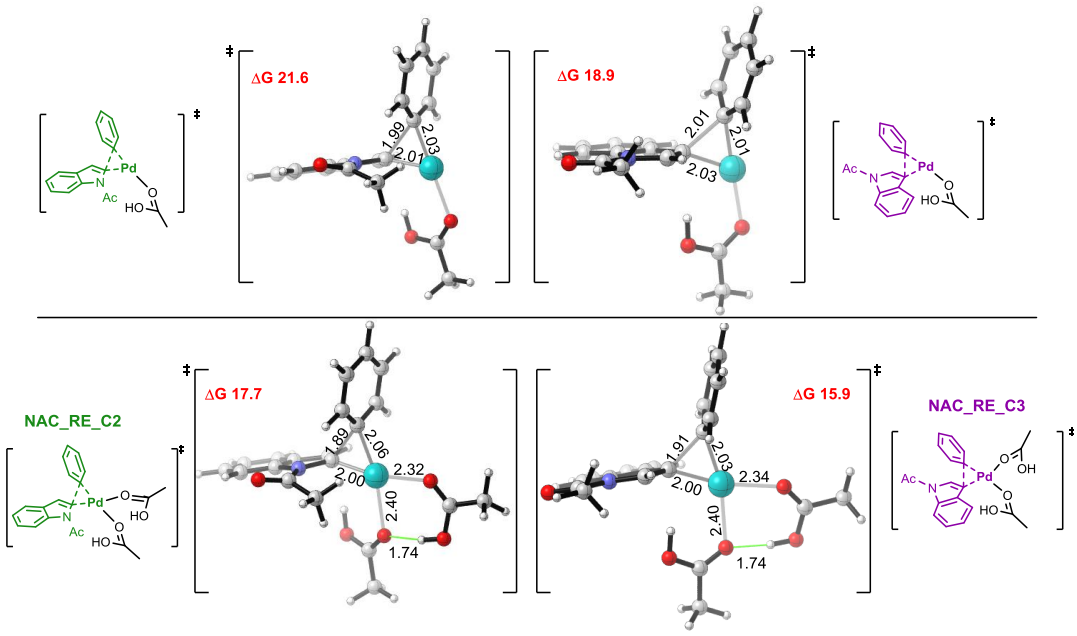

Figure 13. Reductive elimination TS for (top) tri-coordinate Pd(II) and (bottom) four coordinate Pd(II). All energies given in kcal/mol. All bond lengths in Å.

The calculated NPA charge on Pd did not differentiate much between C2 and C3 RE TSs in both the tri coordinate species (C2 Pd: 0.3; C3 Pd: 0.2) or the four coordinate RE TSs (C2 Pd: 0.4; C3 Pd: 0.3). The C3 regioisomer carries less positive charge on Pd in the RE TS, which presumably assists in a favourable

transfer of Ph to C3 (as compared to C2). Similar to the C-H activation of benzene, the acetyl group loses co-planar conformation (w.r.t. indole) in the C2 TS, however bond lengths do not illustrate significant disparity in key bond distances within the TS.

4.3.4. Kinetic Isotope Effects

In order to verify our preferred energy profile against experimental KIEs, computed KIE were analysed. These were calculated against DeBoef's observed KIE (**Figure 14**) where the perdeuterated benzene coupled at C3 with a primary kinetic isotope effect measured at 4.0.

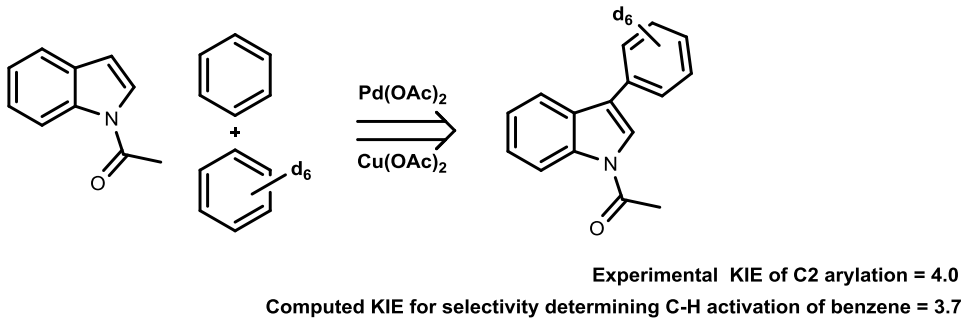

Figure 14. Experimental KIE calculated through competition experiment with perdeuterated benzene and benzene for arylation at C3.

Our calculations examined the selectivity determining C-H activation of benzene and calculated a similar primary KIE of 3.7, in excellent agreement with the experimentally observed KIE. Furthermore, KIE calculations of the reductive elimination step (where perdeuterated benzene is coupled to C3) provided a secondary kinetic isotope effect of 1.0, thus confirming that the experimentally observed KIE is likely to arise through the selectivity determining C-H activation of benzene, corroborating our reaction pathway to the arylation of C3.

4.3.5. Summary

Examining the selectivity determining step further (i.e. C-H activation of benzene), the calculated selectivity of C3:C2 regioisomer has a $\Delta\Delta G^{\ddagger}$ of 1.5 kcal/mol (between Ph_Ts_C2 and Ph_TS_C3) which provides a predicted selectivity of 10:1 (C3:C2). To attain the 5:1 (C3:C2) selectivity achieved in experimental conditions by DeBoef, $\Delta\Delta G^{\ddagger}$ between the two regioisomers would require to be 1.1 kcal/mol – a difference of 0.4 kcal/mol. Therefore, we can conclude our calculations and associated energy profile illustrate good agreement with experimental selectivity of the C3 arylated regioisomer and associated KIE.

Our calculations show that via this pathway (**Figure 15**), the Cu-Pd species provides a favourable C-H bond cleavage at C3 of N-acetyl indole. The computed energy changes for the formation of a mixed Pd-Cu species was shown to be favourable, however, postulated Pd-Ag species is far less likely to form under the reaction conditions. Selectivity is influenced by the catalyst (i.e. $PdCu(OAc)_4$) exhibiting less distortion in the C-H activation TS geometry. There is a relationship between the addition of $Cu(OAc)_2$ and $Pd(OAc)_2$ in both Fagnou and DeBoef's approaches, with the DeBoef experiment requiring Cu to increase yield of the C3 arylated product (yield of C2 remains unchanged with changing amounts of Cu and absence of Pd results in no reaction), we believe a dimeric Pd-Cu catalytic species will assist in the initial C-H activation step.

Following the initial C-H activation of N-acetyl indole, the dissociation of $Cu(OAc)_2$ is required to create a monomeric Pd(II) species, which is calculated to undertake the selectivity determining C-H activation of benzene. The arylation of N-acetyl indole is completed in the final step through reductive elimination of a 16 electron Pd(II) species, which also favours C3 selectivity.

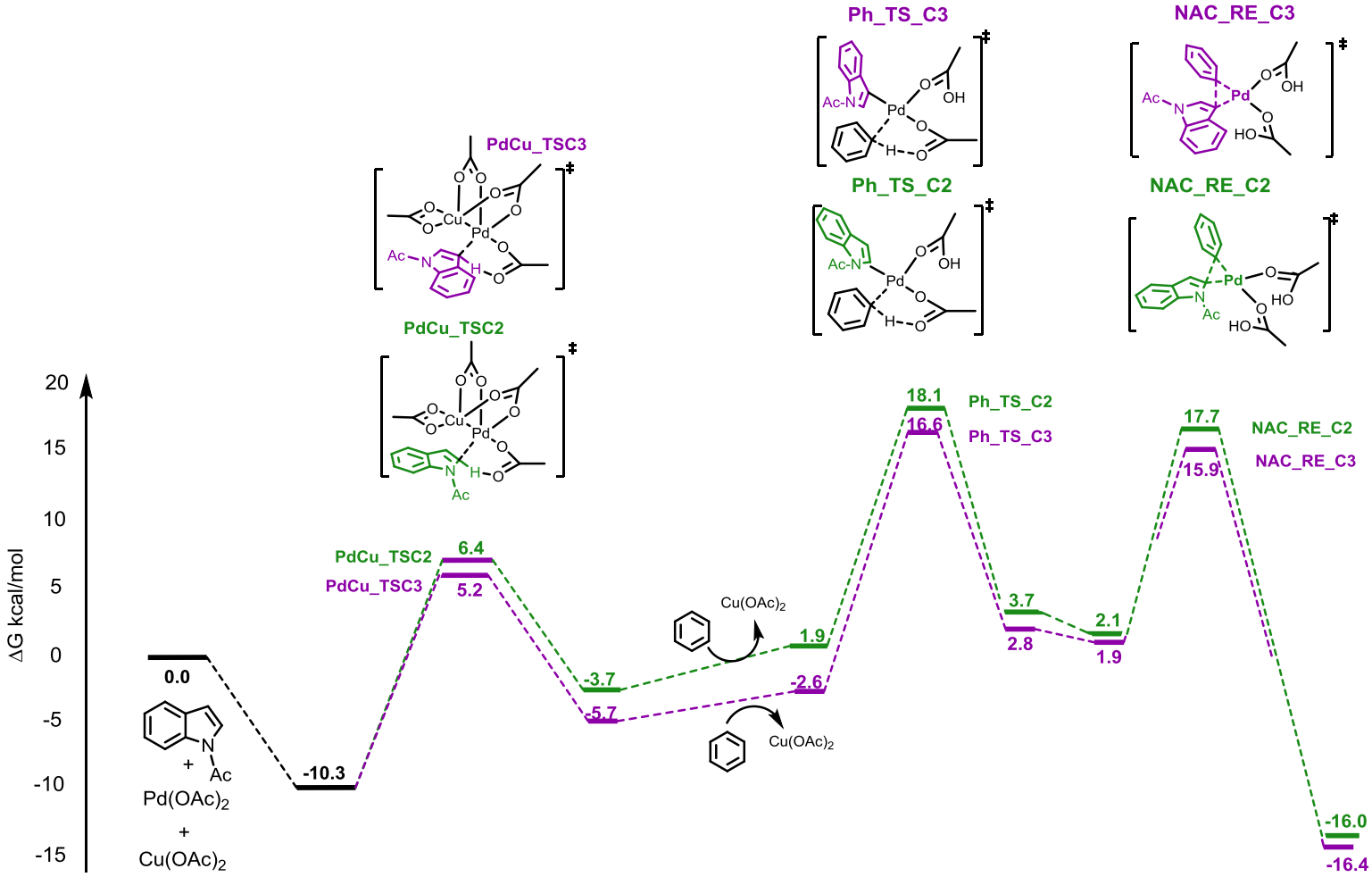

Figure 15. Free energy profile for arylation of N-acetyl indole with $PdCu(OAc)_4$ undertaking the initial activation of N-indole. The selectivity determining step is the C-H activation of benzene (2nd step). All values in kcal/mol

4.3.6. Alternative catalytic cycle

For completeness we calculated an alternative set of mechanistic events, whereby the activation of benzene is the first step (**1**) followed by the subsequent activation of N-acetyl indole and completed via a reductive elimination step (**Figure 16**). As the experiment is conducted with an excess of benzene (~30 equivalents) this is indeed possible. As seen in Chapter 3, a wide range of Pd catalytic species (monomeric and bimetallic) have been calculated for the initial activation of the benzene species.

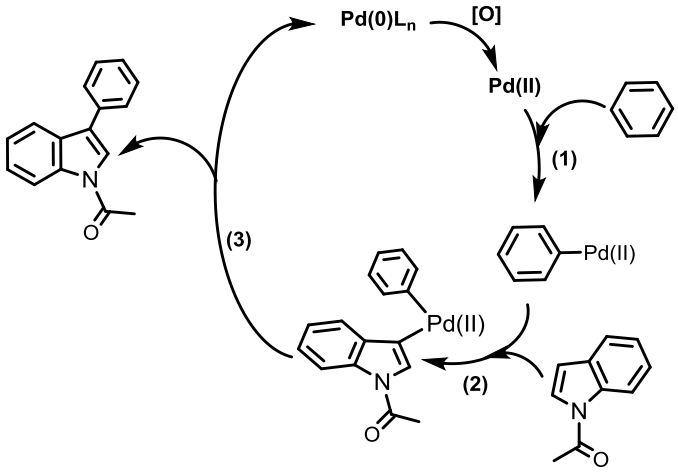

Figure 16. Catalytic cycle with initial C-H activation of benzene of N-acetyl indole, where initial activation occurs at benzene (**1**) followed by C-H activation at the C3 position of indole with PhPd(II) catalyst (**2**) and reductive elimination to produce the C3 arylated product (**3**).

4.3.7. Initial C-H activation of benzene

We calculated the initial activation of benzene through a polymetallic $PdCu(OAc)_4$ catalyst. It was presumed in the absence of Ag(I)OAc it is less likely that aggregated Pd clusters would be disrupted into monomeric Pd(II). Our initial calculations therefore focused on the CMD mechanism via the six membered intramolecular deprotonation TS. Here, the lowest energy resting state is still the η^2 precomplex formed between the Pd-Cu catalyst and the π-system of N-acetyl indole at ΔG -10.3 kcal/mol. Upon dissociation from N-acetyl indole, $PdCu(OAc)_4$ proceeds to coordinate to the π system of benzene, in an η^2 coordination mode leading to a precomplex higher in Gibbs free energy at ΔG -5.5 kcal/mol (**Figure 17**). This is subsequently followed by coordination of Pd η^1 to benzene in CMD TS, where C-H bond cleavage is calculated at ΔG 6.3 kcal/mol.

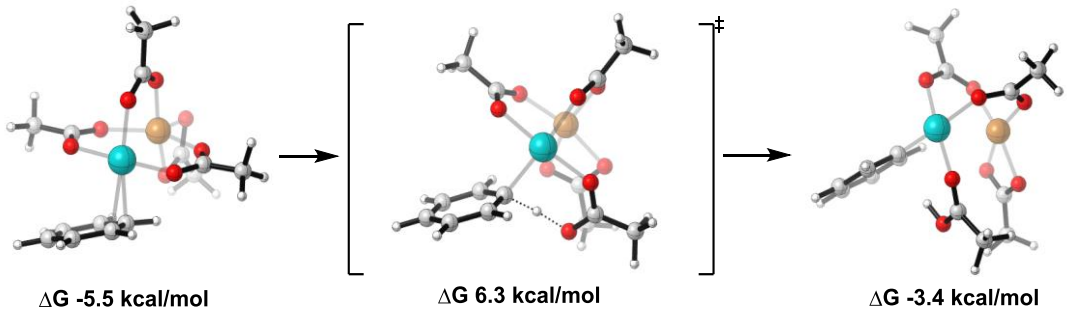

Figure 17. Precomplex, TS and post TS geometries of C-H activation of benzene with $PdCu(OAc)_4$. All values in kcal/mol.

Upon deprotonation of benzene, we calculated the dissociation of $Cu(OAc)_2$, to give PhPd(II)OAc-AcOH as the active catalytic species (i.e. monomeric Pd(II) to undertake the activation of N-acetyl indole). The alternative Pd(II) species where a ligand dissociates in the form of acetic acid was also calculated (i.e. PhPd(II)OAc). However, this pathway was energetically less competitive and was therefore disregarded (with respect to the activation of N-acetyl indole). The catalytic PhPd(II)OAc-AcOH species coordinates η^2 to N-acetyl indole as seen in the initial resting state as the energetically stable precomplex prior to the CMD TS for both C3 and C2 activation.

The C-H activation at the C2 position (ΔG 9.8 kcal/mol) is more favourable TS than that compared to C-H activation C3 (ΔG 11.0 kcal/mol). This is contrast to what was observed in the previous section where the C-H bond cleavage for the C3 position was preferred with a $PdCu(OAc)_4$ catalyst. The C-H bond cleavage of N-acetyl indole with PhPd(II)OAc-AcOH displays an endergonic reaction profile for both C2 and C3 regioisomers, where the acetic acid ligand *cis* to the ambiphillic acetate ligand establishes an intramolecular H-bond with the lone pair on oxygen in OAc and the proton on acetic acid (**Figure 18**).

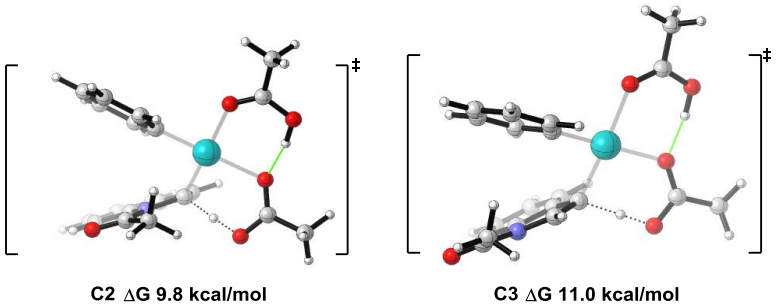

Figure 18. Optimized TS geometries for the C-H activation of N-acetyl indole with PhPd(II)OAc-AcOH. Intramolecular H bond shown in green. All values in kcal/mol

The reaction continues through a relatively stable post-abstraction intermediate, where Pd(II) is coordinated to the either C2 (ΔG 2.1 kcal/mol) or the C3 position (ΔG 1.9 kcal/mol). The phenyl group assumes a *cis* disposition to N-acetyl indole, priming itself for the C-C bond forming three-centred reductive elimination step. The reductive elimination TS is calculated to favour reductive elimination at the C3 position, illustrating a switch in selectivity compared with the initial C-H activation event. The arylation event is a highly exergonic process which leads to a slightly more stable C3 product (by 0.4 kcal/mol). The final C-C bond forming reductive elimination step (as seen in the previous section, NAC_RE_C3 & NAC_RE_C2) is also calculated to be selectivity determining via these set of events (**Figure 19**). Preference for the C3 product via the reductive elimination TS is observed, which concurs with observed experimental selectivity observed by both Fagnou and DeBoef.

The selectivity calculated via the $\Delta\Delta G^{\ddagger}$ of 1.8 kcal/mol is calculated at 19:1 (C3:C2), predicting excellent selectivity for the C3 isomer. However, as noted in the previous section, the calculated KIE for reductive elimination for arylation at C3 is calculated to be 1.0, which does not concur with experimental value of a primary kinetic isotope effect of 4.0 attained by DeBoef (**Figure 14**), and therefore we favour the catalytic cycle observed in the previous section, where C-H activation is undertaken by a Pd-Cu catalytic species on N-acetyl indole first.

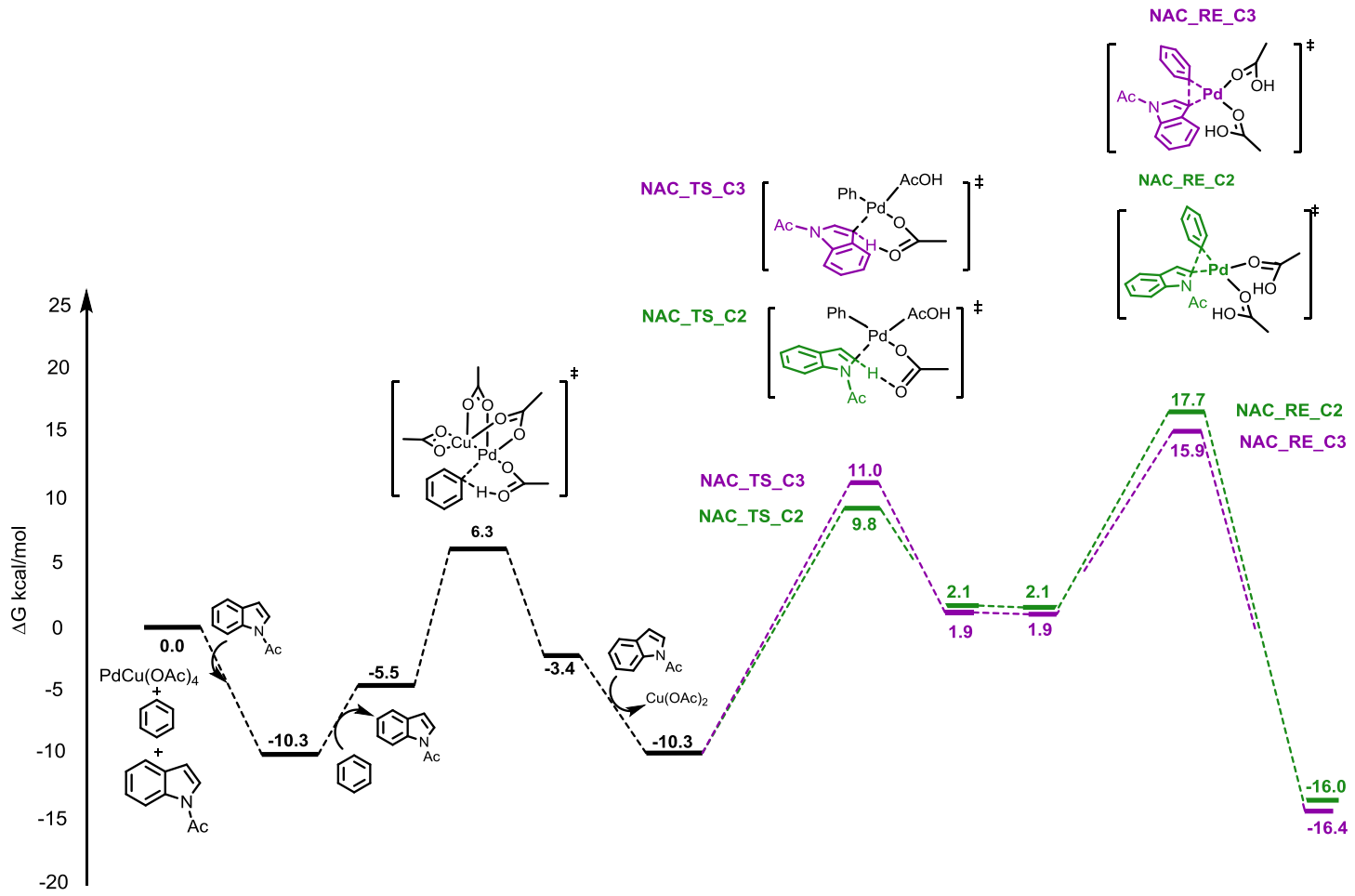

Figure 19. Free energy profile for the activation of benzene with $PdCu(OAc)_4$ first followed by subsequent C-H activation at C2 or C3 of N-acetyl indole. All values in kcal/mol.

4.4. Conclusions

The arylation of N-acetyl indole to give the C3 regioisomer is reliant upon the co-catalyst system of Pd/Cu. Our calculations show that a bimetallic catalytic species provides a favourable C-H activation of N-acetyl indole for the C3 position which can be explained through a distortion-interaction model. In the absence of Cu, the monomeric $Pd(OAc)_2$ species provides preference for activation at C2. This preference could explain why Ag(I)OAc elicits regioselective preference for the C2 position – with silver oxidant cleaving aggregated Pd clusters.The selectivity determining step is the cleavage of the C-H bond in the electron-poor benzene species by Pd(II). This step is lower in energy for the Pd(II) catalyst which has N-acetyl indole ligated at the C3 position as opposed to the C2 position. The calculated KIEs (3.7) is consistent to the primary kinetic isotope effect observed in experiment (4.0). The selectivity is also in good agreement (10:1) to the experimental (5:1), with a disparity of 0.4 kcal/mol in $\Delta\Delta G^{\ddagger}$ accounting for the calculated:observed selectivity.

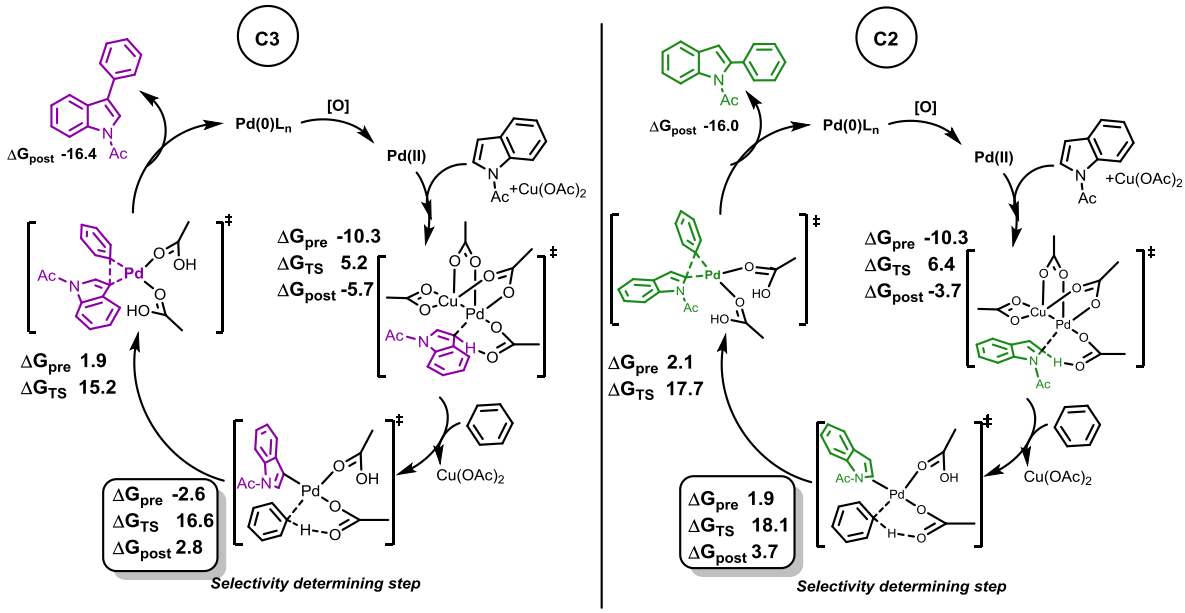

Figure 20. Catalytic cycle leading to C3 arylation of N-acetyl indole. The selectivity determining step is the C-H activation of benzene. All values in kcal/mol.

Chapter 4 *References*

[1] World Drug Index 2007. Thompson Scientific
[2] Vitaku, E.; Smith, D.T.; Njardarson, J.T. *J. Med. Chem.*, **2014**, *57*, 10257.
[3] Ithara, T. *J. Chem. Soc., Chem. Commun.* **1981**, *5*, 254.
[4] Ithara, T. *J. Org. Chem.* **1985**, *50*, 5272.
[5] (a) Stuart, D. R.; Fagnou, K. *Science*. **2007**, *316*, 1172; (b) Chen, X.; Engle, K. M.; Wang, D. H.; Yu, J. Q. *Angew. Chem., Int. Ed.* **2009**, *48*, 5094; (c) Lyons, T. W.; Sanford, M. S. *Chem. Rev.* **2010**, *110*, 1147; (d) Yeung, C. S.; Dong, V. M. *Chem. Rev*. **2011**, *111*, 1215; (e) Liu, C.; Zhang, H.; Shi, W.; Lei, A. *Chem. Rev*. **2011**, *111*, 1780; (f) Lyons, T. W.; Hull, K. L.; Sanford, M. S. *J. Am. Chem. Soc.* **2011**, *133*, 4455; (f) Beck, E. M.; Grimster, N. P.; Hatley, R.; Gaunt, M. J.; *J. Am. Chem. Soc.* **2006**, *126*, 2528; (g) Xi, P.; Yang, F.; Qin, S.; Zhao, D.; Lan, J.; Gao, G.; Hu, C, You, J. *J. Am. Chem. Soc.* **2010**, *132*, 1822; (h) Jiao, L.Y.; Oestreich, M. *Org. Lett.* **2013**, *15*, 5374.
[6] Potavathri, S.; Dumas, A. S.; Dwight, T. A.; Naumiec, G. R.; Hamman, J. M.; DeBoef, B. *Tetrahedron Letters*, **2008**, *49*, 4050.
[7] Wu, M.; Luo, J.; Xiao, F.; Zhang, S.; Deng, G. J.; Luoa, H. A.; *Adv. Synth. Catal.* **2012**, *354*, 335.
[8] (a) Gong, X.; Song, G.; Zhang, H.; Li, X. *Org. Lett.* **2011,** *13*, 1766; (b) Chen, S.; Liao, Y.; Zhao, F.; Qi, H.; Liu, S.; Deng, J. D. *Org Lett*. **2014**, *16*, 1618.
[9] Stuart, D.R.; Villemure, E.; Fagnou, K. *J. Am. Chem. Soc*. **2007**, *129*, 12072.
[10] Phipps, R.J; Grimster, N.P; Gaunt, M. J. *J. Am. Chem. Soc.* **2008**, *130*, 8172.
[11] Yang, Y-F.; Cheng, G-J.; Liu, P.; Leow, D.; Sun, T-Y.; Chen, P.; Zhang, X.; Yu, J.Q.; Wu, Y-D.; Houk, K. N. *J. Am. Chem. Soc*. **2014**, *136*, 344.
[12] Anand, M.; Sunoj, R. B.; Schaefer, H. F. *J. Am. Chem. Soc*., **2014**, *136*, 5535.
[13] Meir, R.; Kozuch, S.; Uhe, A.; Shaik, S. *Chem.Eur. J*. **2011**, *17*, 7623.
[14] Gorelsky S. I.; Lapointe D.; Fagnou, K. *J. Org. Chem.* **2012**, *77*, 658.
[15] (a) Kitahama, K.; Frech, R. *J. Chem. Phys.* **1985**, *82*, 720; (b) Wadt, WR.; Hay, PJ.; *J. Chem. Phys.* **1985**, *82*, 284.
[16] Feller, D. *J. Comp. Chem.*, **1996**, *17*, 1571.
[17] Roy, E. L.; Hay, J.; Martin, R. L. *J. Chem. Theory. Comput.* **2008**, *4*, 1029.
[18] (a) Barone, C.; Cossi, M.; *J. Phys. Chem. A.* **1998**, *102*, 1995; (b) Barone, C.; Rega, N.; Schimani, G.; Cossi, M. *J. Comput. Chem.* **2003**, *24*, 669.
[19] (a) Ribeiro, R. F.; Marenich, A. V.; Cramer, C. J.; Truhlar D. G. *J. Phys. Chem. B*, **2011**, *115*, 14556; (b) Grimme, S. *Chem. Eur. J.* **2012**, *18*, 9955.
[20] Curtiss, L. A.; Raghavachari, K.; Redfern, P. C.; Rassolov, V.; Pople, J. A. *J. Chem. Phys*. **1998**, *109*, 7764; (b) Baboul, A. G.; Curtiss, L. A.; Redfern, P. C.; Raghavachari, K. *J. Chem. Phys.* **1999**, *110*, 7650.
[21] Legault, C. Y. *CYLView*, version 1.0b. http://www.cylview.org, (accessed December 2012).
[22] Reed, A. E.; Weinhold, F. *J. Chem. Phys.* **1983,** *78*, 4066 (b) Reed, A. E.; Weinstock, R. B.; Weinhold, F. *J. Chem. Phys*. **1985,** *83*, 735.
[23] NBO 6.0. E. D. Glendening, J. K. Badenhoop, A. E. Reed, J. E. Carpenter, J. A. Bohmann, C. M. Morales, C. R. Landis, and F. Weinhold, Theoretical Chemistry Institute, University of Wisconsin, Madison (2013).
[24] Zhao, Y.; Truhlar, D.G. *Theor. Chem. Account.* **2006**, *120*, 215.
[25] (a) Brandon, R. W.; Claridge, D. V. *Chem. Commun*. **1968**, 677; (b) Sloan, O. D.; Thornton, *P. Inorg. Chim. Acta* **1986**, *120*, 173.
[26] Zeist, W. J-V.; Bickelhaupt, F. M. *Org. Biomol. Chem.* **2010**, *8*, 3118; (b) Fernandez, I.; Bickhelhaupt, F. M. *Chem. Soc. Rev.* **2014**, *43*, 4953.
[27] Ess, D. H.; Houk, K. N. *J. Am. Chem. Soc.* **2007**, *129*, 10646; (b) Green, A.G.; Liu, P.; Merlic, C. A. Houk, K. N. *J. Am. Chem. Soc.* **2014**, *136*, 4575.
[28] Petit, A.; Flygare, J.; Miller, A. T.; Winkel, G.; Ess, D. H. *Org. Lett.* **2012**, *14*, 3680.
[29] Sakaki, S.; Biswas, B.; Sugimoto, M. *Organometallics* **1998**, *17*, 1278; (b) Sakaki, S.; Kai, S.; Sugimoto, M. *Organometallics* **1999**, *18*, 4825.

Chapter 5

DFT and kinetic studies of TFA tuned coupling of simple arenes: biphenyl, 2- and 4-methoxybiphenyl

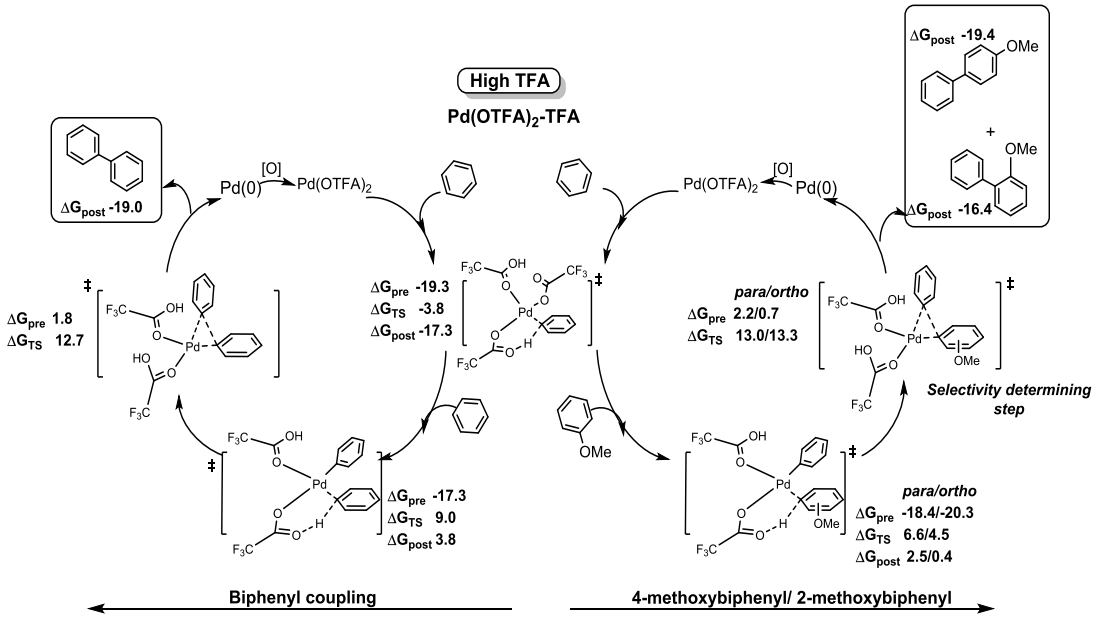

5.1. Introduction

Traditional approaches to forming unsymmetrical biaryls in organic synthesis have focused on utilizing traditional transition metal cross-coupling methods such as the Negishi,[1] Suzuki[2] and Stille[3] protocols. The effectiveness of such methods is widely established and they remain a powerful synthetic methodology in the creation of C-C bonds. However, alternative approaches utilizing direct arylation are now becoming increasingly prominent for biaryl formation via C-H activation.[4,5] Enhancements to C-C bond forming protocol in intermolecular oxidative cross-couplings (via oxidative arylation) employing Pd catalysis has led to the creation of homo- and hetero-biaryls with simple arenes as substrates.[6,7,8]

Lu and co-workers have reported a novel methodology whereby they could increase selectivity of the hetero-biaryl oxidative cross-coupling of benzene and anisole by "tuning" the concentration of trifluoroacetic acid (TFA)[9] (**Figure 1**). Here, the reaction could be tuned to provide less of benzene homocoupling and more of the unsymmetrical biaryl (2-methoxybiphenyl and 4-methoxybiphenyl) dependent upon the concentration of TFA with a $Pd(OAc)_2$ catalyst. The reaction is performed with an excess of benzene, presumably to avoid anisole homo-coupling (*vide infra*) and potassium persulfate functions as a terminal oxidant for Pd(0).

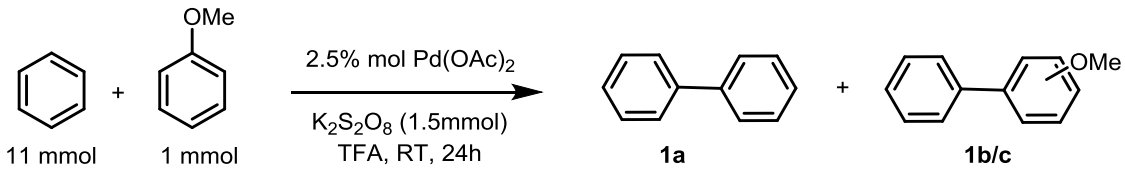

When TFA= 6.3 mmol
1a/1b-c = 56/44; **1b/c** (*para:ortho:meta*) 71:29:0

When TFA= 0.63 mmol
1a/1b-c = 21/79; **1b/c** (*para:ortho:meta*) 69:31:0

Figure 1. Concentration-tuned intermolecular cross-coupling of simple arenes developed by Lu and coworkers. High [TFA] gives biphenyl **1a** as major product, whereas low [TFA] gives 2-/4-methoxybiphenyl **1b/c** as the major product.

When the reaction was conducted with 6.3 mmol of TFA, the homo-coupled biphenyl product (**1a**) was obtained marginally in excess, whereas with a ten-fold decrease of TFA the unsymmetrical hetero-coupled methoxybiphenyl (**1b/c**) formed selectively as the major product. The selectivity (79:21) is moderate, however, the ability to form the

heterocoupled product is synthetically extremely valuable and understanding the mechanism is therefore to importance towards designing ever more selective systems. It is also noteworthy that regardless of reaction conditions, the *para* regioisomer (4-methoxybiphenyl) was preferred over the *ortho* regioisomer (2-methoxybiphenyl), despite the availability of the *ortho* site as a statistically more likely (*ortho:para* 2:1) site for activation.

The proposed catalytic cycle by the authors postulates an initial C-H activation to occur at benzene (due to the greater concentration) followed by activation of anisole to yield the unsymmetrical biaryl product. However, little mention is made regarding mechanism which would lead to these coupled products. Work on C-H activation and arylation of benzene[10], pyrroles[11] and other arenes[12] using a Pd(II) catalyst with ambiphilic carboxylate ligands supported the 'proton-shuttle' assisted mechanism (later termed CMD). Examples of the C-H activation step as rate-determining via KIE experiments have been forthcoming[13], suggesting that the initial C-H activation is important in arenes and heteroarenes alike. Based on our understanding and work in previous chapters, we propose the following catalytic cycle (**Figure 2)** which proceeds through (**1**) initial activation of the benzene substrate (present in excess), followed by (**2**) concentration 'tuned' activation to form - either the biphenyl in high [TFA] or 2- or 4-methoxybiphenyl in low [TFA]. The cycle is completed by reductive elimination (**3**) creating a new C-C bond.

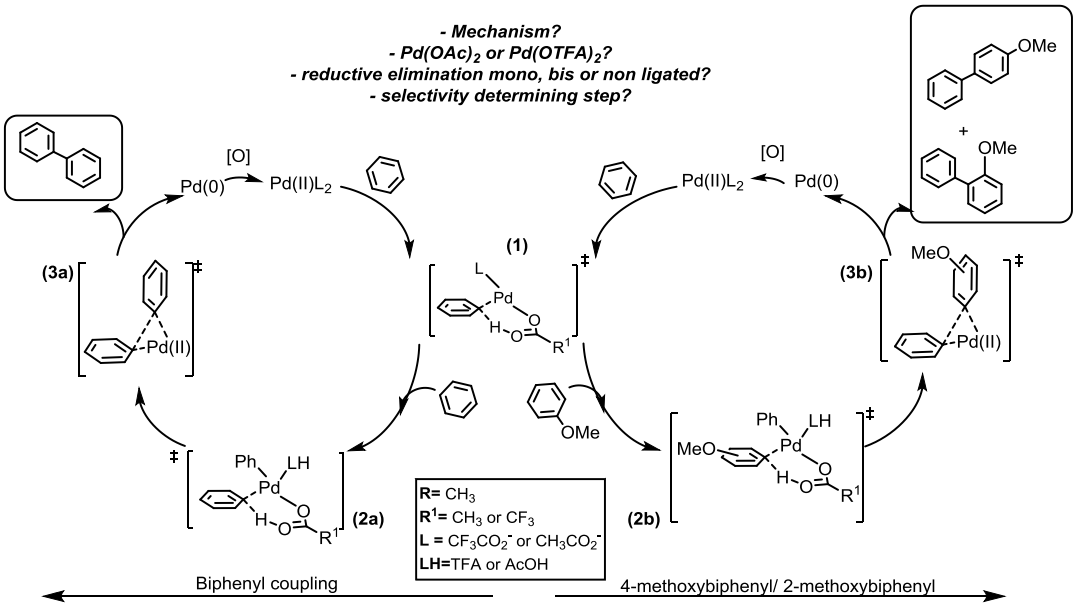

Figure 2. Proposed catalytic cycles for the formation of biphenyl and unsymmetrical biaryl product.

The potential mechanism of the reaction was not explicitly commented on by the authors, therefore, based on our work and previous literature, the intramolecular ambiphilic deprotonation CMD mechanism is likely to be favoured in the initial C-H activation. For this catalytic cycle, the mechanism for C-H activation is unknown and the catalytic species undertaking activation could proceed via a range of Pd(II) catalytic species – acknowledged by the authors. In high concentration of TFA, $Pd(OAc)_2$ could convert to $Pd(OTFA)_2$ (*in situ*)[14] and in lower concentrations TFA could act as a coordinating solvent to $Pd(OAc)_2$, therefore calculations encompassing all possible catalytic species are required.

In this chapter DFT calculations have been applied to elucidate the reaction mechanism of this reaction. Quantum chemical studies of catalysis are commonly performed using free energies computed relative to a standard state – in the gas phase 1 atm is typically used, while in solution this value is 1 mol/l. However, by assuming that each species is present at the same constant concentration, the effect of changes in concentration is neglected on the individual chemical potentials. This is clearly important in computing relative rates of reactants which are present in different amounts, and moreover in modelling the effect of concentration of additives on the reaction selectivity. Fundamentally, the rate of each step is the product of a rate constant (which can, in principle, be computed with DFT) and a concentration term(s). In this chapter to address this, we will utilize a kinetic modelling simulation, in combination with DFT calculations, to model reaction conditions.

Our investigation sought to utilize DFT and kinetic modelling to characterize the catalytic cycles of $Pd(OAc)_2$/$Pd(OTFA)_2$ (and their solvated analogs) implicit in the biphenyl/methoxbiphenyl coupling, thus establishing the mechanism, the selectivity determining step and the nature of catalytic species inherent to this concentration tuned cross-coupling.

5.2. Computational methods

This work was conducted at AstraZeneca, Macclesfield under the supervision and guidance of Dr Simone Tomasi, and with helpful assistance of Dr Ian Ashworth.

The computational protocol used for this chapter follows the methodology presented in section 2.2., Chapter 2. Modifications made to the methodology (for work presented in this chapter) are mentioned herein.

Initial geometry optimizations were performed with the **ω**B97XD functional and split-valance polarized 6-31G(d) basis set for C, N, O, F and H atoms, whilst the LANL2DZ double-zeta valence basis set and associated effective core potential (ECP) were used to describe Pd.[15] Single point energies were computed on all optimized geometries with the larger valence triple-zeta 6-311+G(d,p) and LANL2TZ basis set obtained from the EMSL Basis Set Exchange[16,17] A fine grid density was used for numerical integration in all DFT calculations.

The effects of solvent (benzene ε= 2.27) were incorporated through the use of a conductor-like polarizable continuum model (CPCM), defining the solute cavity with UFF radii[18] by conducting single point calculations on optimized geometries. A smooth damping function centred about a frequency of 100 cm^{-1} was used to switch between the harmonic approximation for vibrations above this value and the free-rotor approximation below.[19] All structures are depicted with CYLview [20] or ChemDraw. All energies presented within this work are Gibbs (ΔG) free energies calculated via:

$$\Delta G_{solv} = \Delta E_{solv} + (\Delta G_{gas} - \Delta E_{gas})$$

The NBO program [21] analyses the many-electron molecular wavefunction in regards to localized electron-pair bonding units. The program carries out the determination of natural atomic orbitals (NAOs), natural bond orbitals (NBOs), and natural localized molecular orbitals (NLMOs), and uses these to perform natural population analysis (NPA) which is used in this chapter to describe the charge present on individual atoms. The sum of these individual charges is used to determine unit charge on benzene, phenyl, anisole and the catalytic Pd species in the reaction.

Kinetic profiles used to determine reaction kinetics were created using the Berkeley-Madonna[22] package which utilizes a differential equation solver to compute rate constants through the application of the Rosenbrock Integration Algorithm (also

referred to as the Stiff ordinary differential equation method).[23] Multi-step kinetic schemes were constructed to represent the reaction pathways investigated. Initial concentrations of reactants were incorporated into our models (benzene: 0.011, anisole: 0.001, Pd(II): 0.00025g). The effect of TFA was presumed to change the nature of the catalytic species (as proposed by the authors). Therefore rapid conversion of $Pd(OAc)_2$ to the various Pd(II) systems studied was assumed in higher concentrations of TFA and explicit solvent concentration of TFA was not modelled. The reoxidation of Pd(0) to regenerate the active Pd(II) catalyst was assumed to be relatively fast, and was modelled as the fastest step in the reaction (compared to explicitly calculated steps).

Optimized solvent corrected Gibbs energies (as referred to above) for both transition states and intermediates were used to calculate $k_{forward}$ and $k_{reverse}$, the rate constant for each experimental step following the theoretical relationship between rate and Transition State Theory, TST, through utilizing Eyring equation. As such kinetic profiles could be created with calculated TS energies.

for reaction

$$A + B \longrightarrow [TS_{AB}]^{\ddagger}$$

rate is equal to

$$\text{Rate} = k[A][B]$$

can also be determined via TST and Eyring Equation

$$k_{TST} = \left(\frac{k_B T}{h}\right) e^{\frac{-\Delta G^{\ddagger}}{RT}}$$

where
$K_B = 1.38 \times 10^{-23}$ J K^{-1}
T = temperature (K)
$h = 6.62 \times 10^{-34}$ J s
e = exponential term
$\Delta G^{\ddagger}$ = calculated Gibbs free energy of TS (kcal/mol)

Using the initial concentrations used experimentally, temperature (K) and calculated *k* values, we have constructed mechanistic models and created a dynamic kinetic profile for our mechanistic pathways based on the computed rate constants. Graphical representation of kinetic profiles can be obtained which provide the mass of the respective reactants, intermediates and substrates as a function of time. Our DFT calculations allowed us to use standard free energies of activation from our energetic profiles to characterize the forward (k_{fwrd}) and reverse (k_{rev}) reactions. Gibbs free energy values were inserted into the Eyring equation calculating *k* values which were used in our differential terms. For all kinetic profiles the reaction was modelled at room temperature, 298K.

5.3. Results

5.3.1. DFT calculations of benzene coupling

Our calculations focused on characterizing the catalytic cycle leading to biphenyl formation, proceeding through the initial C-H activation of benzene (**Figure 3**). Both $Pd(OAc)_2$ and $Pd(OTFA)_2$, and their solvated analogues $Pd(OAc)_2$-TFA and $Pd(OTFA)_2$-TFA were calculated as the catalytic species for the complete catalytic cycle. We postulated that in high TFA concentrations, ligand exchange could occur and lead to change in selectivity.[24] Similarly, in low concentrations we presume that TFA may elicit an effect as a coordinating ligand. Therefore for completeness, all four catalytic species were calculated for the initial cleavage of the benzene C-H bonds.

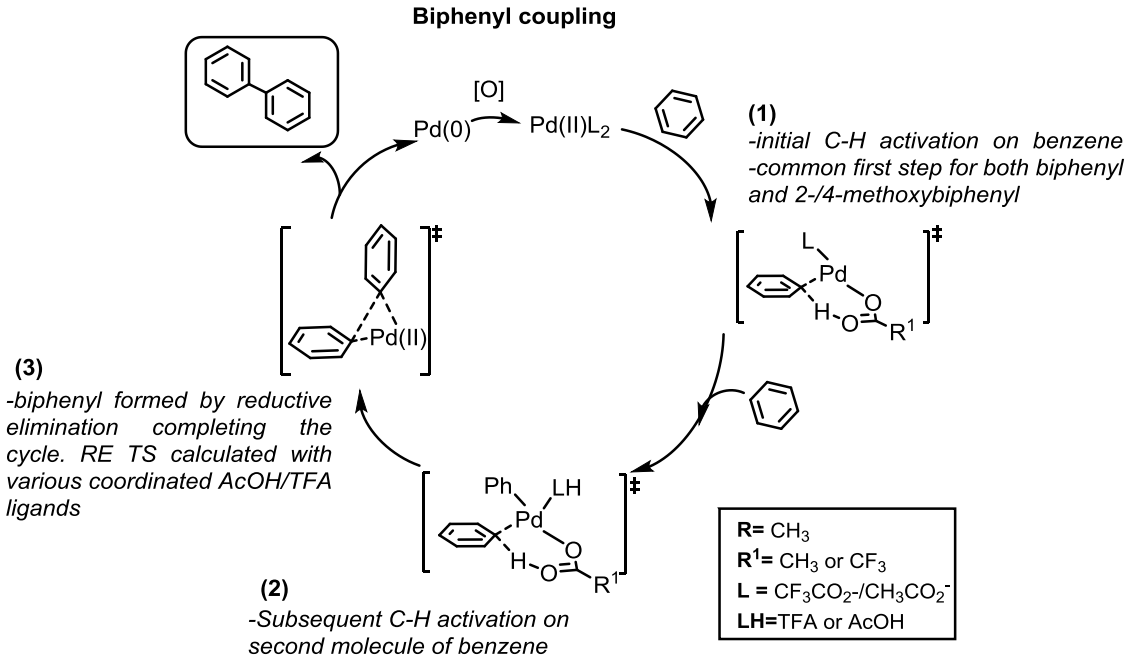

Figure 3. Initial DFT calculations on proposed catalytic cycle of biphenyl formation.

As established in previous chapters, the CMD mechanism proceeds through initial η^2 coordination of the Pd(II) species on benzene, in the precomplex, before changing hapticity to η^1 in the TS where H-abstraction and palladation occur via an ambiphilic acetate or trifluoracetate ligand. This is followed by a second activation of benzene leading to biphenyl formation, which occurs via a second CMD C-H activation.

Amongst the catalytic species, initial activation of benzene with $Pd(OAc)_2$ (**Ben_1**) is shown to proceed via an endergonic reaction process (1.5 kcal/mol), whereas the other catalytic Pd(II) species proceed with C-H activation in an exergonic reaction profile –

there is preference for the TFA assisted mechanism, with $Pd(OTFA)_2$-TFA (**Ben_4**) providing the lowest energy landscape (relative to the separated reactants). Explicit coordination of TFA on Pd assists both $Pd(OAc)_2$-TFA (**Ben_2**) and $Pd(OTFA)_2$-TFA in providing overall lower energy transition states for the initial and subsequent C-H activation of benzene. For $Pd(OAc)_2$ the initial C-H activation TS of benzene (ΔG 18.4 kcal/mol) is lowered with the solvation of TFA (**Ben_2**) in $Pd(OAc)_2$-TFA (ΔG 8.2 kcal/mol). The initial C-H activation TS of benzene (**Figure 4**) with $Pd(OTFA)_2$-TFA is also lower (ΔG -3.8 kcal/mol) than $Pd(OTFA)_2$ (**Ben_3**: ΔG 9.1 kcal/mol).

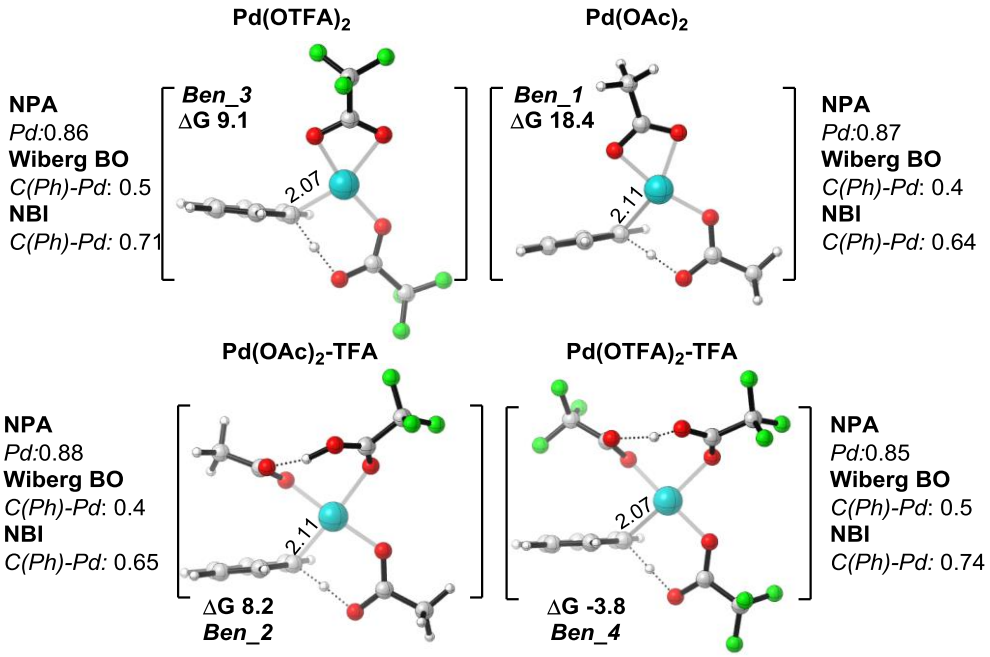

Figure 4. Optimized geometries of C-H activation TS of benzene. Wiberg Bond Order, NPA and NBI for each corresponding TS is shown. Pd-C bond length given in Å. All energies in kcal/mol and given against separated reactants, which is constant amongst all systems studied within this chapter. All calculations conducted using ωB97XD/6-31g(d)/LANL2DZ.

NBO calculations in the initial C-H activation of benzene yield no substantial change in the charge on Pd (NPA) amongst all catalytic species. However, the formation of C(Ph)-Pd bond in the transition state (Wiberg Bond Order) and the interaction strength of the C(Ph)-Pd bond (Natural Binding Index, NBI) indicated (a) formation of an earlier and stronger transition state bond with trifluroacetate ligated Pd. This is also suggested by the C-Pd bond length being shorter in the TS for $Pd(OTFA)_2$ and $Pd(OTFA)_2$-TFA. Following the initial activation of benzene, the subsequent C-H activation was calculated via an intramolecular deprotonation mechanism. Here, Pd(II)

now contains a Ph ligand *cis* to the benzene being activated. The reaction proceeds through characteristic dihapto coordination of Pd with the π system of benzene, and simultaneous proton abstraction and palladation (**Figure 5**). This process displays a significant preference (against separated reactants) to deprotonation via $Pd(OTFA)_2$-TFA mechanism (**Ben_4b**) over the other solvated 16 electron counterparts in **Ben_1b** and **Ben_2b** and the 14 electron PhPd(II)OTFA **(Ben_3b)**. This indicates that using the TFA ligand provides a general energetic advantage in terms of lowering the TS ΔG amongst the studied species.

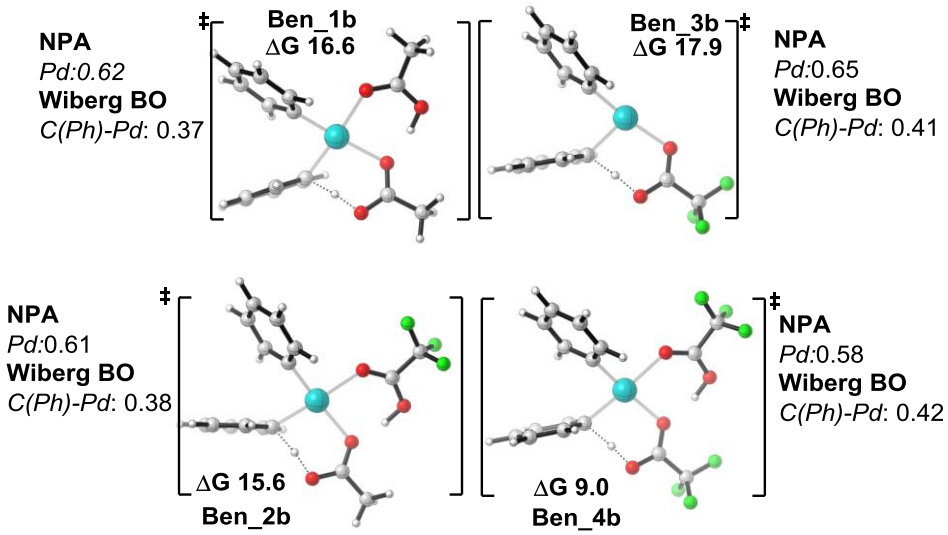

Figure 5. The second C-H activation of benzene with various Pd(II) catalysts. All energies in kcal/mol.

The biphenyl product is formed via a reductive elimination step. The lead authors did not explicitly specify the mechanistic rationale behind the C-C bond forming reaction. However, it is presumed that reductive elimination via a three centred transition state is most likely to account for cross-coupled products. Our calculations focused on C-C bond formation through 16 (**Ben_1_RE**, **Ben_2_RE** and **Ben_4_RE**) and 14 electron (**Ben_3_RE**) Pd(II) undergoing reductive elimination with both Ph groups in required *cis* disposition in the TS **(Figure 6**), upon which Pd(0) is expelled and the biphenyl product formed.

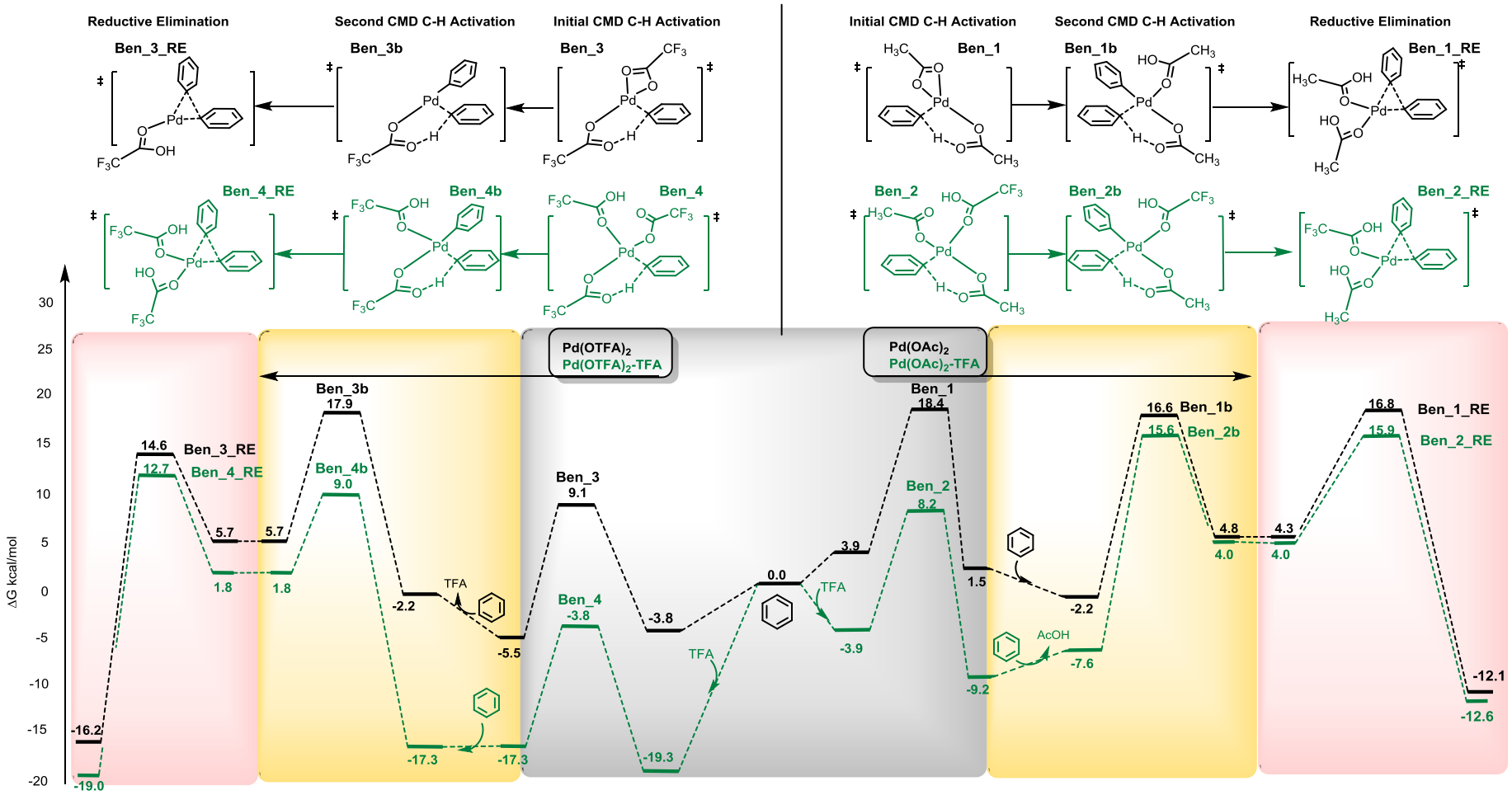

Figure 6. Free energy profile for biphenyl formation via $Pd(OAc)_2$ and $Pd(OAc)_2$-TFA (right) and $Pd(OTFA)_2$ and $Pd(OTFA)_2$-TFA (left). All values in kcal/mol and calculated against separated reactants.

5.3.2. DFT calculations of benzene-anisole coupling

After modelling various Pd(II) catalysts for biphenyl coupling catalytic cycle, our calculations focussed on the activation of anisole (**Figure 7**). This would be in direct competition with the second C-H activation of benzene in a catalytic cycle which has a common step (step **1**). We modelled the C-H activation of the *ortho* and the *para* position of anisole via the CMD mechanism with Pd(II) catalysts containing a Ph ligand from the initial activation of benzene (step **2b**). The reaction would conclude with reductive elimination forming either 2 or 4-methoxybiphenyl (step **3b**).

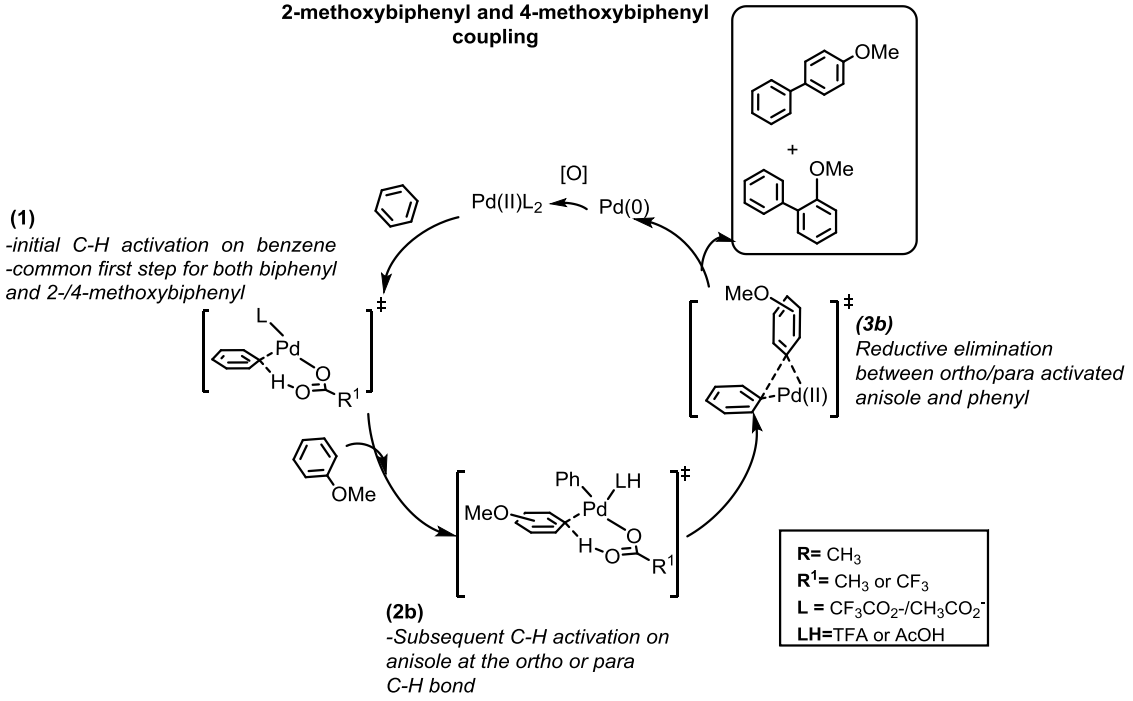

Figure 7. Initial DFT calculations on proposed catalytic cycle of methoxybiphenyl.

5.3.3. DFT calculations of 4-methoxybiphenyl coupling

Following from the (**1**) initial activation of benzene (**2**) the activation of the *para* position of anisole was modelled with a second CMD C-H activation followed by (**3**) C-C bond formation via a reductive elimination to create 4-methoxybiphenyl (**Figure 9**). The activation of anisole at the *para* position proceeds through the two characteristic features in the CMD mechanism (**1**) initial dihapto coordination of Pd to the π system and (**2**) subsequent deprotonation with an ambiphilic intramolecular ligand in either OAc of OTFA thus leading to a diarylated Pd(II) species.

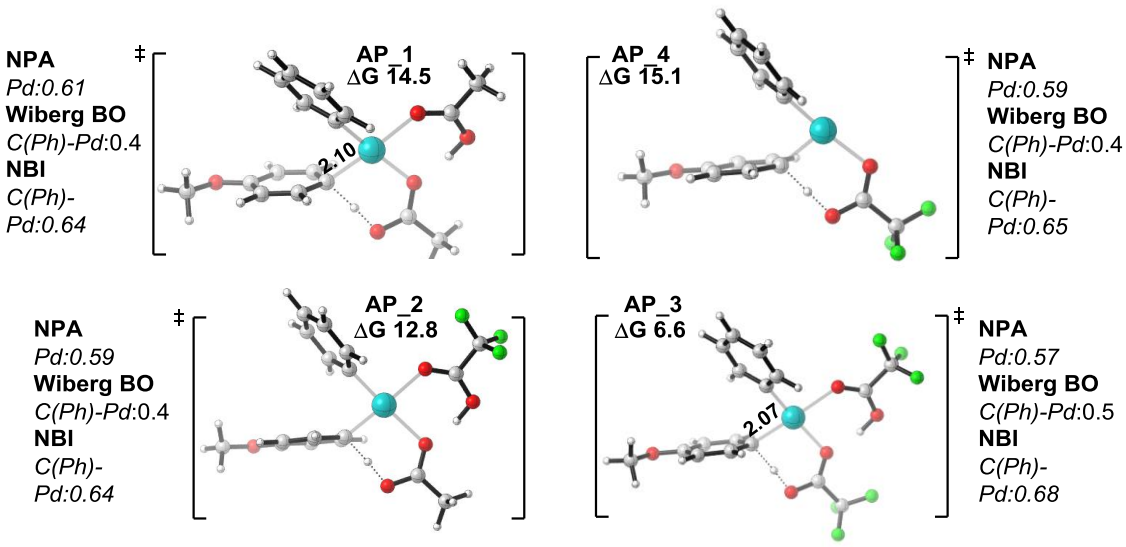

Figure 8. Optimized geometries of the activation of C(*para*)-H of anisole with various Pd(II) catalysts containing a Ph ligand from the initial activation of benzene. All energies in kcal/mol. All bond lengths in Å.

Cleavage of the anisole *para* C-H bond was lowered significantly where two TFA ligands are affixed to the Pd centre (**AP_4**), and displayed a stronger NBI index and Wiberg Bond Order between the C(*para*)-Pd bond than the other TSs (**Figure 8**). We would expect **AP_4** and **AP_3** to be viable catalytic species when large amounts of TFA are used. Similarly in lower concentrations of TFA **AP_1** and **AP_2** are viable. Here (**AP_1** and **AP_2**) the catalytic species undertaking the C-H activation of anisole has retained AcOH from the initial activation of benzene with $Pd(OAc)_2$ in **AP_1**.

The alternative pathway, in lower amounts of TFA, would involve a solvent coordinated Pd(II) catalyst activating benzene ($Pd(OAc)_2$-TFA) followed by dissociation of AcOH. The reaction is completed through a reductive elimination creating 4-methoxybiphenyl product and regenerating a Pd(0) species. Again the lowest energy TS for the reductive elimination (relative to separated reactants) was for the $Pd(OTFA)_2$-TFA pathway (**AP4_Ben_RE**).

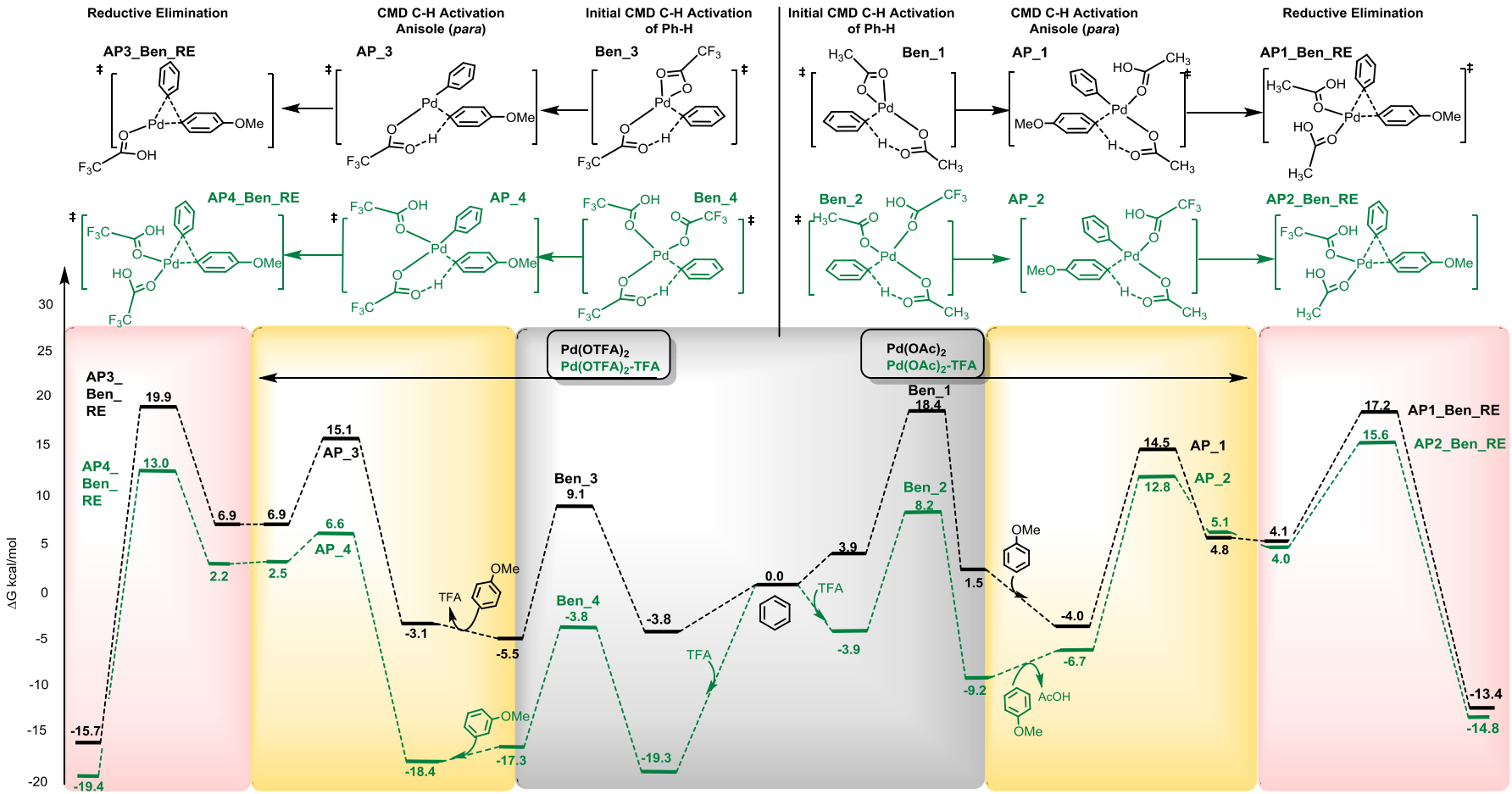

Figure 9. Free energy profile for the coupling of 4-methoxybiphenyl with $Pd(OAc)_2$, $Pd(OAc)_2$-TFA (right) and $Pd(OTFA)_2$ and $Pd(OTFA)_2$ –TFA (left) All values are in kcal/mol

5.3.4. DFT calculations of 2-methoxybiphenyl coupling

In the reaction the *ortho* position of anisole is coupled with Ph. Interestingly, the *ortho* position is activated and coupled in much lower amounts than the *para* isomer, even though statistically there are 2 *ortho* sites for C-H activation compared to one *para*. In both high and low concentrations of TFA, the *ortho* activated product is produced in significantly lower ratios (High $[H]^+$ *para:ortho* 71:29, low $[H]^+$ *para:ortho 69:31*). Our calculations focused on elucidating the preference in chemoselectivity, and also characterize the catalytic cycle for 2-methoxybiphenyl. The cycle would proceed from the initial C-H activation of benzene, followed by the C-H activation at the *ortho* position of anisole (**Figure 10**).

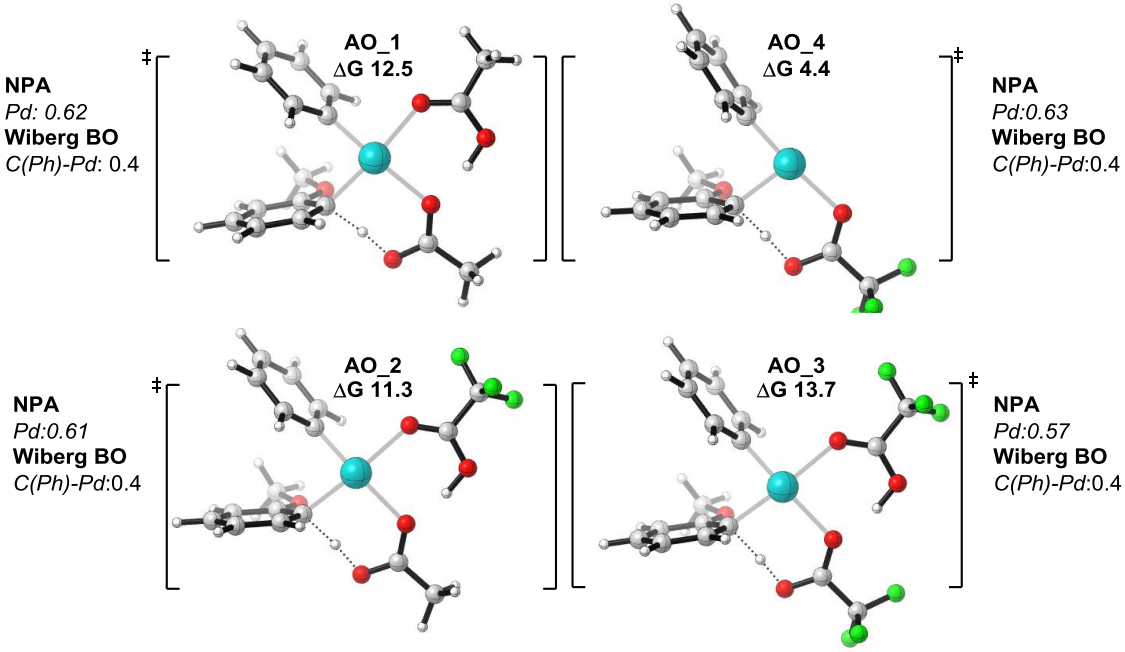

Figure 10. Optimized geometries of the anisole C(*ortho*)-H activation with Pd(II) catalysts proceeding from the initial activation of benzene. All energies in kcal/mol.

Following the *ortho* C-H activation, the catalytic cycle completed through a reductive elimination event, leading to a new C-C bond at the *ortho* position of anisole and Ph. As evident from computational studies into formation of 4-methoxybiphenyl the reductive elimination TS is predicted to be selectivity and rate determining in the formation of 2-methoxybiphenyl (**Figure 11**).

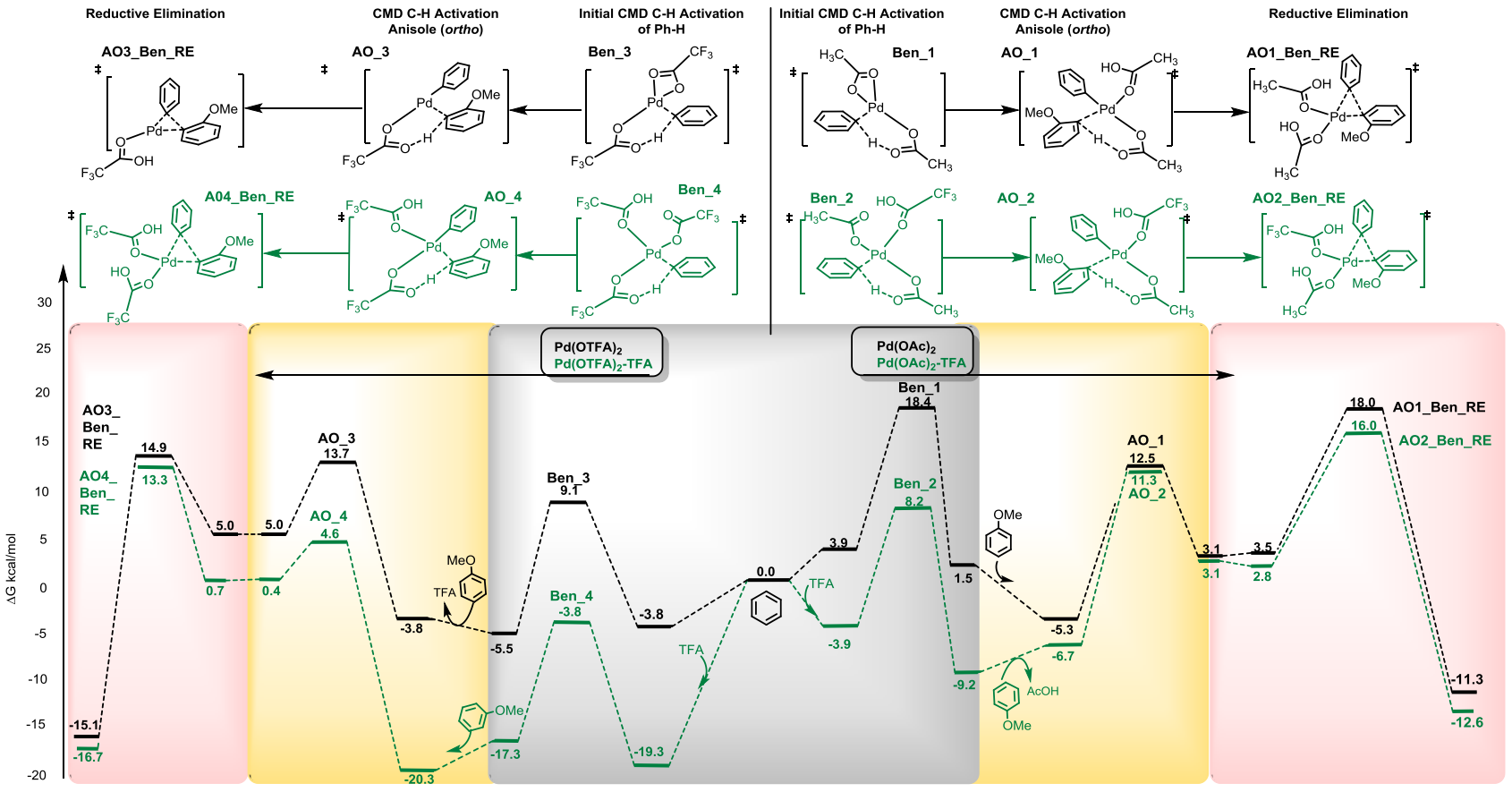

Figure 11. Free energy profile for the coupling of 2-methoxybiphenyl with $Pd(OAc)_2$, $Pd(OAc)_2$-TFA (right) and $Pd(OTFA)_2$ and $Pd(OTFA)_2$ –TFA (left) All values are in kcal/mol.

5.3.6. Kinetic profiling using Berkeley Madonna

5.3.6.1. Kinetic profile of $Pd(OTFA)_2$-TFA: High [TFA]

Upon the completed calculation of the three potential product pathways via the CMD mechanism, we could compare the mechanistic rates of formation via kinetic modelling. Here, kinetic schemes were constructed, and the application of the Eyring equation allowed us to model rates of formation and dissociation for each step. As the reaction proceeds from the initial activation of benzene, we modelled the anisole (*ortho:para*) and benzene pathways in a competitive reaction profile.

For the reaction proceeding via high [TFA] loading, the reaction pathway modelled was $Pd(OTFA)_2$-TFA, as the species along this reaction coordinate are more stable than with $Pd(OTFA)_2$ and $Pd(OAc)_2$. In principle a kinetic model could consider the interconversion of all possible catalyst forms. However, in practice this is extremely difficult since many possible mechanisms and their associated forward and reverse rate constants would have to be explicitly included. Based on the computed free energies for the formation of biphenyl, 4-methoxybiphenyl and 2-methoxybiphenyl (**Figure 6, 9, 11**) we constructed a mechanistic model for all three products as depicted in **Figure 12**. All rate constants are obtained from the DFT-computed activation parameters, except the reoxidation of the catalyst following reductive elimination (since this step has not been computed explicitly). We make the assumption that this is relatively fast, with an apparent activation barrier of 6.0 kcal/mol such that this step is not turnover-limiting. In the case of a high TFA concentration, the initial resting state is a complex formed between the catalyst and benzene and so we have included this pre-equilibrium (relative to the separated reagent and catalyst) into the model using the computed free energy of complexation.

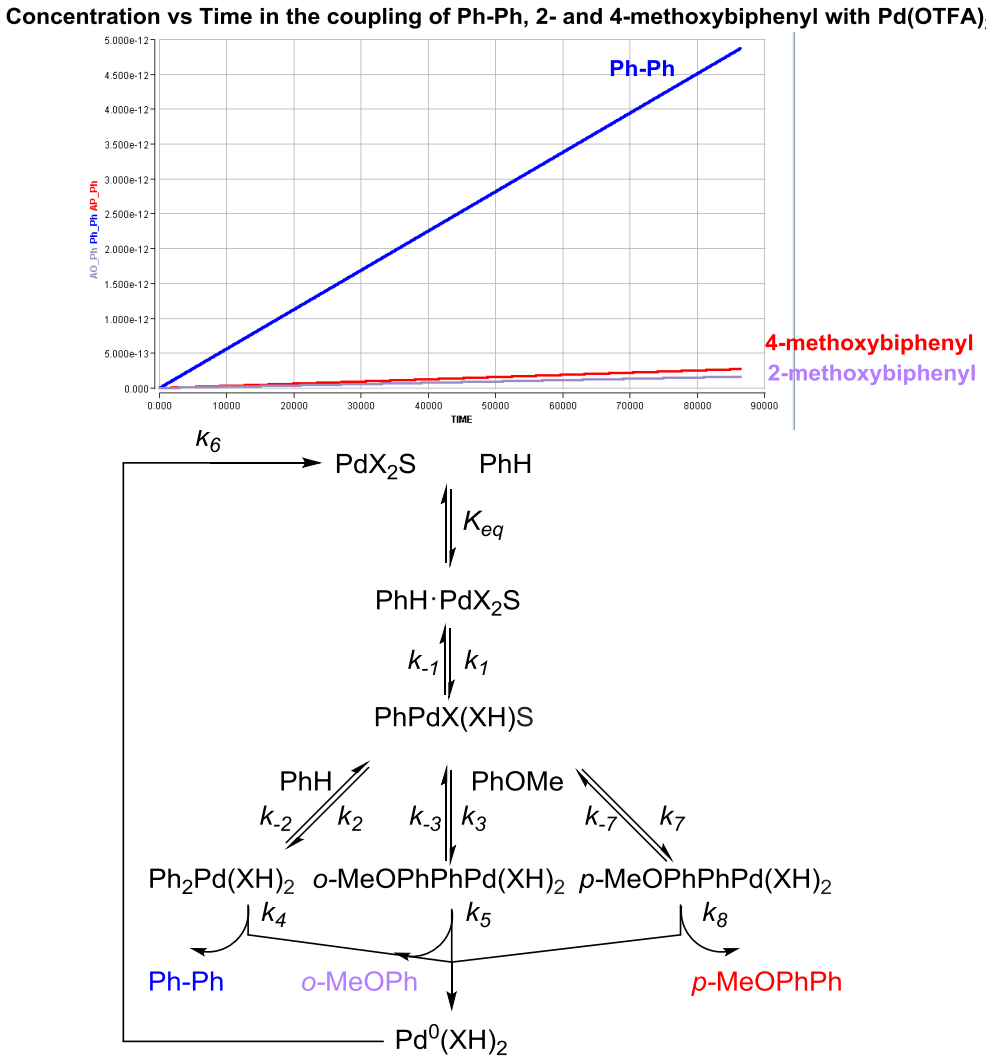

Figure 12. Kinetic simulation modelling formation of biphenyl, 2- and 4-methoxybiphenyl with $Pd(OTFA)_2$-TFA. The kinetic model constructed to model rates of reaction of observed products, proceeding from a common precomplex PhH PdX_2S, where X=OTFA and S=TFA.

In experiment, the reaction produces the biphenyl: 4-methoxybiphenyl/2-methoxybiphenyl adducts in the ratio 56:44 (*para:ortho* 71:29). From our kinetic model, it is apparent that the magnitudes of the rates are grossly underestimated, with relatively little conversion after 24 hours. Nevertheless, it is encouraging that the *para*-isomer is correctly favoured relative to the *ortho* heterocoupled product in the kinetic simulation. The preference of benzene is also exaggerated in this model. Consideration of the underlying DFT-computed reaction profile helps to understand this selectivity: the reductive elimination step limits the turnover for all products, and the relative stabilities of these TSs are in the order Ben_4_RE < AP4_Ben_RE < AO4_Ben_RE (i.e. the biphenyl forming TS is the most stable). The modest computed free energy differences between these

structures (the biphenyl TS is 0.3 kcal/mol more stable that the *para*-isomer, which in turn is 0.3 kcal/mol more stable that the *ortho*-isomer) actually matches well with the observed ratios. However, once the larger excess of benzene is accounted for in the kinetic model the homocoupling is favoured even more so. The kinetic model demonstrates that different concentrations may be accounted for in a model of a complex reaction in combination with computed activation parameters.

5.3.5.2. Kinetic profile of $Pd(OAc)_2$-TFA: Low [TFA]

In low amounts of TFA the heterocoupling of anisole with benzene dominates over biphenyl coupling in the ratio 71:29. Our calculations modelled both $Pd(OAc)_2$ and $Pd(OAc)_2$-TFA as possible catalytic species in low concentrations of TFA. The preference of the *para* isomer is still evident (p:o 69:31) and therefore suggests an inherent selectivity bias for the 4 position in the coupling of anisole and benzene with Pd(II). Using a similar logic to that applied in our discussion relevant to high TFA concentrations, we restrict our analysis to the more stable $Pd(OAc)_2$-TFA reaction profile. Analysis of the computed free energy profile for all three products suggest that, again, the reductive elimination TS is the point at which the selectivity is determined. Satisfyingly, the DFT relative stabilities now put the *para*-heteroadduct as the most stable reductive elimination TS, which fits with the switch to this as the major product observed experimentally. This pathway is now more stable than the biphenyl homocoupling by 0.3 kcal/mol – the effect is subtle. However, the experimental trend towards increased heterocoupling is reproduced computationally.

Our kinetic model of the $Pd(OAc)_2$-TFA catalyze pathway utilized the same form as used previously in **Figure 12**, although now using the appropriate rate constants derived from the DFT calculations for the expected catalyst at lower TFA concentrations. The simulated formation of the three products under these conditions is shown in **Figure 13**. The overall level of conversion is noticeably faster than for the previous system since the energetic span of the catalytic cycle is reduced for this catalyst. Importantly, during the time which there is still anisole remaining, the correct major product is predicted to be formed most quickly (*para*-methoxybiphenyl, red line). After around 2 hours the biphenyl

adduct is seen to "take over" as the major product – this is simply the result of a larger amount of benzene in the reaction mixture which is still present after the anisole has been consumed. This is an example of how kinetic modelling accounts for time-dependent selectivity, which would be absent in most e.g. steady state models of reactivity. Our results suggest that the regime in which the reaction is stopped (or the catalyst becomes inactive) is during the period where the anisole is yet to be fully consumed, since the heterocoupled product is obtained in excess.

The calculated $\Delta\Delta G^{\ddagger}$ between the *ortho* and *para* isomer of 0.4 kcal/mol at 25ºC in the reductive elimination TS corresponds to a selectivity of 66:33 (p:o), in good agreement with the selectivity of 69:31 observed in experiment.

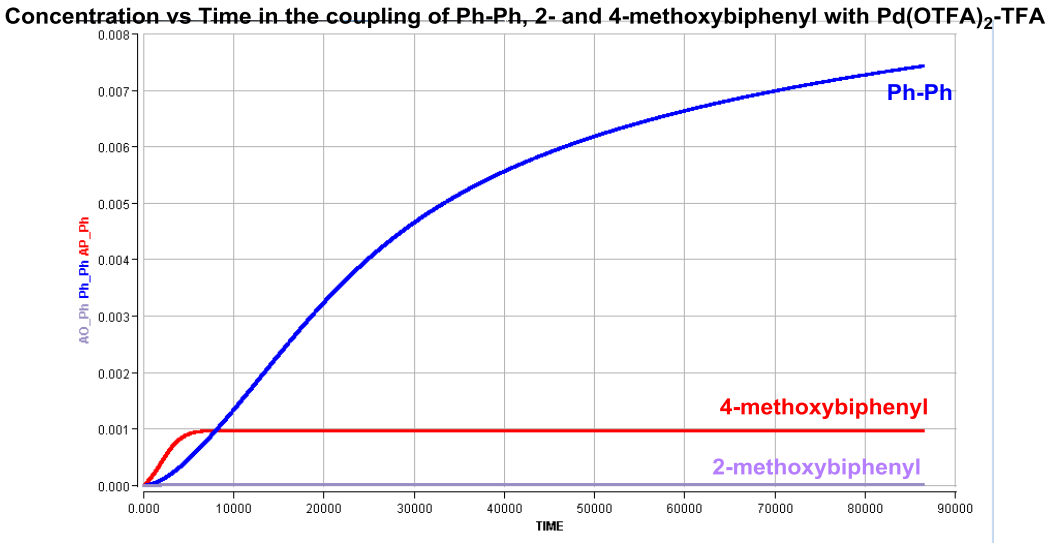

Figure 13. Kinetic simulation modelling formation of biphenyl, 2- and 4-methoxybiphenyl with $Pd(OAc)_2$-TFA over 24 hours.

5.3.6. Summary

In 2- and 4-methoxybiphenyl C-H activation at the *ortho* position is calculated to be more amenable to C-H bond cleavage than the analogous *para* C-H activation, and lower ΔG_{TS} (against separated reactants) of the *ortho* C-H TS vs. *para* C-H TS is consistent amongst all studied catalytic species (**Figure 14**). NBO calculations predict the total overall charge on anisole (Σ NPA Anisole) to be lower when activating at the *ortho* position as opposed to the *para*. Through NBO analysis it is evident that lower ΔG_{TS} (kcal/mol) is exhibited when charge separation between the Pd catalyst and anisole substrate is low (where *charge separation*= ΣNPA anisole – ΣNPA Pd catalyst). Low charge separation is predominant in the C-H activation TS of the *ortho* position of anisole.

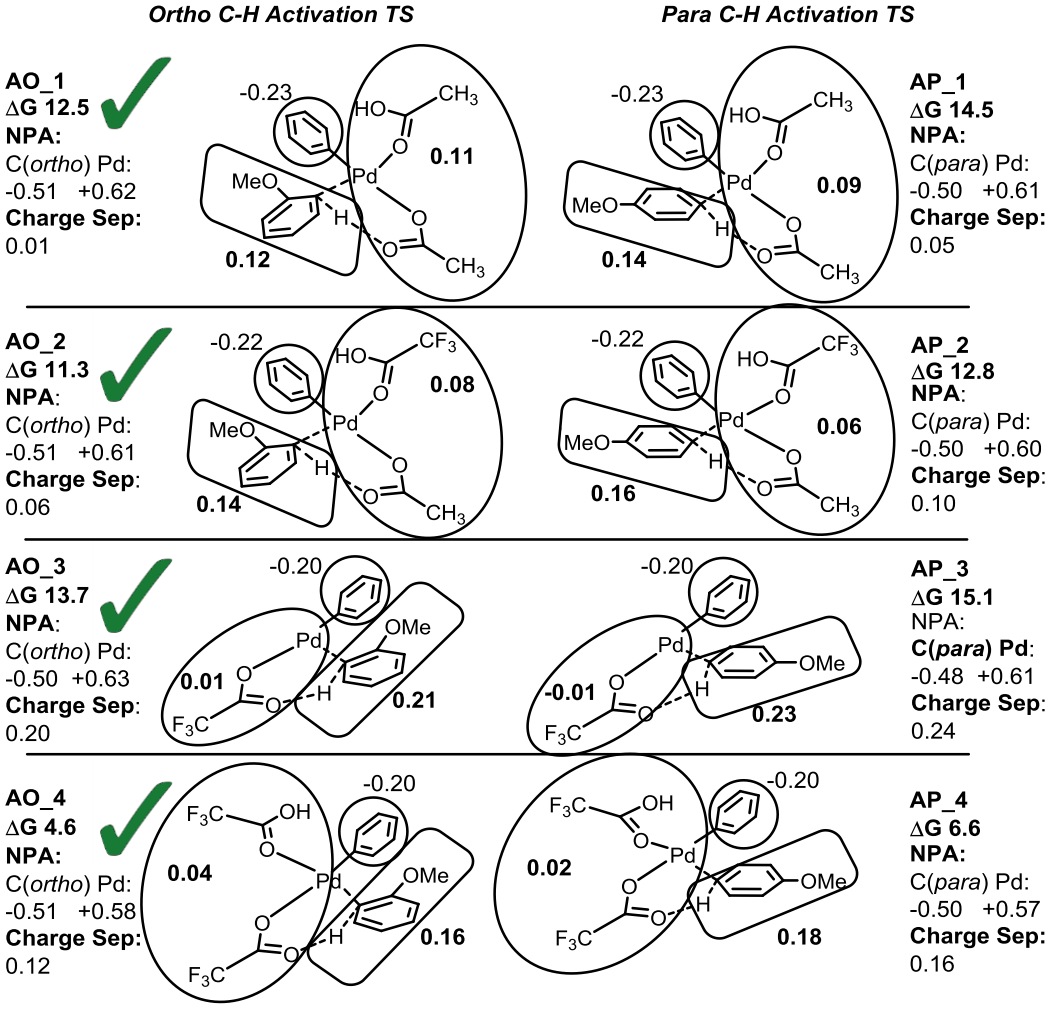

Figure 14. Charge separation of anisole C-H activation between *ortho* and *para* C-H activation. Total charge of anisole (Σ NPA anisole), phenyl (Σ NPA phenyl) and Pd catalyst (Σ NPA Pd +carboxylate ligands) shown next to each unit. All energy values given in kcal/mol.

Reductive elimination is the selectivity determining step in our catalytic cycles (for both high and low TFA concentration) and the *para* isomer is favoured over *ortho*. In the RE TS, lower charge separation between anisole and phenyl leads to a lower ΔG_{TS} , as seen with the C-H activation of anisole in **Figure 14** . The *para* isomer contains less charge separation between the anisole and phenyl unit, leading to a lower ΔG_{TS} (**Figure 15**).

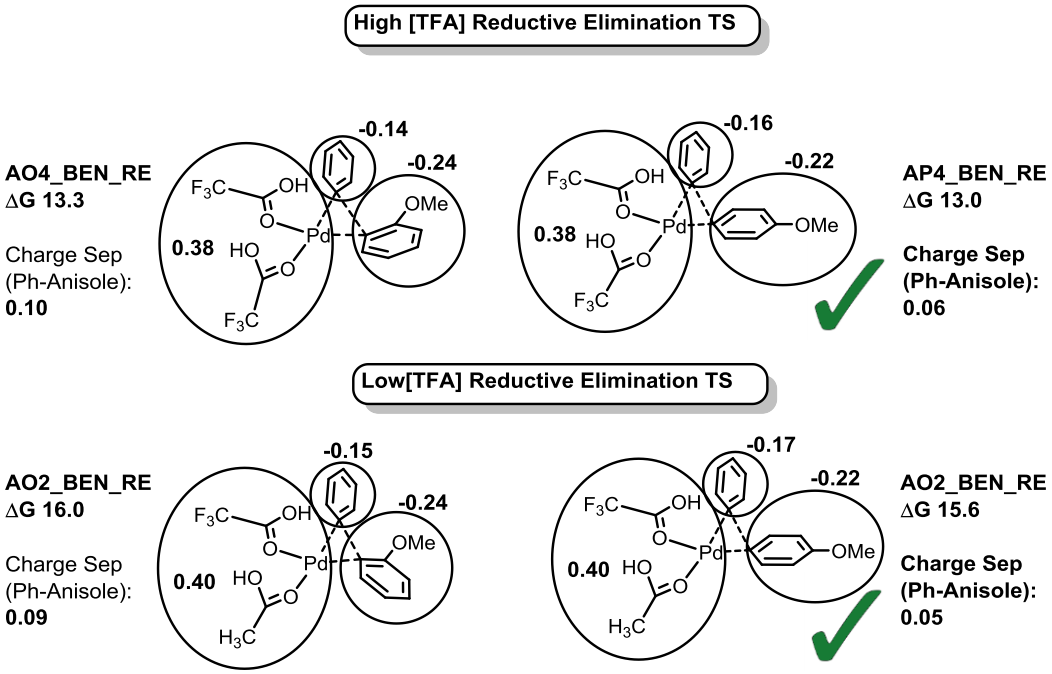

Figure 15. Charge separation of anisole- phenyl in RE TS (*ortho* and *para)*. Total charge of anisole (Σ NPA anisole), phenyl (Σ NPA phenyl) and Pd catalyst (Σ NPA Pd+carboxylate ligands) shown next to each unit. All energy values given in kcal/mol.

The *para* product (4-methoxybiphenyl) is calculated to be more stable than 2-methoxybiphenyl (in all catalytic species). The phenyl unit (at the *ortho* position in 2-methoxybiphenyl) has to bend out of plane to avoid a steric clash with the methoxy group on anisole, thus distorting co-planarity between the two arenes. This distortion is accentuated in the *ortho* product where the C-C-C-C dihedral angle is calculated at 118º (**Figure 16**) whereas the *para* isomer displays a dihedral of 150º, thus distorting less from the ideal 180º dihedral which would correspond to planarity between both arenes in the coupled products.

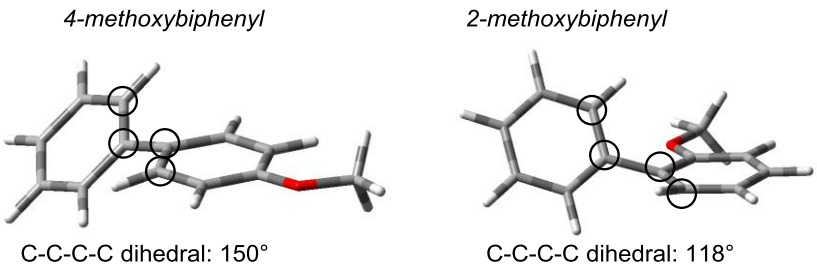

Figure 16. Dihedral angles on 2 and 4-methoxybiphenyl illustrating the distortion in planarity from 180º.

5.5. Conclusions

From our DFT studies and kinetic modelling of this system, we assume that the concentration of TFA leads to a change in catalyst undertaking C-H activation. In high [TFA], the catalytic species is likely to exist as $Pd(OTFA)_2$-TFA (as opposed to $Pd(OAc)_2$). Based on DFT calculated relative energies reductive elimination TSs are in agreement with the biphenyl formation as the major product. Using computed DFT activation parameters we have been able to construct a novel kinetic model for the catalytic cycle which accounts for the differing concentrations of the reactants. Within this model, biphenyl formation is predicted to form fastest. For lower concentrations of TFA, we propose the involvement of $Pd(OAc)_2$-TFA which is successfully able to account for the switch in selectivity observed experimentally, to favour the heterocoupled *para*-isomer. Construction of a kinetic model for this catalytic cycle is also in agreement with the observed product selectivity. Interestingly, this simulation also predicts a change in chemoselectivity towards the biphenyl product as anisole is consumed, which would not be possible using standard transition state modelling.

In both cases, the catalytic cycle proceeds with the initial activation of benzene, before either (a) activation of benzene or (b) activation of anisole at *para/ortho* and is completed with a four coordinate 16 electron reductive elimination TS, which is also the selectivity determining step. Therefore previous literature examples which support initial C-H activation of arenes to be rate-determining are not supported in our calculations in this cross-coupling. We predict that a TS with less charge separation between anisole and phenyl will provide a favourable TS energy for C-H activation and as evident in the *para* RE TSs.

Chapter 5 *References*

[1] King, A. O.; Okukado, N.; Negishi, E. *J. Chem. Soc., Chem. Commun.* **1977,** 683.

[2] Miyaura, N.; Yamada, K.; Suzuki, A. *Tetrahedron Letters* **1979**, *20*, 3437.

[3] Milstein, D.; Stille, J. K. *J. Am. Chem. Soc*. **1978**, *100*, 3636. (b) Milstein, D.; Stille, J. K. *J. Am. Chem. Soc*. **1979**, *101*, 4992.

[4] (a) Lane, B. S.; Brown, M. A.; Sames, D. *J. Am. Chem. Soc*. **2005**, *127*, 8050; (b) Kalyani, D.; Deprez, N. R.; Desai, L. V.; Sanford, M. S. *J. Am. Chem. Soc*. **2005**, *127*, 7330; (c) Daugulis, O.; Zaitsev, V. G. *Angew. Chem., Int. Ed*. **2005**, *44*, 4046; (d) Wakui, H.; Kawasaki, S.; Satoh, T.; Miura, M.; Nomura, M. *J. Am. Chem. Soc.* **2004**, *126*, 8658; (e) Huang, Q.; Fazio, A.; Dai, G.; Campo, M. A.; Larock, R. C. *J. Am. Chem. Soc.* **2004**, *126*, 7460; (f) Campeau, L. C.; Parisien, M.; Leblanc, M.; Fagnou, K. *J. Am. Chem. Soc*. **2004**, *126*, 9186; (g) Kakiuchi, F.; Kan, S.; Igi, K.; Chatani, N.; Murai, S. *J. Am. Chem. Soc*. **2003**, *125*, 1698; (h) Bedford, R. B.; Limmert, M. E. *J. Org. Chem*. **2003**, *68*, 8669; (i) Hong, W.; Qui, Y.; Yao, Z.; Qang, Z.; Jiang, S. *Tetrahedron Lett.* **2011**, *38*, 4916; (j) Park, C.-H.; Ryabova, V.; Seregin, I. V.; Sromek, A. W.; Gevorgyan, V. *Org. Lett*. **2004**, *6*, 1159; (k) Kapdi, A. *Dalton Trans.* **2014**, *43*, 3021; (l) Topczewski, J. A.; Sanford, M. A. *Chem. Sci*. **2015,** *6*, 70.

[5] Kuhl, N.; Hopkinson, M. N.; Welcel-Delord, J.; Glorius, F. *Angew. Chem. Int. Ed.* **2012**, *41*, 10236.

[6] (a) Wei, Y.; Su, W. *J. Am. Chem. Soc.* **2010**, *132*, 16377. (b) Wang, X.; Leow, D.; Yu, J. Q. *J. Am. Chem. Soc.* **2011**, *133*, 13864; (c) Dong, J.; Huang, Y.; Qin, X.; Cheng, Y.; Hao, J.; Wan, D.; Li, W.; Liu, W.; You, P. *Chem. Eur. J*. **2012**. *20*, 6158.

[7] Ricci, P.; Kramer, K.; Larossa, I. *J. Am. Chem. Soc.* **2014**, *136*, 18082.

[8] Hu, F.; Szostak, M. *ChemCatChem.* **2015**, *7*, 1061.

[9] Li, R.; Jiang, L.; Lu, W. *Organometallics*. **2006**, *25*, 5973.

[10] Lafrance, M.; Fagnou, K. *J. Am. Chem. Soc*., **2006**, *128*, 16496.

[11] Cho, B.S.; Bae, H.J.; Chung, Y. K. *J. Org. Chem.* **2015**, *80*, 5302.

[12] Ferguson, D.M.; Rudolph, S.R.; Kalyani, D. *ACS. Catal*, **2014**, *4*, 2395; (b) Laha, J.K.; Jethava. K.P.; Dayal, N. *J. Org. Chem.* **2014**, *79*, 8010.

[13] Wu, G.; Zhou, J.; Zhang, M.; Hu, P.; Su, W. *Chem. Commun.* **2012**, *48*, 8964.

[14] Zhang, H.; Shi, R.; Gan, P; Liu, C.; Ding, A.; Wang, Q.; Lei, A. *Angew. Chem. Int. Ed.* **2012**, *51*¸ 5204.

[15] (a) Kitahama, K.; Frech, R. *J. Chem. Phys.* **1985**, *82*, 720; (b) Wadt, W. R.; Hay, P. J.; *J. Chem. Phys.* **1985**, *82*, 284.

[16] Feller, D. *J. Comp. Chem.* **1996,** *17*, 1571.

[17] Roy, E. L.; Hay, J.; Martin, R. L. *J. Chem. Theory. Comput.* **2008**, *4*, 1029.

[18] (a) Barone, C.; Cossi, M. *J. Phys. Chem. A.* **1998**, *102*, 1995; (b) Barone, C.; Rega, N.; Schimani, G.; Cossi, M. *J. Comput. Chem.* **2003**, *24*, 669.

[19] (a) Ribeiro, R. F.; Marenich, A. V.; Cramer, C. J.; Truhlar D. G. *J. Phys. Chem. B*, **2011**, *115*, 14556; (b) Grimme, S. *Chem. Eur. J*. **2012**, *18*, 9955.

[20] Legault, C. Y. *CYLView*, version 1.0b. http://www.cylview.org, (accessed Aug 1 2012).

[21] NBO 6.0. E. D. Glendening, J. K. Badenhoop, A. E. Reed, J. E. Carpenter, J. A. Bohmann, C. M. Morales, C. R. Landis, and F. Weinhold, Theoretical Chemistry Institute, University of Wisconsin, Madison (2013).

[22] Macey, R.; Oster, G.; Zahley, T. *Berkeley Madonna* **2000**

[23] Rosenbrock, H. H. *Comput. J.* **1963**, *5*, 329.

[24] Zhao, X.; Yueng, C. S.; Dong, V. M. *J. Am. Chem. Soc.* **2010**, *132*, 5837; (b) Zhou, L.; Lu, W. *Organometallics*. **2012**, *31*, 2124.

Chapter 6

DFT studies of C-H activation in Pd (II) catalyzed coupling of *p*-xylene

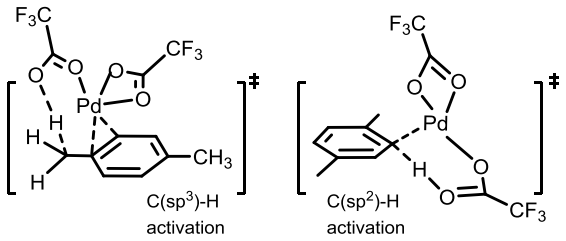

6.1. Introduction

Affording selective aryl C-H functionalization through oxidative coupling is a challenging process. The functionalization of unreactive, unfunctionalized carbon-carbon bonds has been well studied experimentally and can be achieved through traditional transition metal catalyzed cross-coupling methods.[1] Recently, advances in synthetic methodology have enabled the construction of organic molecules, through insertion of Pd catalysts selectively into C-H bonds[2] including the activation of benzylic C(sp^3)-H bonds with $Pd(OAc)_2$[3] and other transition metals.[4] The activation of benzylic C-H bonds as opposed to aryl C-H bonds, although not unprecedented, is rare without the inclusion of directing or activating groups. In toluene, where the benzylic C-H bond is ~30 kcal/mol weaker than a sp^2 aryl C-H bond, the latter is more prone to cleavage.[5] Presumably, where Pd catalysts are employed, π-coordination with the aryl group facilitates C-H activation; especially where the CMD mechanistic manifold has (through coordination of carboxylate ion) has been known to affect C-H cleavage.[6]

Lu[7] optimized a Pd(II) catalytic system where the cleavage of the C-H bond could be dictated through tuning of the concentration of TFA (**Figure 1**). Through changing the concentration of acid in the reaction, the observed regioisomer could be changed from biaryl to diarylmethane. Therefore, through this simple tuning of acid (TFA) sp^3 benzylic activation (**B**) was observed at high concentrations (20.0 mmol) while the regioselectivity is reversed at lower concentrations (0.25 mmol of TFA) leading to the biaryl regioisomer (**A**) as the major product.

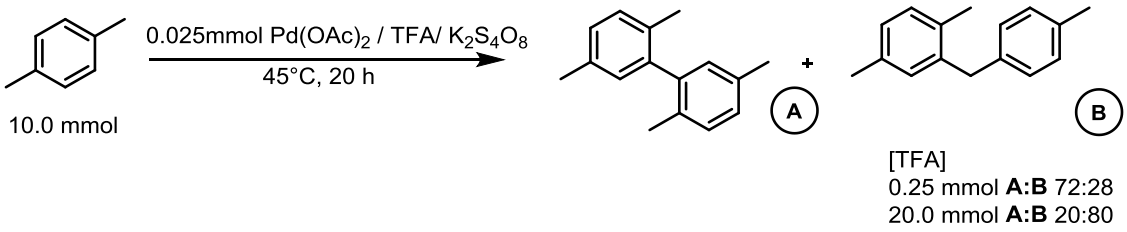

Figure 1. Concentration tuned coupling of *p*-xylene to give biaryl (A) or diarylmethane (B)

The experimentally observed sp^2-sp^2 selectivity of the homocoupled *p*-xylene product is produced with low concentration of TFA (0.25 mmol), where successive aryl C(sp^2)-H activations on *p*-xylene produce the biaryl product as the major regioisomer. The authors proposed a tentative mechanism consisting of a Pd(0)/(II) catalytic cycle, where

the formation of the homocoupled product is achieved through two C-H activation events and reductive elimination (**Figure 2**).

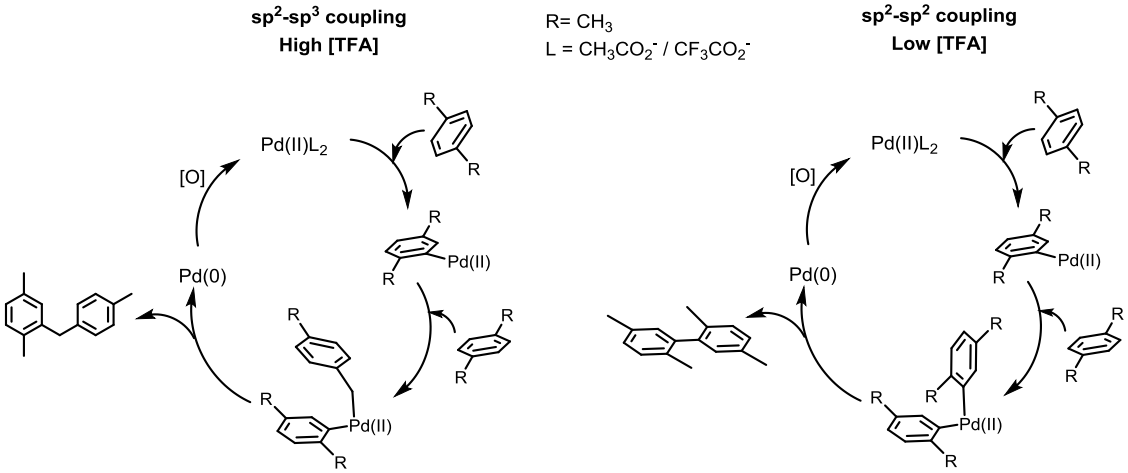

Figure 2. Proposed catalytic cycles (by Lu and coworkers) for the couplings of *p*-xylene.

The authors acknowledged that ligand exchange on Pd could occur (i.e. carboxylate ligands exchanging from CH_3COO^- to CF_3COO^-). Therefore, the authors could not ascertain which Pd(II) catalytic species was responsible in the chemoselectivity of the homocoupling, with both $Pd(OTFA)_2$ and $Pd(OAc)_2$ potential catalytic species. In fact, recent computational and experimental work[8] examining the CMD mechanism with both $Pd(OAc)_2$ and $Pd(OTFA)_2$ shows that using $Pd(OTFA)_2$ as the Pd(II) catalyst lowers C-H activation barriers by ~12.0 kcal/mol in the intramolecular hydroarylation of coumarin versus $Pd(OAc)_2$. Therefore $Pd(OTFA)_2$ could outcompete $Pd(OAc)_2$ as a more competitive catalytic species (upon ligand exchange).

Aromatic C-H activation has been proposed to occur via a Pd(II) catalyst attacking the aryl C-H bond electrophilically to form an aryl Pd(II) intermediate. In low [TFA] it was proposed that the reactivity of sp^3 benzylic C-H bonds was diminished, thus the second activation would occur at the sp^2 C-H bond of *p*-xylene, followed by reductive elimination to give the diaryl Pd(II) aryl-aryl intermediate. This would readily undergo reductive elimination to provide the homocoupled product.

In contrast, it was suggested by the authors that high [TFA] renders a more amenable environment to cleavage at the sterically less hindered benzylic C-H bond, preferring benzylic C-H activation as opposed to aryl sp^2 C-H activation. The benzylic activation was proposed to arise through electrophilic attack on C-H through a Pd(II) aryl species

from the initial activation of the sp^2 C-H bond. However, our BDE calculations confirm the benzylic C-H bond to be significantly weaker (~25 kcal/mol) since the benzylic radical is more stable and therefore initial cleavage at the benzylic position should not be considered unfeasible (**Figure 3**).

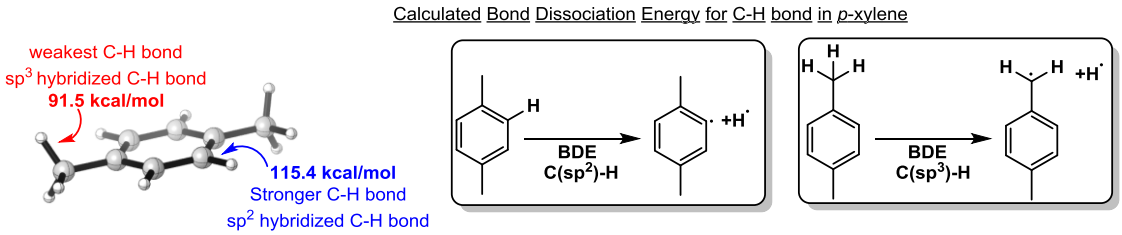

Figure 3. Bond Dissociation Enthalpy (BDE) for sp^2 and sp^3 C-H bonds of *p*-xylene calculated at G3B3. All values in kcal/mol

The sp^3 radical (i.e. benzylic radical) is thermodynamically more stable. The resonance stabilization associated with the delocalization of the unpaired electron and the aromatic system of *p*-xylene is not possible in the C(sp^2) radical. Kinetically, however, in general it is more difficult to achieve cleavage of an C(sp^3)-H bond as compared with C(sp^2)-H bond when Pd-catalysis is involved. These is due to the former lacking filled high-energy or empty low-energy orbitals (e.g. π, π^*) in close enough proximity to interact with the metal.

As the reaction undergoes coupling at the benzylic position with stoichiometric amounts of $Pd(OAc)_2$ without the need for oxidants or bases, the authors suggested that a Pd(IV) cycle or proton abstraction mechanism was unlikely to affect arene C-H bond cleavage and could therefore be excluded from these processes.[9] The activation of aryl sp^2 hybridized C-H bonds via synergy of computation and experiment through the metalation deprotonation pathway (i.e. CMD) is well documented.[6] However, recent studies investigating the cleavage of unactivated sp^3 C-H bonds with Pd(0)/Pd(II) catalysts have also exhibited a strong agreement for a proton abstraction mechanism leading to desired diaryl products, with Fagnou[10], Houk[11] and Baudoin[12] providing insight into activation via an intramolecular CMD mechanism (**Figure 4**), amongst others.[13,14,15]

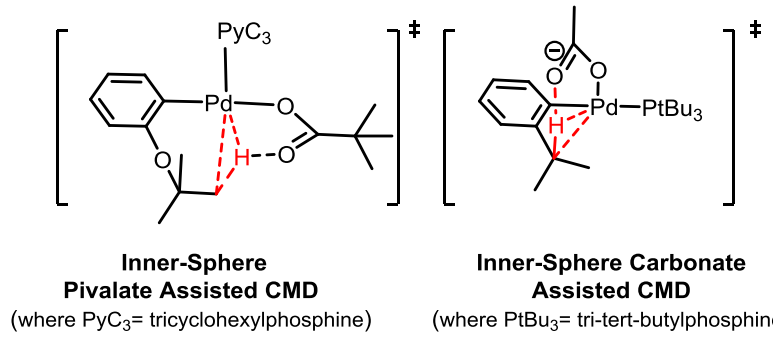

Figure 4. Inner sphere sp^3 CMD intramolecular C-H activation as proposed by Fagnou and Baudoin through an agostic interaction (M-H-C) between Pd—H—C (shown in red).

The inner sphere CMD TS has an agostic three-centre two-electron interaction between the C-H σ bond (which is cleaved) and the Pd centre (Figure 4). With cleavage of sp^3 C-H known and preferred versus sp^2 C-H bonds with Pd(II) catalysts containing carboxylate ion ligands[16] the mechanistic rationale behind such couplings and the related C-H activation are an extremely important topic, and have received significant focus.[17] Our work sought to employ DFT calculations to examine mechanistic events inherent to the regioselective activation and subsequent coupling in the experimental work by Lu and coworkers.

It should also be noted that the selectivity observed in experiment needs to be reassessed to factor the statistical effect of sites of activation (i.e. C-H bonds) in *p*-xylene. With four C(sp^2)-H sites available per molecule of *p*-xylene, and six C(sp^3)-H positions this statistical factor must be taken into consideration. Therefore in low [TFA] where the observed selectivity is 72:28 (sp^2-sp^2:sp^3-sp^2), a $\Delta\Delta G^{\ddagger}$ of 0.6 kcal/mol would correspond to this value. However, applying the selectivity factor (**Figure 5**), the innate selectivity would be accurately reassigned as $\Delta\Delta G^{\ddagger}$ 0.85 kcal/mol. Similarly, the experimental selectivity in high [TFA] is 20:80 (sp^2-sp^2:sp^3-sp^2) which corresponds to $\Delta\Delta G^{\ddagger}$ of 0.62 kcal/mol. We have considered the effects of statistics in the selectivity, although this is a relatively small correction (<0.3 kcal/mol), which may be smaller than computational error.

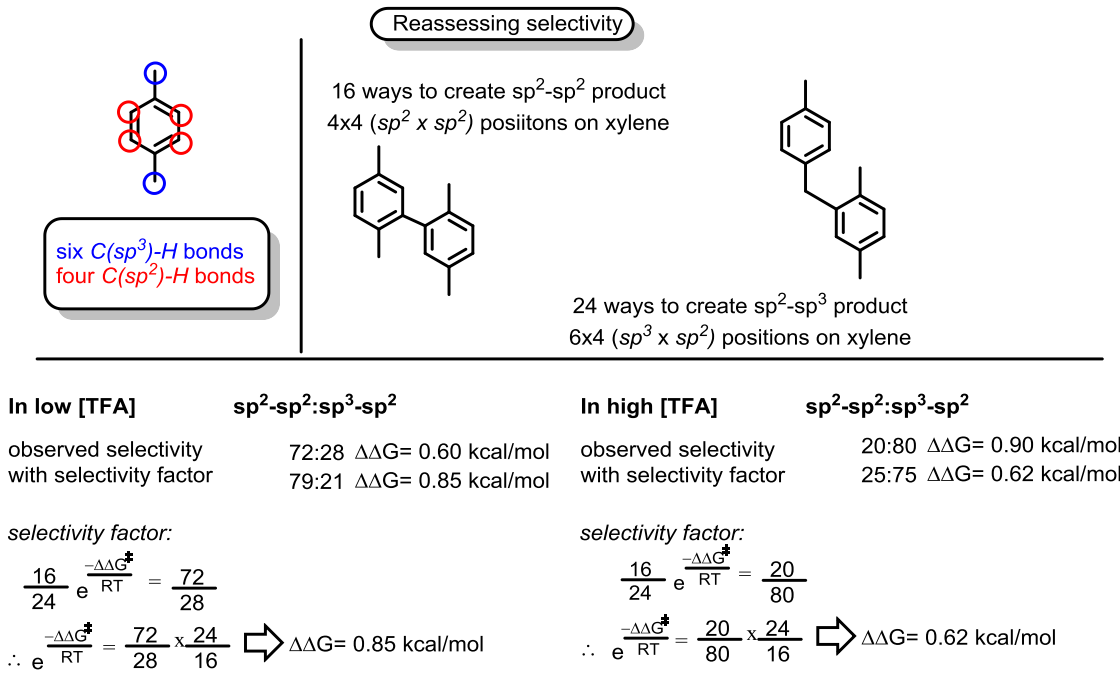

Figure 5. Applying selectivity factor to account for statistical significance of C(sp^2)-H and C(sp^3)-H bonds in xylene.

6.2. Computational methods

The computational protocol used within this chapter follows methodology presented in section 2.2., Chapter 2. Modifications made to the computational methodology (for work presented in this chapter) are mentioned herein.

Initial geometry optimizations were performed with the **ω**B97XD functional and split-valance polarized 6-31G(d) basis set for C, H, F and O atoms, whilst the LANL2DZ double-zeta valence basis set and associated effective core potential (ECP) were used to describe Pd.[18] Single point energies were computed on all optimized geometries with the larger valence triple-zeta 6-311+G(d,p) and LANL2TZ basis set obtained from the EMSL Basis Set Exchange.[19,20] A fine grid density was used for numerical integration in all DFT calculations.

Free energies were evaluated at 318K including zero point vibrational energies. The effects of solvent (*p*-xylene ε= 2.275) were incorporated through the use of a conductor-like polarizable continuum model (CPCM), defining the solute cavity with UFF radii[21] by conducting single point optimizations on optimized geometries A smooth damping function centred about a frequency of 100 cm^{-1} was used to switch between the harmonic approximation for vibrations above this value and the free-rotor approximation below.[22] Bond dissociation energies (BDE) were calculated through enthalpy calculations using the G3B3 composite method, where structures and zero point vibrational energies are calculated at the B3LYP/6-31g(d) level of theory.[23]All energies presented within this work are Gibbs (ΔG) free energies against separated reactants and calculated via:

$$\Delta G_{solv} = \Delta E_{solv} + (\Delta G_{gas} - \Delta E_{gas})$$

The NBO 6.0 program[24] was used to calculate Wiberg Bond Orders to assess bond formation between atoms and assess Natural Population Analysis (NPA)[25] to calculate the natural charge on atoms, as well as the Natural Binding Index (NBI) signifying the strength of the bond.

6.3. Results

6.3.1. Proposed catalytic cycles

Our mechanistic proposition for C-H activation focused on a proton abstraction mechanism via an intramolecular (CMD) or intermolecular (S_E3) mechanism for sp^2 and sp^3 C-H bonds. Two catalytic cycles were characterized, (**1**) the reaction proceeding through common C(sp^2)-H activation followed by the subsequent C(sp^3)-H or C(sp^2)-H activation or (**2**) two independent C-H activations where either C(sp^2)-H or C(sp^3)-H activation occur independently before an arylated Pd catalyst undertakes a C(sp^2)-H activation (**Figure 6**).

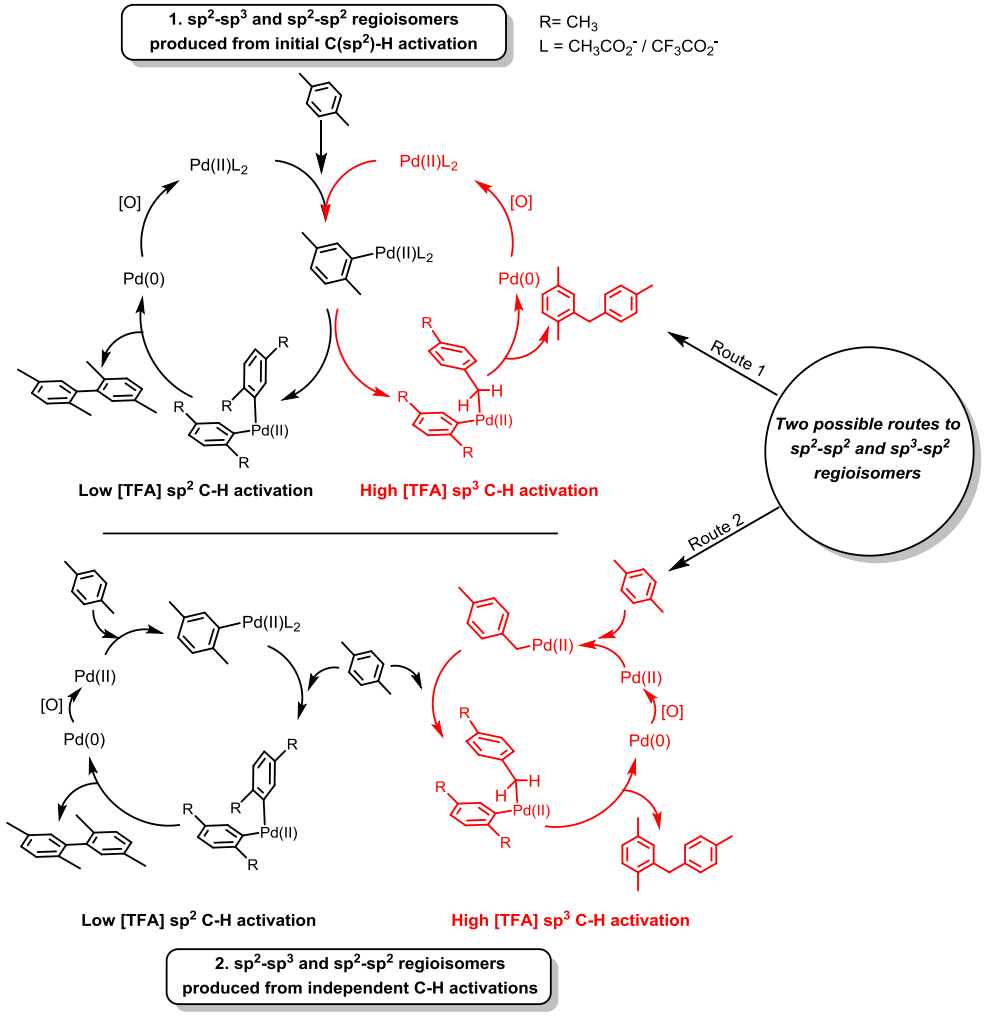

Figure 6. Proposed catalytic cycles proceeding via a common sp^2 intermediate (*left*) as proposed by authors, or via two independent C-H activation events (*right*).

Both $Pd(OAc)_2$, $Pd(OTFA)_2$ and their solvated analogs (where TFA is a neutral two electron σ donor to the Pd centre) were calculated undertaking cleavage of sp^2 and sp^3

C-H bonds in *p*-xylene. The oxidant ($K_2S_2O_8$) was found not to affect selectivity or turnover in experiment. Therefore, the reaction owes selectivity to a combination of catalyst and concentration of TFA.

6.3.2. sp^2-sp^2 activation

The catalytic species could change depending on the concentration of TFA. It was suggested by Lu and coworkers that higher concentrations could yield a $Pd(OTFA)_2$ species through catalytic turnover and/or ligand exchange. In low concentrations, the possibility of $Pd(OAc)_2$ or $Pd(OAc)_2$ with an additional neutral ligand (TFA) cannot be ruled out. Therefore C-H activation with all such postulated catalytic Pd(II) species was calculated, including 'ligandless' $Pd(OAc)_2$ and $Pd(OTFA)_2$ as well as their solvated variants, in the form of $Pd(OAc)_2$-TFA and $Pd(OTFA)_2$-TFA. The authors proposed the catalytic cycle to proceed via initial activation at the C(sp^2)-H bond, in both high and low concentrations of TFA. This section concentrates on the homocoupling (sp^2-sp^2) of *p*-xylene (**Figure 7**).

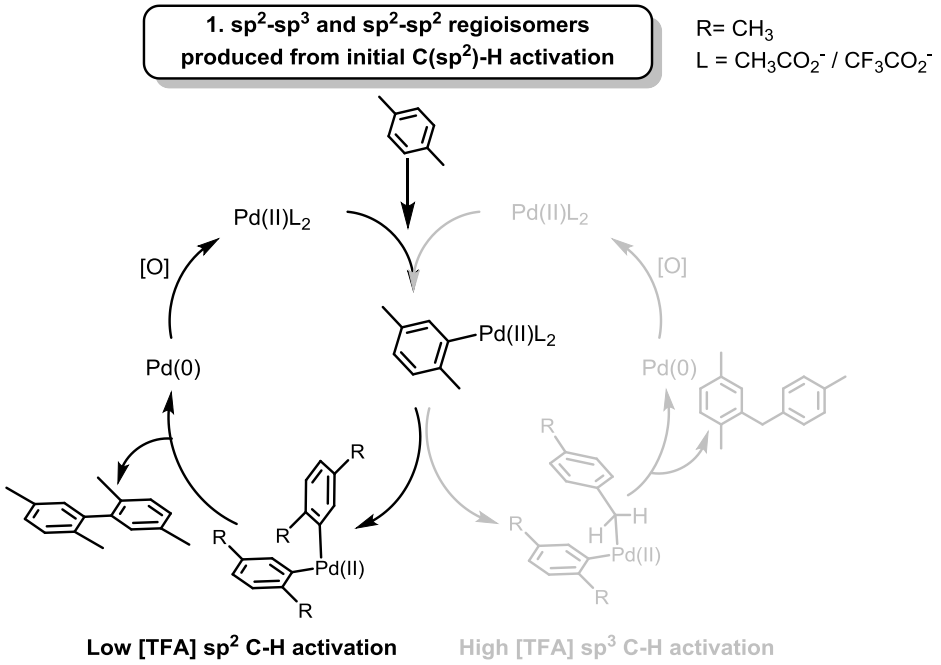

Figure 7. Examining the proposed catalytic cycle in the homocoupling of p-xylene through a double C(sp^2)-H activation (*left, black*).

The CMD mechanism proceeds through a Pd(II) *p*-xylene precomplex, where η^2 complexation of Pd occurs with the π system of *p*-xylene. The coordination allows for Pd(II) to assume square planar geometry in the precomplex, which is concomitant to the CMD TS. The initial coordination proceeds with orientation to the square planar, four coordinate geometry associated with Pd (II) 16 valence electron species. Hapticity of Pd(II) to the aryl changes from η^2 to η^1 allowing for a concerted

palladation/deprotonation event by either $CH_3CO_2^-$ or $CF_3CO_2^-$ (depending on the catalytic species). The deprotonation of C-H occurs involves simultaneous palladation of the Pd(II) species to the C(sp^2) position (

Figure 8) .

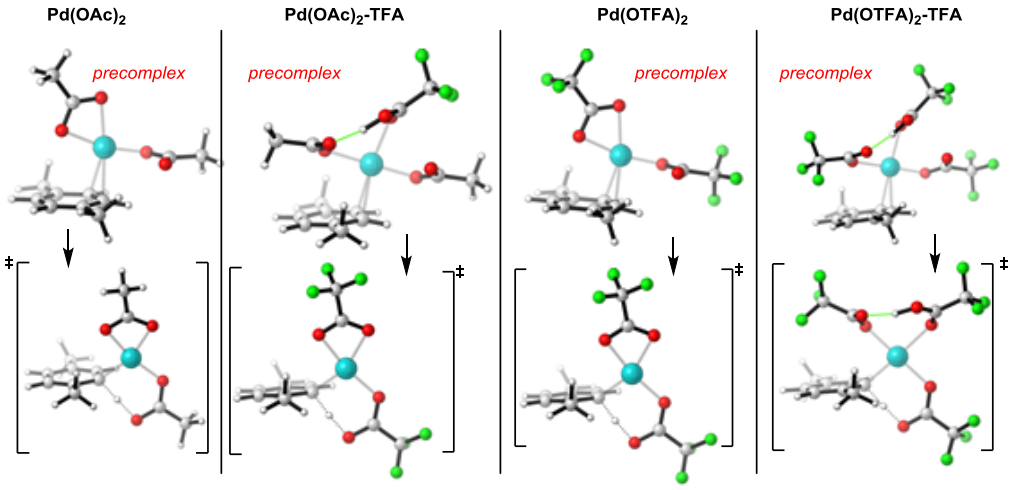

Figure 8. Optimized geometry of precomplex *(top)* and corresponding TS (*bottom*) of CMD mechanism for *p*-xylene. All studied Pd(II) species shown. Here OTFA= anionic CF_3COO^- and TFA= neutral CF_3COOH.

Our calculations illustrated that exchanging the carboxylate ligand from OAc^- to $OTFA^-$ establishes a trend in Gibbs free energy in the initial C-H deprotonation via the CMD mechanism. It is noted that the $OTFA^-$ ligands produce catalytic species that lower ΔG in the CMD TS for sp^2 C-H activation. Gibbs free energy for the CMD TS decreases in the order *$Pd(OAc)_2$ > $Pd(OAc)_2$-TFA > $Pd(OTFA)_2$ > $Pd(OTFA)_2$-TFA*, indicating that the OTFA ligand exerts a greater TS stabilizing influence than the OAc ligand, and that additional solvation by TFA further stabilizes the TSs (presumably because of a combination of bite-angle relief on going from η^2 carboxyl to two η^1 carboxyls, and better charge delocalization) (**Figure 9**).

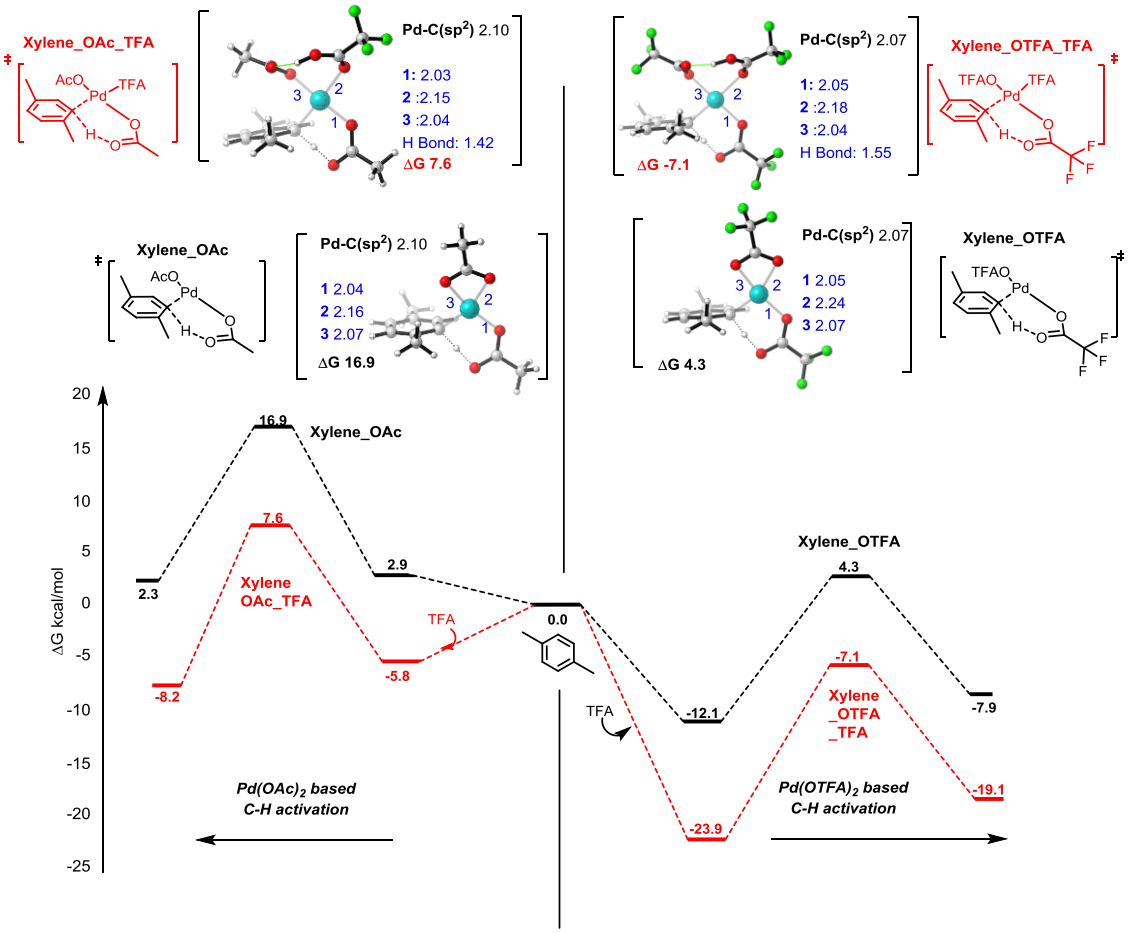

Figure 9. Gibbs free energy profile for the initial CMD C-H activation with different Pd(II) species. All values in kcal/mol. All energies against separated reactants, which is constant amongst all energy profiles within this chapter.

Calculations showed that coordination of TFA creating solvated Pd(II) catalysts (i.e. **Xylene_OAc_TFA** and **Xylene_TFA_TFA**) also caused $\Delta G^{\ddagger}$ to be lowered. The reaction was shown to occur more readily with the ligation of a neutral TFA molecule occupying an open coordination site on Pd(II) – exemplified by **Xylene_OAc** (ΔG 16.9 kcal/mol) being higher in energy than **Xylene_OAc_TFA** (ΔG 7.6 kcal/mol) suggesting TFA plays an important role in the activation of *p*-xylene, whether it be by changing the catalyst to $Pd(OTFA)_2$ or by providing an extra ligand to the Pd centre – as apparent with $Pd(OAc)_2$-TFA (**Xylene_OAc_TFA**) and as seen in **Figure 9**.

Explicit coordination of TFA provides the lowest energy pathways, i.e. $Pd(OAc)_2$-TFA and $Pd(OTFA)_2$-TFA (ΔG -7.1 kcal/mol) are shown to be most energetically favourable for $C(sp^2)$-H activation.

Therefore we presume that in low [TFA] the catalytic species could certainly exist as $Pd(OAc)_2$-TFA and in higher [TFA] the catalytic species is either $Pd(OTFA)_2$/$Pd(OTFA)_2$-TFA, assuming ligand exchange.

Using NBO calculations it was discovered that solvated species had a higher formal bond order (Wiberg Bond Order) for Pd–C(sp^2) in the TS and stronger binding (NBI) than their ligandless counterpart. Stronger bonding (for C-Pd) within the TS was unrelated to the natural charge on Pd(II), with the actual positive charge of the metal centre constant amongst all studied species (**Table 1**).

Species	Wiberg Pd-C	Charge on Pd	NBI
$Pd(OAc)_2$	**0.44**	0.85	**0.66**
$Pd(OAc)_2$-TFA	**0.46**	0.86	**0.68**
$Pd(OTFA)_2$	**0.54**	0.84	**0.73**
$Pd(OTFA)_2$-TFA	**0.55**	0.84	**0.74**

Table 1. Wiberg bond order for Pd-C(sp^2), Natural Population Analysis of Pd and Natural Binding Index (NBI) between Pd-C(sp^2) shown for relevant CMD TS.

Also, $Pd(OTFA)_2$ /$Pd(OTFA)_2$-TFA catalytic species were shown to have a higher bond order in the CMD TS for Pd-C(sp^2) compared to OAc based catalysts (Table 1). Furthermore, the TS geometry shows shorter bond lengths for Pd-C(sp^2) (**Figure 9**) in TFA based Pd(II) catalytic species, i.e. $Pd(OTFA)_2$ and $Pd(OTFA)_2$-TFA than $Pd(OAc)_2$ and $Pd(OAc)_2$-TFA suggesting stronger bonding between Pd and C(sp^2). This suggestion is supported by NBI calculations (with 1 signifying strong and 0 weaker bonding) in **Table 1**– where the Pd-C(sp^2) bond is stronger in $Pd(OTFA)_2$ and $Pd(OTFA)_2$-TFA species suggesting triflouroacetate ligands do enhance CMD TS by providing a stronger bond order, binding strength and overall lower $\Delta G^{\ddagger}$.

Second sp^2 C-H activation

Following from the first C(sp^2)-H activation of *p*-xylene , the Pd(II) species now has an aryl ligand. Dissociation of either AcOH or TFA must occur for subsequent coordination and C(sp^2)-H activation of the second *p*-xylene unit. The CMD mechanism was modelled for this activation with initial η^2 coordination of the Pd(II)ArX (where Ar = sp^2-activated *p*-xylene and X= OAc/OTFA) to the π system of *p*-xylene. This was a precursor to the subsequent CMD C-H activation TS of *p*-xylene. We investigated the reaction proceeding from our lowest energy initial C-H activations, from **Xylene_OAc_TFA** and **Xylene_OTFA_TFA** (seen in **Figure 9**). Bisligated species were preferred for the second activation, with lower Gibbs free energy barriers to activation (**Figure 10**). Presumably this is because of the electronic stability afforded from having 16 rather than 14 valence electrons about the Pd centre.

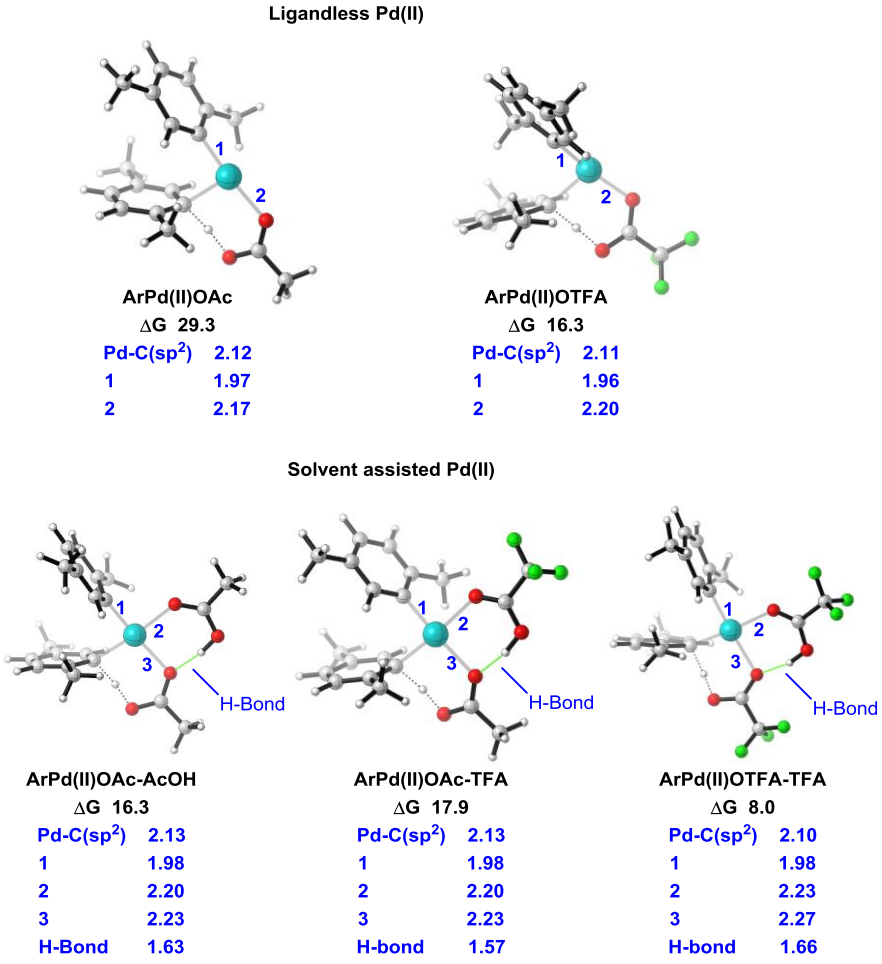

Figure 10. Optimized geometries of second sp^2 CMD C-H activation with non-solvated (*top*) and solvent assisted (*bottom*) following initial C-H activation. All bond lengths in Å. All energy values in kcal/mol

NBO calculations showed that a lower natural charge of Pd is observed where OTFA/TFA ligands are coordinated to the Pd centre as compared with OAc/AcOH ligands. Further analysis of the NBO calculations suggest that electron deficient Pd (i.e. possessing higher natural charge) does provide any distinct benefit in the palladation/ C-H activation event (**Figure 11**). Higher charge on Pd has a correlation with higher ΔG exhibited in the CMD TS (R^2=0.77). The Wiberg Bond order is higher in the Pd-C(sp^2) bond in the second activation for ArPd(II)OTFA-TFA and ArPd(II)OTFA, which is reflected in shorter bond distances as opposed to ArPd(II)OAc-AcOH and ArPd(II)OAc (as seen in **Figure 10**)

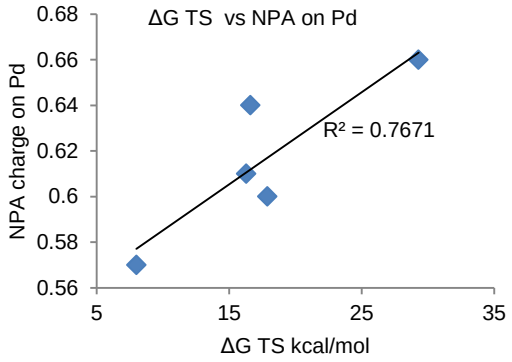

TS Species	ΔG(TS)	Pd Charge	Wiberg
ArPd(II)OAc	**29.3**	**0.66**	0.39
ArPd(II)OTFA	**16.3**	**0.64**	0.42
ArPd(II)OAc-AcOH	**16.3**	**0.61**	0.37
ArPd(II)OAc-TFA	**17.9**	**0.60**	0.39
ArPd(II)OTFA-TFA	**8.0**	**0.57**	0.42

Figure 11. Correlation between Pd charge in CMD TS and resulting TS free energy of calculated species. Data tabulated on the right. Wiberg bond order is for the Pd-C(sp^2); all values in kcal/mol.

The *p*-xylene homocoupling is a result of a three-centred reductive elimination event leading to the formation a C-C bond and upon expulsion of Pd(0), the sp^2-sp^2 coupled product (**Figure 12**). Reductive elimination proceeds through a three-centred, mechanism where two aryl groups are in *cis* disposition prior to C-C bond formation. Both four coordinate 16 electron and three coordinate 14 electron species were studied.

Amongst the catalytic species studied, it is the four-coordinate 16 electron species which has the lower Gibbs free energy relative to 14 electron species, i.e. ArPd(II)Ar'AcOH is higher in ΔG TS than ArPd(II)Ar'$(AcOH)_2$. Therefore reductive elimination is calculated to proceed with a coordinately saturated square planar Pd(II) species. Preference for a fully saturated square planar reductive elimination species is rationalized by the ability of the two neutral σ donors (OTFA and/or AcOH) to create a smaller, more acute C-Pd-C angle (**Figure 12**). This brings the two aryl groups in closer proximity, signified by the C-Pd-C angle and also the bond lengths in TS where

the 16 electron species exhibits shorter $C(sp^2)$-$C(sp^2)$ bond length in comparison to the 14 electron species.

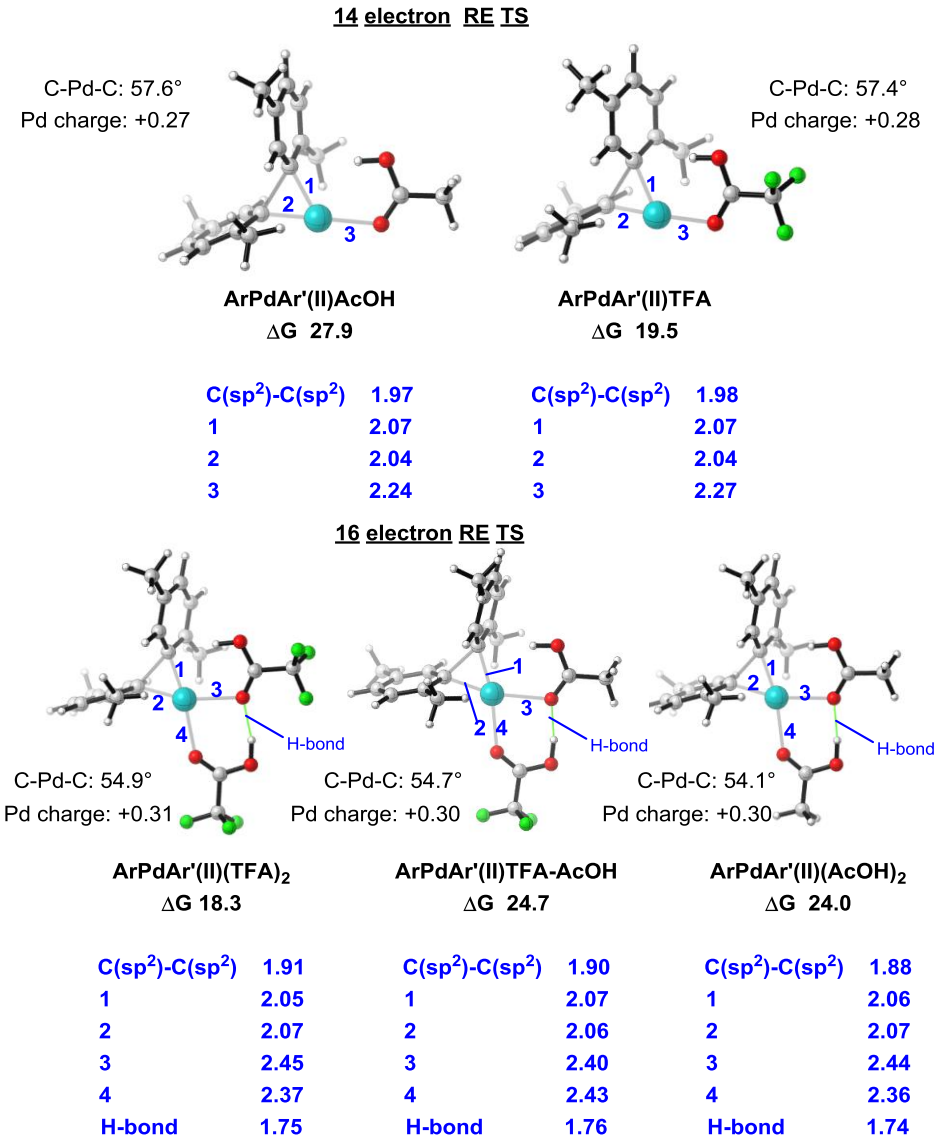

Figure 12. Optimized geometries for reductive elimination TS. 14 electron species, ArPd(II)Ar'AcOH and ArPd(II)Ar'TFA (*top*). 16 electron species ArPd(II)Ar'$(TFA)_2$, ArPd(II)Ar'AcOHTFA and ArPd(II)Ar'$(AcOH)_2$ (left to right, *bottom*). All values in kcal/mol. All bond length in Å

Summary of sp^2-sp^2 activation via CMD mechanism

The role of triflouroacetic acid in the reaction is calculated to be non-innocent. Ligation of TFA to the Pd centre (to create either $Pd(OAc)_2$-TFA or $Pd(OTFA)_2$-TFA) produces a more energetically competitive catalytic CMD TS compared to the ligandless pathways for the initial CMD C-H activation.

Furthermore, $Pd(OTFA)_2$ and $Pd(OTFA)_2$-TFA produce lower C-H activation TSs than their acetate based counterparts via a CMD pathway. The energetic span for the CMD pathway is however a lot higher for the $Pd(OTFA)_2$-TFA pathway – in excess of 40 kcal/mol. In contrast, this span is lower in the $Pd(OAc)_2$-TFA pathway – at 32.0 kcal/mol (**Figure 13**). We believe that the initial precomplex formed by the $Pd(OTFA)_2$-TFA catalyst has been overestimated at ΔG -24.2 kcal/mol which contributes to the large span predicted for the $Pd(OTFA)_2$-TFA complex.

Therefore, where the sp^2 homocoupled product dominates (i.e. in low concentrations of TFA) it is likely that $Pd(OAc)_2$-TFA pathway is the most competitive, where TFA plays the role of coordinating solvent (**Figure 13**, *left*). We believe that the $Pd(OTFA)_2$-TFA pathway (*right*) is more likely in high concentrations of TFA (i.e. where the sp^3-sp^2 product will dominate), and where the high concentration of TFA has created ligand exchange to create $Pd(OTFA)_2$ in the first instance.

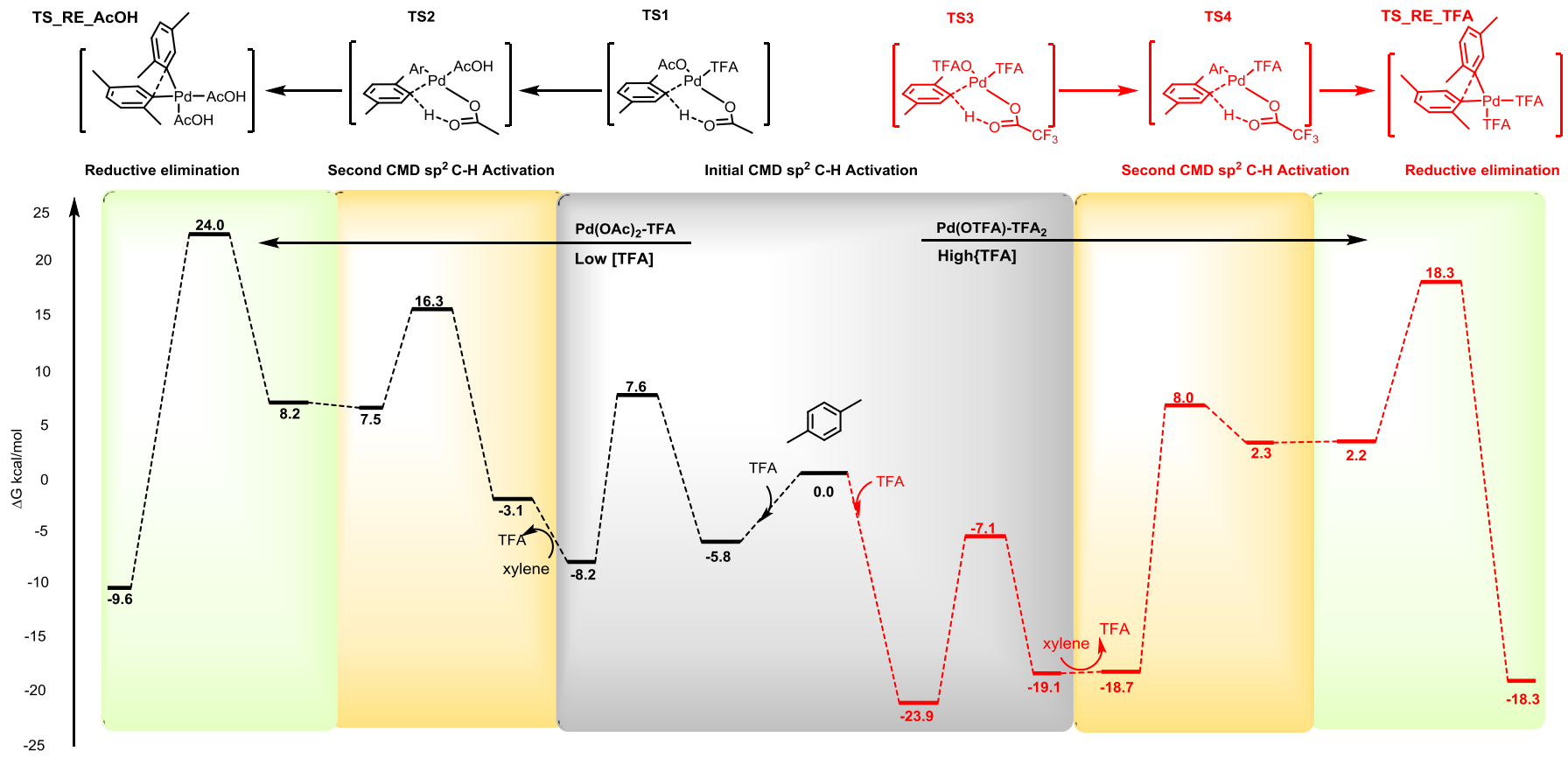

Figure 13. Free energy diagram for the sp^2-sp^2 coupling of *p*-xylene. Energy profiles for $Pd(OAc)_2$-TFA (*left*) and $Pd(OTFA)_2$-TFA (*right*) are shown with the double CMD mechanism both catalytic species. All values are in kcal/mol . All energies against seperated reactants.

6.3.3. Alternative mechanisms for sp^2-sp^2 coupling

6.3.3.1. Carbopalladation (CP)

A carbopalladation mechanism for the second C-H activation as an alternative to CMD was explored. The mechanism is calculated to proceed via *syn*-palladation across the π system of *p*-xylene subsequent to the initial CMD mechanism, therefore competing against successive CMD events (**Figure 14**).

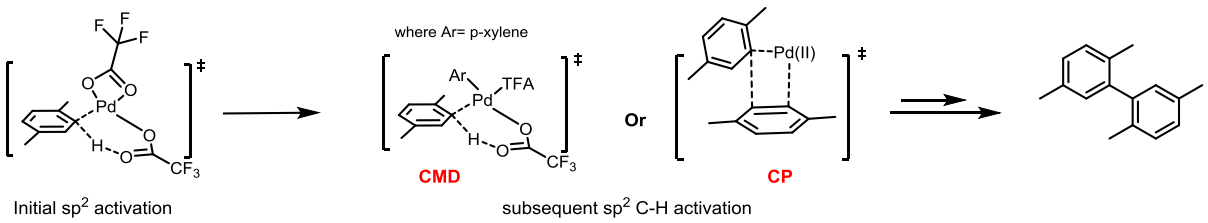

Figure 14. The mechanisitc alternatives for the second sp^2 C-H activation. CMD and Carbopalladation (CP) are both plausible mechanistic events leading to the homocoupled *p*-xylene product.

The TS proceeds via four-membered TS where *syn* addition creates a new C-C bond, transferring the sp^2 aryl ligand to the *ortho* position. The carbopalldation TS is energetically favoured over the CMD event for ArPd(II)OTFA-TFA (**CP:** ΔG -0.3 kcal/mol/ **CMD:** ΔG 8.0 kcal/mol). Interestingly, for a TFA deficient species, (i.e. ArPd(II)OAc-AcOH) CMD is preferred over carbopalladation for the second C-H activation (**CP:** ΔG 18.6 kcal/mol **/ CMD** ΔG 16.3 kcal/mol**) (Figure 15)**.

Carbopalladation leads to the construction of a new C-C bond between the two aryl species with aromaticity of the system restored through an *anti* E2 intermolecular base-assisted deprotonation restoring π character and expelling Pd(0) from the homocoupled *p*-xylene product which completes the catalytic cycle. The traditional syn *β*-hydride elimination event is not possible due to inability of C-C bond rotation in *p*-xylene. Deprotonation and subsequent rearomatization of *p*-xylene requires proton abstraction with the TFA conjugate base, expelling Pd(0). Calculations show this to be a low energy TS proceeding via lower Gibbs free energy than the reductive elimination event in the CMD mechanism.

The potential of this intermolecular deprotonation is hampered by the lack of free base present in the acidic reaction conditions. The dissociation of either $CF3COO^-$ or CH_3COO^- from Pd could produce the anion in order to undertake deprotonation, or from dissociation of the acid, TFA to the conjugate base pairs (i.e. CF_3COO^- and H^+).

The oxidant ($K_2S_2O_8$ is unlikely to affect intermolecular deprotonation as selectivity and turnover of either product is not affected by altering amounts of the oxidant. However, our calculations suggest that the sp^2-sp^2 coupling could switch from a CMD mechanism in buffered conditions to a Heck-type carbopalladation mechanism in more basic conditions with $Pd(OTFA)_2$ as the catalytic species.

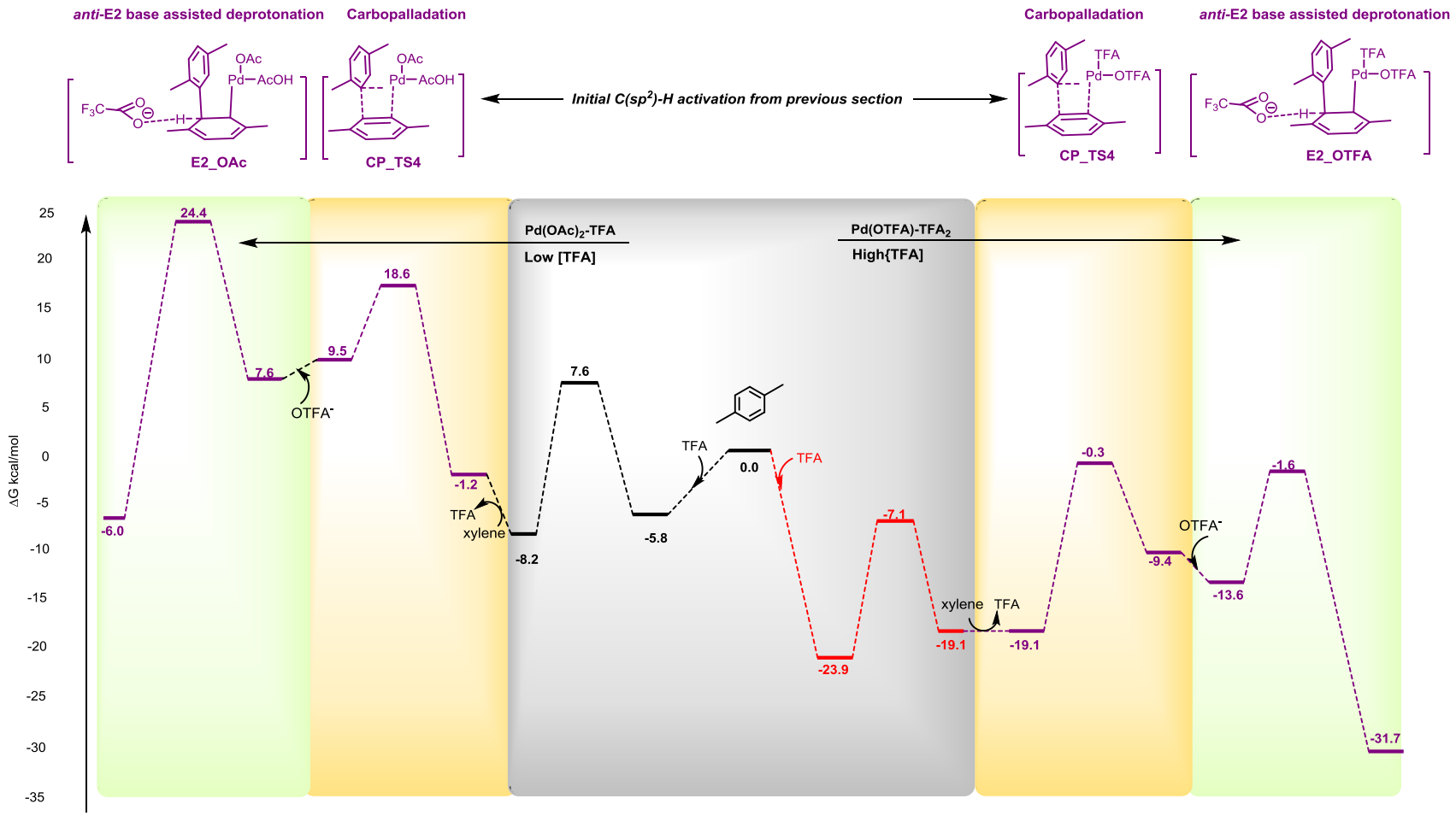

Figure 15. Free energy diagram for the sp^2-sp^2 coupling of *p*-xylene with a carbopalladation mechanism. Energy profiles for $Pd(OAc)_2$-TFA (*left*) and $Pd(OTFA)_2$-TFA (*right*) are shown. All values are in kcal/mol . All energies against seperated reactants.

6.3.3.2. Intermolecular C-H activation: S_E3

The initial C-H of C(sp^2)-H via an intermolecular deprotonation mechanism was also calculated as a competing mechanism for the initial C-H activation. From previous calculations on (hetero)arenes (Chapter 2/3/4) the S_E3 mechanism was shown to be unsuccessful in producing an energetically competitive TS compared to an intramolecular C-H cleavage mechanism (i.e. CMD). This was once again illustrated with the sp^2 C-H activation of *p*-xylene species (**Figure 16**), where each calculated TS was higher in energy than the analogous CMD mechanism.

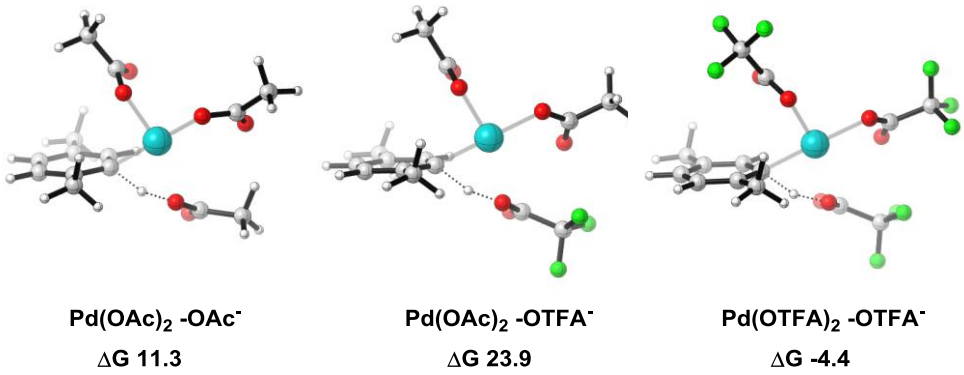

Figure 16. Optimized geometries of S_E3 TS for sp^2 C-H activation of *p*-xylene. All values in kcal/mol and against separated reactants.

All postulated catalytic Pd (II) species were calculated (i.e. $Pd(OAc)_2$-OAc, $Pd(OAc)_2$-OTFA and $Pd(OTFA)_2$-OTFA), with both OAc^- and $OTFA^-$ modelled as the carboxylate anion affecting C-H cleavage in a intermolecular reaction. This mechanistic profile and catalytic cycle would require free base to be available in the reaction in order to affect cleavage which is improbably in the presence of TFA. Our computational results suggest that the CMD pathway would be preferred over the S_E3 pathway for the initial activation of *p*-xylene.

6.3.4. sp^2-sp^3 coupling: Initial C(sp^2)-H activation

The sp^2-sp^3 coupled product is observed as the major product when the reaction employs high [TFA]. Our calculations sought to establish the mechanism leading to benzylic sp^3 C-H activation and subsequent formation of diaryl product. Therefore it is our hypothesis that a mechanism via $Pd(OTFA)_2$ or $Pd(OTFA)_2$-TFA is more likely in such conditions. However, for completeness all catalytic species $Pd(OAc)_2$, $Pd(OAc)_2$-TFA, $Pd(OTFA)_2$ and $Pd(OTFA)_2$-TFA were calculated. This section presents work detailing a catalytic cycle whereby initial C-H activation has occurred via CMD on C(sp^2)-H bond of xylene, and the subsequent step would be the activation of C(sp^3)-H bond on xylene (**Figure 17**, *red*).

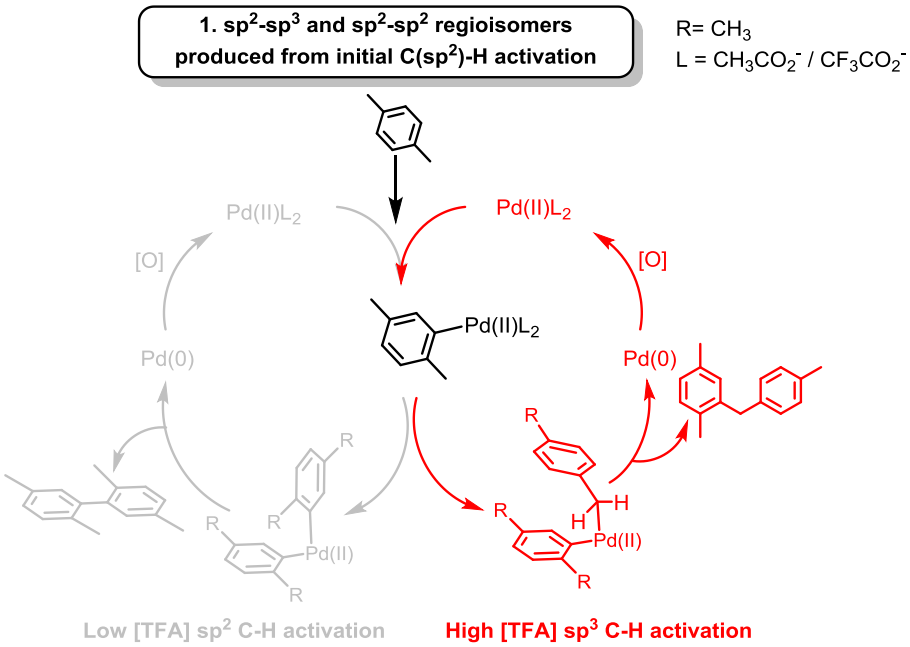

Figure 17. Calculated catalytic cycle of sp^2-sp^3 regioisomer (*right, red*) which proceeds from a common sp^2 C-H activation as observed in the previous section.

The sp^3 C-H bond is devoid of π-orbitals to initiate coordination with the d orbitals of Pd, therefore alternative mechanisms to the conventional intramolecular CMD were investigated. The benzylic C-H cleavage was calculated via an inner sphere CMD process (**Figure 18**). Initial C-H activation for sp^3 C-H bonds via an S_E3 mechanistic pathway or an outer-sphere CMD (as termed by Grubbs and Houk[26]) where an anionic, unbound carboxylate ($OTFA^-$ /OAc^-) undertakes deprotonation was also studied. The outer sphere mechanism is analogous to S_E3.

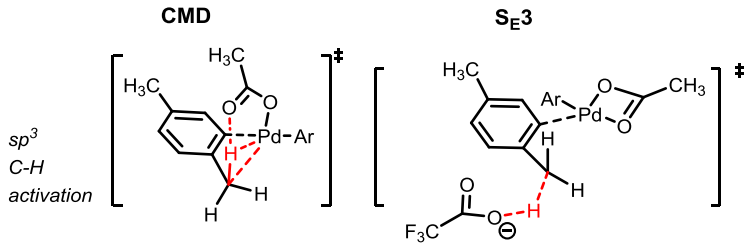

Figure 18. Possible mechanistic events of sp^3 C-H activation. The inner sphere mechanism (*left*) and the outer sphere mechanism/S_E3 mechanism (*right*) for *p*-xylene.

Inner sphere CMD

Calculations into proposed mechanism of C-H activation of the sp^3-sp^2 coupled product sought to elucidate whether initial sp^2 activation followed by sp^3 activation (as proposed by the authors) could account for observed selectivity. A six-membered TS where aryl sp^2 C-H bond cleavage occurs through a concerted palladation and deprotonation event (as calculated in the previous section) is subsequently followed by sp^3 C-H bond cleavage via a CMD inner sphere mechanism in order for the authors proposed catalytic cycle to be feasible. Cleavage at the sp^3 C-H bond cleavage occurs via initial η^2 coordination which provides precomplex **Pre_OAc_Inner** (**Figure 19**). This is the precursor to the sp^3 C-H activation TS, **OAc_Inner_TS** where the elongation of OAc^- (*trans* to sp^2 activated *p*-xylene) occurs in order to undertake deprotonation of the benzylic proton (**Figure 19**).

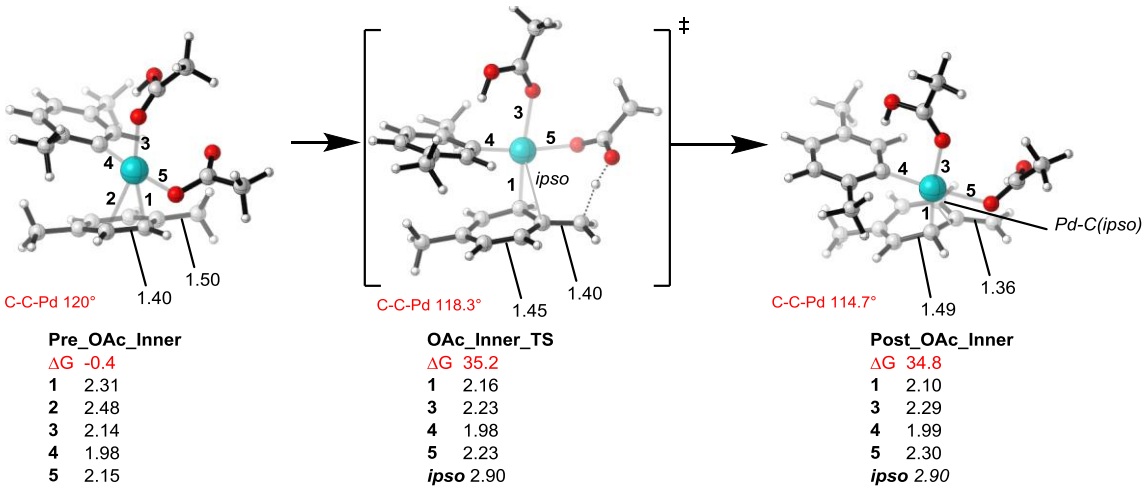

Figure 19. Optimized geometries for the inner sphere CMD mechanism of sp^3 C-H bond cleavage. The precomplex (Pre_OAc_Inner), TS (OAc_Inner_TS) and post abstraction intertermediate (Post_OAc_Inner) are shown. The catalytic species shown is ArPd(II)OAc-AcoH (where Ar=*p*-xylene). All bond lengths in Å. All energies in kcal/mol.

Benzylic C-H bond cleavage retains dihaptacity of Pd (η^2 to the π system) –at the *ortho* and *ipso* positions which is illustrated by the bond length shortening at position **1** from 2.31Å to 2.16Å and the absolute loss of bond **2** (as seen in **Figure 19**) and linkage at the *ipso* position of Pd-C(*ipso)* of 2.90 Å. Disruption of the *p*-xylene π system is observed through the inner sphere mechanism (**Pre_OAc_Inner → OAc_Inner_TS → Post_OAc_Inner**), exemplified by the distortion in planar arrangement of the six-membered *p*-xylene ring and C-C-C bond angle (of 120º) to the *p*-xylene aromatic ring (**Figure 22**). Lengthening of the *p*-xylene C-C aromatic bond to more characteristic single C-C bond length is observed after deprotonation (**Pre_OAc_Inner:** 1.40Å**→ Post_OAc_Inner:** 1.49Å**)**, indicating the transformation from sp^2 to sp^3 character. Optimized TS geometries for all studied species show the shortening of the benzylic C-H bond, indicating increased allylic character (change in the benzylic C-C bond from 1.50Å in **Pre_OAc_Inner** to 1.36 Å in **Post_OAc_Inner)**. The ideal bond angle of the planar aromatic π system of 120º in *p*-xylene distorts in the TS to 114.7º in order to produce the cleaved product **Post_OAc_Inner**, resembling sp^3 hybridization. The allylic C=C bond (post deprotonation) bends out of plane, distorted from its co-planar geometry with the *p*-xylene, creating an undesirable high energy post-abstraction species.

Coordination at the *ortho-ipso* position is essential to affect C-H cleavage via CMD. Optimizations yielded only the η^2 *ortho-ipso* Pd coordinated TS (**Figure 20**). This dihapto Pd coordination was common in all TS amongst all Pd species studied.

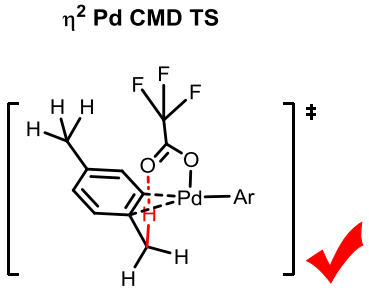

Figure 20. Calculations of benzylic C-H activation favoured η^2 Pd CMD TS coordination geometry.

However, C(sp^3)-H activation via an inner sphere mechanism is a high energy process amongst all catalytic Pd(II) species. This is reflected in calculated C(sp^3)-H activation energies with **ArPd(II)OAc_AcOH** TS (ΔG 35.2 kcal/mol), **ArPd(II)OTFA-TFA** (ΔG= 27.7 kcal/mol) and **ArPd(II)OAc-TFA** (ΔG= 36.3 kcal/mol) - all displaying

high Gibbs free energy (against separated reactants) for the cleavage of an sp^3 C-H bond (**Figure 21**). Our calculations suggest that the abstraction of H^+ from the benzylic position (via this series of events) will be difficult irrespective of the carboxylate ligand present on Pd.

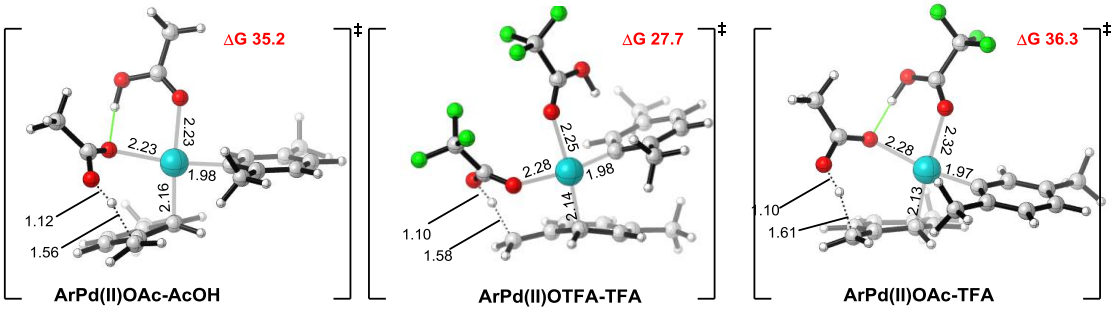

Figure 21. Optimized TS geomtries for C-H bond cleavage at sp^3 via an inner sphere mechanism with an aryl-Pd(II) catalytic species. Free energy values in kcal/mol; bond lengths in Å

The activation of the C(sp^3)-H bond via this set of mechanistic events is a high energy process which produces an unstable post abstraction intermediate (as seen **Post_OAc_Inner** ΔG 34.8 kcal/mol). This is high energy post-abstraction intermediate is observed amongst all studied Pd species (**Table 2**), suggesting that this would be an additional prohibitive effect in achieving C(sp^3)-H activation.

	ArPd(II)OAc-AcoH (ΔG kcal/mol)	ArPd(II)OTFA-TFA (ΔG kcal/mol)	ArPd(II)OAc-TFA (ΔG kcal/mol)
Inner sphere CMD TS of C(sp^3)-H bond on *p*-xylene	**35.2**	**27.7**	**36.3**
Post C(sp^3)-H cleavage intermediate	34.8	27.5	35.9

Table 2. Solvent corrected free energies of TS and post abstraction species resulting from bond cleavage at C(sp^3) -H via an inner sphere mechanism. All values in kcal/mol

Subsequent [1,3] Pd migration allows for reformation of the *p*-xylene π system and benzylic character is restored through a new C(sp^3)-Pd bond The Pd centre is fully saturated in a 16 electron square planar coordination, with the two aryl species in *cis* conformation to each other. This is the precursor to the reductive elimination TS (**Figure 22**).

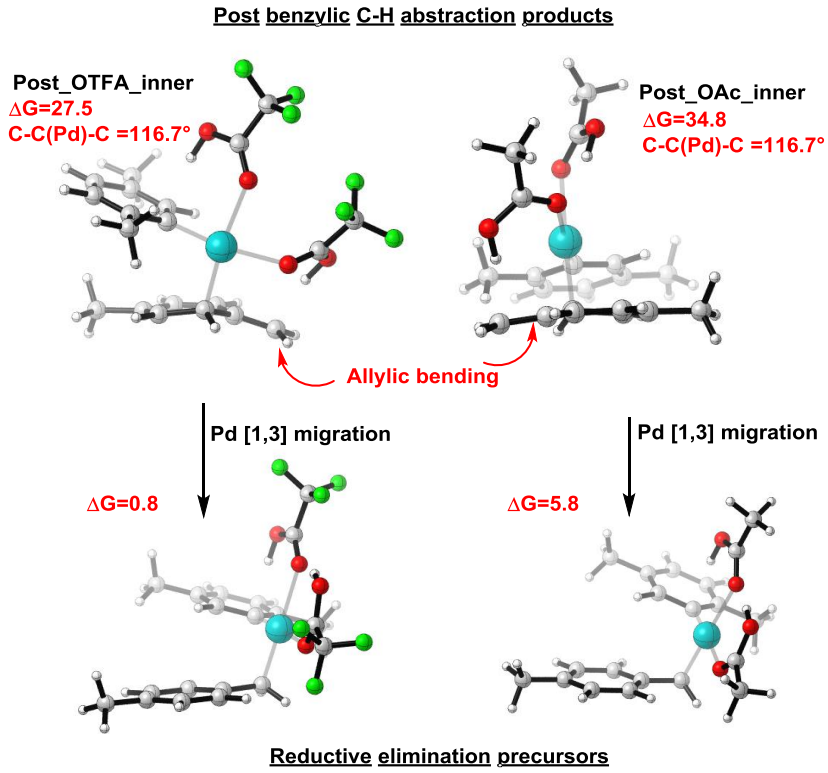

Figure 22. Post abstraction (sp^3 C-H) intermediates and the structure resulting from Pd [1,3] migration to create a new sp^3 C-Pd bond with the arylpalladium(II) species.

The mechanism is completed via and sp^3-sp^2 reductive elimination transition state, which can proceed via a three-centred transition state between C(sp^2)-C(sp^3). Our calculations show that the two rings choose not to adopt π-π stacking coordination upon optimization in the TS geometry. The sp^3 and sp^2 activated aryl ligands reside in the required *cis* conformation leading to C-C bond formation and expulsion of Pd(0) to complete the catalytic cycle and regenerate Pd(0) (**Figure 23**). A four coordinate reductive elimination, 16 electron TS is calculated to give the lowest Gibbs free energy (against separated reactants) for the C-C bond forming process.

Therefore, the reaction was modelled with both acid (TFA and AcOH) ligands attached to the Pd centre. The neutral TFA or AcOH ligands coordinated to the Pd(II) centre adopt conformations which allow a lone pair of electrons on the *cis* carboxylate ligand to form an O—H—O intramolecular hydrogen bond between the TFA and OTFA/ AcOH and OAc (**Figure 23**).

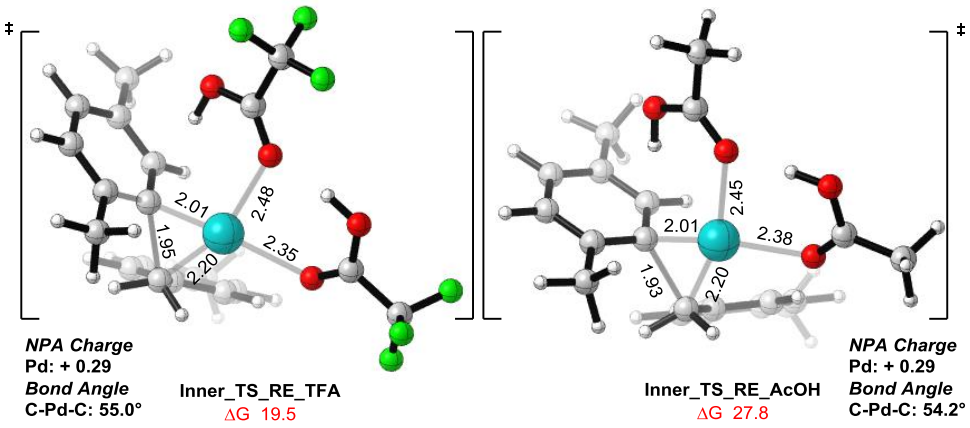

Figure 23. Optimized geometries for the 16 electron reductive elimination TS for sp^3-sp^2 coupling. Key bond distance are shown in Å. All energy values are in kcal/mol

The reductive elimination event for the sp^3-sp^2 diaryl formation is higher in energy in comparison to the analogous 16 electron sp^2-sp^2 reductive elimination event for both $Pd(OAc)_2$ (**sp^2-sp^2** ΔG 24.0 kcal/mol ; **sp^3-sp^2** ΔG 27.8 kcal/mol) and $Pd(OTFA)_2$ (**sp^2-sp^2** ΔG 18.3 kcal/mol; **sp^3-sp^2** ΔG 19.5 kcal/mol). This is not entirely surprising as orbitals with more s character are less directional and lead to better overlap in the reductive elimination transition state, therefore sp^2-sp^2 overlap is expected to be favourable compared to sp^3-sp^2 overlap.

Selectivity: sp^2-sp^2 coupling vs sp^2-sp^3 coupling

Suggestions of the mechanism proceeding through a catalytic cycle whereby sp^2 C-H activation provides the initial aryl-Pd(II) species is unlikely to occur according to our calculations.

Our calculations show that C(sp^3)-H activation is severely hampered by the production of a high energy, unstable post abstraction intermediate, which makes these set of events highly prohabitive in energy. In addition to the large TS energies, the slow step via this mechanistic set of events is predicted to be the reductive elimination transition state. However, the sp^2-sp^2 regioisomer is preferred in both $Pd(OAc)_2$-TFA and $Pd(OTFA)_2$-TFA through the slow, rate determining reductive elimination TS.

The sp^2-sp^2 coupling is favoured via this catalytic cycle irrespective of catalytic species. Therefore, the combination of the high energy second activation and the predicition of only the sp^2-sp^2 regioisomer in the slow reductive elimination step renders this pathway unlikely to be responsible for providing the sp^3-sp^2 regioisomer.

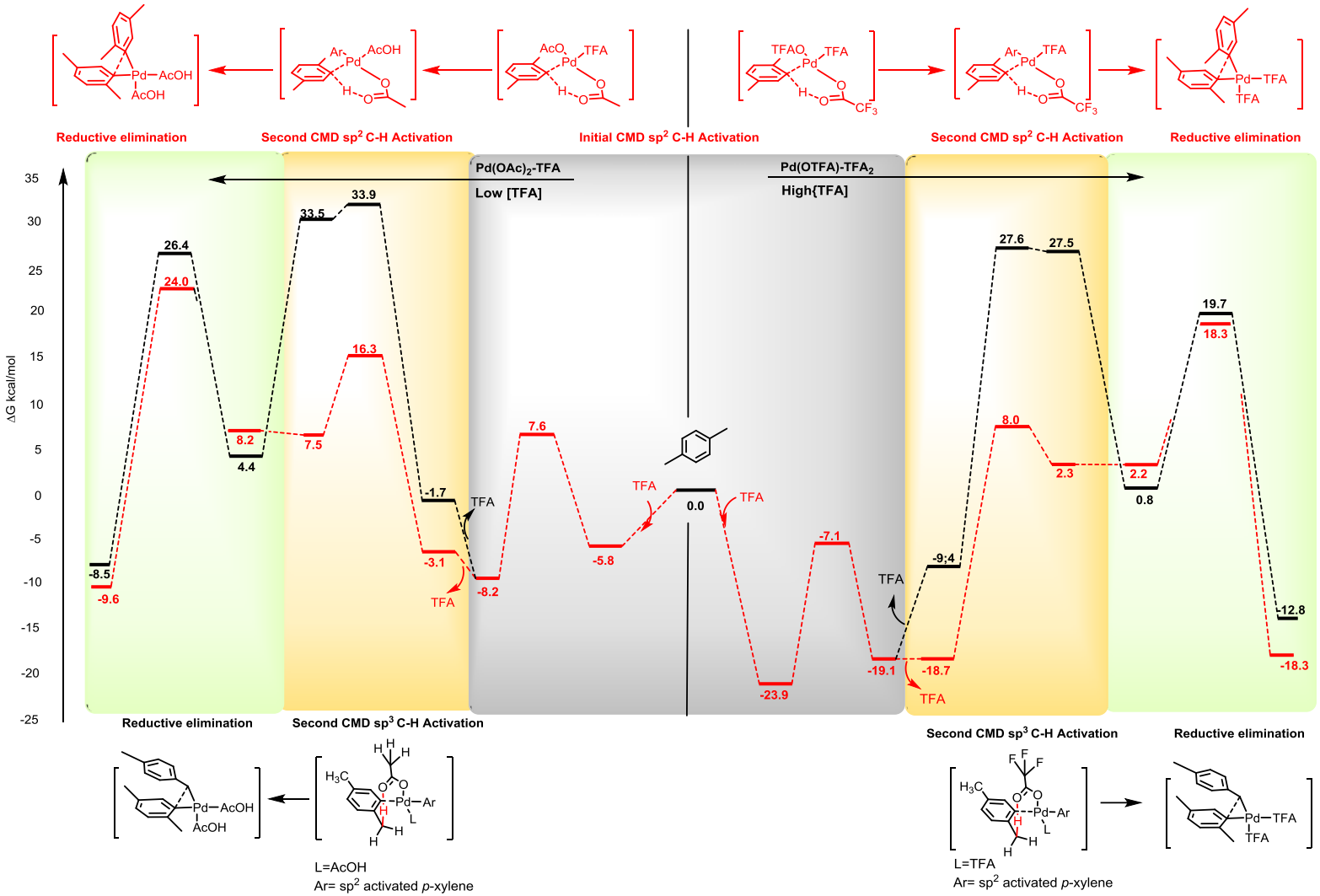

Figure 24. Free energy profile of CMD mechanism for sp^2-sp^2 coupling (red) vs sp^3-sp^2 coupling (black). $Pd(OAc)_2$-TFA (*left*) and $Pd(OTFA)_2$-TFA (*right*) are modelled. All values in kcal/mol.

6.3.5. sp^3–sp^2 C-H coupling: Initial C(sp^3)-H activation

Initial C-H activation at the benzylic position followed by subsequent C(sp^2)-H activation was calculated as an alternative mechanism. Calculations in the previous section did not provide a favourable energy landscape for C(sp^3)-H cleavage occurring after initial C(sp^2)-H cleavage. Therefore, we investigated the potential of two independent catalytic cycles which would lead to both sp^3-sp^2 and sp^2-sp^2 products. Our investigation therefore concentrated on characterising the initial cleavage of the C(sp^3)-H bond with $Pd(OAc)_2$, $Pd(OAc)_2$-TFA, $Pd(OTFA)_2$ and $Pd(OTFA)_2$-TFA (**Figure 25**).

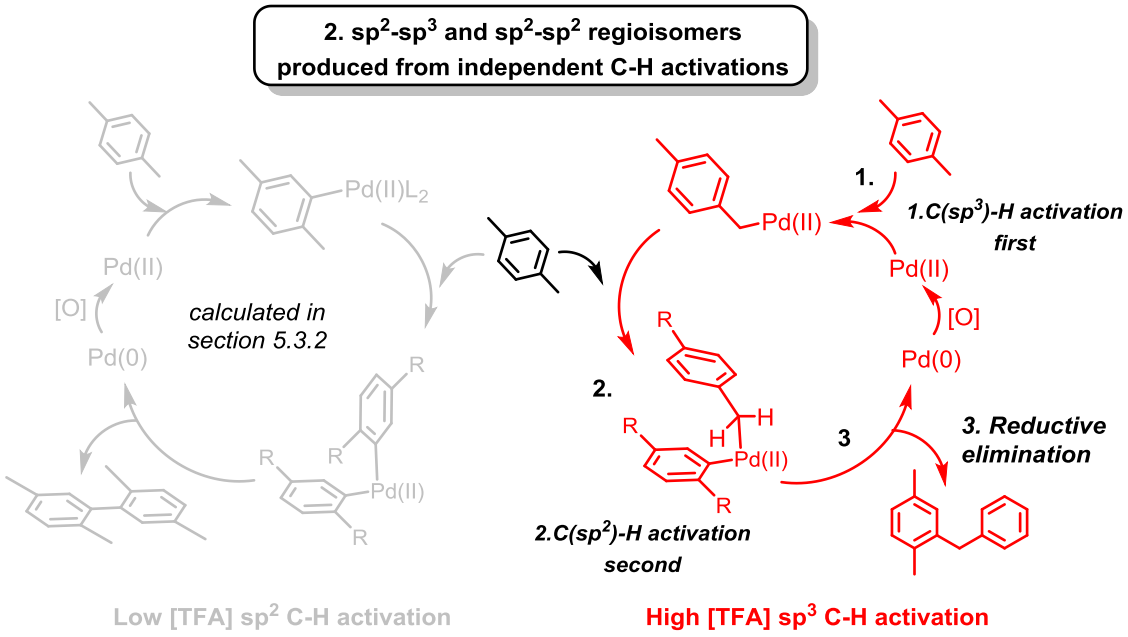

Figure 25. Calculated catalytic cycle in this section, proceeding from initial C(sp^3)-H activation with various Pd(II) catalysts.

A CMD mechanism invoking the M-H-C three centred agostic interaction was not apparent upon TS optimization. The Pd species undertakes η^1 coordination to the *ortho* position on *p*-xylene and no Pd-H-C(sp^3) agostic bond is observed (**Figure 26**). Instead, the C(sp^3)-H bond cleavage favours an eight membered intermolecular deprotonation TS.

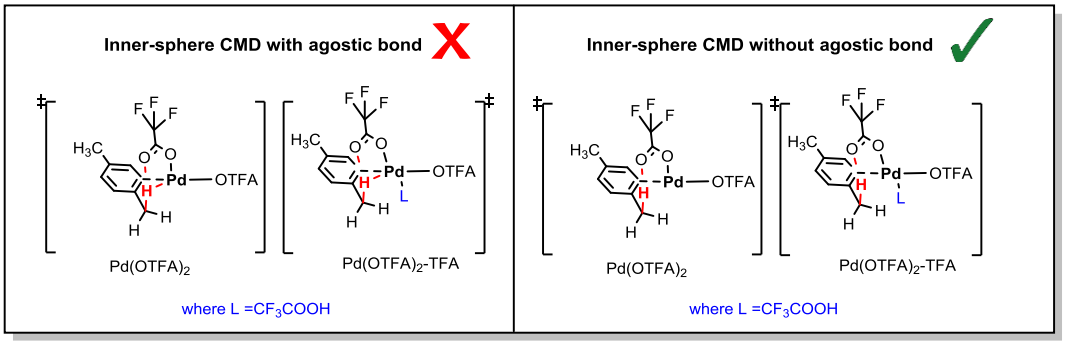

Figure 26. Inner sphere mechanism occurring at sp^3 C-H via an agostic bond. This was not located in the mechanism with optimizations favouring an intermolecular eight-membered CMD mechanism at the benzylic position.

Inner Sphere CMD

The initial C-H activation of the sp^3 C-H bond was calculated with non-solvated Pd(II) catalysts, $Pd(OTFA)_2$ (**Inner _TS_OTFA2**) and $Pd(OAc)_2$ (**Inner_TS_OAc2**) and solvated counterparts where a TFA ligand was coordinated *trans* to the *p*-xylene ring . The C-H bond cleavage at the benzylic position occurs through an eight-membered TS, with Pd(II) coordination changing from η^2 to the π-system (in the precomplex) to η^2 at the *ortho-ipso* position (in the TS) to allow for intramolecular deprotonation via CMD at the C(sp^3)-H bond (**Figure 27**).

The lowest energy TSs for C(sp^3)-H cleavage were calculated to be for the solvated catalysts, where $Pd(OTFA)_2$-TFA (ΔG 12.7 kcal/mol) and $Pd(OAc)_2$-TFA (ΔG 29.7 kcal/mol) were lower in energy than their non-solvated catalytic species. Intermolecular C-H activation with $Pd(OAc)_2$ was calculated to be undesirable, with a large TS energy relative to separated reactants (ΔG 34.9 kcal/mol), however, a lower Gibbs free energy for the TS was predicted with $Pd(OTFA)_2$ (ΔG 21.7 kcal/mol). From this energy landscape our investigation focused on the most likely species in low [TFA], which was calculated to be $Pd(OAc)_2$-TFA (presuming TFA acts merely as a coordinating solvent) and in high [TFA] we favour $Pd(OTFA)_2$-TFA (presuming ligand exchange occurs with large concentration of TFA). Our initial calculations suggest that C(sp^3)-H cleavage is more amenable with $Pd(OTFA)_2$-TFA than other catalytic species.

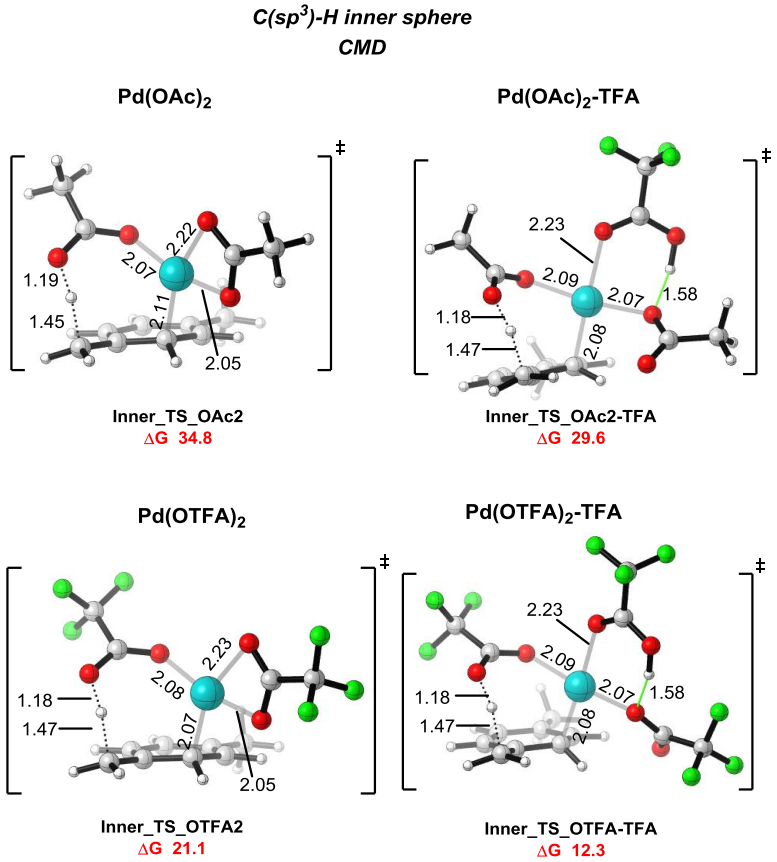

Figure 27. Optimized TS geometry of sp^3 C-H bond cleavage with Pd(II) catalytic species. All values in kcal/mol. All bond lengths in Å.

In the preferred TS for C(sp^3)-H activation (i.e. **Inner_TS_OAc2-TFA** & **Inner TS_OTFA_TFA)** the reaction is calculated to proceed via an eight membered TS with all coordinating ligands monodentate, creating a saturated square planar Pd(II) TS geometry. The addition of the TFA molecule creates an intramolecular hydrogen bond between the carboxylate ligand *cis* to it providing additional stabilization in both cases. Unlike Fagnou *et. al*. and Badouin *et. al.* where intramolecular benzylic C-H bond cleavage was calculated to incorporate a three-centre M-H-C agostic bonding interaction, [27] no such interaction is observed between here as judged by the relatively long distance between Pd-H of 2.92Å (as seen in **Inner_TS_OTFA-TFA, Figure 28**). Therefore we predict an intermolecular deprotonation via an eight membered cyclic structure to be favoured for the initial C(sp^3)-H activation.

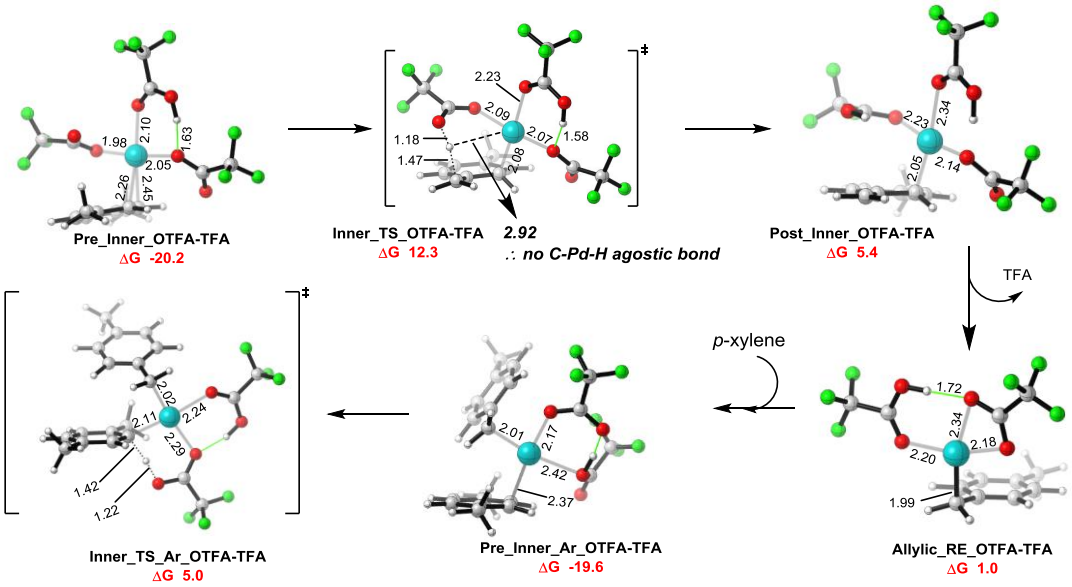

Figure 28 Optimized geometries of the CMD mechanism with initial sp^3 activation with $Pd(OTFA)_2$-TFA followed by C-H bond cleavage at sp^2 C-H bond. All bond lengths in Å. All values in kcal/mol

Cleavage of the benzylic C-H bond induces *exo*-methylene character (CH_2=C) and the loss of aromaticity of *p*-xylene, resulting in a new sp^3 hybridized Pd-C intermediate (**Post_Inner_OTFA-TFA)**. The post abstraction product does not result in a high energy, unstable species as observed with the cleavage with an sp^2 aryl-Pd(II) species (seen in the previous section). Presumably, the overall co-planarity of the substrate contributes to the stability of this intermediate (**Figure 28**).

The aryl-Pd(II) species required for the second activation is produced via a facile [1,3] migration of Pd and dissociation of TFA (**Allylic_RE_OTFA-TFA**). This rearrangement creates the sp^3 C-Pd benzylic species and leads to the reformation of the π system in *p*-xylene. Dissociation of TFA from the Pd centre is essential from **Allylic_RE_OTFA-TFA** to allow for a vacant coordination site on Pd. This facilitates the subsequent coordination of another *p*-xylene unit (**Pre_Inner_Ar_OTFA_TFA**) prior to the sp^2 C-H activation. Subsequent sp^2 C-H cleavage is calculated to occur at the C(sp^2) -H bond via the CMD mechanism (**Inner_Ts_Ar_OTFA-TFA)**, where the sp^3 aryl-Pd(II) species (produced form the initial activation of C(sp^3)-H) coordinates to the π system of *p*-xylene η^2 prior to initiating proton abstraction via a six-membered intramolecular deprotonation TS, simultaneously creating a new C(sp^2)-Pd bond.

It was observed that π-π stacking conformation between the two *p*-xylene rings (in the second activation of the C(sp^2)-H bond) was not present upon TS optimization, with the

sp^3 activated *p*-xylene opting to 'twist' away from a direct 'face to face' stacking interaction (**Figure 29**). It is noted that such interactions and associated benefits are a contentious topic and extend beyond the scope of examination here.[28] However, the preference to 'twist' around the Pd-C(sp^3) bond allows for C-H-π interaction between C-H of the benzylic group and the π-system of the sp^3-activated *p*-xylene, with resultant bond lengths indicative of the weak van der Waal type interaction.[29] This interaction is not evident in the second C-H activation TS in sp^2-sp^2 biaryl and perhaps compensates as an alternative stabilizing interaction in this step.

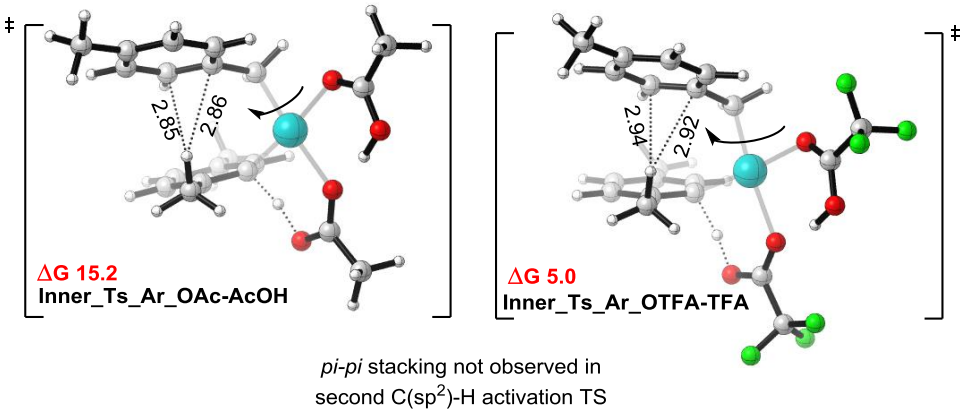

Figure 29. Activation of sp^2 C-H with sp^3aryl-Pd(II) species. C-H-π interactions are shown. The ability of the sp^3-aryl to rotate around its axis is illustrated. All values in kcal/mol. Bond distances in Å

This C-H bond cleavage via an sp^3-arylPd(II) catalyst (**Inner_Ts_Ar_OTFA-TFA**) was calculated for both $Pd(OTFA)_2$-TFA and $Pd(OAc)_2$-TFA pathways. Both corresponding CMD TS were lower in Gibbs free energy than CMD via an sp^2-arylPd(II) catalyst. Upon the completion of the second C-H activation, the Pd(II) diaryl species is produced which is the precursor to the reductive elimination, which proceeds with the same TS as observed in the previous section (**Figure 23**).

Selectivity: sp^2-sp^2 coupling vs sp^3-sp^2 coupling

The sp^2-sp^2 product is favoured with both sets of catalysts. The cleavage of the C(sp^3)-H is calculated as a high energy process for $Pd(OAc)_2$-TFA (C(sp^3)-H ΔG 29.6 kcal/mol; C(sp^2)-H ΔG 7.6 kcal/mol). We presume $Pd(OAc)_2$-TFA would exist in lower concentration of TFA, where the sp^2-sp^2 regioisomer is favoured. The preference for the sp^2-sp^2 regioisomer is shown by our calculations proceeding via the inner sphere CMD mechanism with $Pd(OAc)_2$-TFA (**Figure 30**).

For C(sp^3)-H activation with $Pd(OTFA)_2$-TFA the energy required for proton abstraction is lower (than $Pd(OAc)_2$-TFA) at ΔG 12.7 kcal/mol. In higher concentrations of TFA, the sp^3-sp^2 isomer is produced as the major product, and we expect through catalytic turnover, that the species undertaking activation would be $Pd(OTFA)_2$. However, the selectivity determining step here is the reductive elimination

However, for $Pd(OTFA)_2$-TFA the reductive elimination TS is favoured for the biaryl over the diaryl by only 1.2 kcal/mol (**sp^3** TS ΔG 19.5 kcal/mol; **sp^2** ΔG 18.3 kcal/mol). Therefore, changing the catalytic species assists in decreasing the $\Delta\Delta G^{\ddagger}$ between the sp^2-sp^2 and sp^3-sp^2 reductive elimination TSs.

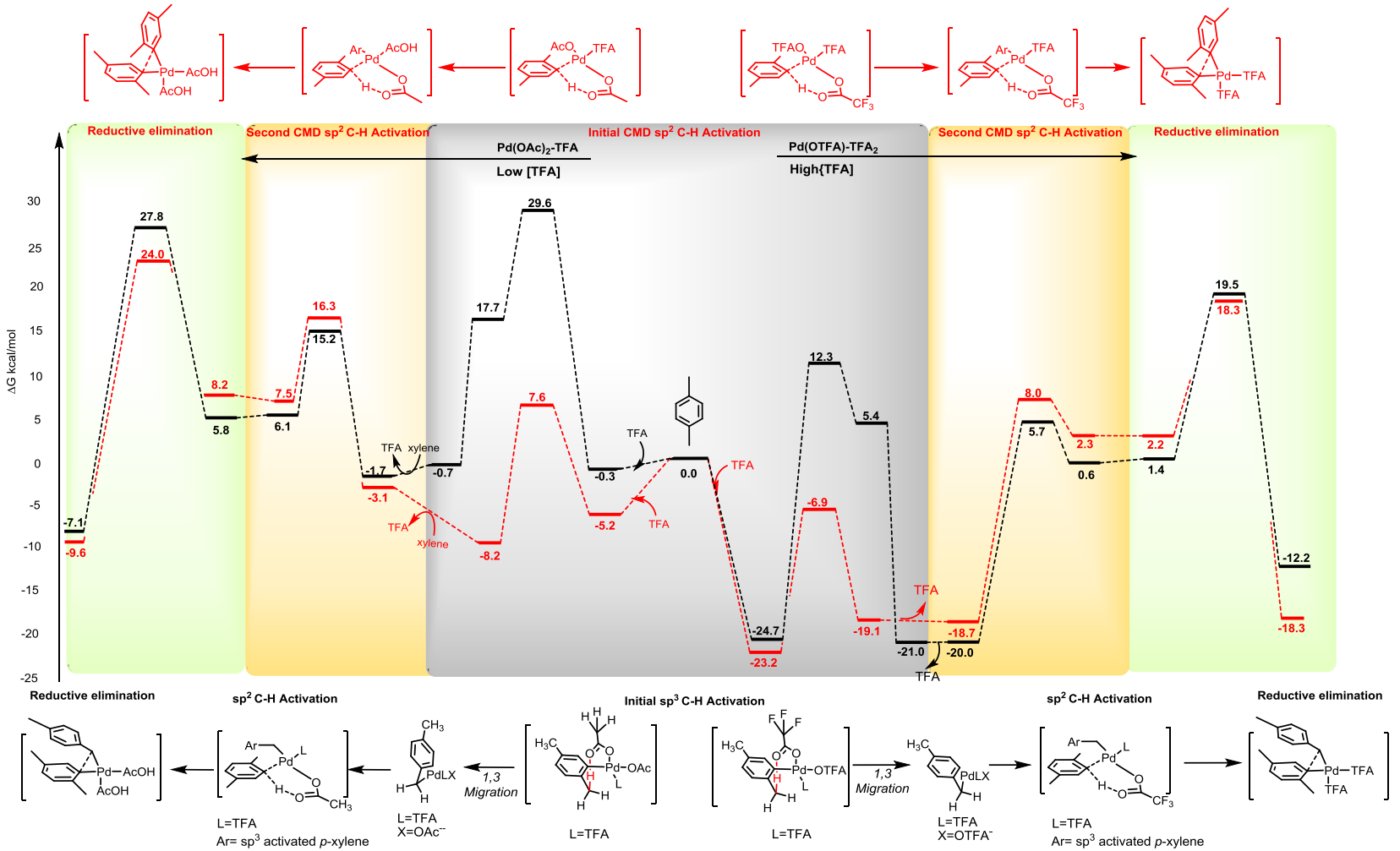

Figure 30. Free energy profile for the double CMD activation of both sp^2-sp^2 homocoupling (*red*) and sp^3-sp^2 coupling (*black*) for both $Pd(OTFA)_2$-TFA (*right*) and $Pd(OAc)_2$-TFA (*left*). All values in kcal/mol

6.3.6. Alternative mechanisms for sp^3-sp^2 coupling

6.3.6.1. Outer sphere CMD: S_E3

The intermolecular outer sphere mechanism was investigated as an alternative method of initial C(sp^3)-H activation. Cleavage of the C-H bond occurring initially at the benzylic C(sp^3)-H was calculated with $OTFA^-$ as the intermolecular base. Both $Pd(OAc)_2$ and $Pd(OTFA)_2$ were modelled in order to observe whether the S_E3 mechanism .

Selectivity was favoured towards C(sp^2)-H activation through this mechanism, however, the initial activation of C(sp^3)-H with $Pd(OTFA)_2$-$OTFA^-$ (at ΔG 2.3 kcal/mol) as compared to the inner sphere CMD (ΔG 12.3 kcal/mol) was lower via this mechanism. Therefore we believe that in high concentrations of TFA this may also exist as a viable mechanistic pathway for the initial activation of the benzylic C(sp^3)-H bond, where $OTFA^-$ could act as an external anion for assisting in intermolecular deprotonation whilst Pd(II) coordinates η^2 *ortho-ipso* to *p*-xylene.

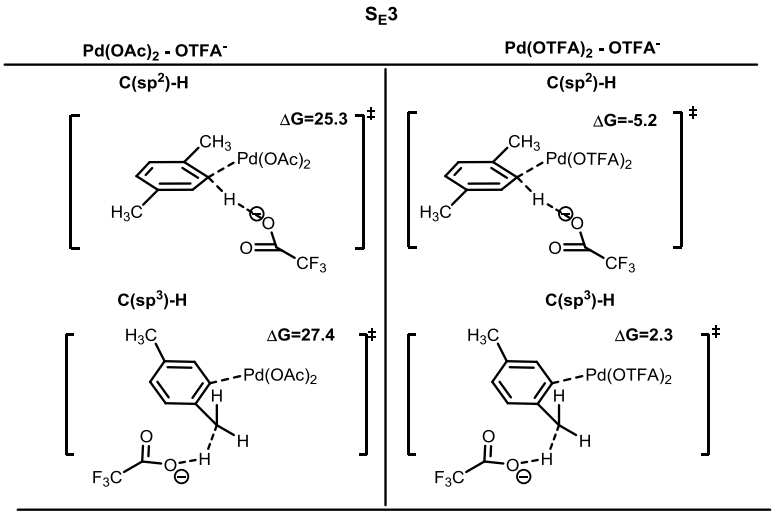

Figure 31. C(sp^2)-H activation favoured via the S_E3 activation over C(sp^3) activation.

6.3.6.2. sp^3-sp^2 Carbopalladation

The carbopalladation mechanism was also investigated for completeness. In order for carbopalladation to occur (leading to eventual diaryl sp^3-sp^2 product), initial activation would have to occur at sp^3 (via a CMD mechanism) followed by *syn*-carbopalladation with the Pd(II) catalytic species and the π-system of *p*-xylene (**Figure 32**).

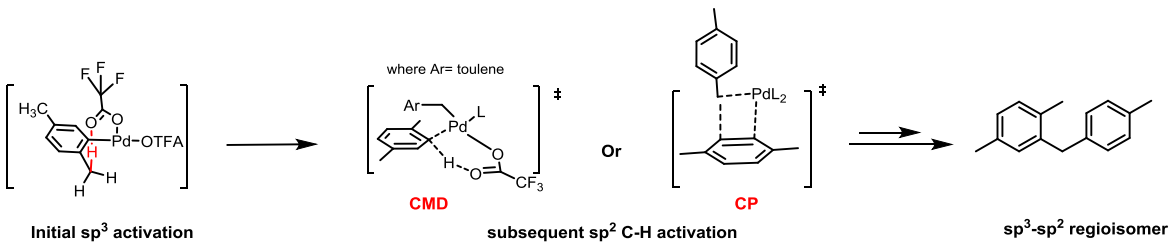

Figure 32. The mechanistic routes towards creation of the diaryl sp^3-sp^2 regioisomer. For carbopalladation to occur, sp^3 activation must occur first.

As such, this mechanistic profile could be seen as direct competition for the second CMD activation of the sp^2 C-H bond cleavage. The TS for both $Pd(OAc)_2$-TFA (**CP_OAc_sp^3)** pathway and $Pd(OTFA)_2$-TFA (**CP_OTFA_sp^3**) pathway were optimized (**Figure 33**),

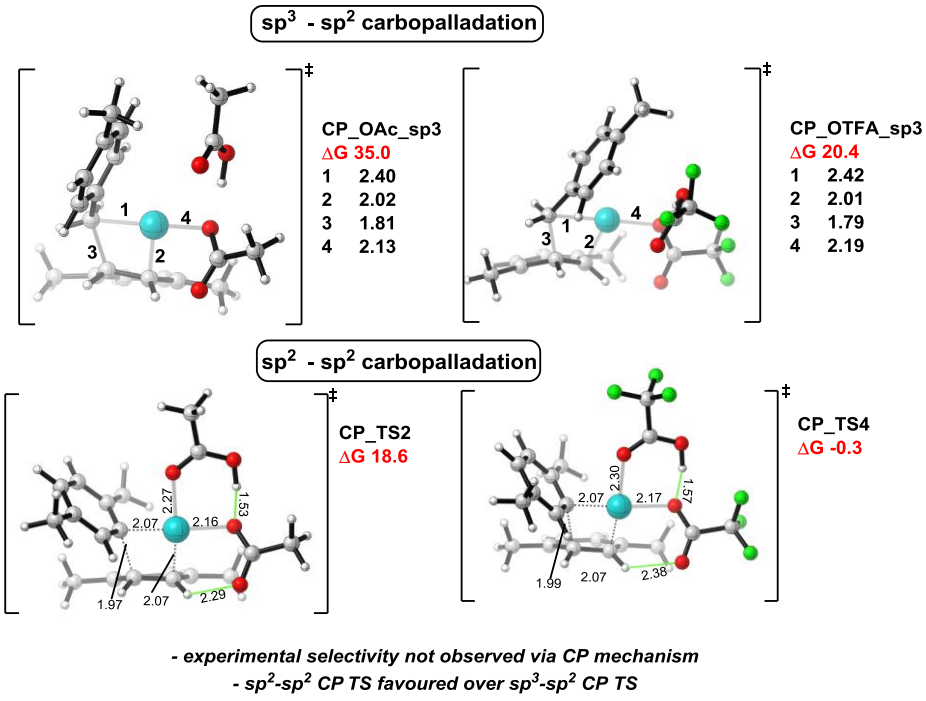

Figure 33 Optimized geometries for the Pd(II) catalyzed carbopalladation of sp^3-sp^2 *p*-xylene. Dissociation of TFA ligands is observed in the sp^3-sp^2 TS. All energy values in kcal/mol. No selectivity for the sp^3-sp^2 species is observed. All bond lengths in Å

However, both activations were higher than the respective sp^2-sp^2 carbopalladation, therefore biasing selectivity to the sp^2-sp^2 product irrespective of catalytic species. Additionally, the CP TS sp^3-sp^2 is higher than the analogous CMD TS for sp^3-sp^2 activation for both the $Pd(OAc)_2$-based pathway (CMD: ΔG 15.2 kcal/mol; CP: ΔG 35.0 kcal/mol) and $Pd(OTFA)_2$ based pathway (CMD: ΔG 5.7 kcal/mol; CP: ΔG 20.4 kcal/mol). Therefore, the CP pathway was discounted as a possible mechanistic route to experimental selectivity.

6.4. Conclusions

DFT computations have been used to characterize the mechanism of Pd-catalyzed C-H activation at the benzylic position of p-xylene. This reaction is atypical, in that an sp^3-hybridized C-H bond undergoes palladation in the presence of several other available sp^2 C-H bonds, for which C-H activation has been much more widely studied. Our analysis of the possible transition structures for this reaction show that concerted metalation-deprotonation is viable at this position, while the Pd is coordinated to the arene ring in a six-membered TS. In contrast to previously studied intramolecular examples, this intermolecular process does not display any appreciable Pd-H interaction in the proton abstraction TS. Mechanistically, we can rule out the sequential activation of C(sp^2)-H followed by C(sp^3)-H since this gives rise to a much greater activation barrier than when this sequence of events is reversed.

The formation of the typical biaryl product, the result of two C(sp^2)-H activations is computed to be favoured for the catalyst system at low concentrations of TFA, the result of a lower barrier towards reductive elimination to form the new C-C bond. This agrees with experiment, although the magnitude of this selectivity is exaggerated computationally. Having characterized the reaction mechanism with four distinct catalyst species, we have also studied the competing pathways for catalyst species relevant to conditions of higher concentrations of TFA. Here, the energetic gap between reductive elimination TSs for the two distinct products is diminished from 3.8 to 0.8 kcal/mol, indicating a greater proportion of the sp^3-sp^2 coupled product will form at higher acid concentrations, as seen experimentally (although the flip in selectivity is not reproduced computationally). As in earlier chapters, these results indicate that the kinetics of Pd-catalyzed C-H activation, while important for the overall rate, are not decisive in determining product selectivity. Where this not the case, it would be

difficult to observe any C(sp^3)-H activation whatsoever since it is much more difficult than the competing C(sp^2)-H activation. However, subsequent step(s) such as reductive elimination are important, and our computations with different catalyst species indicate that the relative energetics of this step can indeed be influenced by the additives/solvent present in the reaction, which will influence selectivity.

Chapter 6 *References*

[1] (a) Handbook of C–H transformations, ed. G. Dyker, Wiley-VCH, Weinheim, *2005* (b) Topics in Current Chemistry, ed. J.Q. Yu.; Z. Shi, Springer, *2010*, vol. 292.

[2] (a) Alberico, D.; Scott, M. E.; Lautens, M. *Chem. Rev*. **2007**, *107*, 174; (b) Jazzar, R.; Hitce, J.; Renaudat, A.; Sofack-Kreutzer, J.; Baudoin, O. *Chem. Eur. J*. **2010**, *16*, 2654; (c) Kuhl, N.; Hopkinson, M. N.; Wencel-Delord, J.; Glorius, F. *Angew. Chem., Int. Ed*. **2012**, *51*, 10236.

[3] (a) Zaitsev, V.G.; Shabashov, D.; Daugulis, O. *J. Am. Chem. Soc.* **2005**, *127*, 13154; (b) Wang, D-H.; Wasa, M.; Yu, J.Q. *J. Am. Chem. Soc.* **2008**, *130*, 7190; (c) Zhang, Q.; Yin, X.-S.; Zhao, S.; Fang, S-L.; Shi, B-F. *Chem. Commun*. **2014**, *50*, 8353; (d) He, J.; Li, S.; Deng, Y.; Fu, H.; Laforteza, B. N.; Spangler, J. E.; Homs, A.; Yu, J.Q. *Science* **2014**, *343*, 1216; (e) Curto, J. M.; Kowlowski, M.N. *J. Am. Chem. Soc.* **2015**, *137*, 18.

[4] (a) Johansson, L.; Ryan, B. O.; Romming, C.; Tilset, M. *J. Am. Chem. Soc*. **2001**, *123*, 6579; (b) Heyduk, A. F.; Driver, T. G.; Labinger, J. A.; Bercaw, J. E. *J. Am. Chem. Soc.* **2004**, *126*, 15034; (c) Driver, T. G.; Day, M. W.; Labinger, J. A.; Bercaw, J. E. *Organometallics* **2005**, *24*, 3644; (d) Driver, T. G.; Williams, T. J.; Labinger, J. A.; Bercaw, J. E. *Organometallics* **2007**, *26*, 294.

[5] Blanksby, S. J.; Ellison, G. B. *Acc. Chem. Res.* **2003**, *36*, 255.

[6] (a) Lapointe, D.; Fagnou, K. *Chem. Lett.* **2010,** *39*, 1118; (b) Balcells, D.; Clot, E.; Eisenstein, O. *Chem. Rev.* **2010**, *110*, 749; (c) Ackermann, L. *Chem. Rev*. **2011**, *111*, 1315; (d) Ackermann, L. Acc. *Chem. Res.* **2014**, *47*, 281; (e) Musaev, D. G.; Figg, T. M.; Kaledin, A. L. *Chem. Soc. Rev.* **2014,** *43*, 5009; (f) Davies, D. L.; Donald, S. M. A.; Macgregor, S. A. *J. Am. Chem. Soc.* **2005**, *127*, 13754; (g) Lafrance, M.; Fagnou, K. *J. Am. Chem. Soc.* **2006**, *128*, 16496; (h) García-Cuadrado, D.; Braga, A. A. C.; Maseras, F.; Echavarren, A. M. *J. Am. Chem. Soc.* **2006**, *128*, 1066; (i) García-Cuadrado, D.; de Mendoza, P.; Braga, A. A. C.; Maseras, F.; Echavarren, A. M. *J. Am. Chem. Soc.* **2007**, *129*, 6880; (j) Lafrance, M.; Gorelsky, S. I.; Fagnou, K. *J. Am. Chem. Soc.* **2007**, *129*, 14570; (k) Gorelsky, S. I.; Lapointe, D.; Fagnou, K. *J. Am. Chem. Soc.* **2008**, *130*, 10848; (l) Tang, S.-Y.; Guo, Q.-X.; Fu, Y. *Chem. Eur. J.* **2011**, *17*, 13866. (m) Zhang, S.; Shi, L.; Ding, Y. *J. Am. Chem. Soc.* **2011**, *133*, 20218; (n) Musaev, D. G.; Kaledin, A.; Shi, B.-F.; Yu, J. Q. *J. Am. Chem. Soc.* **2012**, *134*, 1690; (p) Giri, R.; Lan, Y.; Liu, P.; Houk, K. N.; Yu, J. Q. *J. Am. Chem. Soc.* **2012**, *134*, 14118; (q) Sanhueza, I. A.; Wagner, A. M.; Sanford, M. S.; Schoenebeck, F. *Chem. Sci*. **2013**, *4*, 2767; (r) Yang, Y.-F.; Cheng, G-J.; Liu, P.; Leow, D.; Sun, T.-Y.; Chen, P.; Zhang, X.; Yu, J. Q.; Wu, Y-D.; Houk, K. N. *J. Am. Chem. Soc.* **2014**, *136*, 344; (s) Anand, M.; Sunoj, R. B.; Schaefer, H. F., III. *J. Am. Chem. Soc.* **2014,** *136*, 55359; (t) Cheng, G.-J.; Yang, Y.-F.; Liu, P.; Chen, P.; Sun, T.-Y.; Li, G.; Zhang, X.; Houk, K. N.; Yu, J. Q.; Wu, Y.-D. *J. Am. Chem. Soc*. **2014**, *136*, 894.

[7] Rong, Y.; Li, R.; Lu, W. *Organometallics*, **2007**, *26*, 4376.

[8] Nedd, S.; Alexandrova, A. N. *Phys. Chem. Chem. Phys.* **2015**, *17*, 1347.

[9] Hull, K. L.; Lanni, E. L.; Sanford, M. S. *J. Am. Chem. Soc*. **2006**, *128*, 14047.

[10] Rousseaux, S.; Davi, M.; Sofack-Kreutzer, J.; Pierre, C.; Kefalidis, C. E.; Clot, E.; Fagnou, K.; Baudoin, O. *J. Am. Chem. Soc.* **2010**, *132*, 10706.

[11] Giri, R.; Lan, Y.; Lui P.; Houk, K.N.; Yu J. Q. *J. Am. Chem. Soc.* **2012,** *134*, 14118.

[12] Chaumontet, M.; Piccardi, R.; Audic, N.; Hitce, J.; Peglion, J.-L.; Clot, E.; Baudoin, O. *J. Am. Chem. Soc.* **2008**, *130*, 15157.

[13] Haines, B. E.; Musaev, D. G. *ACS Catal.* **2015**, *5*, 830.

[14] Larionov, E.; Masafumi, N.; Katayev, D.; Besnard, C.; Kundig, E. P. *Chem. Sci.* **2013**, *4*, 1195.

[15] Haller, L. J. L.; Page, M. J.; Macgregor, S. A.; Mahon, M. F.; Whittlesey, M. K. *J. Am. Chem. Soc.* **2009**, *131*, 4604.

[16] Y. Dang, S.; Qu, J. W.; Nelson, H. D.; Pham, Z.-X.; Wang, X. *J. Am. Chem. Soc.* **2015**, *137*, 2006.

[17] Baudoin, O. *Chem. Soc. Rev.* **2011**, *40*, 4902.

[18] (a) Kitahama, K.; Frech, R. *J. Chem. Phys.* **1985**, *82*, 720; (b) Wadt, W.R.; Hay, P. J. *J. Chem. Phys.* **1985**, *82*, 284.

[19] Feller, D. *J. Comp. Chem.* **1996**, *13*, 1571.

[20] Roy, E. L.; Hay, J.; Martin, R. L.; *J. Chem. Theory. Comput.* **2008**, *4*, 1029.

[21] (a) Barone, C.; Cossi, M. *J. Phys. Chem. A.* **1998**, *102*, 1995; (b) Barone, C.; Rega, N.; Schimani, G.; Cossi, M. *J. Comput. Chem.* **2003**, *24*, 669.

[22] (a) Ribeiro, R. F.; Marenich, A. V.; Cramer, C. J.; Truhlar D. G. *J. Phys. Chem. B*, **2011**, *115*, 14556; (b) Grimme, S. *Chem. Eur. J.* **2012**, *18*, 9955.

[23] Curtiss, L. A.; Raghavachari, K.; Redfern, P. C.; Rassolov, V.; Pople, J. A. *J. Chem. Phys*. **1998**, *109*, 7764; (b) Baboul, A. G.; Curtiss, L. A.; Redfern, P. C.; Raghavachari, K. *J. Chem. Phys.* **1999**, *110*, 7650.

[24] NBO 6.0. E. D. Glendening, J. K. Badenhoop, A. E. Reed, J. E. Carpenter, J. A. Bohmann, C. M. Morales, C. R. Landis, and F. Weinhold, Theoretical Chemistry Institute, University of Wisconsin, Madison (2013).

[25] Reed, A. E.; Weinhold, F. *J. Chem. Phys.* **1983,** *78*, 4066; (b) Reed, A. E.; Weinstock, R. B.; Weinhold, F. *J. Chem. Phys*. **1985,** *83*, 735.

[26] Cannon. J.S.; Zou. L.; Liu, P.; Lan, Y.; O'Leary, D.J.; Houk, K.N.; Grubbs, R.H. *J. Am. Chem. Soc.* **2014,** *136*, 6733.

[27] Brookhart, M.; Green, M.L.H.; Parkin, G. *Proc. Natl. Acad. Sci.* **2007**, *104*, 6908.

[28] Martinez, C. R.; Iverson, B. L. *Chem. Sci.* **2012**, *3*, 2191; (b) Grimme, S. *Angew. Chem. Int. Ed*. **2008**, *47*, 3430.

[29] Tsuzuki S. *Annu. Rep. Prog. Chem., Sect. C: Phys. Chem***. 2012**, *108*, 69.

Appendix

Basis Sets:

6-31G: Pople split valence basis set: six primitive Gaussians for the contracted core functions, with a double-zeta valence basis of three contracted primitives and a further primitive.

6-311G: Pople triple-zeta valence basis set.

6-31+G: Indicates augmentation of the basis set with an additional s and one set of p functions with small exponents on heavy atoms to describe spatially diffuse MOs.

6-31++G: As above with additional diffuse s functions on hydrogens.

6-31++G: As above with additional diffuse s functions on hydrogens.

LANL2DZ: the LANL2DZ basis set which for fourth row elements uses a nonrelativistic [Ar] 18-electron core and for fifth row elements uses a relativistic [Kr] 36-electron core with double-zeta split valence functions.

LANL2TZ(f): As above with triple-zeta split valence functions and an additional f polarization

List of structures

Chapter 2

Optimizations at ωB97XD on *Gaussian* 09. Imaginary frequencies shown for all TS structures.

Structure	Reference	Energy (Hartree)	Gibbs (Hartree)	Imaginary Frequency (cm^{-1})
N-methyl indole		-402.98718	-402.85339	
$Pd(OAc)_2$		-583.56678	-583.49194	
AcOH		-229.00694	-228.96392	
$PhB(OH)_2$		-408.12029	-408.01955	
Benzene		-232.16100	-232.08026	
Transmetalation first followed by CMD				
Four-membered transmetalation precomplex of $Pd(OAc)_2$ and $PhB(OH)_2$	**CB1**	-991.70053	-991.50770	
Four-membered transmetalation TS of $Pd(OAc)_2$ and $PhB(OH)_2$	**CB2**	-991.67864	-991.48689	-149.54
Four-membered transmetalation product of $Pd(OAc)_2$ and $PhB(OH)_2$		-991.71924	-991.52745	
Six-membered transmetalation precomplex of $Pd(OAc)_2$ and $PhB(OH)_2$	**CC1**	-991.70054	-991.50734	
Six-membered transmetalation TS of $Pd(OAc)_2$ and $PhB(OH)_2$	**CC2**	-991.69193	-991.49957	-160.13
Six-membered transmetalation product of $Pd(OAc)_2$ and $PhB(OH)_2$		-991.73428	-991.54136	
Catalytic species formed from Indole following six-membered transmetalation of $Pd(OAc)_2$ and $PhB(OH)_2$	**CD1**	-586.68296	-586.57151	
Precomplex of N-methyl indole and PdPhOAc	**CD2**	-989.72871	-989.46419	
C3 CMD TS of N-methyl indole and PdPhOAc	**F1**	-989.68019	-989.42124	-1178.05
C2 CMD TS of N-methyl indole and PdPhOAc	**D1**	-989.67541	-989.41634	-1193.98
Product of C3 CMD TS of N-methyl indole and PdPhOAc		-989.69620	-989.43280	
Product of C2 CMD TS of N-methyl indole and PdPhOAc		-989.70172	-989.43724	
Precursor to Reductive elimination of Ph and N-methyl indole at C2		-989.70172	-989.43724	
Reductive elimination TS of Ph and N-methyl indole at C2	**D2**	-989.68877	-989.42508	-277.96
C2 arylated product from reductive elimination TS		-989.74103	-989.47523	
Precursor to Reductive elimination of Ph and N-methyl indole at C3		-989.69619	-989.43356	
Reductive elimination TS of Ph and N-methyl indole at C3	**F2**	-989.68567	-989.42189	-292.91

Structure	Reference	Energy (Hartree)	Gibbs (Hartree)	Imaginary Frequency (cm^{-1})
C3 arylated product from reductive elimination TS		-989.74070	-989.47578	
Solvent-assisted (AcOH) six-membered transmetalation precomplex between $Pd(OAc)_2$ and $PhB(OH)_2$	**T1**	-1220.74429	-1220.49266	
Solvent-assisted (AcOH) six-membered transmetalation TS between $Pd(OAc)_2$ and $PhB(OH)_2$	**T2**	-1220.72370	-1220.47061	-112.74
Solvent-assisted (AcOH) six-membered transmetalation product $Pd(OAc)_2$ and $PhB(OH)_2$	**T3**	-1220.76946	-1220.51732	
Catalytic species PhPdOAc-AcOH	**DA1**	-815.74297	-815.57149	
Precomplex of N-methyl indole and PdPhOAc-AcOH	**CE2**	-1218.77086	-1218.44688	
C3 CMD TS of N-methyl indole and PdPhOAc-AcOH	**FB1**	-1218.73299	-1218.41558	-1137.70
Product of C3 CMD TS of N-methyl indole and PdPhOAc-AcOH		-1218.74087	-1218.41871	
C2 CMD TS of N-methyl indole and PdPhOAc-AcOH	**DB1**	-1218.72908	-1218.41107	-1208.95
Product of C2 CMD TS of N-methyl indole and PdPhOAc-AcOH		-1218.74559	-1218.42317	
Precursor to Reductive elimination of Ph and N-methyl indole at C3 (solvent assisted)		-1218.74087	-1218.41871	
Reductive elimination TS of Ph and N-methyl indole at C3 (solvent assisted)	**FB2**	-1218.72044	-1218.39940	-307.54
C3 arylated product from reductive elimination TS (solvent-assisted)		-1218.78010	-1218.45636	
Precursor to Reductive elimination of Ph and N-methyl indole at C2 (solvent assisted)		-1218.74849	-1218.42542	
Reductive elimination TS of Ph and N-methyl indole at C2 (solvent assisted)	**DB2**	-1218.72560	-1218.40394	-302.58
C2 arylated product from reductive elimination TS (solvent-assisted)		-1218.77824	-1218.45337	
CMD followed by transmetalation				
Precomplex of CMD TS between N-methyl indole and $Pd(OAc)_2$	**A1**	-986.58531	-986.35923	
CMD TS of N-methyl indole at C2 with $Pd(OAc)_2$	**A2**	-986.55162	-986.33010	-1169.50
Product of CMD TS of $Pd(OAc)_2$ and N-methyl indole at C2	$\mathbf{A2_{prod}}$	-986.57225	-986.34658	
CMD TS of N-methyl indole at C3 with $Pd(OAc)_2$	**AA3**	-986.55466	-986.33233	-1128.42
Product of CMD TS of $Pd(OAc)_2$ and N-methyl indole at C3	$\mathbf{AA_{prod}}$	-986.56911	-986.34387	
Precomplex of CMD TS between N-methyl indole and $Pd(OAc)_2$-AcOH	**A1-AcOH**	-1215.63037	-1215.34435	
CMD TS of N-methyl indole at C2 with $Pd(OAc)_2$-AcOH	**A2-AcOH**	-1215.59775	-1215.31733	-1130.95
Product of CMD TS of $Pd(OAc)_2$-$AcOH_2$ and N-methyl indole at C2	$\mathbf{A2\text{-}AcOH_{prod}}$	-1215.61707	-1215.33230	

Structure	Reference	Energy (Hartree)	Gibbs (Hartree)	Imaginary Frequency (cm^{-1})
CMD TS of N-methyl indole at C3 with $Pd(OAc)_2$-AcOH	**A3-AcOH**	-1215.60137	-1215.32066	-1128.37
Product of CMD TS $Pd(OAc)_2$-AcOH and N-methyl indole at C3	**A3-$AcOH_{prod}$**	-1215.61217	-1215.32838	
Four membered transmetalation at C2 palladated indole: precomplex		-1165.67804	-1165.38999	
Four membered transmetalation at C2 palladated indole: TS	**FM-TS2**	-1165.63656	-1165.35165	-195.91
Four membered transmetalation at C2 palladated indole: product		-1165.68868	-1165.40329	
Four membered transmetalation at C3 palladated indole: precomplex		-1165.68040	-1165.39416	
Four membered transmetalation at C3 palladated indole: TS	**FM-TS3**	-1165.63565	-1165.35015	-221.58
Four membered transmetalation at C3 palladated indole: product		-1165.68361	-1165.39803	
Six membered transmetalation at C2 palladated indole: precomplex		-1165.65944	-1165.37396	
Six membered transmetalation at C2 palladated indole: product		-1165.69248	-1165.40661	
Six membered transmetalation at C3: palladated indole: precomplex		-1165.65815	-1165.37160	
Six membered transmetalation at C3 palladated indole: TS	**SM-TS3**	-1165.64615	-1165.36132	-300.98
Six membered transmetalation at C3 palladated indole: product		-1165.68553	-1165.39932	
Solvent assisted (AcOH) six membered transmetalation at C3: palladated indole: H-Bond precomplex		-1394.70948	-1394.3652	
Solvent assisted (AcOH) six membered transmetalation at C3: palladated indole: H-Bond TS	**SM-TS3-Hbond**	-1394.69315	-1394.34979	-270.10
Solvent assisted (AcOH) six membered transmetalation at C3: palladated indole: H-Bond product		-1394.72630	-1394.38222	
Solvent assisted (AcOH) six membered transmetalation at C2: palladated indole: H-Bond precomplex		-1394.71299	-1394.36838	
Solvent assisted (AcOH) six membered transmetalation at C2: palladated indole: H-Bond TS	**SM-TS2-Hbond**	-1394.69902	-1394.35397	-246.63
Solvent assisted (AcOH) six membered transmetalation at C2: palladated indole: H-Bond product		-1394.73660	-1394.39139	
Solvent assisted (AcOH) six membered transmetalation at C3: palladated indole: polar-π bond precomplex		-1394.70669	-1394.36172	
Solvent assisted (AcOH) six membered transmetalation at C3: palladated indole: polar-π bond TS	**SM-TS3-Polar**	-1394.69400	-1394.35103	-264.00
Solvent assisted (AcOH) six membered transmetalation at C3: palladated indole: polar-π bond product		-1394.73339	-1394.39075	
Solvent assisted (AcOH) six membered transmetalation at C2: palladated indole: polar-π bond precomplex		-1394.71221	-1394.36608	

Structure	Reference	Energy (Hartree	Gibbs (Hartree)	Imaginary Frequency (cm^{-1})
Solvent assisted (AcOH) six membered transmetalation at C2: palladated indole: polar-π bond TS	**SM-TS2-Polar**	-1394.70232	-1394.35853	-258.40
Solvent assisted (AcOH) six membered transmetalation at C2: palladated indole: polar-π bond product		-1394.74192	-1394.39749	
Reductive elimination: "Non"ligated precomplex at C2		-760.64913	-760.44448	
Reductive elimination: "Non"ligated TS at C2		-760.63917	-760.43348	-267.37
Reductive elimination: Product from "Non" RE TS – C2 arylated N-methyl indole		-760.69664	-760.48943	
Reductive elimination: "Non"ligated precomplex at C3		-760.64703	-760.44233	
Reductive elimination: "Non"ligated TS at C3		-760.63841	-760.43336	-270.16
Reductive elimination: Product from "Non" RE TS – C3 arylated N-methyl indole		-760.69666	-760.48961	
Reductive elimination: "Mono"ligated precomplex at C2		-989.70172	-989.43724	
Reductive elimination: "Mono"ligated TS at C2		-989.68877	-989.42508	-277.96
Reductive elimination: Product from "Mono" RE TS – C2 arylated N-methyl indole		-989.74103	-989.47523	
Reductive elimination: "Mono"ligated precomplex at C3		-989.69619	-989.43356	
Reductive elimination: "Mono"ligated TS at C3		-989.68567	-989.42189	-292.91
Reductive elimination: Product from "Mono" RE TS – C3 arylated N-methyl indole		-989.74070	-989.47578	
Reductive elimination: "Bis"ligated precomplex at C2		-1218.74849	-1218.42542	
Reductive elimination: "Bis"ligated TS at C2	**RE2-Bis**	-1218.72560	-1218.40394	-302.58
Reductive elimination: Product from "Bis" RE TS – C2 arylated N-methyl indole		-1218.77824	-1218.45337	
Reductive elimination: "Bis"ligated precomplex at C3		-1218.74087	-1218.41871	
Reductive elimination: "Bis"ligated TS at C3	**RE3-Bis**	-1218.72044	-1218.39940	-307.54
Reductive elimination: Product from "Bis" RE TS – C3 arylated N-methyl indole		-1218.78010	-1218.45636	
$B(OH)_2OAc$ resulting from dissociation after transmetalation		-405.128019	-404.93531	

List of structures

Chapter 3

Bond Dissociation Energy calculations of N-methyl indole using G3B3

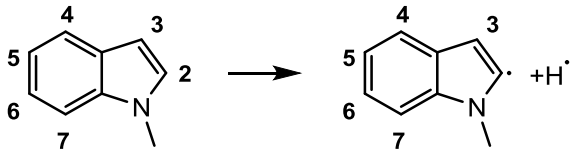

Structure	G3B3 Enthalpy (Hartree)
Indole	-402.810615
H Radical	-0.498726
Indole C2 radical	-402.120535
Indole C3 radical	-402.118633
Indole C4 radical	-402.12971
Indole C5 radical	-402.129201
Indole C6 radical	-402.129672
Indole C7 radical	-402.128964

Model studies: benzene as a prototypical arene

Optimizations conducted at ωB97XD on *Gaussian* 09. Imaginary frequencies shown for all TS structures. CEPA and SCS-MP2 single points conducted on Orca.

Structure	Reference	Energy (Hartree)	Gibbs (Hartree)	Imaginary Frequency (cm^{-1})
Benzene		-232.16101	-232.08659	
PdPhOAc		-586.68296	-586.57986	
PdPhOAc-DMF		-832.01730	-834.96107	
Precomplex of Benzene and PdPhOAc		-818.85412	-818.65501	
CMD TS: Benzene C-H activation with PdPhOAc	**TS_1**	-818.83140	-818.63650	-1163.30
Product from Benzene C-H activation with PdPhOAc		-818.86421	-818.66781	
Precomplex to reductive elimination TS of Benzene and PdPhOAc		-818.86421	-818.66783	-291.32
Reductive elimination TS of Benzene and PdPhOAc	**TS_2**	-818.85517	-818.65687	
Product from Reductive elimination of Benzene and PdPhOAc		-818.91024	-818.71080	
Precomplex of Benzene and PdPhOAc-DMF		-1067.32922	-1067.03442	

CMD TS: Benzene C-H activation with PdPhOAc-DMF	-1067.30084	-1067.00987	-1163.30
Product from Benzene C-H activation with PdPhOAc-DMF	-1067.32327	-1067.03069	
Precomplex to reductive elimination TS of Benzene and PhPdOAc-DMF	-1067.32327	-1067.03071	
Reductive elimination TS of Benzene and PdPhOAc-DMF	-1067.30395	-1067.01040	-291.32
Product from Reductive elimination of Benzene and PdPhOAc-DMF	-1067.35709	-1067.06387	

Benzene Single Point Energy (Hartree)	PdPhOAc Single Point Energy (Hartree)	PdPhOAc-DMF Single Point Energy (Hartree)	Method
-232.19608	-586.67395	-835.18893	M062X
-231.56283	-584.91336	-832.824189	SCS-MP2
-232.31363	-587.00896	-835.64765	B3LYP DFTD3
-231.62539	-585.02154	N/A	CEPA

Structure	Reference	Single Point Energy (Hartree)	Method
CMD TS: Benzene C-H activation with PdPhOAc	**TS_1**	-818.85254	M062X
Reductive elimination TS of Benzene and PdPhOAc	**TS_2**	-818.87971	M062X
CMD TS: Benzene C-H activation with PdPhOAc-DMF		-1067.36140	M062X
Reductive elimination TS of Benzene and PdPhOAc-DMF		-1067.36869	M062X
CMD TS: Benzene C-H activation with PdPhOAc	**TS_1**	-816.46682	SCS-MP2
Reductive elimination TS of Benzene and PdPhOAc	**TS_2**	-816.50016	SCS-MP2
CMD TS: Benzene C-H activation with PdPhOAc-DMF		-1064.37298	SCS-MP2
Reductive elimination TS of Benzene and PdPhOAc-DMF		-1064.38612	SCS-MP2
CMD TS: Benzene C-H activation with PdPhOAc	**TS_1**	-819.31356	B3LYP+DFTD3
Reductive elimination TS of Benzene and PdPhOAc	**TS_2**	-819.32993	B3LYP+DFTD3
CMD TS: Benzene C-H activation with PdPhOAc-DMF		-1067.9439	B3LYP+DFTD3
Reductive elimination TS of Benzene and PdPhOAc-DMF		-1067.9403	B3LYP+DFTD3
CMD TS: Benzene C-H activation with PdPhOAc	**TS_1**	-816.63053	CEPA
Reductive elimination TS of Benzene and PdPhOAc	**TS_2**	-816.64924	CEPA

Structure	Reference	Energy (Hartree)	Gibbs (Hartree)	Imaginary Frequency (cm^{-1})
$Pd(OAc)_2$		-583.56679	-583.49195	
$Pd_2(OAc)_4$		-1167.20135	-1167.03072	
$PdAg(OAc)_3$		-957.80873	-957.68979	
$PdCu(OAc)_4$		-1236.62898	-1236.45991	
DMF		-248.42829	-248.34731	
AcOH		-229.00695	-228.96392	
N-methyl indole		-402.98718	-402.85340	
N-Piv indole		-634.19873	-633.97573	
Acetate anion (OAc^-)		-228.42157	-228.39229	
CMD C-H activation of benzene followed by N-methyl indole				
Benzene and $Pd(OAc)_2$:Precomplex	**BL_1**	-815.73678	-815.56562	
Benzene and $Pd(OAc)_2$: CMD C-H activation TS	**BL_TS**	-815.70995	-815.54290	-1091.83
Benzene and $Pd(OAc)_2$:Product	**BL_2**	-815.73843	-815.56706	
Benzene and $Pd(OAc)_2$-DMF: Precomplex	**BP_1**	-1064.1938	-1063.9241	
Benzene and $Pd(OAc)_2$-DMF: TS	**BP_TS**	-1064.163	-1063.8978	-1056.84
Benzene and $Pd(OAc)_2$-DMF: Product	**BP_2**	-1064.1909	-1063.9213	
Benzene and $Pd(OAc)_2$-AcOH: Precomplex	**BNP_1**	-1044.77284	-1044.5434	
Benzene and $Pd(OAc)_2$-AcOH: TS	**BNP_TS**	-1044.746571	-1044.521	-1028.25
Benzene and $Pd(OAc)_2$-AcOH: Product	**BNP_2**	-1044.775858	-1044.5463	
Benzene and $Pd_2(OAc)_4$:Precomplex		-1399.3672	-1399.1004	
Benzene and $Pd_2(OAc)_4$: CMD C-H activation TS		-1399.341	-1399.0788	-1123.88
Benzene and $Pd_2(OAc)_4$:Product		-1399.3677	-1399.1001	
Benzene and $PdAg(OAc)_3$: CMD C-H activation TS		-1189.9559	-1189.7561	-1125.22
Precomplex: η^2 PhPd(II)OAc with N-methyl indole	**Pre_1**	-989.72871	-989.4642	
CMD C-H TS: N-methyl indole and PhPd(II)OAc at C2	**C2_CMD1**	-989.67541	-989.41635	
Product from CMD C-H TS N-methyl indole and PhPd(II)OAc at C2		-989.70171	-989.43729	
CMD C-H TS: N-methyl indole and PhPd(II)OAc at C3	**C3_CMD1**	-989.68019	-989.42124	
Product from CMD C-H TS N-methyl indole and PhPd(II)OAc at C3		-989.69621	-989.4328	
Precursor to Reductive elimination TS: N-methyl indole C2: PhPd(II)AcOH		-989.70172	-989.43725	

Structure	Reference	Energy (Hartree)	Gibbs (Hartree)	Imaginary Frequency (cm^{-1})
Reductive elimination TS: N-methyl indole at C2 and PhPd(II)AcOH	**C2_RE_1**	-989.68877	-989.42508	-277.96
Product from Reductive elimination of N-methyl indole and PhPd(II)OAc: C2 arylated product		-989.74104	-989.47524	
Precursor to Reductive elimination TS: N-methyl indole at C3 and PhPd(II)AcOH		-989.6962	-989.43356	
Reductive elimination TS: N-methyl indole at C3 and PhPd(II)AcOH	**C3_RE_1**	-989.68568	-989.4219	-292.91
Product from Reductive elimination of N-methyl indole and PhPd(II)OAc: C3 arylated product		-989.7407	-989.47579	
Precomplex: η^2 PhPd(II)OAc-DMF with N-methyl indole	**Pre_2**	-1238.1792	-1237.8164	
CMD C-H TS: N-methyl indole and PhPd(II)OAc-DMF at C2	**C2_CMD_P**	-1238.1427	-1237.7855	-1151.16
Product from CMD C-H TS N-methyl indole and PhPd(II)OAc-DMF at C2		-1238.1626	-1237.8007	
CMD C-H TS: N-methyl indole and PhPd(II)OAc-DMF at C3	**C3_CMD_P**	-1238.146	-1237.7883	-1169.61
Product from CMD C-H TS N-methyl indole and PhPd(II)OAc-DMF at C3		-1238.1575	-1237.7957	
Precursor to Reductive elimination TS: N-methyl indole at C2 and PhPd(II)AcOH-DMF		-1238.1651	-1237.8027	
Reductive elimination TS: N-methyl indole at C2 and PhPd(II)AcOH-DMF	**C2_RE_P**	-1238.1402	-1237.7794	-311.65
Product from Reductive elimination of N-methyl indole and PhPd(II)OAc-DMF: C2 arylated product		-1238.1983	-1237.8345	
Precursor to Reductive elimination TS: N-methyl indole at C3 and PhPd(II)AcOH-DMF		-1238.1575	-1237.7958	
Reductive elimination TS: N-methyl indole at C3 and PhPd(II)AcOH-DMF	**C3_RE_P**	-1238.1348	-1237.7748	-303.51
Product from Reductive elimination of N-methyl indole and PhPd(II)OAc-DMF: C3 arylated product		-1238.1973	-1237.8333	
Precomplex: η^2 PhPd(II)OAc-AcOH with N-methyl indole	**Pre_3**	-1218.770863	-1218.4469	
CMD C-H TS: N-methyl indole and PhPd(II)OAc-AcOH at C2	**C2_CMD_NP**	-1218.72908	-1218.4111	-1208.95
Product from CMD C-H TS N-methyl indole and PhPd(II)OAc-AcOH at C2		-1218.745591	-1218.4232	
CMD C-H TS: N-methyl indole and PhPd(II)OAc- AcOH at C3	**C3_CMD_NP**	-1218.73299	-1218.4156	-1137.70
Product from CMD C-H TS N-methyl indole and PhPd(II)OAc- AcOH at C3		-1218.740874	-1218.4187	

Structure	Reference	Energy (Hartree)	Gibbs (Hartree)	Imaginary Frequency (cm^{-1})
Precursor to Reductive elimination TS: N-methyl indole at C2 and PhPd(II)AcOH-AcOH		-1218.748493	-1218.4254	
Reductive elimination TS: N-methyl indole at C2 and PhPd(II)AcOH-AcOH	**C2_RE_NP**	-1218.725604	-1218.4039	-307.54
Product from Reductive elimination of N-methyl indole and PhPd(II)OAc-AcOH: C2 arylated product		-1218.778242	-1218.4534	
Precursor to Reductive elimination TS: N-methyl indole at C3 and PhPd(II)AcOH-AcOH		-1218.740873	-1218.4187	
Reductive elimination TS: N-methyl indole at C3 and PhPd(II)AcOH-AcOH	**C3_RE_NP**	-1218.720448	-1218.3994	-302.58
Product from Reductive elimination of N-methyl indole and PhPd(II)OAc-AcOH: C3 arylated product		-1218.780109	-1218.4564	
Pd Dimers with N-methyl indole: CMD C-H activation				
Precomplex of C2 CMD TS C-H activation: $Pd_2(OAc)_4$		-1570.21446	-1569.89266	
C2 CMD TS C-H activation: $Pd_2(OAc)_4$		-1570.17986	-1569.86286	-1167.07
Product of C2 CMD TS C-H activation: $Pd_2(OAc)_4$		-1570.20239	-1569.88065	
Precomplex of C3 CMD TS C-H activation: $Pd_2(OAc)_4$		-1570.22272	-1569.89883	
C3 CMD TS C-H activation: $Pd_2(OAc)_4$		-1570.18736	-1569.86953	-1120.58
Product of C3 CMD TS C-H activation: $Pd_2(OAc)_4$		-1570.19942	-1569.87714	
Precomplex of C2 CMD TS C-H activation: $PdCu(OAc)_4$		-1639.65691	-1639.33583	
C2 CMD TS C-H activation: $PdCu(OAc)_4$		-1639.62274	-1639.30518	-1157.99
Product of C2 CMD TS C-H activation: $PdCu(OAc)_4$		-1639.64512	-1639.32384	
Precomplex of C3 CMD TS C-H activation: $PdCu(OAc)_4$		-1639.66422	-1639.33965	
C3 CMD TS C-H activation: $PdCu(OAc)_4$		-1639.63197	-1639.31373	-1118.56
Product of C3 CMD TS C-H activation: $PdCu(OAc)_4$		-1639.64339	-1639.32051	
Precomplex of C2 CMD TS C-H activation: $PdAg(OAc)_3$		-1360.81835	-1360.54758	
C2 CMD TS C-H activation: $PdAg(OAc)_3$		-1360.80070	-1360.53324	-1137.14
Product of C2 CMD TS C-H activation: $PdAg(OAc)_3$		-1360.84617	-1360.57260	
Precomplex of C3 CMD TS C-H activation: $PdAg(OAc)_3$		-1360.83194	-1360.55919	
C3 CMD TS C-H activation: $PdAg(OAc)_3$		-1360.80389	-1360.53658	-1164.30

Structure	Reference	Energy (Hartree)	Gibbs (Hartree)	Imaginary Frequency (cm^{-1})
Product of C3 CMD TS C-H activation: $PdAg(OAc)_3$		-1360.81421	-1360.54280	
C2 CMD TS C-H activation: $PdCu(OAc)_4$ – "switch"		-1752.91024	-1752.58181	-429.01
C3 CMD TS C-H activation: $PdCu(OAc)_4$- "switch"		-1752.90926	-1752.58261	-969.36
C2 CMD TS C-H activation: $PdAg(OAc)_3$- "switch"		-1360.73372	-1360.46597	-155.64
Pd Dimers with N-Piv indole: CMD C-H activation				
Precomplex of N-Piv Indole C3 CMD TS C-H activation: $PdCu(OAc)_4$		-1870.86726	-1870.45313	
N-Piv Indole C3 CMD TS: $PdCu(OAc)_4$		-1870.84305	-1870.43335	-1026.41
Product of N-Piv Indole C3 CMD TS C-H activation: $PdCu(OAc)_4$		-1870.85957	-1870.44663	
Precomplex of N-Piv Indole C2 CMD TS C-H activation: $PdCu(OAc)_4$		-1870.87052	-1870.45700	
N-Piv Indole C2 CMD TS: $PdCu(OAc)_4$		-1870.83360	-1870.42424	-1176.14
Product of N-Piv Indole C2 CMD TS C-H activation: $PdCu(OAc)_4$		-1870.84763	-1870.43594	
Precomplex of C2 CMD TS C-H activation: $Pd_2(OAc)_4$		-1801.42881	-1801.01498	
C2 CMD TS C-H activation: $Pd_2(OAc)_4$		-1801.39081	-1800.98247	-1167.07
Product of C2 CMD TS C-H activation: $Pd_2(OAc)_4$		-1801.40592	-1800.99386	
Precomplex of C3 CMD TS C-H activation: $Pd_2(OAc)_4$		-1801.42469	-1801.00956	
C3 CMD TS C-H activation: $Pd_2(OAc)_4$		-1801.39864	-1800.99012	-1120.58
Product of C3 CMD TS C-H activation: $Pd_2(OAc)_4$		-1801.41575	-1801.00231	
C-H Activation of N-methyl indole followed by benzene C-H activation				
Precomplex of N-methyl indole C-H activation: $Pd(OAc)_2$		-986.58532	-986.35924	
CMD TS of N-methyl indole C2: $Pd(OAc)_2$		-986.55163	-986.33011	-1169.50
Product of N-methyl indole C2 C-H activation: $Pd(OAc)_2$		-986.57225	-986.34659	
CMD TS of N-methyl indole C3: $Pd(OAc)_2$		-986.55466	-986.33233	-1128.42
Product of N-methyl indole C3 C-H activation: $Pd(OAc)_2$		-986.56912	-986.34388	
Precomplex of N-methyl indole C-H activation: $Pd(OAc)_2$-DMF		-1235.04512	-1234.71955	
CMD TS of N-methyl indole C2: $Pd(OAc)_2$-DMF		-1235.00764	-1234.68796	-1145.61
Product of N-methyl indole C2 C-H activation: $Pd(OAc)_2$-DMF		-1235.02726	-1234.70384	

Structure	Reference	Energy (Hartree)	Gibbs (Hartree)	Imaginary Frequency (cm^{-1})
CMD TS of N-methyl indole C3: $Pd(OAc)_2$-DMF		-1235.00940	-1234.68995	-1130.44
Product of N-methyl indole C3 C-H activation: $Pd(OAc)_2$-DMF		-1235.02057	-1234.69776	
Precomplex of N-methyl indole C-H activation: $Pd(OAc)_2$-AcOH		-1215.63345	-1215.34694	
CMD TS of N-methyl indole C2: $Pd(OAc)_2$-AcOH	**NMe_C2_ AcOH**	-1215.59775	-1215.31733	-1130.99
Product of N-methyl indole C2 C-H activation: $Pd(OAc)_2$-AcOH		-1215.61707	-1215.33231	
CMD TS of N-methyl indole C3: $Pd(OAc)_2$-AcOH	**NMe_C3_ AcOH**	-1215.60138	-1215.32066	-1128.37
Product of N-methyl indole C3 C-H activation: $Pd(OAc)_2$-AcOH		-1215.61217	-1215.32838	
Precomplex of benzene C-H activation with C3Indole-Pd(II)OAc		-989.70823	-989.44443	
CMD TS of benzene C-H activation with C3Indole-Pd(II)OAc		-989.66018	-989.40178	-1098.25
Product of benzene C-H activation with C3Indole-Pd(II)OAc		-989.69425	-989.43093	
Precomplex of benzene C-H activation with C2Indole-Pd(II)OAc		-989.71186	-989.44801	
CMD TS of benzene C-H activation with C2Indole-Pd(II)OAc		-989.66300	-989.40406	-1092.65
Product of benzene C-H activation with C2Indole-Pd(II)OAc		-989.69790	-989.43385	
Precomplex of benzene C-H activation with C3Indole-Pd(II)OAc-DMF		-1238.15988	-1237.79581	
CMD TS of benzene C-H activation with C3Indole Pd(II)OAc-DMF		-1238.13259	-1237.77384	-1062.88
Product of benzene C-H activation with C3Indole- Pd(II)OAc-DMF		-1238.16149	-1237.79852	
Precomplex of benzene C-H activation with C2Indole- Pd(II)OAc-DMF		-1238.16324	-1237.80022	
CMD TS of benzene C-H activation with C2Indole- Pd(II)OAc-DMF		-1238.13649	-1237.77711	-1105.56
Product of benzene C-H activation with C2Indole- Pd(II)OAc-DMF		-1238.16476	-1237.80289	
Precomplex of benzene C-H activation with C3Indole-Pd(II)OAc-AcOH		-1218.74648	-1218.42465	
CMD TS of benzene C-H activation with C3Indole- Pd(II)OAc-AcOH		-1218.71470	-1218.39655	-1264.71
Product of benzene C-H activation with C3Indole- Pd(II)OAc-AcOH		-1218.73523	-1218.41274	
Precomplex of benzene C-H activation with C2Indole- Pd(II)OAc-AcOH		-1218.74966	-1218.42709	
CMD TS of benzene C-H activation with C2Indole- Pd(II)OAc-AcOH		-1218.71910	-1218.40126	-1275.03
Product of benzene C-H activation with C2Indole- Pd(II)OAc-AcOH		-1218.73986	-1218.41666	

Structure	Reference	Energy (Hartree)	Gibbs (Hartree)	Imaginary Frequency (cm^{-1})
Alternative mechanisms: S_E3 activation of N-methyl indole				
C2 S_E3 C-H activation TS with PdPhOAc	**TS_5**	-1218.17807	-1217.87306	-966.36
C2 Product of S_E3 C-H activation TS with PdPhOAc		-1218.21694	-1217.90787	
C3 S_E3 C-H activation TS with PdPhOAc	**TS_3**	-1218.17688	-1217.87264	-1086.93
C3 Product of S_E3 C-H activation TS with PdPhOAc		-1218.20387	-1217.89475	
Precursor to reductive elimination TS at C2 with PdPhOAc		-1218.21694	-1217.90786	
Reductive elimination TS at C2 with PdPhOAc	**TS_6**	-1218.19033	-1217.88146	-261.63
Product of reductive elimination TS at C2 with PdPhOAc		-1218.23166	-1217.93419	
Precursor to reductive elimination TS at C3 with PdPhOAc		-1218.20387	-1217.89475	
Reductive elimination TS at C3 with PdPhOAc	**TS_4**	-1218.17691	-1217.86925	-281.65
Product of reductive elimination TS at C3 with PdPhOAc		-1218.22746	-1217.93029	
C3 S_E3 C-H activation TS with PdPhOAc-DMF		-1466.62897	-1466.22317	-1155.62
C3 Product of S_E3 C-H activation TS with PdPhOAc-DMF		-1466.65056	-1466.24013	
Precursor to reductive elimination TS at C3 with PdPhOAc-DMF		-1466.65685	-1466.24780	
Reductive elimination TS at C3 with PdPhOAc-DMF		-1466.62247	-1466.21413	-322.42
Product of reductive elimination TS at C3 with PdPhOAc-DMF		-1466.69596	-1466.28671	
Precursor to S_E3 C3 C-H activation with PdPhOAc-AcOH		-1447.24863	-1446.88034	
C3 S_E3 C-H activation TS with PdPhOAc-AcOH		-1447.22292	-1446.86115	-1132.31
C3 Product of S_E3 C-H activation TS with PdPhOAc-AcOH		-1446.88250	-1447.25005	
Precursor to reductive elimination TS at C3 with PdPhOAc-AcOH		-1447.25005	-1446.88250	-314.19
Reductive elimination TS at C3 with PdPhOAc-AcOH		-1447.21885	-1446.85246	
Product of reductive elimination TS at C3 with PdPhOAc-AcOH		-1447.27820	-1446.90806	
Alternative mechanisms: Heck-type carbopalladation of N-methyl indole				
Precursor to Heck-type carbopalladation with PhPdOAc		-989.72871	-989.46419	
C2 arylation with PdPhOAc				
Carobopalladation TS with PhPdOAc		-989.70225	-989.43628	-361.92

Structure	Reference	Energy (Hartree)	Gibbs (Hartree)	Imaginary Frequency (cm^{-1})
Product of Heck-type carbopalldation with PhPdOAc		-989.73033	-989.46400	
Precursor to E2 elimination with OAc^-		-1218.20658	-1217.89575	
E2 elimination TS with OAc^-		-1218.18143	-1217.87666	-1206.93
C2 arylated product		-1218.23166	-1217.92134	
C3 arylation with PdPhOAc				
Carobopalladation TS with PhPdOAc		-989.69691	-989.43205	-326.70
Product of Heck-type carbopalldation with PhPdOAc		-989.73433	-989.46756	
Precursor to E2 elimination with OAc^-		-1218.19992	-1217.88950	
E2 elimination TS with OAc^-		-1218.18962	-1217.88394	-943.90
C3 arylated product		-1218.22746	-1217.91713	
C2 arylation with PdPhOAc-DMF				
Precursor to Heck-type carbopalladation with PhPdOAc-DMF		-1238.17921	-1237.81642	
Carobopalladation TS with PhPdOAc-DMF		-1238.15181	-1237.78848	-352.17
Product of Heck-type carbopalldation with PhPdOAc-DMF		-1237.66476	-1237.31384	
Precursor to E2 elimination with OAc^-		-1466.65193	-1466.24364	
E2 elimination TS with OAc^-		-1466.63286	-1466.22939	-1269.43
C2 arylated product		-1466.66061	-1466.25107	
C3 arylation with PdPhOAc-DMF				
Carobopalladation TS with PhPdOAc-DMF		-1238.14854	-1237.78605	-320.34
Product of Heck-type carbopalldation with PhPdOAc-DMF		-1238.18458	-1237.82004	
Precursor to E2 elimination with OAc^-		-1466.66404	-1466.25303	
E2 elimination TS with OAc^-		-1466.64787	-1466.24441	-1178.55
C3 arylated product		-1466.68537	-1466.27340	
C2 arylation with PdPhOAc-AcOH				
Precursor to Heck-type carbopalladation with PhPdOAc-AcOH		-1218.77048	-1218.44614	
Carobopalladation TS with PhPdOAc-AcOH		-1218.74584	-1218.42240	-355.25

Structure	Reference	Energy (Hartree)	Gibbs (Hartree)	Imaginary Frequency (cm^{-1})
Product of Heck-type carbopalldation with PhPdOAc-DMF		-1218.77048	-1218.44614	
Precursor to E2 elimination with OAc^-		-1447.24426	-1446.87644	
E2 elimination TS with OAc^-		-1447.22321	-1446.86177	-1238.27
C2 arylated product		-1447.27159	-1446.90284	
C3 arylation with PdPhOAc-AcOH				
Precursor to Heck-type carbopalladation with PhPdOAc-AcOH		-1218.76267	-1218.43922	
Carobopalladation TS with PhPdOAc-AcOH		-1218.74207	-1218.41952	-322.42
Product of Heck-type carbopalldation with PhPdOAc-DMF		-1218.77696	-1218.45042	
Precursor to E2 elimination with OAc^-		-1447.24574	-1446.48110	
E2 elimination TS with OAc^-		-1447.23238	-1446.86997	-1168.57
C3 arylated product		-1447.27011	-1446.90370	

List of structures

Chapter 4

Structure	Reference	Energy (Hartree)	Gibbs (Hartree)	Imaginary Frequency (cm^{-1})
N-acetyl indole		-516.29586	-516.15432	
Benzene		-232.16101	-232.08026	
Acetic Acid		-229.00695	-228.96392	
DMF		-248.42829	-248.34731	
$Pd(OAc)_2$		-583.56679	-583.49195	
$Cu(OAc)_2$		-653.00882	-652.93447	
$Cu_2(OAc)_4$		-1306.02210	-1305.85363	
$Ag_2(OAc)_2$		-748.44713	-748.38611	
$PdCu(OAc)_4$		-1236.62898	-1236.45991	
$PdAg(OAc)_3$		-957.80873	-957.68979	
$Pd_3(OAc)_6$		-1750.84990	-1750.58306	
$Pd_2(OAc)_4$		-1167.20135	-1167.03072	
C-H activation via CMD of N-acetyl indole with Pd(II) catalysts				
Precomplex of CMD at C2: $Pd(OAc)_2$		-1099.89119	-1099.65692	
CMD TS at C2: $Pd(OAc)_2$		-1099.85984	-1099.63008	-1219.55
Product of CMD at C2: $Pd(OAc)_2$		-1099.88187	-1099.64694	
Precomplex of CMD at C3: $Pd(OAc)_2$		-1099.89116	-1099.65657	
CMD TS at C3: $Pd(OAc)_2$		-1099.85626	-1099.62636	-910.73
Product of CMD at C3: $Pd(OAc)_2$		-1099.87822	-1099.64362	
Precomplex of CMD: $Pd(OAc)_2$-DMF		-1348.35229	-1348.01818	
CMD TS at C2: $Pd(OAc)_2$-DMF		-1348.31775	-1347.98947	-1169.35
Product of CMD at C2: $Pd(OAc)_2$-DMF		-1348.33344	-1348.00041	
CMD TS at C3: $Pd(OAc)_2$-DMF		-1348.31268	-1347.98440	-1110.63
Product of CMD at C3: $Pd(OAc)_2$-DMF		-1348.33067	-1347.99934	

Structure	Reference	Energy (Hartree)	Gibbs (Hartree)	Imaginary Frequency (cm^{-1})
Precomplex of CMD: $Pd(OAc)_2$-AcOH		-1328.93771	-1328.64341	
CMD TS at C2: $Pd(OAc)_2$-AcOH		-1328.90698	-1328.61660	-1162.20
Product of CMD at C2: $Pd(OAc)_2$-AcOH		-1328.92266	-1328.62914	
CMD TS at C3: $Pd(OAc)_2$-AcOH		-1328.90344	-1328.61521	-1076.39
Product of CMD at C3: $Pd(OAc)_2$-AcOH		-1328.92135	-1328.62850	
Precomplex of CMD at C2: $PdCu(OAc)_4$		-1752.96384	-1752.63375	
CMD TS at C2: $PdCu(OAc)_4$	**PdCu_TS C2**	-1752.93207	-1752.60666	-1154.81
Product of CMD at C2: $PdCu(OAc)_4$		-1752.95170	-1752.62089	
Precomplex of CMD at C3: $PdCu(OAc)_4$		-1752.96630	-1752.63507	
CMD TS at C3 $PdCu(OAc)_4$	**PdCu_TS C3**	-1752.93497	-1752.60890	-1165.75
Product of CMD at C3: $PdCu(OAc)_4$		-1752.95337	-1752.62212	
CMD TS at C2: $PdAg(OAc)_3$		-1474.10825	-1473.83262	-1149.77
CMD TS at C2: $PdAg(OAc)_3$ – rotation of acetyl group		-1474.10937	-1473.83280	-1143.87
CMD TS at C3: $PdAg(OAc)_3$		-1474.10680	-1473.83169	-1146.60
CMD TS at C3 $PdCu(OAc)_4$: coordination with Cu		-1752.90926	-1752.58261	-738.22
CMD TS at C2 $PdCu(OAc)_4$: coordination with Cu		-1752.91024	-1752.58181	-513.53
CMD TS at C2: $Pd(OTFA)_2$		-1695.11377	-1694.93573	-1205.50
CMD TS at C3: $Pd(OTFA)_2$		-1695.11382	-1694.93633	-1117.88
CMD C-H activation of benzene with C2 indole-Pd(OAc)AcOH: precomplex		-1332.05798	-1331.72576	
CMD C-H activation of benzene with C2 indole-Pd(OAc)AcOH: TS		-1332.03019	-1331.70106	-592.61
CMD C-H activation of benzene with C2 indole-Pd(OAc)AcOH: product		-1332.04691	-1331.71545	
CMD C-H activation of benzene with C2 indole-Pd(OAc): TS	**Ph_TS_C2**	-1102.96951	-1102.70151	-1207.52
CMD C-H activation of benzene with C3 indole-Pd(OAc)AcOH: precomplex		-1332.05840	-1331.72998	
CMD C-H activation of benzene with C3 indole-Pd(OAc)AcOH: TS	**Ph_TS_C3**	-1332.02825	-1331.70118	-1262.13
CMD C-H activation of benzene with C3 indole-Pd(OAc)AcOH: product		-1332.04844	-1331.71545	
CMD C-H activation of benzene with C3 indole-Pd(OAc): TS		-1102.97025	-1102.70270	-1099.81

Reductive elimination of N-acetyl indole and Ph at C2 with PdPhOAc-AcOH: precomplex		-1332.05145	-1331.72000	
Reductive elimination of N-acetyl indole and Ph at C2 with PdPhOAc-AcOH: TS	**NAC_RE_C2**	-1332.02854	-1331.69933	-321.65
Reductive elimination of N-acetyl indole and Ph at C2 with PdPhOAc-AcOH: product		-1332.09423	-1331.76054	
Reductive elimination of N-acetyl indole and Ph at C2 with PdPhOAc: TS		-1102.9908	-1102.71895	-291.91
Reductive elimination of N-acetyl indole and Ph at C3 with PdPhOAc-AcOH: precomplex		-1332.05149	-1331.71992	
Reductive elimination of N-acetyl indole and Ph at C3 with PdPhOAc-AcOH: TS	**NAC_RE_C3**	-1332.03094	-1331.70141	-307.55
Reductive elimination of N-acetyl indole and Ph at C3 with PdPhOAc-AcOH: product		-1332.09292	-1331.75963	
Reductive elimination of N-acetyl indole and Ph at C3 with PdPhOAc: TS		-1102.9956	-1102.72340	-309.55
Activation of benzene with $PdCu(OAc)_{4:}$ precomplex		-1468.81728	-1468.56191	
Activation of benzene with $PdCu(OAc)_{4:}$ TS		-1468.78450	-1468.53360	-1040.14
Activation of benzene with $PdCu(OAc)_{4:}$ product		-1468.81113	-1468.55678	
Precomplex of N-acetyl indole CMD TS at C2 with PdPhOAc-AcOH		-1332.07809	-1331.74579	
N-acetyl indole CMD TS at C2 with PdPhOAc-AcOH	**NAC_TS_C2**	-1332.04028	-1331.71259	-1178.89
Product of N-acetyl indole CMD TS at C2 with PdPhOAc-AcOH		-1332.05213	-1331.72044	
Precomplex of N-acetyl indole CMD TS at C3 with PdPhOAc-AcOH		-1332.06914	-1331.73701	
N-acetyl indole CMD TS at C3 with PdPhOAc-AcOH	**NAC_TS_C3**	-1332.03882	-1331.71113	-1083.73
Product of N-acetyl indole CMD TS at C3 with PdPhOAc-AcOH		-1332.05162	-1331.71969	

List of structures

Chapter 5

Optimizations conducted at ωB97XD on *Gaussian 09*

Structure	Reference	Energy (Hartree)	Gibbs (Hartree)	Imaginary Frequency (cm^{-1})
Anisole		-346.64846	-346.53760	
Benzene		-232.16101	-232.08026	
Acetic Acid		-229.0069	-228.96392	
$Pd(OAc)_2$		-583.56679	-583.49195	
$Pd(OTFA)_2$		-1178.81150	-1178.78636	
TFA		-526.63379	-526.61821	
C-H activation of benzene with $Pd(OAc)_2$. Biphenyl				
Precomplex to 1st C-H activation of benzene		-815.73677	-815.56579	
1st C-H activation TS of benzene	**Ben_1**	-815.70988	-815.54281	-1094.2382
Product from 1st C-H activation of benzene		-815.73845	-815.56664	
Precomplex to 2nd C-H activation of benzene		-1047.92093	-1047.65387	
2nd C-H activation TS of benzene	**Ben_1b**	-1047.88737	-1047.62352	-1280.17
Product from 2nd C-H activation of benzene		-1047.90639	-1047.63888	
Precursor to reductive elimination TS		-1047.90622	-1047.63947	
Reductive elimination TS of biphenyl	**Ben_1_RE**	-1047.88942	-1047.62280	-312.49
Biphenyl product		-1047.94212	-1047.67353	
C-H activation of benzene with $Pd(OAc)_2$-TFA. Biphenyl				
Precomplex to 1st C-H activation of benzene		-1342.40460	-1342.20197	
1st C-H activation TS of benzene	**Ben_2**	-1342.38002	-1342.18241	-973.78
Product from 1st C-H activation of benzene		-1342.41030	-1342.20776	
Precomplex to 2nd C-H activation of benzene		-1345.55443	-1345.31250	
2nd C-H activation TS of benzene	**Ben_2b**	-1345.51331	-1345.27581	-1294.33
Product from 2nd C-H activation of benzene		-1345.53210	-1345.29135	

Structure	Reference	Energy (Hartree)	Gibbs (Hartree)	Imaginary Frequency (cm^{-1})
Precursor to reductive elimination TS		-1345.53205	-1345.29174	
Reductive elimination TS of biphenyl	**Ben_2_RE**	-1345.51684	-1345.27681	-321.95
Biphenyl product		-1345.56796	-1345.32518	
C-H activation of benzene with $Pd(OTFA)_2$. Biphenyl				
Precomplex to 1st C-H activation of benzene		-1410.99792	-1410.87795	
1st C-H activation TS of benzene	**Ben_3**	-1410.96573	-1410.85111	-1148.17
Product from 1st C-H activation of benzene		-1410.99074	-1410.87134	
Precomplex to 2nd C-H activation of benzene		-1116.49502	-1116.31182	
2nd C-H activation TS of benzene	**Ben_3b**	-1116.46456	-1116.28689	-1276.5810
Product from 2nd C-H activation of benzene		-1116.48846	-1116.30707	
Precursor to reductive elimination TS		-1116.48846	-1116.30710	
Reductive elimination TS of biphenyl	**Ben_3_RE**	-1116.47948	-1116.29720	-286.62
Biphenyl product		-1116.53529	-1116.35143	
C-H activation of benzene with $Pd(OTFA)_2$-TFA. Biphenyl				
Precomplex to 1st C-H activation of benzene		-1937.67273	-1937.52000	
1st C-H activation TS of benzene	**Ben_4**	-1937.64161	-1937.49435	-1105.40
Product from 1st C-H activation of benzene		-1937.66558	-1937.51361	
Precomplex to 2nd C-H activation of benzene		-1643.18578	-1642.97058	
2nd C-H activation TS of benzene	**Ben_4b**	-1643.14210	-1642.93003	-1246.67
Product from 2nd C-H activation of benzene		-1643.15516	-1642.93945	
Precursor to reductive elimination TS		-1643.15506	-1642.93929	
Reductive elimination TS of biphenyl	**Ben_4_RE**	-1643.14040	-1642.92516	-311.04
Biphenyl product		-1643.19674	-1642.97951	
C-H activation of benzene then anisole with $Pd(OAc)_2$. 4-methoxybiphenyl				
Precomplex to 2nd C-H activation of anisole (*para*)		-1162.41310	-1162.11471	
C-H activation TS of anisole (*para*) with PhPdOAc-AcOH	**AP_1**	-1162.37890	-1162.08371	-1258.58

Structure	Reference	Energy (Hartree)	Gibbs (Hartree)	Imaginary Frequency (cm^{-1})
Product from C-H activation of anisole (*para*)		-1162.39359	-1162.09514	
Precursor to reductive elimination TS		-1162.39368	-1162.09719	
Reductive elimination TS of anisole (*para*)	**AP1_Ben_RE**	-1162.37625	-1162.07959	-318.60
4-methoxybiphenyl product		-1162.43360	-1162.13395	
C-H activation of benzene then anisole with $Pd(OAc)_2$-TFA : 4-methoxybiphenyl				
Precomplex to 2nd C-H activation of anisole (*para*)		-1460.04714	-1459.77371	
C-H activation TS of anisole (*para*) with PhPdOAc-TFA	**AP_2**	-1460.00515	-1459.73712	-1253.88
Product from C-H activation of anisole (*para*)		-1460.01939	-1459.74724	
Precursor to reductive elimination TS		-1460.01952	-1459.74817	
Reductive elimination TS of anisole (*para*)	**AP2_Ben_RE**	-1460.00384	-1459.73281	-305.67
4-methoxybiphenyl product		-1460.06094	-1459.78704	
C-H activation of benzene then anisole with $Pd(OTFA)_2$: 4-methoxybiphenyl				
Precomplex to 2nd C-H activation of anisole (*para*)		-1230.98746	-1230.77374	
C-H activation TS of anisole (*para*) with PhPdOTFA	**AP_3**	-1230.95750	-1230.74860	-1273.73
Product from C-H activation of anisole (*para*)		-1230.97593	-1230.76266	
Precursor to reductive elimination TS		-1230.97589	-1230.76349	
Reductive elimination TS of anisole (*para*)	**AP3_Ben_RE**	-1230.96668	-1230.75374	-289.13
4-methoxybiphenyl product		-1231.02278	-1230.80818	
C-H activation of benzene then anisole with $Pd(OTFA)_2$-TFA : 4-methoxybiphenyl				
Precomplex to 2nd C-H activation of anisole (*para*)		-1757.67892	-1757.43124	
C-H activation TS of anisole (*para*) with PhPdOTFA-TFA	**AP_4**	-1757.63424	-1757.39135	-1163.09
Product from C-H activation of anisole (*para*)		-1757.64273	-1757.39520	
Precursor to reductive elimination TS		-1757.64265	-1757.39635	
Reductive elimination TS of anisole (*para*)	**AP4_BEN_RE**	-1757.62759	-1757.38199	-302.13
4-methoxybiphenyl product		-1757.68625	-1757.43836	

Structure	Reference	Energy (Hartree)	Gibbs (Hartree)	Imaginary Frequency (cm^{-1})
C-H activation of benzene then anisole with $Pd(OAc)_2$. 2-methoxybiphenyl				
Precomplex to 2nd C-H activation of anisole (*ortho*)		-1162.41498	-1162.11610	
C-H activation TS of anisole (*ortho*) with PhPdOAc-AcOH	**AO_1**	-1162.38268	-1162.08770	-1222.85
Product from C-H activation of anisole (*ortho*)		-1162.39682	-1162.09930	
Precursor to reductive elimination TS		-1162.39705	-1162.09881	
Reductive elimination TS of anisole (*ortho*)	**AO_1_Ben_RE**	-1162.37708	-1162.07892	-313.41
2-methoxybiphenyl product		-1162.43074	-1162.12990	
C-H activation of benzene then anisole with $Pd(OAc)_2$-TFA. 2-methoxybiphenyl				
Precomplex to 2nd C-H activation of anisole (*ortho*)		-1460.04869	-1459.77608	
C-H activation TS of anisole (*ortho*) with PhPdOAc-TFA	**AO_2**	-1460.00914	-1459.74045	-1237.06
Product from C-H activation of anisole (*ortho*)		-1460.02290	-1459.75021	
Precursor to reductive elimination TS		-1460.02296	-1459.75056	
Reductive elimination TS of anisole (*ortho*)	**AO_2_Ben_RE**	-1460.00494	-1459.73329	-315.31
2-methoxybiphenyl product		-1460.05778	-1459.78280	
C-H activation of benzene then anisole with $Pd(OTFA)_2$. 2-methoxybiphenyl				
Precomplex to 2nd C-H activation of anisole (*ortho*)		-1230.99013	-1230.77496	
C-H activation TS of anisole (*ortho*) with PhPdOTFA	**AO_3**	-1230.96119	-1230.75176	--1224.16
Product from C-H activation of anisole (*ortho*)		-1230.97909	-1230.76617	
Precursor to reductive elimination TS		-1230.97909	-1230.76617	
Reductive elimination TS of anisole (*ortho*)	**AO_3_Ben_RE**	-1230.96863	-1230.75501	-285.42
2-methoxybiphenyl product		-1231.02389	-1230.80811	
C-H activation of benzene then anisole with $Pd(OTFA)_2$-TFA. 2-methoxybiphenyl				
Precomplex to 2nd C-H activation of anisole (*ortho*)		-1757.68052	-1757.43328	
C-H activation TS of anisole (*ortho*) with PhPdOTFA-TFA	**AO_4**	-1757.63832	-1757.39511	-1124.28
Product from C-H activation of anisole (*ortho*)		-1757.64663	-1757.39968	
Precursor to reductive elimination TS		-1757.64663	-1757.39967	

Structure	Reference	Energy (Hartree)	Gibbs (Hartree)	Imaginary Frequency (cm^{-1})
Reductive elimination TS of anisole (*ortho*)	**AO_4_Ben_RE**	-1757.62894	-1757.38251	-321.55
2-methoxybiphenyl product		-1757.68304	-1757.43431	

Kinetic models with Berkeley-Madonna

$Pd(OAc)_2$-TFA:

METHOD STIFF

STARTTIME = 0
STOPTIME=86400
DT = .001

;INITIAL VALUES
init Benzene =0.011
init PdOAc2 = 0.00025
init PdOAc2_Benzene = 0
init Anisole = 0.001
init Ph_Pd_OAc_AcOH = 0
init PhPhPdAcOH2 = 0
init AO_Ph_Pd_AcOH2 = 0
init AP_Ph_Pd_AcOH2 = 0
init AO_Ph = 0
init AP_Ph = 0
init Ph_Ph = 0
init PdAcOH2=0

;REACTION TEMP
x=273+Temp
Temp=25

;DIFFERENTIAL MODEL: Benzene followed by anisole (para)
R3=k3*Anisole*Ph_Pd_OAc_AcOH
Rr3=kr3*AP_Ph_Pd_AcOH2
R5=k5*AP_Ph_Pd_AcOH2
;reoxidation
R6=k6*PdAcOH2

;DIFFERENTIAL MODEL: benzene followed by anisole (ortho)
R7=k7*Anisole*Ph_Pd_OAc_AcOH
Rr7=kr7*AO_Ph_Pd_AcOH2
R8=k8*AO_Ph_Pd_AcOH2

;Differential model: Benzene – Benzene
Rpq=kpq*PdOAc2*Benzene
Rpqr=kpqr*PdOAc2_Benzene
R1=k1*PdOAc2_Benzene
Rr1=kr1*Ph_Pd_OAc_AcOH
R2=k2*Ph_Pd_OAc_AcOH*Benzene
Rr2=kr2*PhPhPdAcOH2
R4=k4*PhPhPdAcOH2

```
; DIFFERENTIAL TERMS
d/dt(Benzene)=Rpqr-Rpq+Rr2-R2
d/dt(PdOAc2)=R6-Rpq+Rpqr
d/dt(PdOAc2_Benzene)=Rpq-Rpqr
d/dt(Anisole)=Rr3-R3-R7+Rr7
d/dt(Ph_Pd_OAc_AcOH)= R1+rr2+Rr3-Rr1-R2-R3-R7+Rr7
d/dt(PhPhPdAcOH2)= R2-Rr2-R4
d/dt(AO_Ph_Pd_AcOH2)=R7-Rr7-R8
d/dt(AP_Ph_Pd_AcOH2)= R3-Rr3-R5
d/dt (AO_Ph)=R8
d/dt (AP_Ph)=R5
d/dt (Ph_Ph)=R4
d/dt (PdAcOH2)=R4+R5-R6+R8

;Constants
kb=1.38*10^-23
h=6.626*10^-34
T=x
;x is temp defined, thus allowing the term 'temp' to be the variable. See above

;EYRING EQ
;Ph-Ph
k1=((kb*T)/h)*expEaRT_f1
expEaRT_f1=exp(-12.1/((0.001987*x)))
kr1=((kb*T)/h)*expEaRT_r1
expEaRT_r1=exp(-17.4/((0.001987*x)))
k2=((kb*T)/h)*expEaRT_f2
expEaRT_f2=exp(-24.8/((0.001987*x)))

kr2=((kb*T)/h)*expEaRT_r2
expEaRT_r2=exp(-11.6/((0.001987*x)))
k4=((kb*T)/h)*expEaRTr3
expEaRTr3=exp(-11.9/((0.001987*x)))

;benzene-anisole (ortho)
k7=((kb*T)/h)*expEaRTf2
expEaRTf2=exp(-20.5/((0.001987*x)))
kr7=((kb*T)/h)*expEaRTr2
expEaRTr2=exp(-8.2/((0.001987*x)))
k8=((kb*T)/h)*expEaRTr3a
expEaRTr3a=exp(-12.9/((0.001987*x)))

;Benzene-anisole (para)
k3=((kb*T)/h)*expEaRTfor2
expEaRTfor2=exp(-20.2/((0.001987*x)))
kr3=((kb*T)/h)*expEaRTrev2
expEaRTrev2=exp(-7.7/((0.001987*x)))
k5=((kb*T)/h)*expEaRTre3
expEaRTre3=exp(-10.5/((0.001987*x)))

;reoxidation term
k6=((kb*T)/h)*expEaRT4
expEaRT4=exp(-6.0/((0.001987*x)))
;pre-equilbrium terms
kpq=((kb*T)/h)*expEaRTpq
expEaRTpq=exp(-2.4/((0.001987*x)))
kpqr=((kb*T)/h)*expEaRTpqr
expEaRTpqr=exp(-6.3/((0.001987*x)))
```

$Pd(OTFA)_2$-TFA

```
METHOD STIFF

STARTTIME = 0
STOPTIME=86400
DT = .001

;INITIAL VALUES
init Benzene =0.011
init PdOAc2 = 0.00025
init PdOAc2_Benzene = 0
init Anisole = 0.001
init Ph_Pd_OAc_AcOH = 0
init PhPhPdAcOH2 = 0
init AO_Ph_Pd_AcOH2 = 0
init AP_Ph_Pd_AcOH2 = 0
init AO_Ph = 0
init AP_Ph = 0
init Ph_Ph = 0
init PdAcOH2=0

;REACTION TEMP
x=273+Temp
Temp=25

;DIFFERENTIAL MODEL: Benzene followed by anisole (para)

R3=k3*Anisole*Ph_Pd_OAc_AcOH
Rr3=kr3*AP_Ph_Pd_AcOH2
R5=k5*AP_Ph_Pd_AcOH2
;reoxidation
R6=k6*PdAcOH2

;DIFFERENTIAL MODEL: Benzene followed by anisole (ortho)
R7=k7*Anisole*Ph_Pd_OAc_AcOH
Rr7=kr7*AO_Ph_Pd_AcOH2
R8=k8*AO_Ph_Pd_AcOH2

;Differential model – Benzene-Benzene

Rpq=kpq*PdOAc2*Benzene
Rpqr=kpqr*PdOAc2_Benzene
R1=k1*PdOAc2_Benzene
Rr1=kr1*Ph_Pd_OAc_AcOH
R2=k2*Ph_Pd_OAc_AcOH*Benzene
Rr2=kr2*PhPhPdAcOH2
R4=k4*PhPhPdAcOH2

; DIFFERENTIAL TERM
d/dt(Benzene)=Rpqr-Rpq+Rr2-R2
d/dt(PdOAc2)=R6-Rpq+Rpqr
d/dt(PdOAc2_Benzene)=Rpq-Rpqr
d/dt(Anisole)=Rr3-R3-R7+Rr7
d/dt(Ph_Pd_OAc_AcOH)= R1+rr2+Rr3-Rr1-R2-R3-R7+Rr7
d/dt(PhPhPdAcOH2)= R2-Rr2-R4
d/dt(AO_Ph_Pd_AcOH2)=R7-Rr7-R8
d/dt(AP_Ph_Pd_AcOH2)= R3-Rr3-R5
```

```
d/dt (AO_Ph)=R8
d/dt (AP_Ph)=R5
d/dt (Ph_Ph)=R4
d/dt (PdAcOH2)=R4+R5-R6+R8

;Constants
kb=1.38*10^-23
h=6.626*10^-34
T=x
;x is temp defined, thus allowing the term 'temp' to be the variable. See above

;EYRING EQ
;Ph-Ph
k1=((kb*T)/h)*expEaRT_f1
expEaRT_f1=exp(-15.5/((0.001987*x)))
kr1=((kb*T)/h)*expEaRT_r1
expEaRT_r1=exp(-13.5/((0.001987*x)))
k2=((kb*T)/h)*expEaRT_f2
expEaRT_f2=exp(-26.3/((0.001987*x)))
kr2=((kb*T)/h)*expEaRT_r2
expEaRT_r2=exp(-7.2/((0.001987*x)))
k4=((kb*T)/h)*expEaRTr3
expEaRTr3=exp(-10.9/((0.001987*x)))

;benzene-anisole (ortho)
k7=((kb*T)/h)*expEaRTf2
expEaRTf2=exp(-21.9/((0.001987*x)))
kr7=((kb*T)/h)*expEaRTr2
expEaRTr2=exp(-4.2/((0.001987*x)))
k8=((kb*T)/h)*expEaRTr3a
expEaRTr3a=exp(-12.9/((0.001987*x)))

;BENZEne-para

k3=((kb*T)/h)*expEaRTfor2
expEaRTfor2=exp(-23.9/((0.001987*x)))
kr3=((kb*T)/h)*expEaRTrev2
expEaRTrev2=exp(-4.1/((0.001987*x)))
k5=((kb*T)/h)*expEaRTre3
expEaRTre3=exp(-10.5/((0.001987*x)))

;reoxidation term
k6=((kb*T)/h)*expEaRT4
expEaRT4=exp(-6.0/((0.001987*x)))

;pre-equilbrium terms
kpq=((kb*T)/h)*expEaRTpq
expEaRTpq=exp(-2.4/((0.001987*x)))
kpqr=((kb*T)/h)*expEaRTpqr
expEaRTpqr=exp(-21.7/((0.001987*x)))
```

List of structures

Chapter 6

Optimizations conducted at ωB97XD on *Gaussian 09*

BDE calculations conducted at G3B3

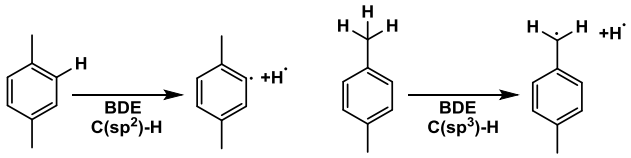

Structure	G3B3 Enthalpy (Hartree)
xylene	-310.60336
H Radical	-0.498726
$C(sp^2)$-H radical	-309.92073
$C(sp^3)$-H radical	-309.95877

Structure	Reference	Energy (Hartree)	Gibbs (Hartree)	Imaginary Frequency (cm^{-1})
Xylene		-310.77356	-310.64228	
$Pd(OAc)_2$		-583.56679	-583.49498	
$Pd(OTFA)_2$		-1178.81150	-1178.78940	
TFA		-526.63379	-526.62024	
AcOH		-229.00695	-228.96551	
OTFA anion, $OTFA^-$		-526.08776	-526.08616	
CMD C-H activation: sp^2-sp^2 activation of *p*-xylene				
Precomplex to $C(sp^2)$-H activation with $Pd(OAc)_2$	**Xylene_OAc**	-894.35494	-894.13457	
$C(sp^2)$-H activation with $Pd(OAc)_2$: CMD TS		-894.32819	-894.11284	-1043.05
Product of $C(sp^2)$-H activation with $Pd(OAc)_2$		-894.35309	-894.13267	
Precomplex to $C(sp^2)$-H activation with $Pd(OAc)_2$-TFA	**Xylene_OAc_TFA**	-1421.02816	-1420.77529	
$C(sp^2)$-H activation with $Pd(OAc)_2$-TFA: CMD TS		-1420.99980	-1420.75333	-904.14
Product of $C(sp^2)$-H activation with $Pd(OAc)_2$-TFA		-1421.02655	-1420.77559	
Precomplex to $C(sp^2)$-H activation with $Pd(OTFA)_2$		-1489.61671	-1489.44860	

$C(sp^2)$-H activation with $Pd(OTFA)_2$: CMD TS	**Xylene_OTFA**	-1489.58533	-1489.42305	-1098.40
Product of $C(sp^2)$-H activation with $Pd(OTFA)_2$		-1489.60664	-1489.43953	
Precomplex to $C(sp^2)$-H activation with $Pd(OTFA)_2$-TFA		-2016.29687	-2016.09437	
$C(sp^2)$-H activation with $Pd(OTFA)_2$-TFA: CMD TS	**Xylene_OTFA_TFA**	-2016.26204	-2016.06684	-1092.28
Product of $C(sp^2)$-H activation with $Pd(OTFA)_2$-TFA		-2016.28261	-2016.08354	
CMD C-H activation Second sp^2 C-H activation of *p*-xylene				
Precomplex to $C(sp^2)$-H activation with PhPdOAc		-976.11625	-975.80530	
$C(sp^2)$-H activation with PhPdOAc: CMD TS		-976.06257	-975.75858	-1188.15
Product of $C(sp^2)$-H activation with PhPdOAc		-976.09202	-975.78229	
Precomplex to $C(sp^2)$-H activation with PhPdOTFA		-1273.71713	-1273.43321	
$C(sp^2)$-H activation with PhPdOTFA: CMD TS		-1273.69597	-1273.41635	-1271.44
Product of $C(sp^2)$-H activation with PhPdOTFA		-1273.74916	-1273.46479	
Precomplex to $C(sp^2)$-H activation with PhPdOAc-AcOH		-1205.15376	-1204.78548	
$C(sp^2)$-H activation with PhPdOAc-AcOH: CMD TS	**TS2**	-1205.11759	-1204.75327	-1246.44
Product of $C(sp^2)$-H activation with PhPdOAc-AcOH		-1205.13454	-1204.76498	
Precomplex to $C(sp^2)$-H activation with PhPdOAc-TFA		-1502.78766	-1502.44555	
$C(sp^2)$-H activation with PhPdOAc-TFA: CMD TS		-1502.74384	-1502.40551	1273.71
Product of $C(sp^2)$-H activation with PhPdOAc-TFA		-1502.76132	-1502.41899	
Precomplex to $C(sp^2)$-H activation with PhPdOTFA-TFA		-1800.41942	-1800.10270	
$C(sp^2)$-H activation with PhPdOTFA-TFA: CMD TS	**TS4**	-1800.37305	-1800.06022	-1220.89
Product of $C(sp^2)$-H activation with PhPdOTFA-TFA		-1800.38388	-1800.06784	
sp^2-sp^2 Reductive elimination				
Precomplex to sp^2-sp^2 reductive elimination TS: ArPdAr'(II)AcOH		-976.09226	-975.78204	
Reductive elimination TS: ArPdAr'(II)AcOH		-976.07603	-975.76569	-293.62
sp^2-sp^2 product from reductive elimination of ArPdAr'(II)AcOH		-976.13625	-975.82381	
Precomplex to sp^2-sp^2 reductive elimination TS: ArPdAr'(II)$(AcOH)_2$		-1205.13469	-1204.76551	
Reductive elimination TS: ArPdAr'(II)$(AcOH)_2$	**TS_RE_ACOH**	-1205.10910	-1204.74233	-307.07

sp^2-sp^2 product from reductive elimination of ArPdAr'(II)$(AcOH)_2$		-1205.17133	-1204.80129	
Precomplex to sp^2-sp^2 reductive elimination TS: ArPdAr'(II)AcOH-TFA		-1502.76145	-1502.41918	
Reductive elimination TS: ArPdAr'(II)AcOH-TFA		-1502.73713	-1502.39598	-300.92
sp^2-sp^2 product from reductive elimination of ArPdAr'(II)AcOH-TFA		-1502.79363	-1502.45105	
Precomplex to sp^2-sp^2 reductive elimination TS: ArPdAr'(II)TFA		-1273.71713	-1273.43321	
Reductive elimination TS: ArPdAr'(II)TFA		-1273.70105	-1273.41674	-291.24
sp^2-sp^2 product from reductive elimination of ArPdAr'(II)TFA		-1273.76197	-1273.47462	
Precomplex to sp^2-sp^2 reductive elimination TS: ArPdAr'(II)$(TFA)_2$		-1800.38391	-1800.06794	
Reductive elimination TS: ArPdAr'(II)$(TFA)_2$	**TS_RE_TFA**	-1800.36124	-1800.04513	-299.90
sp^2-sp^2 product from reductive elimination of ArPdAr'(II)$(TFA)_2$		-1800.42630	-1800.10760	
$C(sp^3)$-H activation after initial $C(sp^2)$-H activation: Inner Sphere CMD				
Precomplex to $C(sp^3)$-H activation: Inner sphere CMD with ArPd(II)OAc-AcOH	**Pre_OAc_inner**	-1205.15251	-1204.78408	
$C(sp^3)$-H activation: Inner sphere CMD TS with ArPd(II)OAc-AcOH	**OAc_Inner_TS**	-1205.08991	-1204.72498	-586.12
Product of $C(sp^3)$-H activation: With ArPd(II)OAc-AcOH	**Post_OAc_Inner**	-1205.09095	-1204.72395	
Precomplex to $C(sp^3)$-H activation: Inner sphere CMD with ArPd(II)OAc-TFA		-1502.78637	-1502.44329	
$C(sp^3)$-H activation: Inner sphere CMD TS with ArPd(II)OAc-TFA		-1502.71611	-1502.37738	-592.93
Product of $C(sp^3)$-H activation: With ArPd(II)OAc-TFA		-1502.71715	-1502.37520	
Precomplex to $C(sp^3)$-H activation: Inner sphere CMD with ArPd(II)OTFA-TFA		-1800.40622	-1800.08760	
$C(sp^3)$-H activation: Inner sphere CMD TS with ArPd(II)OTFA-TFA		-1800.34429	-1800.02995	-619.10
Product of $C(sp^3)$-H activation: With ArPd(II)OTFA-TFA	**Post_OTFA_inner**	-1800.34510	-1800.02816	
Initial $C(sp^3)$-H activation: Inner Sphere CMD				
Precomplex to $C(sp^3)$-H activation: Inner sphere CMD with $Pd(OAc)_2$		-894.35350	-894.13335	
$C(sp^3)$-H activation: Inner sphere CMD TS with $Pd(OAc)_2$	**Inner_TS_OAc2**	-894.29859	-894.08288	-1561.63
Product of $C(sp^3)$-H activation: With $Pd(OAc)_2$		-894.31363	-894.09469	

Precomplex to $C(sp^3)$-H activation: Inner sphere CMD with $Pd(OAc)_2$-TFA		-1421.01823	-1420.76606	
$C(sp^3)$-H activation: Inner sphere CMD TS with $Pd(OAc)_2$-TFA	**Inner_TS_OAc2-TFA**	-1420.96390	-1420.71639	-1668.60
Product of $C(sp^3)$-H activation: With $Pd(OAc)_2$-TFA		-1420.98340	-1420.73305	
Precomplex to $C(sp^3)$-H activation: Inner sphere CMD with $Pd(OTFA)_2$		-1489.60185	-1489.43427	
$C(sp^3)$-H activation: Inner sphere CMD TS with $Pd(OTFA)_2$	**Inner_TS_OTFA2**	-1489.55780	-1489.39469	-1523.10
Product of $C(sp^3)$-H activation: With $Pd(OTFA)_2$		-1489.61672	-1489.44872	
Precomplex to $C(sp^3)$-H activation: Inner sphere CMD with $Pd(OTFA)_2$-TFA	**Pre_Inner_OTFA_TFA**	-2016.28810	-2016.08819	
$C(sp^3)$-H activation: Inner sphere CMD TS with $Pd(OTFA)_2$-TFA	**Inner_TS_OTFA-TFA**	-2016.22920	-2016.03274	-1505.67
Product of $C(sp^3)$-H activation: With $Pd(OTFA)_2$-TFA	**Post_Inner_OTFA-TFA**	-2016.24365	-2016.04371	
Product after [1.3] Pd migration with PdOAcAcOH		-894.36052	-894.36052	
Product after [1.3] Pd migration with PdOAcTFA	**Allylic_RE_OTFA-TFA**	-1489.63664	-1489.46812	
CMD C-H activation: $C(sp^2)$-H activation after initial Inner Sphere CMD $C(sp^3)$-H activation				
Precomplex to $C(sp^2)$-H activation with ArPdOAc-AcOH		-1205.15528	-1204.78622	
$C(sp^2)$-H activation TS with ArPdOAc-AcOH		-1205.12376	-1204.75792	-1254.67
Product from $C(sp^2)$-H activation with ArPdOAc-AcOH		-1205.13978	-1204.76920	
Precomplex to $C(sp^2)$-H activation with ArPdOTFA-TFA		-1273.72661	-1273.44312	
$C(sp^2)$-H activation TS with ArPdOTFA-TFA		-1273.69711	-1273.41233	-1237.64
Product from $C(sp^2)$-H activation with ArPdOTFA-TFA		-1273.76705	-1273.47915	
sp^2-sp^3 reductive elimination				
Precomplex to 14 electron reductive elimination TS with Ar'Pd(II)Ar-TFA		-1273.72661	-1273.44312	
14 electron reductive elimination TS with Ar'Pd(II)Ar-TFA		-1273.69711	-1273.41233	-286.64
Product to 14 electron reductive elimination TS with Ar'Pd(II)Ar-TFA		-1273.76705	-1273.47915	
Precomplex to 14 electron reductive elimination TS with Ar'Pd(II)Ar- AcOH		-976.14045	-975.82601	
14 electron reductive elimination TS with Ar'Pd(II)Ar- AcOH		-976.07132	-975.76100	-282.72
Product to 14 electron reductive elimination TS with Ar'Pd(II)Ar-AcOH		-976.10073	-975.79105	

Precomplex to 16 electron reductive elimination TS with Ar'Pd(II)Ar$(TFA)_2$	**Pre_Inner_ArOTFA-TFA**	-1800.38942	-1800.07131	
16 electron reductive elimination TS with Ar'Pd(II)Ar$(TFA)_2$	**Inner_TS_AR_OTFA-TFA**	-1800.35847	-1800.04268	-363.40
Product to 16 electron reductive elimination TS with Ar'Pd(II)Ar$(TFA)_2$		-1800.41807	-1800.09853	
Precomplex to 16 electron reductive elimination TS with Ar'Pd(II)Ar$(AcOH)_2$		-1205.13901	-1204.76993	
16 electron reductive elimination TS with Ar'Pd(II)Ar$(AcOH)_2$	**Inner_TS_AR_OAc-AcOH**	-1205.10584	-1204.73712	-366.20
Product to 16 electron reductive elimination TS with $(AcOH)_2$		-1205.16679	-1204.79622	
Alternative mechanisms: sp^2-sp^2				
sp^2-sp^2 carbopalladation with PdPhOTFA-TFA: precomplex		-1800.41843	-1800.10267	
sp^2-sp^2 carbopalladation with PdPhOTFA-TFA: TS	**CP_TS4**	-1800.39284	-1800.07394	-336.64
sp^2-sp^2 carbopalladation with PdPhOTFA-TFA: product		-1800.41178	-1800.09006	
E2 elimination precomplex with PdPhOTFA-TFA and $OTFA^-$		-2326.54997	-2326.21180	
E2 elimination TS with PdPhOTFA-TFA and $OTFA^-$		-2326.53089	-2326.19892	-1297.26
E2 elimination product with PdPhOTFA-TFA and $OTFA^-$		-2326.57992	-2326.24377	
sp^2-sp^2 carbopalladation with PdPhOAc-AcOH: precomplex		-1205.15271	-1204.78384	
sp^2-sp^2 carbopalladation with PdPhOAc-AcOH: TS	**CP_TS2**	-1205.12407	-1204.75311	-342.45
sp^2-sp^2 carbopalladation with PdPhOAc-AcOH: product		-1205.14242	-1204.76915	
E2 elimination precomplex with PdPhOAc-AcOH and $OTFA^-$		-1731.27164	-1730.88224	
E2 elimination TS with PdPh OAc-AcOH and $OTFA^-$		-1731.24712	-1730.86350	-1313.08
E2 elimination product with PdPh OAc-AcOH and $OTFA^-$		-1731.29371	-1730.90840	
S_E3 TS: C(sp^2)-H activation with $Pd(OAc)_2$ and $OTFA^-$		-1420.44180	-1420.20894	-1308.67
S_E3 TS: C(sp^2)-H activation with $Pd(OTFA)_2$ and $OTFA^-$		-2015.73412	-2015.55198	-1363.58
Alternative mechanisms: S_E3 and CP for C(sp^3)-H				
S_E3 TS: C(sp^3)-H activation with $Pd(OAc)_2$ and $OTFA^-$		-1420.43976	-1420.20752	-957.34
S_E3 TS: C(sp^3)-H activation with $Pd(OTFA)_2$ and $OTFA^-$		-2015.72436	-2015.54301	-1278.26
sp^3-sp^2 carbopalladation with PdPhOAc-AcOH: TS	**CP_sp3_OAc**	-1205.09126	-1204.71958	-275.49
sp^3-sp^2 carbopalladation with PdPhOTFA-TFA: TS	**CP_sp3_OTFA**	-1800.36097	-1800.03943	-218.91